

Diss. ETH no. 19138

**ENGINEERING BIO-PHARMACEUTICAL
MICRO- AND NANO-PARTICLES USING
SUPERCRITICAL CARBON DIOXIDE AS
ANTI-SOLVENT**

Dissertation submitted to the

ETH ZURICH

for the degree of

DOCTOR OF SCIENCES

presented by

Johannes Kluge

Process Engineer, ETH Zurich

born on January 3rd, 1980

Citizen of Germany

Accepted on the recommendation of

Prof. Dr. Marco Mazzotti (ETH Zurich), examiner

Prof. Dr. Raffaele Mezzenga (ETH Zurich), co-examiner

Dr. Gerhard Muhrer (Novartis Pharma AG), co-examiner

Zurich 2010

Acknowledgements

First and foremost, I'd like to express my extraordinary gratitude to Professor Marco Mazzotti for accepting me as a PhD student and giving me the possibility to carry out this work as a member of his research group. I consider myself very privileged to have him as a supervisor and want to thank him for supporting and motivating me with a lot of momentum and genuine enthusiasm, but also especially for being patient when necessary.

Many thanks to Dr. Gerhard Muhrer for his enduring commitment to this project, and especially for finding the time for a relaxed and fruitful discussion every once in a while - his continued interest and support has been a great source of motivation to me. I also thank him for being a co-examiner of this thesis.

I am also grateful to Professor Raffaele Mezzenga for his interest in my work and for accepting the task of being a co-examiner.

Thanks a lot to all the other members of the Mazzotti Group, former and present, who have made the time at this institute so valuable. I am especially grateful to Francesco Fusaro; I have enjoyed a lot working together with him in good collaboration. There are many happy memories, like Johanna Schell welcoming me every morning in the office, or Michel Kempkes and Christian Lindenberg teaching me how to ski, only to mention a few, that I would like to acknowledge here.

I would also like to thank Marco Furlan and Marco Lattuada from the Institute for Chemical and Bioengineering, for letting me participate in their work and also for sharing their ideas in a cooperation that has been very important to this project.

Thanks also to Nathalie Casas, Eyal Spier and Lisa Joss, who have carried out their Master and Semester Theses in relation to this project.

I have appreciated a lot the enthusiasm they have brought with them and the energy they invested in this work. Special thanks also to the laboratory technicians and assistant, Daniel Trottmann, Chris Rohrbach and Markus Huber, who, by sharing their rich experience, have always been a strong support.

Last but not least, I am very grateful to Agne for her continuous and everlasting support and for her patience with me, and I want to thank my family and friends who have supported me unconditioned where ever possible. This work is dedicated to them.

Zurich, May 2010

Johannes Kluge

Abstract

The combination of active pharmaceutical ingredients (APIs) with polymeric excipients into functional drug-polymer co-formulations bears huge potential for innovations in the field of drug formulation technology. However, tapping this potential requires novel and innovative processes, tailored to the particular needs of this range of products. In this category fall a number of techniques exploiting the favorable properties of near- and supercritical fluids, especially of supercritical CO₂ (scCO₂), as antisolvents and solvent extracting agents. Such processes may be exploited for the direct manufacturing of high quality products exhibiting a maximum degree of purity. The aim of this work is to contribute to the development of such technology towards practical implementation on an industrial scale. First, pharmaceutical applications are identified where drug-polymer composites represent an especially promising strategy towards innovative products. Then, an experimental setup implemented at the Separation Processes Laboratory at ETH is used to evaluate the potential of supercritical processes in this field, especially by highlighting the quality of manufactured products using suitable analytical techniques.

A first study concerns APIs that are sparingly soluble in water. In order to improve their bioavailability upon oral administration, such drugs are often combined with a water-soluble polymeric excipient. In this context, co-formulations of the sparingly soluble anticonvulsant phenytoin and the water-soluble polymer poly-(vinyl pyrrolidone)-K30 (PVP) have been precipitated using dense scCO₂ as an antisolvent. While the pure API was precipitated in the form of needle-shaped crystals, the pure polymer yielded spherical and fully amorphous nanoparticles. Co-precipitation of both substances yielded products in which the drug was stabilized in the fully amorphous polymer matrix up to a phenytoin content of 40 wt.%; the morphology of these products was very similar to pure PVP. In products exhibiting a drug content in excess of 40 wt.%, phenytoin was also present in crystalline form. The same threshold concentration was found to apply at different operating conditions. Fully amorphous products did not recrystallize upon one year of storage at ambient

conditions, and hence are considered to be long-term stable.

A second and more comprehensive study focuses on the manufacturing of micro- and nanoparticles of the bio-compatible and bio-degradable polymer poly-lactic-co-glycolic acid (PLGA). This water-insoluble polymer is widely used for the administration of sensitive biopharmaceuticals and in order to achieve controlled and prolonged drug release. In all these applications, the size of composite particles plays an important role. Therefore, the potential of manufacturing such particles by a novel process called Supercritical Fluid Extraction of Emulsions (SFEE) is investigated. First, the process is compared to conventional manufacturing techniques in order to highlight its general advantages. Moreover, different strategies are introduced that may be used for the encapsulation of drugs. Then, it is demonstrated in a series of experiments how process parameters like the PLGA concentration and the stirring rate during emulsion preparation may be varied in order to produce particles of pure PLGA with average sizes ranging between 100 nm and a few μm in a controlled and reproducible manner. Finally, three different methods for the encapsulation of lysozyme into composite particles have been investigated and evaluated experimentally. Using the most successful method, an encapsulation efficiency of 48.5% has been achieved.

Further, the encapsulation of the non-steroidal antiinflammatory drug ketoprofen (KET) into PLGA is investigated. Here, the stability of composite nanoparticles is of interest, and has been investigated during one week of storage in aqueous suspension. Depending on their drug content, products could be grouped into three different categories according to their stability behavior. Products containing less than 5 wt.% KET were observed to be stable, while for polymeric particles containing in excess of 10 wt.% KET a significant decrease in drug content could be observed over time, together with the formation of KET crystals by recrystallization. Products with a drug content in between 5 to 10 wt.% exhibited a metastable behavior, i.e. their drug content remained constant while crystals were absent, however the addition of KET crystals led to desupersaturation and a decrease in drug content. In all sus-

pensions equilibrated with crystals of racemic KET, particles were observed to approach a KET level of approximately 5 wt.%, independent of their initial drug content. This behavior is rationalized assuming a solubility of approximately 5 wt.% for KET in PLGA at ambient temperature, together with a metastable zone extending to levels of at least 10 wt.%.

Based on this concept, the solubility of KET in PLGA has been determined in an extended range of temperatures between 0°C and 50°C. Also the effect of KET chirality has been investigated by using two different crystalline forms of KET, namely enantiopure S-KET and a racemic compound, RS-KET, in equilibration experiments. It was found that the level of KET established in PLGA at equilibrium increases with temperature, e.g. from 6.9 wt.% at 20°C to 25.8 wt.% at 40°C for the case of S-KET. At each temperature level, the solubility of KET in PLGA was lower for equilibration with RS-KET, significantly higher for equilibration with S-KET, and the highest for simultaneous equilibration with both crystalline species. Experimental solubility data of KET in PLGA were also used in a model where the polymer solution was described by the Sanchez-Lacombe equation of state.

Finally, the SFEE based manufacturing of biocompatible magnetic nanocomposites made of magnetite nanocrystals dispersed in PLGA nanoparticles has been investigated. The influence of those parameters affecting the final particle size distribution and morphology, primarily the concentration of emulsifier and the magnetite content, has been investigated, so as to optimize the process. Analysis of the products indicated that narrower size distributions are obtained with larger amounts of emulsifier and lower amounts of magnetite. Using ricinoleic acid-stabilized magnetic nanocrystals, magnetite was observed to be distributed inhomogeneously in the polymer and to accumulate on one hemisphere of the particle, hence the morphology of the composite particles tended to be of Janus type. Using magnetite nanoparticles functionalized by polylactide, a much more homogeneous distribution of magnetite in the PLGA particles could be achieved.

Zusammenfassung

Die Kombination von pharmazeutischen Wirkstoffen mit polymerischen Zuschlagstoffen birgt ein grosses Innovationspotential im Bereich pharmazeutischer Formulierungen. Um dieses Potential voll auszuschöpfen, werden neue Verfahren benötigt, welche optimal auf den Produktbereich Wirkstoff-Polymer Ko-Formulierungen zugeschnitten sind. In diesen Bereich fallen Prozesse, welche die vorteilhaften Eigenschaften von nah- bzw. überkritischem CO₂ als Antilösungsmittel ausnützen. Mit solchen Verfahren können direkt und ohne weitere Arbeitsschritte Produkte hergestellt werden, welche insbesondere bezüglich ihrer Reinheit eine hohe Produktqualität aufweisen. Die vorliegende Arbeit soll dazu beitragen, dass solche Verfahren möglichst rasch zur industriellen Anwendung gelangen. Dazu werden zunächst pharmazeutische Anwendungsbereiche beschrieben, in denen besonders Ko-Formulierungen zu innovativen Produkten führen können. Mit Hilfe einer am Institut für Verfahrenstechnik realisierten Anlage werden dann verschiedene Herstellungsverfahren sowie die Qualität der damit hergestellten Produkte experimentell ausgewertet.

Die erste Studie behandelt schlecht wasserlösliche Wirkstoffe, welche zwecks einer verbesserten Bioverfügbarkeit oft mit einem gut wasserlöslichen Polymer zu einer Ko-formulierung verarbeitet werden. In diesem Zusammenhang wurde die gemeinsame Ausfällung von Phenytoin, einem schwer löslichen Wirkstoff, und Polyvinylpyrrolidon (PVP), einem wasserlöslichen Polymer, aus einer Lösung mittels superkritischem CO₂ als Antilösungsmittel untersucht. Hierbei wurde der Wirkstoff in Form von nadelförmigen Kristallen und das Polymer in Form von viel kleineren amorphen Nano-Kugeln ausgefällt; es ergaben sich also für beide Stoffe separat jeweils sehr unterschiedliche Produkte. Bei gemeinsamen Fällungsexperimenten konnte der Wirkstoff bis zu einer Konzentration von 40 Gew.% in der amorphen Polymermatrix stabilisiert werden; bei noch höheren Wirkstoffgehalten war Phenytoin im Produkt zusätzlich auch in kristalliner Form zu finden. Die Produktmorphologien und auch der Schwellenwert von 40 Gew.% für das Auftreten von Kristallen haben

sich als weitgehend unabhängig von Prozessparametern wie Temperatur und Druck erwiesen. Vollständig amorphe Produkte mit einem Wirkstoffgehalt unter 40 Gew.% zeigten über mehrere Jahre keine Anzeichen für Rekristallisation von Phenytoin und können somit als langfristig stabil bezeichnet werden.

Eine zweite und umfangreichere Studie beschäftigt sich mit der Herstellung von Partikeln des bioabbaubaren und biokompatiblen Polymers Poly(lactid-co-glycolid) (PLGA). Dieses Polymer ist wasserunlöslich, und daher geeignet für die Herstellung von Mikropartikeln zwecks kontrollierter Wirkstofffreisetzung oder zielgerichteter Wirkstoffverabreichung (Targeting). Da bei solchen Anwendungen die Partikelgrösse eine wichtige Rolle spielt, wird in dieser Arbeit die Herstellung solcher Partikel mittels Superkritischer Fluid Extraktion von Emulsionen (SFEE) untersucht. Zunächst wird beschrieben, welche Vorteile dieses Verfahren gegenüber anderen Herstellungsprozessen auszeichnet. Weiter werden verschiedene Strategien vorgestellt, mittels welcher die Einkapsulierung von Wirkstoffen erreicht werden kann. Dann wird in einer Serie von Experimenten gezeigt, wie über Parameter wie die PLGA-Konzentration in der Emulsion oder die Rührgeschwindigkeit bei der Emulsionsherstellung die Partikelgrösse zwischen ca. 100 nm und einigen μm gezielt kontrolliert werden kann. In einem letzten Schritt werden drei verschiedene Strategien zur Einkapsulierung von Lysozym experimentell ausgewertet und miteinander verglichen. Hierbei erreicht die beste Methode eine Einkapsulierungseffizienz von 48%.

Weiter wird die Einkapsulierung von Ketoprofen (KET), einem entzündungshemmenden Wirkstoff, in PLGA beschrieben. Hier ist vor allem die Produktstabilität von Interesse, welche in wässriger Suspension über einen Zeitraum von einer Woche beobachtet wurde. In Abhängigkeit vom Wirkstoffgehalt konnten die Produkte in drei verschiedene Kategorien eingeteilt werden. Solche mit weniger als 5 Gew.% KET waren stabil, während bei Produkten mit über 10 Gew.% KET eine deutliche Abnahme des Wirkstoffgehalts beobachtet werden konnte, einhergehend mit der Rekristallisation von KET. Produkte mit einem Gehalt zwischen 5 und 10 Gew.% KET zeigten ein metastabiles Verhalten, d.h. der Wirkstoffgehalt blieb in der Abwesenheit von Kristallen un-

verändert, eine Zugabe von KET-Kristallen führte jedoch zu einer Abnahme des Wirkstoffgehalts in den Partikeln der Ko-formulierung. Unabhängig vom Wirkstoffgehalt am Anfang haben alle Suspensionen, welche mit kristallinem KET ins Gleichgewicht gebracht wurden, allmählich einen Wirkstoffgehalt von 5 Gew.% erreicht. Dies wird damit erklärt, dass bei Umgebungstemperatur die Gleichgewichtslöslichkeit von KET in PLGA bei 5 Gew.% liegt.

Basierend auf dem eben vorgestellten Konzept wurde weiter die Löslichkeit von KET in PLGA in einem erweiterten Temperaturbereich zwischen 0°C und 50°C ermittelt. Zudem wurde bei KET der Einfluss der Chiralität auf die Löslichkeit untersucht. Dazu wurden zwei unterschiedliche Kristallformen von KET, nämlich enantiomerenreines S-KET und ein racemischer Mischkristall RS-KET, verwendet. Wie erwartet nimmt die Löslichkeit von KET in PLGA mit steigender Temperatur zu. Bei allen Temperaturen wurde für RS-KET eine wesentlich niedrigere Löslichkeit ermittelt als für S-KET, wobei die höchste Löslichkeit für gleichzeitiges Equilibrieren mit S-KET und RS-KET gemessen wurde. Die experimentellen Daten wurden für ein Modell des Löslichkeitsverhaltens herangezogen, in dem die Polymerlösung mit der Sanchez-Lacombe Zustandsgleichung beschrieben wurde.

Schliesslich wurde die Enkapsulierung von Magnetit-Nanopartikeln in PLGA mittels SFEE untersucht, wobei eine möglichst hohe Beladung der Partikel mit Magnetit sowie die Herstellung möglichst kleiner Partikel mit einer möglichst engen Grössenverteilung erreicht werden sollte. Untersucht wurde, welchen Einfluss die Konzentration des die Emulsion stabilisierenden Netzmittels auf die Produktqualität hat. Eine wichtige Rolle spielt auch die Funktionalisierung der Magnetit-Nanopartikel: Mit Ricinolsäure funktionalisierter Magnetit war ungleichmässig und einseitig in den PLGA-Partikeln verteilt, somit ergaben sich vorwiegend sogenannte Januspartikel. Hingegen war mit Polylactide funktionalisierter Magnetit auch bei höheren Konzentrationen gleichmässig im PLGA verteilt.

Table of Contents

1	Introduction	1
1.1	A Pharmaceutical Perspective	2
1.2	Supercritical Fluids in Particle Formation	7
1.3	Particle Formation using Supercritical Fluids as Antisolvents	10
1.3.1	Precipitation of Pharmaceuticals using scCO_2 as Antisolvent	11
1.3.2	Precipitation of Polymers using scCO_2 as Antisolvent	15
1.3.3	Co-Precipitation of Drugs and Polymers	18
1.3.4	Supercritical Fluid Extraction of Emulsions	21
1.4	Particle Formation: Crystallization vs. Liquid-Liquid Phase Split	22
1.5	Results of earlier Research in our Lab	26
1.5.1	Gas AntiSolvent Recrystallization (GAS)	27

1.5.2	Precipitation with Compressed Antisolvent (PCA)	32
1.5.3	Conclusions from previous work	38
1.6	Structure of the thesis	39
2	Drug-polymer co-formulation by CO₂ anti-solvent precipitation	43
2.1	Introduction	43
2.1.1	Drug-Polymer Co-Formulation	43
2.1.2	PCA Process	45
2.2	Materials and Methods	47
2.2.1	Materials	47
2.2.2	Experimental Setup and Procedure	47
2.2.3	Product characterization	49
2.3	Experimental Results	51
2.3.1	Co-Precipitation of PVP and Phenytoin	51
2.3.2	Effect of Drug to Polymer Ratio	56
2.3.3	Effect of Concentration Changes in the Initial Solution	59
2.3.4	Long-Term Stability of Co-Formulations	60
2.4	Discussion and Conclusions	61
2.4.1	Thermodynamics of a four-component system	63
2.5	Conclusion	72

3	PLGA micro- and nanocomposites by SFEE: Encapsulation of lysozyme	75
3.1	Introduction	75
3.2	Background	77
3.2.1	Formation of PLGA particles	77
3.2.2	PLGA particles by supercritical fluid processes	77
3.2.3	PLGA composite particles	81
3.3	Materials and Methods	83
3.3.1	Materials	83
3.3.2	Emulsion Preparation	84
3.3.3	SFEE: Experimental Setup and Procedure	85
3.3.4	Product Characterization	87
3.4	Experimental Results	88
3.4.1	SFEE processing of PLGA	88
3.4.2	Effect of PLGA Concentration	88
3.4.3	Effect of Emulsion Stirring Rate	92
3.4.4	Encapsulation of Lysozyme	93
3.5	Discussion and Conclusions	96
4	PLGA micro- and nanocomposites by SFEE: Encapsulation of ketoprofen	99
4.1	Introduction	99

4.2	Materials and Methods	103
4.2.1	Materials	103
4.2.2	Emulsion Preparation and SFEE processing	104
4.2.3	Product Characterization	104
4.3	Experimental Results	106
4.3.1	SFEE processing of pure PLGA and pure Ketoprofen	108
4.3.2	Co-formulation of PLGA and Ketoprofen via SFEE	110
4.3.3	Stability of co-formulations upon seeding	112
4.3.4	Co-Formulation by Impregnation	115
4.3.5	KET solubility in PLGA	117
4.4	Discussion and Conclusions	120
4.4.1	SFEE processing of pure PLGA and Ketoprofen	120
4.4.2	KET-PLGA co-formulation	121
4.4.3	Concluding remarks	123
4.5	Nomenclature	124
5	Solubility of Ketoprofen in Colloidal PLGA	125
5.1	Introduction	125
5.2	Experimental	128
5.2.1	Materials	128
5.2.2	Emulsion Preparation and SFEE processing	129
5.2.3	Preparation of Ketoprofen crystals	129

5.2.4	Equilibration-Impregnation Experiments	130
5.2.5	Equilibration by De-supersaturation	131
5.2.6	Product Characterization	132
5.3	Results and Discussion	133
5.3.1	Equilibration-Impregnation Experiments	135
5.3.2	Equilibration by De-supersaturation	138
5.3.3	Modeling Equilibrium between KET and PLGA	142
5.3.4	Results	147
5.3.5	Equilibration and Glass Transition Temperature	150
5.4	Conclusion	152
5.5	Nomenclature	154
6	Design of biocompatible magnetite-PLGA nano-composites using SFEE	155
6.1	Introduction	155
6.2	Materials and Methods	159
6.2.1	Materials	159
6.2.2	Preparation of magnetite nanocrystals	160
6.2.3	Preparation of polymer composites	162
6.2.4	Samples characterization	164
6.3	Results and Discussion	165
6.3.1	Process Design	165

6.3.2	Effect of operating parameters on size and morphology	168
6.3.3	Non Janus type morphology	180
6.4	Conclusions	181
7	Conclusions and Outlook	183
7.1	Conclusions	183
7.2	Outlook	187
7.2.1	CO ₂ -assisted High-Pressure Homogenization	188
7.2.2	SFEE processing of crystalline Solids: Recrystallization from Emulsions	194
	List of Figures	242
	List of Tables	244

Chapter 1

Introduction

The intention of this first chapter is to introduce the basic concepts and ideas behind this thesis. As shown in Figure 1.1, the project has a multidisciplinary background, and therefore it is advisable to have a look from different perspectives in order to gain a broad overview. First, we present the pharmaceutical perspective, giving a motivation about the type of products that is targeted and about foreseen applications. Then, we introduce supercritical fluid technology, and more specifically processes in particle manufacturing using supercritical CO₂ as antisolvent and solvent extracting agent, in order to give an overview about the manufacturing techniques investigated. Further, two different mechanisms of phase separation that may occur in antisolvent precipitation are introduced, namely crystallization and liquid-liquid phase separation. The final section of this chapter provides an outlook on the structure of the thesis.

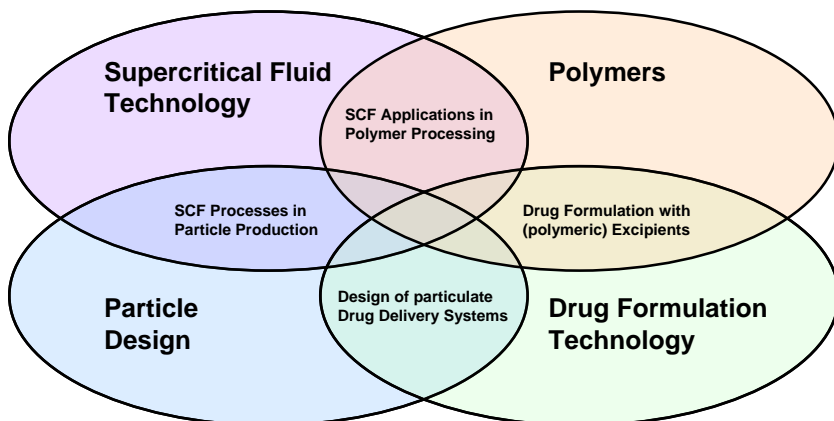


Figure 1.1: Multidisciplinary background of this thesis project.

1.1 A Pharmaceutical Perspective

It is quite a commonplace that healthcare causes tremendous costs and that the pharmaceutical industry has its fair share in this market. Hence one should expect that in this prospering business, the number of newly developed pharmaceuticals is steadily increasing. However, only a brief glimpse at statistics of the US Food and Drug Administration (FDA) is required to disprove this conjecture: whereas the number of new molecular entities (NME's) approved as drugs by the FDA has been remarkably constant during the last 60 years, oscillating around 20 NMEs annually, it is the cost of drug development that has risen exponentially at an annual rate of 13% over the same timeframe, currently exceeding 1.5 billion US\$ per approved NME (Munos, 2009). The obvious difficulty in bringing forward NME based drugs is steadily increasing the importance of lifecycle management for already existing drug products, and therefore it is not surprising that a large majority of new drug applications

(NDAs) currently approved by the FDA is based on active pharmaceutical ingredients that have already been approved previously (Cohen, 2005).

Feasible strategies for extending the lifecycle of a pharmaceutical product are usually based on the design of innovative drug products providing added value as compared to the already existing product. This may be a measurable improvement of therapeutic performance, for instance based on more favorable pharmacokinetics, or facilitated patient compliance, e.g. by enabling a more favorable delivery pathway. The design of improved drug products includes in many cases innovations on the field of drug formulation technology such as particle engineering or the design of functional drug-polymer composites, both fields that have gained considerable attention in recent time. It is worthwhile giving a few examples of novel delivery concepts that are enabled by such innovation.

A first example refers to drugs that are administered orally in form of a pill. Here, complete liberation of the drug has to be achieved during the residence time of the pill in the gastrointestinal tract so as to enable a large fraction of the administered dose to reach systemic circulation - this fraction is called the bioavailability of the drug. An important group of orally administered drugs defined as Class II substances according to the Biopharmaceutical Classification System (BCS), is characterized by very low solubility in aqueous media while permeability across the gastrointestinal membranes is high. Class II substances are generally prone to exhibit a low bioavailability, which is correlated to their *in vitro* kinetics of dissolution (Amidon et al., 1995). Among the possible approaches to enhance both dissolution rate and bioavailability, the coformulation with water-soluble polymeric excipients has generally great potential in this area. The presence of such polymers in the drug formulation may improve bioavailability mainly by two mechanisms. First, the dispersion

of pharmaceutical crystals in water-soluble excipients improves wetting and tablet disintegration, thus leading to accelerated dissolution. This effect can also be achieved by mere physical mixing of the two compounds and does not involve any change in drug morphology. However, a more effective method aims at dissolving the drug in the polymer matrix at a molecular level, so as to stabilize the drug in an amorphous state, i.e. in a so called solid dispersion or solid solution (Leuner and Dressman, 2000). By this, the formation of a stable crystal lattice is hindered, and the solubility of the drug is increased, thus leading to a great enhancement of bio-availability.

The second example concerns active pharmaceutical ingredients that are sensitive biomolecules. Once distributed in the body, many of them are subject to rapid degradation, and hence they have only a short therapeutic half-life. In order to maintain a therapeutic level of the drug in the body, the drug has to be administered in regular intervals, e.g. several times a day. This leads to reduced patient compliance, especially in the case of parenteral delivery and for drugs that need to be administered over a long therapy horizon. Here, a more effective therapy may be achieved by drug administration in the form of a controlled release delivery system from which the drug is released in a specific location and at a certain rate, thus maintaining a constant and optimal therapeutic level of drug at the desired site of action. Such controlled release formulations are typically manufactured by incorporating the drug into microparticles of a suitable polymeric carrier (Varde and Pack, 2004). In contrast to the first example, water-insoluble polymeric carriers are now required, from which the drug is released for instance by diffusion out of the particles or by the erosion of the polymer matrix by biodegradation. It has been found that several important parameters with strong influence on the release rates depend on the size of composite microspheres (Berk-

land et al., 2003); thus, drug formulation in form of composite particles exhibiting a uniform size distribution in the desired size range represents a key prerequisite for a precise control of drug release rates (Berkland et al., 2002).

Third, many pharmaceuticals - especially those used for cancer treatment in chemotherapy - are characterized by a narrow therapeutic range, referring to an optimal level of the drug in the body. This level should preferably stay in the range between a lower bound below which the drug does not exhibit a therapeutic effect and an upper bound above which toxic side effects of the drug become dominant. For these drugs that are potentially toxic, a small dosage in combination with an accumulation of the drug at the desired site of action can help reducing the side effects caused by the toxicity of the drug. This is possible by a more favorable drug distribution within the body, approaching targeted drug delivery to the desired site of action. There are a number of different concepts as to how such targeted delivery may be achieved, and some of these involve drug-polymer composites. For instance, magnetically responsive composite nanoparticles may allow to influence the distribution of or drug release from drug-polymer co-formulation particles in the body by means of a magnetic field. Another example is the targeted delivery of drugs to the pulmonary system by inhalation. For this case, it has been shown that drug particles in the narrow size range of 1 to 3 μm are most efficient, and hence tight control of particle size is required in the manufacturing of products for which this pathway of drug delivery has been selected (Gupta and Hickey, 1991).

These three examples should demonstrate the huge potential of drug-polymer co-formulations for the development of improved drug products for a large variety of different pharmaceutical applications. Clearly, the choice of materials, i.e. the drug and the polymer used in the co-

formulation, will be different in each of the applications presented, and so will be the specific criteria that are applied in an assessment on product quality. However, a number of important questions are rather general and have to be addressed independent of the materials that are being used. Here, a good example is the issue of long term stability of composite particles consisting of a solid solution of the drug in the polymer matrix. The entrapment of the active ingredient into the polymeric material may be thermodynamically unfavorable, especially if high drug loadings are desired, or if the mutual affinity between drug and polymer is low. Such co-formulations would bear the risk of reduced long-term stability and shelf life, and this aspect represents a major hurdle with respect to potential applications (Vasanthavada et al., 2005). Hence, the design and development of such co-formulations requires information about the compatibility of drug and polymer, in order to select a promising polymer excipient forming stable co-formulations and allowing for maximal drug load. However, there is still a lack of such data, as well as of robust and reliable experimental methods to generate such information in an accurate and efficient manner.

Physical mixing represents the simplest method to produce a co-formulation of a drug and a polymer, however, mixing is restricted to the level of particles, and mixing on a molecular level cannot be achieved. The latter may be attained through melt extrusion (Six et al., 2003; Miller et al., 2007), however this process requires temperatures sufficient to melt the polymer matrix, and therefore it is not suitable for the processing of temperature-sensitive materials. Impregnation is feasible if drug and polymer have sufficient affinity for each other, but long timescales are required to achieve equilibration between drug and polymer through diffusion; in this context, supercritical fluids may be exploited as plasticizing agents in order to accelerate impregnation (Ki-

mic and Vecchione, 2003). A number of processes start with a common solution of drug and polymer from which the solvent is subsequently removed, e.g. by spray drying (Filipovic-Grcic et al., 2003), solvent evaporation, using an emulsion process, or by antisolvent precipitation. The application of supercritical fluid methods in this context is discussed in the following.

1.2 Supercritical Fluids in Particle Formation

A large majority of more than 98% of applications related to the supercritical fluid technology relies on supercritical carbon dioxide (scCO₂) (Pasquali et al., 2008). For CO₂, the state of a supercritical fluid is reached above its critical point at 31.1°C and 73.9 bar, i.e. at comparably mild temperatures and reasonable pressures. At these conditions, scCO₂ exhibits properties midway between gas-like and liquid-like; for instance, its density and viscosity may be adjusted continuously between gas-like and liquid-like values, simply by variation of pressure or temperature. As a process solvent, scCO₂ has favorable properties since it is non-toxic, non-inflammable and inert in many applications as well as cheap, available in abundance and considered environmentally benign as compared to most organic solvents. Moreover, it is easily separated from the final product by evaporation when returning to atmospheric pressure, i.e. without any further action.

These favorable properties make clear that scCO₂ is widely applicable, and not surprisingly, it is used on an industrial scale in an increasing number of processes. The most significant are Supercritical Extraction (SE), where scCO₂ takes the role of a solvent used to extract e.g. sensi-

tive biomolecules from natural matter (Reverchon and De Marco, 2006), and Supercritical Fluid Chromatography (SFC), where scCO_2 is used as a mobile phase in adsorption-based separations (Taylor, 2009). On the other hand, many scCO_2 -based processes are still considered emerging technologies, or even solutions in search of a problem. The main reason here is that using scCO_2 is often considered technically challenging, mainly because of the high operating pressures that require costly equipment and make it difficult to observe processes or to implement probes and monitoring devices unless this is planned carefully in advance. Regarding possible applications there is a strong tendency to favor conventional techniques as long as they are feasible, and hence the breakthrough of scCO_2 -based technology in these areas requires most of all a demonstration that such methods lead to innovative products that are not easily obtained in a more conventional way.

The class of still-emerging supercritical fluid technologies comprises a number of processes concerning the formation of particles. These have been divided into four groups (Pasquali and Bettini, 2008):

- Processes where scCO_2 acts as a solvent (RESS)
- Processes where scCO_2 acts as a propellant and atomizing agent (CO_2 -assisted spray drying, CAN-BD, SAA)
- Processes where scCO_2 acts as a plasticizer (PGSS)
- Processes where scCO_2 acts as an antisolvent (GAS, PCA, SAS, SEDS, ASES) or solvent extracting agent (SFEE)

The first three categories shall only be explained briefly. ScCO_2 is used as a solvent in a process called Rapid Expansion of a Supercritical Solution (RESS). In this process, supercritical medium is saturated with

a solute, followed by rapid depressurization and expansion through a nozzle. The expansion step causes a drastic and instantaneous decrease of solvent power respectively build-up of supersaturation, leading to the formation of very small particles of uniform size (Debenedetti et al., 1993). RESS has been used for the micronization of a number of pharmaceutical substances (Turk, 2009), however, the practical applicability of RESS is limited by the fact that comparably few drugs, such as ibuprofen (Charoenchaitrakool et al., 2000), are sufficiently well-soluble in scCO_2 .

The fact that scCO_2 is miscible with, or at least partly soluble in most solvents is exploited in processes using scCO_2 as a propellant and atomizing agent. These processes are called CO_2 -assisted spray drying, CO_2 -Assisted Nebulization with a Bubble Dryer, CAN-BD (Sievers et al., 2001) or Supercritical Assisted Atomization, SAA (Reverchon and Antonacci, 2006). In these processes, a solution saturated with CO_2 at high pressure is subsequently expanded and atomized through a nozzle. CO_2 acts both as pneumatic agent that atomizes the solution in fine droplets, and as cosolute expanding from the inside of the primary droplets, thus leading to their further atomization upon decompression. As in spray drying, the formation of solid particles is achieved by an additional stream of drying gas, e.g. nitrogen. A considerable advantage of this type of processes as compared to other supercritical techniques in particle formation is that also aqueous solutions may be processed.

Some substances, especially polymers, uptake CO_2 by sorption, leading to swelling of the polymer matrix and to a significant plasticization. For amorphous polymers this leads to a decrease in the glass transition temperature; this has been investigated in more detail for PLGA (Liu and Tomasko, 2007; Pini et al., 2008) and PMMA (Liu et al., 2005; Rajendran et al., 2005). A similar effect is observed in semicrystalline

polymers such as PEG and PCL, where a decrease in the melting point has been measured (Lian et al., 2006). The plasticizing effect of CO₂ on such substances may be exploited in a process called Particles from Gas Saturated Solutions, PGSS (Weidner et al., 1996). In PGSS the solid to form particles is melted, and the melt is simultaneously saturated and expanded by addition of scCO₂, leading to a low viscosity gas saturated solution. Particles are formed by expanding this solution over a nozzle, leading to the formation of fine particles by atomization. Since there is no solvent used in this process, particles solidify immediately due to the drastic decrease in pressure and temperature induced by the expansion.

1.3 Particle Formation using Supercritical Fluids as Antisolvents

ScCO₂ is a rather bad solvent for most pharmaceuticals and polymers, however, it is well-miscible with most organic solvents such as alcohols, ethers and esters, water being the most prominent exception. Thus, when a solute of interest is dissolved in a suitable organic solvent, and the solution is mixed with scCO₂ in a second step, this leads in many cases to a drastic lowering of the solvent power and induces precipitation of particles. This is employed in a number of processes using scCO₂ as antisolvent and solvent extracting agent, representing indeed the most widely applicable method of using supercritical fluids in processes concerning the formation of particles. The single processes differ mainly in the way solution and antisolvent are contacted. In the Gas AntiSolvent crystallization (GAS) process, the solution is loaded into a batch precipitator, which is subsequently pressurized with CO₂. With increasing vapor pressure, CO₂ dissolves into the solution and causes an expan-

sion of the liquid accompanied by a decrease in solvent power, which finally leads to the precipitation of particles (Gallagher et al., 1989). On the other hand, the Precipitation using Compressed Antisolvent (PCA) process is based on the continuous mixing of solution and scCO_2 in a two substance nozzle placed at the inlet of a high pressure vessel that is initially filled with scCO_2 (Randolph et al., 1993; Bodmeier et al., 1995). In the case of PCA, mass transfer between solution and scCO_2 is more efficient, and therefore buildup of supersaturation and precipitation of particles happens much faster as in the GAS process. For the continuous process, a number of modifications have been proposed, aiming for instance at improved mixing by optimized design of the injection device. While each of them has been named with its own acronym, for instance Solution Enhanced Dispersion by Supercritical fluids (SEDS), Aerosol Spray Extraction System (ASES) or simply Supercritical Antisolvent processing (SAS), it is worth highlighting that all these processes exhibit actually many similarities, but no fundamental differences.

Supercritical Antisolvent Processes have been applied to a large range of materials (Shariati and Peters, 2003), especially for pharmaceutical (Foster et al., 2003), polymeric (Yeo and Kiran, 2005) or energetic materials (Pourmortazavi and Hajimirsadeghi, 2005).

1.3.1 Precipitation of Pharmaceuticals using scCO_2 as Antisolvent

Since this study targets the precipitation of pharmaceuticals and polymeric excipients used in drug formulation, a list of interesting examples in this area is presented in the following. Table 1.1 comprises a selection of studies concerning the precipitation of drug substances using scCO_2 as antisolvent, with a special focus on class II compounds and biomolecules

such as carotenoids and proteins.

Table 1.1: Selection of studies concerning the manufacturing of drug, polymer and drug-polymer composite products using scCO_2 as antisolvent.

Compound	Process	Reference
Theophylline	GAS, SAS	Subra et al. (2005); Roy et al. (2007)
Phenytoin	GAS, PCA	Muhrer et al. (2006)
Paracetamol	GAS, PCA	Fusaro et al. (2004, 2005)
Salicylic acid	PCA	Lin et al. (2007)
Carbamazepine	GAS	Moneghini et al. (2003)
Itraconazole	GAS, ASES	Barrett et al. (2008)
Paclitaxel	PCA	Niu et al. (2006)
Rifampicin	SAS	Reverchon et al. (2002)
Cefonicid	SAS	Reverchon and De Marco (2004)
Nalmefene HCl	SAS	Adami et al. (2008)
Amoxicillin	SAS	Kalogiannis et al. (2005) Reverchon et al. (2003)
Piroxicam	PCA	Wu et al. (2009)
Lutein	SAS	Miguel et al. (2008)
Lycopene	SAS	Miguel et al. (2006)
β -Carotene	SAS	Franceschi et al. (2009)
Lysozyme	GAS	Muhrer and Mazzotti (2003)
	SAS	Chang et al. (2008)
Insulin	PCA	Snaveley et al. (2002)
Trypsin	SAS	Winters et al. (1996)

Considering that in these studies very different compounds have been precipitated using processes that are in general quite similar, it is interesting to have a look at the various morphologies that have been obtained for these particles. Typical examples are shown in Figure 1.2:

For many substances such as Carbamazepine, Itraconazole, Paracetamol, Phenytoin and Theophylline, clearly crystalline products have been ob-

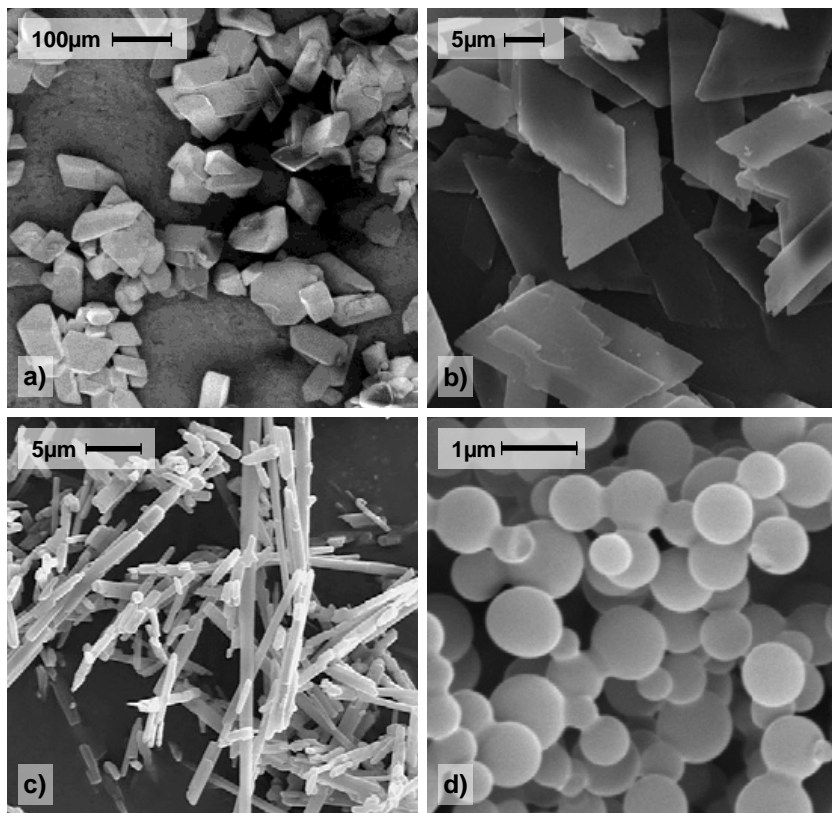


Figure 1.2: Product morphologies obtained by scCO_2 antisolvent precipitation of pure drug substances. a) Paracetamol, compact crystals (Fusaro et al., 2004); b) Theophylline, crystalline platelets (Roy et al., 2007); c) Phenytoin, crystalline needles (Muhrer et al., 2006); d) undisclosed compound, amorphous submicron spherical particles (Muhrer et al., 2003).

tained. This is evident from suitable analytical techniques such as XRD and DSC, but also from the characteristic shape of crystalline particles, ranging from compact crystals (Figure 1.2a) to platelets (1.2b) and

needle-like morphologies (1.2c). A general comparison also shows that typically larger particles are obtained for batch precipitation using the GAS process, where supersaturation is induced slowly due to the gradual addition of antisolvent. On the other hand, smaller particles are produced using continuous processes such as PCA or SEDS, where much higher initial supersaturations are achieved by the continuous mixing of scCO_2 and solution in a mixing device. Batch and continuous processes have been directly compared to each other in a number of studies, often leading to the same conclusion (Muhrrer et al., 2006; Fusaro et al., 2005). However, in some of these studies using different processing techniques had only a marginal influence on the size of product particles (Barrett et al., 2008; Roy et al., 2007), which is especially surprising if one considers the fact that mixing in PCA is typically by orders of magnitude faster as compared to the GAS process (Fusaro et al., 2005). Moreover, crystalline nanoparticles have not been obtained in any of the mentioned studies.

Other substances, especially larger molecules such as Rifampicin, Cefonicid, Nalmefene HCL and Amoxicillin, but also proteins such as lysozyme and insulin, have been found to precipitate in the form of amorphous particles rather than crystals. As shown in Figure 1.2d, such amorphous particles are mostly spherical, sometimes agglomerated, and generally much smaller as compared to the aforementioned crystalline particles, often in the submicron and nanometer range. Due to these properties, precipitation products belonging to the second category are generally very similar to each other regarding their visual appearance in microscopy, and can be easily distinguished from the first class of products, i.e. crystalline precipitates. Interestingly, there are substances where crystals as well as amorphous spheres have been obtained as precipitation products, depending e.g. on the organic solvent that has been used in the otherwise

equivalent precipitation process (Muhler et al., 2003; Reverchon et al., 2002). Hence the question whether crystalline or amorphous precipitation products will be formed cannot always be answered regarding just the precipitating substance; at least sometimes, there are other effects that need to be considered.

1.3.2 Precipitation of Polymers using scCO_2 as Antisolvent

Besides pharmaceuticals, also a large number of polymeric materials have been precipitated using various scCO_2 -based anti-solvent processes. A selection is presented in the following table 1.2 Also in the case of polymeric substances, it is interesting to have a look at morphologies that have been obtained when precipitating these polymers. Some of the polymers, such as PEG, PVA and L-PLA, lead to semicrystalline precipitates. However, these have usually the appearance of micron or submicron irregular shaped particles or of fibers; well developed larger crystals are typically not observed. On the other hand, most of the mentioned polymers exhibit a fully amorphous structure. Equivalent to what has been observed for other substances forming amorphous precipitates, they form typically (sub-)micron spherical particles that are sometimes heavily agglomerated, then forming web-like structures. Distinct spherical particles have been observed e.g. for PVP and Dextran, while web-like morphologies have been obtained for HYAFF, EC and HPMC. As compared to the previous case, semi-crystalline and amorphous precipitates cannot be easily distinguished at first glance due to their generally similar particle size and morphology. This can be seen from the different examples given in Figure 1.3.

As mentioned previously, many polymers are able to uptake CO_2 by

Table 1.2: Selection of studies concerning the manufacturing of drug, polymer and drug-polymer composite products using scCO₂ as antisolvent.

Polymer	Process	Reference
Polystyrene (PS)	PCA	Dixon et al. (1993)
polyvinylpyrrolidone (PVP)	PCA	Muhrer et al. (2006) Wu et al. (2009)
hydroxypropyl-methylcellulose (HPMC)	PCA	Reverchon et al. (2008)
Polyethylene glycol (PEG)	GAS	Martin et al. (2007) Barrett et al. (2008)
Dextran	PCA	(Perez et al., 2004)
Hyaluronic acid (HYAFF)	GAS, PCA	Elvassore et al. (2001a)
Polyvinylalcohol (PVA)	GAS, SAS	Adami et al. (2007)
Ethylcellulose (EC)	SAS	Duarte et al. (2006)
Eudragit EPO	GAS	Garay et al. (2010)
Poly-L-Lactide (L-PLA)	PCA	Perez de Diego et al. (2005); Chen et al. (2007)
Poly-Lactide-co-Glycolide (PLGA)	SEDS	Ghaderi et al. (1999, 2000)
Poly-DL-Lactide (DL-PLA)		
Poly- ϵ -Caprolactone (PCL)		

sorption, leading to swelling of the polymer matrix and to a significant plasticization, i.e. a decrease in the glass transition temperature or melting point. While this interaction of polymer and CO₂ may be exploited in a number of processes such as facilitated melt extrusion (Verreck et al., 2006b,a, 2007), supercritical impregnation (Kikic and Vecchione, 2003) or PGSS, it represents a major handicap for many polymers exhibiting a rather low melting point or glass transition temperature regarding the possibility of precipitation using scCO₂ as antisolvent. Instead of forming solid particles, such polymers precipitate in the presence of scCO₂

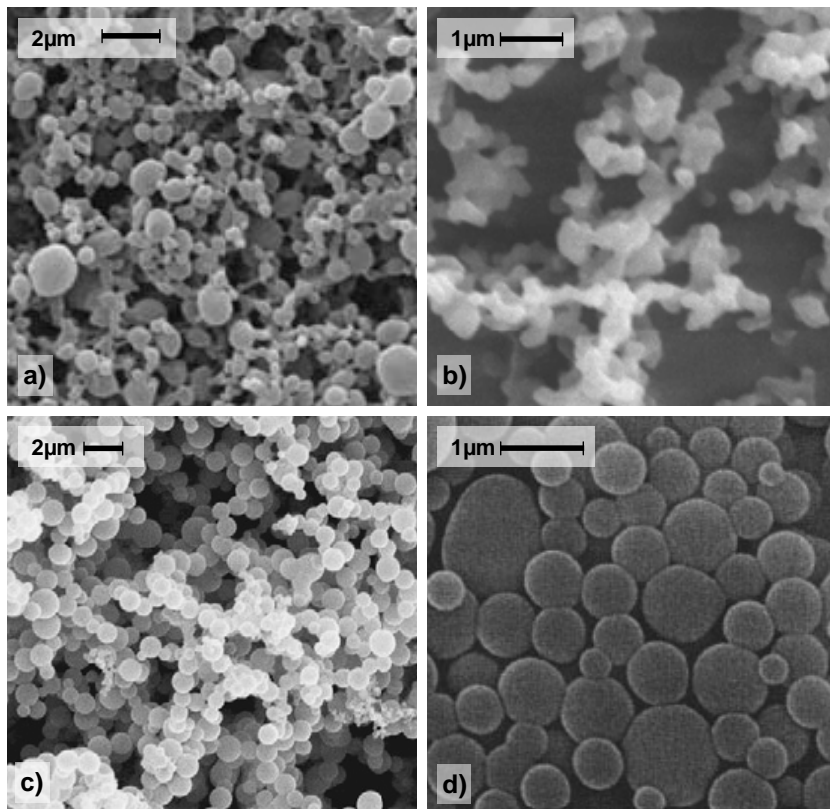


Figure 1.3: Product morphologies obtained by scCO_2 antisolvent precipitation of polymers. a) L-PLA, a water-insoluble semicrystalline polymer (Chen et al., 2007); b) Ethylcellulose, a water-insoluble amorphous polymer (Duarte et al., 2006); c) PVA, a water-soluble semi-crystalline polymer (Adami et al., 2007); d) Dextran, a water-soluble amorphous polymer (Perez et al., 2004).

as droplets in rubbery liquid state, and are prone to agglomeration, coalescence and formation of films, as observed e.g. for PLGA, DL-PLA and PCL (Ghaderi et al., 1999). In these cases, improved formation of

particles has been observed when mixtures of CO₂ and nitrogen were used as antisolvent instead of pure CO₂ (Ghaderi et al., 2000).

1.3.3 Co-Precipitation of Drugs and Polymers

In the co-formulation of drugs and polymers, two or more different materials exhibiting different morphologies are precipitated simultaneously from a homogeneous solution, using scCO₂ as antisolvent. A selection of studies where the formation of drug-polymer composites has been investigated is presented in Table 1.3.

Most of these studies fall in two major focus areas, namely first the co-formulation of sparingly soluble class II compounds, such as Carbamazepine, Felodipine, Itraconazole and Phenytoin, with water-soluble polymers such as PVP, PEG or HPMC, and second the encapsulation of sensitive biomolecules, such as cholesterol and insulin, into water-insoluble polymeric drug delivery systems such as PLA and PLGA. Not surprisingly, observed product morphologies comprise combinations of what is observed for the pure substances (compare Figures 1.2 and 1.3); a selection of drug-polymer composite products is presented in Figure 1.4.

Here it is worth making a few comments. Figure 1.4a shows the product of a co-precipitation experiment with theophylline, a crystalline drug, and L-PLA, a semicrystalline polymer. It can be clearly seen that both substances form separate phases, i.e. rhombic crystals of theophylline and semicrystalline microparticles of L-PLA (Roy et al., 2007). Figure 1.4b shows a co-precipitate of Cholesterol and PLGA. Also here, the drug precipitates separately in the form of elongate crystals. PLGA is amorphous, and forms droplets coating the Cholesterol crystals rather than separate particles (Dave et al., 2006). On the other hand, Figure

1.3 Particle Formation using Supercritical Fluids as Antisolvents

Table 1.3: Selection of studies concerning the manufacturing of drug, polymer and drug-polymer composite products using scCO₂ as antisolvent.

Composites (Drug - Polymer)		Process	Reference
Bupivacaine HCL	PLGA L-PLA	SAS	Lee et al. (2006)
Carbamazepine	PEG	GAS	Moneghini et al. (2001); Sethia and Squillante (2002)
	PVP	GAS	Sethia and Squillante (2004)
Cholesterol	L-PLA	PCA	Perez de Diego et al. (2005)
	PLGA	SAS	Dave et al. (2006)
Itraconazole	PEG	ASES	Barrett et al. (2008)
	HPMC	ASES	Lee et al. (2005)
Theophylline	L-PLA	SAS	Roy et al. (2007)
	HPMC	SAS	Moneghini et al. (2006)
Felodipine	HPMC	SAS	Won et al. (2005)
Insulin	PLA+PEG	GAS	Elvassore et al. (2001b)
Lutein	L-PLA	SAS	Miguel et al. (2008)
β -Carotene	PEG	SAS	Martin et al. (2007)
Lutein	PEG	SAS	Martin et al. (2007)
Phenytoin	PVP	PCA	Muhrer et al. (2006)
Piroxicam	PVP	PCA	Wu et al. (2009)

1.4c shows a co-precipitate consisting of three different materials, i.e. insulin, L-PLA and PEG, that appear well-mixed on the micro-scale, forming submicron and spherical composites (Elvassore et al., 2001b). This example, and also other studies, show that scCO₂ antisolvent precipitation also represents an interesting process for the preparation of polymer blends (Duarte et al., 2006; Lin et al., 2010). Figure 1.4d shows composites of Felodipine and HPMC, and also in this case the drug does not form separate crystals, but is dissolved in the amorphous polymer matrix (Won et al., 2005). Regarding these scenarios, we conclude that

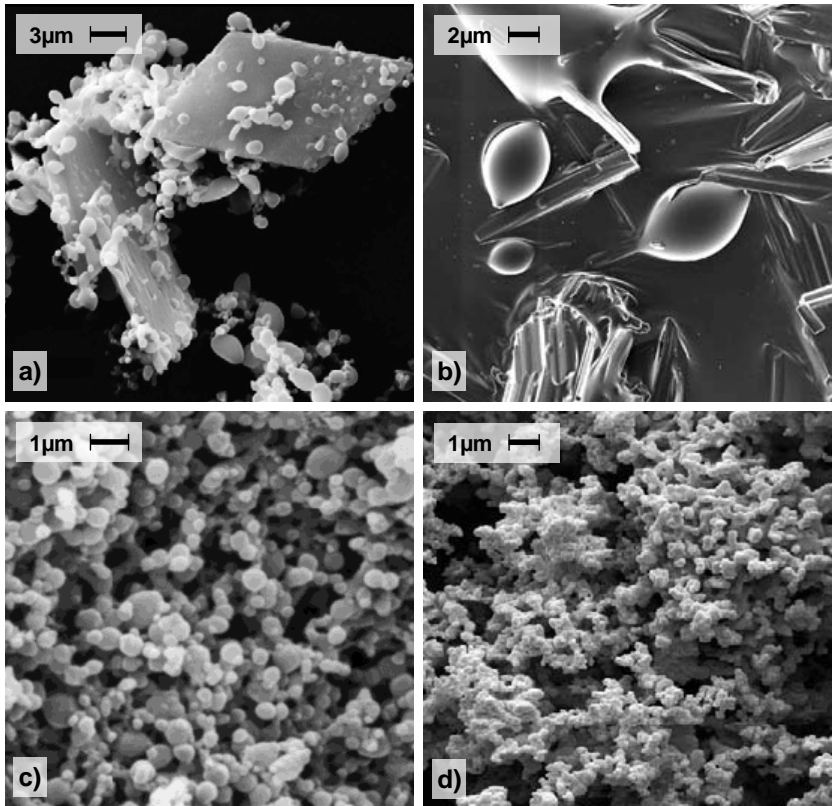


Figure 1.4: Drug-Polymer composite particles obtained by $scCO_2$ antisolvent precipitation. a) Theophylline + L-PLA: Rhombic theophylline crystals can be clearly distinguished from micron-sized polymeric particles (Roy et al., 2007); b) Cholesterol + PLGA: Elongate crystals of cholesterol coated by polymeric droplets (Dave et al., 2006); c) Insulin + PLA + PEG: Submicron composite particles (Elvassore et al., 2001b); d) Felodipine + HPMC: The drug is stabilized in amorphous composite particles, crystals are not present (Won et al., 2005).

the two materials involved in co-precipitation may form separate phases that can be clearly distinguished, or form composite particles and even single phase mixtures. It is generally difficult to predict the outcome of a co-precipitation, but it is always enlightening to study the precipitation of its pure components in order to see what can be expected.

1.3.4 Supercritical Fluid Extraction of Emulsions

ScCO₂ has also been used as solvent extracting agent for the production of particles by supercritical fluid extraction of solvent from an emulsion (SFEE). In this process, an organic solution of the compound to be precipitated is first dispersed in an oil-in-water emulsion and stabilized by a suitable surfactant. Then, the emulsion is continuously mixed with supercritical CO₂ in order to extract the organic solvent from the emulsion droplets. Thereby, a stable suspension of solvent-free product particles in water are obtained, and may be recovered upon depressurization. The process was introduced for the manufacturing of drug - PLGA composites (Chattopadhyay et al., 2006), and recent research activities have focused further on producing PLGA microparticles (Della Porta and Reverchon, 2008). However, it has been demonstrated that also crystalline particles may be precipitated (Shekunov et al., 2006b) by SFEE. Recently this process has been applied for the manufacturing of PLGA-based gene delivery nanoparticles (Mayo et al., 2010).

It has been discussed already that the plasticizing effect of scCO₂ complicates the scCO₂ precipitation of a number of polymers exhibiting a rather low melting point or glass transition temperature, since in the presence of scCO₂ they precipitate as droplets in rubbery liquid state rather than forming solid particles. It is worth mentioning that SFEE is ideally suitable for the processing of such polymers, provided they

are insoluble in water. A number of very interesting materials, such as PLGA, DL-PLA, PCL, PMMA and some types of Eudragit fall into this category. Using SFEE, stable suspensions of solvent-free polymeric droplets in water are obtained, and upon depressurization, the solidified polymer particles may be recovered. Particles produced by SFEE exhibit a characteristic high degree of uniformity, and the size of product particles may be tightly controlled during emulsion preparation.

1.4 Particle Formation: Crystallization vs. Liquid-Liquid Phase Split

In the previous section, we have shown a number of examples for substances that precipitate in the form of crystals, as shown in Figure 1.2a-c, or otherwise in the form of amorphous nanospheres, as shown in Figures 1.2d, 1.3b and 1.3d. The two types of particles differ also with respect to the phase behavior and mechanisms that lead to their formation, and it is worth discussing these differences here in detail, since the distinction between crystallization and liquid-liquid phase separation is an important point in the outline of this thesis.

For crystalline particles, these formation mechanisms are nucleation and growth, as predicted by classical nucleation theory. The typical phase diagram of a ternary system, where crystallization from a binary solution is induced by addition of CO_2 acting as antisolvent, is shown in Figure 1.5a. The process starts at point A, with a solution of drug in a suitable solvent. When CO_2 is added, the process follows the dashed operating line, and after moving into the two-phase region, the mixture is supersaturated (point B). Nucleation of crystals is an activated process and requires a certain induction time. Point C corresponds to the

overall composition in the final state after crystals have formed, where a saturated solution in C_1 is in equilibrium with the pure crystalline drug in C_2 . This type of system is comparably well-investigated and has not only been described qualitatively but also modeled using rigorous mathematical models (Dixon and Johnston, 1991; Kikic et al., 1997; Muhrer et al., 2002).

On the other hand, the typical phase diagram of a ternary system where phase separation of a polymer solution is induced by addition of CO_2 acting as antisolvent is shown in Figure 1.5b. Again, the process starts at point A' , with a solution of an amorphous polymer in a suitable solvent, and the process follows the dashed operating line when CO_2 is added. When moving into the two-phase region, it can be observed that the operating line crosses two curves: first, after crossing the binodal (solid) line in point B' , the solution becomes supersaturated, and then, after crossing the spinodal (dotted) line in point C' , the solution becomes unstable. Liquid-liquid phase separation by spinodal decomposition is then a spontaneous process, i.e. it starts immediately and does not require any induction time. With point D' corresponding to the overall composition, points D'_1 and D'_2 represent the final state, i.e. a polymer-rich and a polymer-lean phase in equilibrium with each other. Also this type of system has already been described previously (Dixon et al., 1993; Lai et al., 1998; Perez de Diego et al., 2005).

Liquid-liquid phase separation and nucleation of a crystalline solid phase have actually a lot in common: they both involve the formation of a new phase (the precipitate) in which the precipitating species is enriched at the cost of the leaner phase. Also, both types of phase separation are caused by the same mechanisms leading to supersaturation, i.e. cooling, solvent evaporation or antisolvent addition. Hence, it is not surprising that the two phase separation mechanisms may under certain conditions

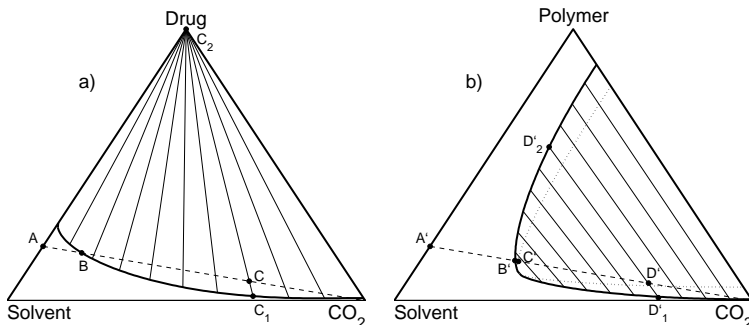


Figure 1.5: a) Precipitation of a crystalline solid using CO_2 as an antisolvent. b) Precipitation of a polymer using CO_2 as an antisolvent.

compete with each other because of either kinetic or thermodynamic reasons, as illustrated in Figure 1.6.

Precipitation of a species exhibiting kinetic competition between crystallization and liquid-liquid phase separation is shown in Figure 1.6a. Again, the process starts at point A with a binary solution and the process follows the dashed operating line when CO_2 is added. At point B, the solution is supersaturated, and crystals are formed if sufficient time is available to overcome the induction time required for formation of nuclei. Under this condition, the system behaves as that illustrated in Figure 1.5a. Otherwise, if CO_2 is added rapidly so as its composition moves beyond point C before the onset of crystallization, the system encounters a spinodal (dotted line) and undergoes a spontaneous liquid-liquid phase separation by spinodal decomposition, i.e. it behaves as the one illustrated in Figure 1.5b. The outcome at the end of the precipitation process in point D is different in the two cases, leading to a stable crystalline phase in the first case, and to a metastable liquid or glassy phase in the second. This kind of kinetic competition is often encountered for

systems that crystallize slowly, such as proteins.

Thermodynamic competition between crystallization and liquid-liquid phase separation is shown in Figure 1.6b. If the process starts at point A', i.e. at low concentration, the operating line leads into a two-phase region where crystals are formed, equivalent to the scenario in Figure 1.5a. On the other hand, if precipitation starts at point A'' with a solution at higher concentration, addition of antisolvent leads first into a liquid-liquid two phase region, and phase separation by liquid-liquid phase split, equivalent to the scenario in Figure 1.5b, cannot be avoided. This type of behavior is exhibited by many substances that are prone to oiling out.

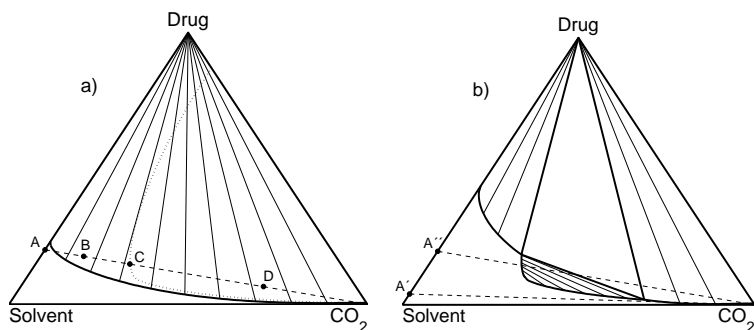


Figure 1.6: Competition between crystallization and liquid-liquid phase separation. a) Kinetic competition, b) Thermodynamic competition

Summarizing, the presented framework gives a rational explanation why two rather different types of product morphologies, namely large crystalline particles and amorphous microspheres, have been observed in scCO_2 antisolvent precipitation of different materials. It proposes that the formation of the two types of particles relies on different mechanisms, namely on nucleation and growth for crystals, as compared to

a liquid-liquid phase separation, probably involving spinodal decomposition, for amorphous particles. With regard to the co-precipitation of drug-polymer composites, it gives an indication that for the two single species a rather different precipitation behavior may be expected, and it highlights the complexity of a system where both species are precipitated together. Regarding Figure 1.6, we conclude that crystallization and liquid-liquid phase separation may interfere with each other, favoring liquid-liquid phase separation and hence formation of amorphous precipitates in systems where supersaturation is achieved rapidly. However, it has to be kept in mind that the crystalline state is usually thermodynamically more favorable, and may be attained during long term storage by recrystallization.

1.5 Results of earlier Research in our Lab

This section presents results of earlier work that has been carried out in our lab, highlighting in more detail the different behavior of crystalline and amorphous materials in precipitation experiments using scCO_2 as antisolvent. Further, we describe more clearly the specific process setups that have been applied, and discuss operating parameters that are expected to have an effect on important product properties such as the obtained particle size. The materials used in these studies fall into the two different categories described in section 1.3.1 for scCO_2 antisolvent precipitation, namely phenytoin and paracetamol precipitating in crystalline form, and lysozyme precipitating in the form of fully amorphous nanoparticles.

1.5.1 Gas AntiSolvent Recrystallization (GAS)

Experimental Setup: A temperature controlled and stirred high pressure vessel with a total volume of 400 ml, equipped with a Pyrex window allowing visual observation of the liquid phase volume expansion and precipitation processes upon CO_2 addition, represents the core of the GAS setup at ETH and is shown schematically in Figure 1.7.

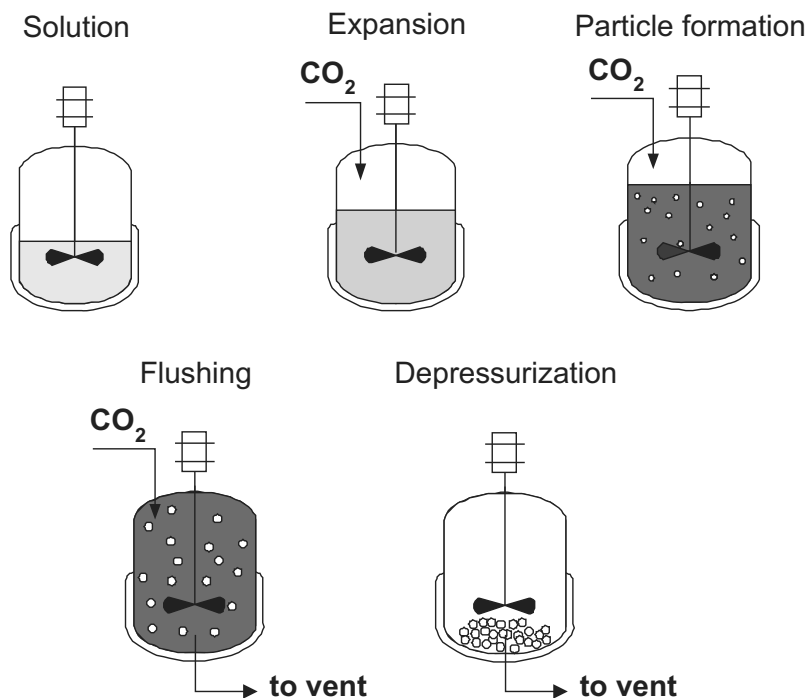


Figure 1.7: Sequence of Steps in Gas AntiSolvent recrystallization (GAS).

Prior to the experiment, organic solutions of the compound to be precip-

itated were prepared, i.e., paracetamol in acetone, phenytoin in acetone or ethanol, and lysozyme in DMSO. A variable amount of the solution, typically 50 ml, was initially loaded into the vessel. Then, CO₂ was delivered at constant mass flow rate and at operating temperature. Feeding was accomplished by bubbling CO₂ directly into the liquid phase in the vessel while stirring at a constant rate of typically about 500 rpm. With increasing pressure, gaseous CO₂ readily dissolves into the organic solvent, leading to an expansion of the liquid phase while reducing its solvent power, finally causing the precipitation of particles. The feed flow rate of CO₂ was kept constant until the precipitation vessel was completely filled with liquid, and the desired final pressure was reached. Then, while remaining at the final pressure, the outlet valve was opened, and flushing with pure CO₂ was continued, in order to remove the organic solvent from the product particles which were retained in the reactor by a sinter metal filter mounted at the bottom of the precipitation vessel. After depressurization, the precipitator was opened, and the product could be harvested in the form of dry solid particles for off-line analysis. A more detailed description of the setup may be found elsewhere (Muhrrer and Mazzotti, 2003). In the GAS process, the specific rate of CO₂ addition, i.e. the flow rate of CO₂ normalized by the initial volume of organic solution in the reactor, is widely considered the most influential operating parameter.

Precipitation of Paracetamol: The precipitation of paracetamol has been investigated in an extensive study using the GAS technique (Fusaro et al., 2004). Selected results of GAS precipitation are shown in Figure 1.8. In these experiments, paracetamol was precipitated from an 8wt.% solution in acetone at a temperature of 25°C, stirring at a rate of 500 rpm, while the specific rate of CO₂ addition was varied. The de-

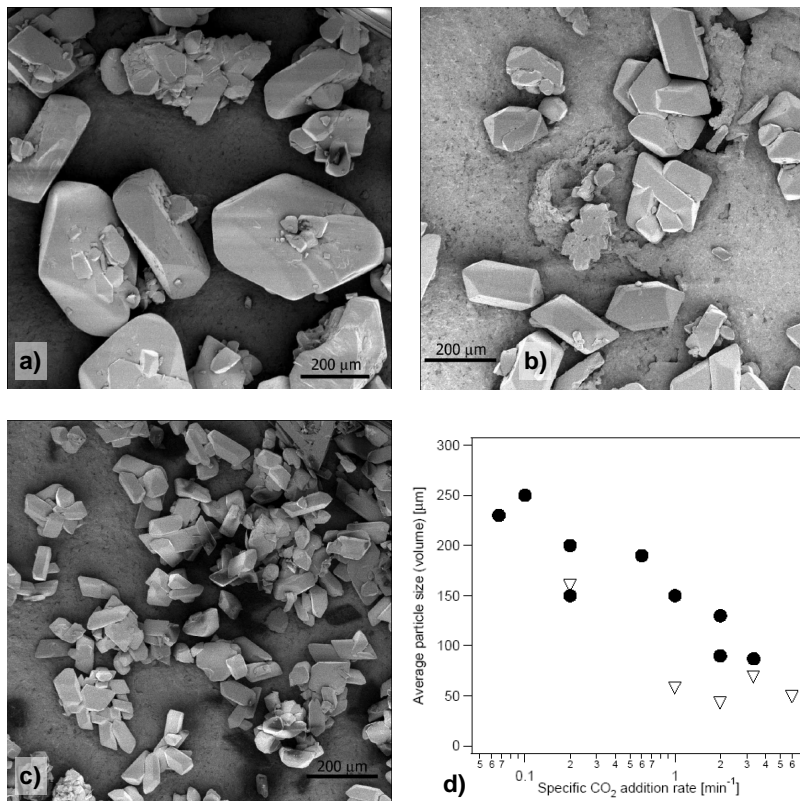


Figure 1.8: Paracetamol crystals precipitated by the GAS process, using specific rates of CO₂ addition of 0.1 min⁻¹ (a), 0.6 min⁻¹ (b), and 2 min⁻¹ (c). Average particle size vs. specific rate of CO₂ addition for a larger set of experiments (d); (∇) experiments carried out using a different GAS setup (Fusaro et al., 2004).

crease in average size in going from low to high CO₂ addition rates can be clearly observed visually from the appearance of particles, but also by plotting the average particle size against the specific CO₂ addition rate, as shown in Figure 1.8d where experimental points lie on a curve

with negative slope. This is also true for the experiments carried out on a different set-up, indicated with a triangle (Fusaro et al., 2004).

Precipitation of Phenytoin: In another study, the precipitation of the anticonvulsant drug phenytoin has been investigated using both GAS and PCA (Muhrrer et al., 2006). Selected results of GAS precipitation are shown in Figure 1.9. In each of these experiments, phenytoin was precipitated from a 3wt.% solution in acetone at 30°C while stirring at 400 rpm; the specific rate of CO₂ addition was varied. Also here, it can be clearly observed from the appearance of particles that the average crystal size and volume markedly decreases with increasing rate of CO₂ addition. Further, a morphological transition from rhombic to more

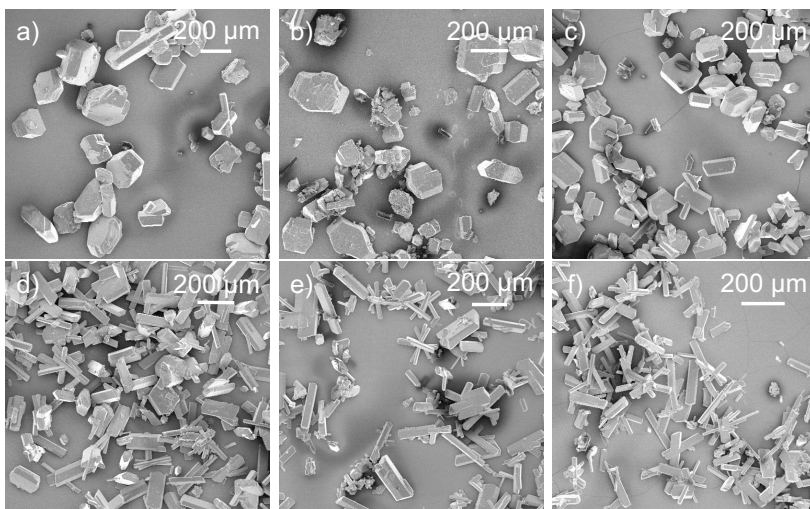


Figure 1.9: Phenytoin crystals precipitated by the GAS process, using specific rates of CO₂ addition of a) 0.07 min⁻¹, b) 0.1 min⁻¹, c) 0.2 min⁻¹, d) 0.5 min⁻¹, e) 1 min⁻¹, f) 2 min⁻¹. The average crystal size decreases with increasing rate of CO₂ addition (Fusaro, 2008).

columnar crystal shapes could be observed with decreasing particle size.

Precipitation of Lysozyme The effect of operating parameters on product quality in the precipitation of lysozyme from DMSO using the GAS process has been investigated in an extensive study (Muhrrer and Mazzotti, 2003). It was found that the average particle size was essentially insensitive to variations of the major operating parameters in the GAS process, namely CO_2 addition rate, initial lysozyme concentration in the solution, and experimental temperature. The effect of the CO_2 addition rate on the average particle size is shown in Figure 1.10 for two different concentrations, representing the upper and lower limit of the concentration range studied.

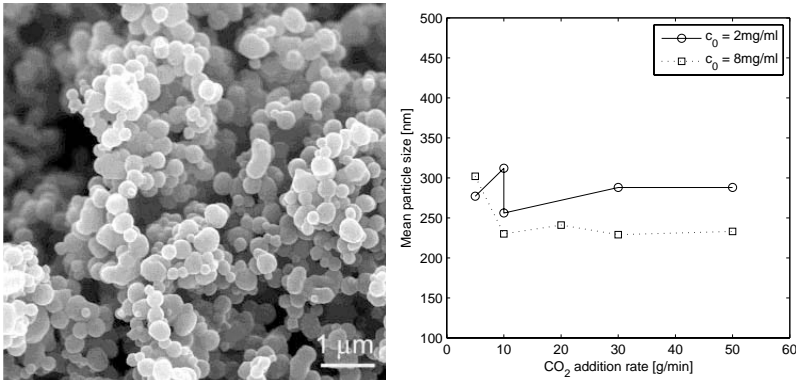


Figure 1.10: Lysozyme precipitation by the GAS process. a) Product precipitated from a 2 g/l solution in DMSO at 25°C , using a CO_2 addition rate of 50 g/min. b) Effect of CO_2 addition rate on the average particle size of lysozyme precipitated at 25°C (Muhrrer and Mazzotti, 2003)

No trend can be observed for the particle size when the CO_2 addition rate is varied between 5 and 50 g/min. For the lowest initial concentration of 2 mg/ml, average particle size varies between 277 and 312 nm, whereas

for the highest concentration of 8 mg/ml, particles are between 233 and 302 nm.

Modeling of the GAS process The formation of particles in the GAS process has also been described in a mathematical model (Muhrrer et al., 2002). The model is based on material balances for the involved species solute, solvent and CO₂; further, liquid-vapor equilibrium between solvent and CO₂ was described using the Peng-Robinson equation of state. Finally a population balance equation was used to describe the evolution of the particle size distribution, including constitutive equations for particle formation and growth. Using this model, the effect of the main operating parameter in GAS, namely the specific rate of CO₂ addition, on the size distribution of product particles could be investigated in simulations. Here it was observed that the size of product particles was strongly decreasing with increasing rate of CO₂ addition. This is rational, since higher rates of CO₂ addition lead to higher supersaturation being attained, which generally favors nucleation over growth, and hence leads to the formation of smaller particles. As may be seen in a comparison of Figures 1.8, 1.9 and 1.10, the trend predicted by the model is also observed experimentally for the crystalline materials paracetamol and phenytoin, however not for amorphous lysozyme.

1.5.2 Precipitation with Compressed Antisolvent (PCA)

Experimental Setup PCA experiments were carried out in a temperature controlled high pressure vessel with a total volume of 900 ml shown schematically in Figure 1.11. In contrast to GAS, PCA is a continuous process, working at a constant operating temperature and pressure, and

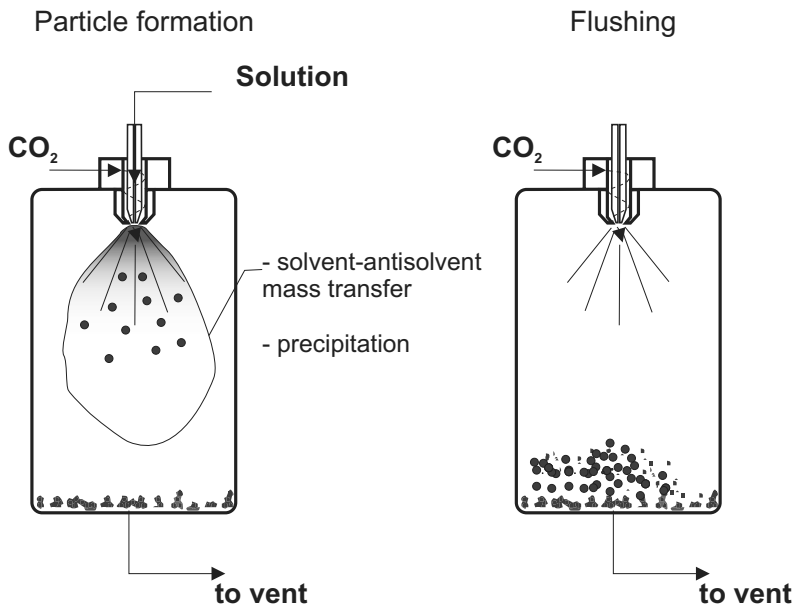


Figure 1.11: Precipitation with Compressed Antisolvent (PCA) process.

involving constant streams, such as feed of scCO_2 and solution as well as the off-gas flux to be vented. The reactor is initially filled with CO_2 , and feed of all streams is started; at this stage, pure organic solvent is fed to the reactor. When steady state is reached with respect to operating temperature, pressure and flow rates, an organic solution of the compound to be precipitated is fed to the reactor, and precipitation is induced when the two streams of organic solution and scCO_2 are mixed at the entrance of the vessel in a two-substance nozzle. Mass transfer between solution and antisolvent, and also the formation of particles is mostly restricted to a zone close to the nozzle outlet, as shown on the left hand side of Figure 1.11. Finally, the reactor content is flushed with

pure CO₂ in order to remove residual solvent from reactor and product (Figure 1.11, right hand side), and the reactor is depressurized to recover the product from the vessel. A more detailed description is provided in Section 2.2.3.

PCA is a steady state process, highlighting the importance of the operating point in terms of pressure and temperature conditions, and especially the state of the solvent-antisolvent binary system at this point. Here, subcritical and supercritical conditions are distinguished. At subcritical conditions, injection of solvent and CO₂ through a nozzle will result in jet break-up into fine droplets, comparable to spray drying, and mass transfer will then be controlled by diffusion into and from the droplet (Werling and Debenedetti, 1999). At supercritical conditions, solvent and CO₂ are completely miscible, and the absence of finite surface tension rules out the formation of droplets (Lengsfeld et al., 2000). In the first case, CO₂ acts as solvent-extracting agent whereas in the second case it acts as anti-solvent. The transition from one domain to the other and its effect on size and morphology of product particles has been investigated in a previous study on the precipitation of P_LLA (Perez de Diego et al., 2005).

Precipitation of Paracetamol by PCA: Precipitation of Paracetamol using PCA has been carried out at supercritical conditions of 313 K and 150 bar, using a 10 g/l ethanol solution at a flow rate of 1 ml/min. The effect of varying the CO₂ flow rate has been investigated in the range between 20 and 150 g/min. Figure 1.12 shows the corresponding volume weighted particle size distributions (PSDs) measured with a Coulter Multisizer (Beckman-Coulter, USA). While the narrowest PSD and the smallest particle size are clearly obtained at the highest CO₂ flow rate of 150 g/min, it can be observed that variations at lower CO₂

flow rates have almost no effect on the PSD of the obtained particles.

Precipitation of Phenytoin by PCA: In a series of PCA experiments, the precipitation of phenytoin from acetone solutions has been investigated (Muhrer et al., 2006). It was found that phenytoin precipitated in the form of fine, medium to high aspect ratio needles at all operating conditions investigated, this particular habit being typi-

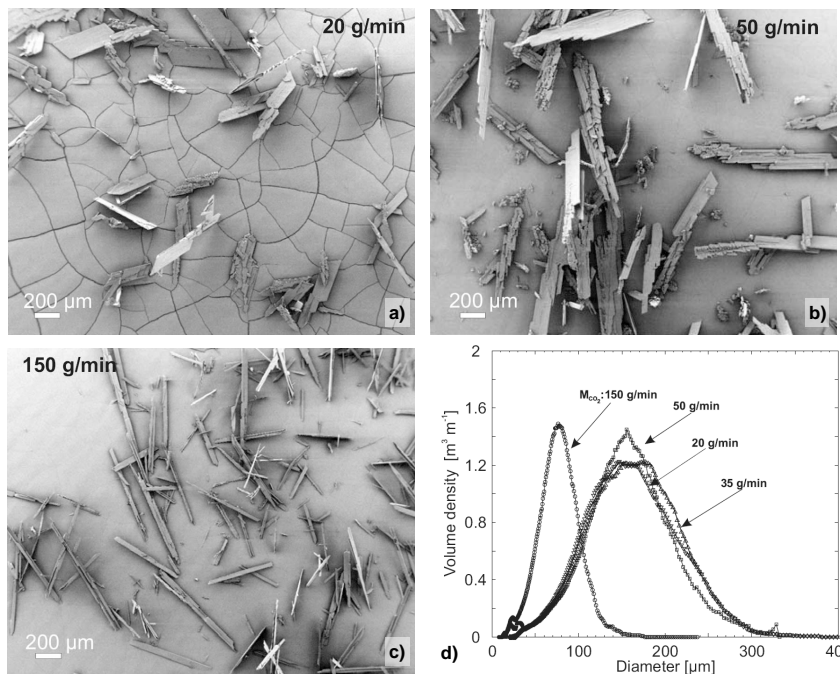


Figure 1.12: Precipitation of Paracetamol using the PCA process. Products obtained at 313 K and 150 bar from a 10 g/l solution at a flow rate of 1 ml/min. CO₂ flow rates are a) 20 g/min, b) 50 g/min and c) 150 g/min. d) Volumetric particle size distributions obtained for these runs (Fusaro , 2008).

cally associated to very high supersaturation levels. Selected results are presented in Figure 1.13. In these experiments the pressure was varied between 95 and 150 bar while keeping the temperature at 50°C; the concentration of phenytoin in the solution was 4 wt.%, the solution flow rate 1 ml/min and the CO₂ flow rate 80 g/min. As shown in Figure 1.13a and b, high aspect ratio needles are formed at 150 bar and 120 bar. On the contrary, at 95 bar, the morphology of the precipitate changes rather dramatically. As shown in Figure 1.13c, the product appears as agglomerates of roughly spherical, fused particles, containing some columnar crystals. This change in morphology is attributed to the near-critical precipitation conditions experienced in the last experiment, where the experimental pressure lies close to the critical pressure of the binary system acetone-CO₂ (90 bar at 50°C).

Precipitation of Lysozyme by PCA: The PCA precipitation of lysozyme from solutions in DMSO has been addressed in a recent and rather comprehensive study, investigating a large range of operating parameters and involving sub- and supercritical as well as liquid precipita-

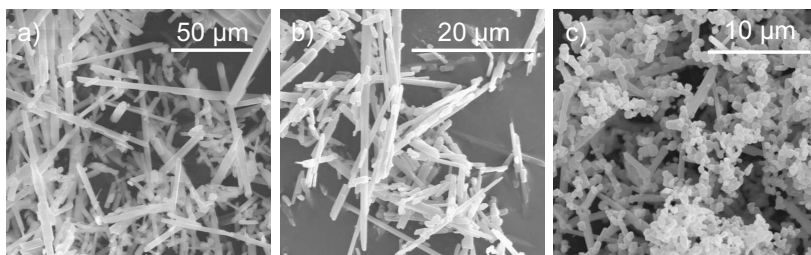


Figure 1.13: Precipitation of Phenytoin using the PCA process. Products obtained at 323 K from a 4 wt.% solution at a flow rate of 1 ml/min, using a CO₂ flow rate of 80 g/min. Operating pressures are a) 150 bar, b) 120 bar and c) 95 bar (Muhrrer et al., 2006).

tion conditions (Fusaro et al., 2009). In this work, particle size distributions have been obtained by image analysis, in order to assess the effect of operating conditions on particle size. As shown in Figure 1.14a-c, it was found that operating in the subcritical region, characterized by

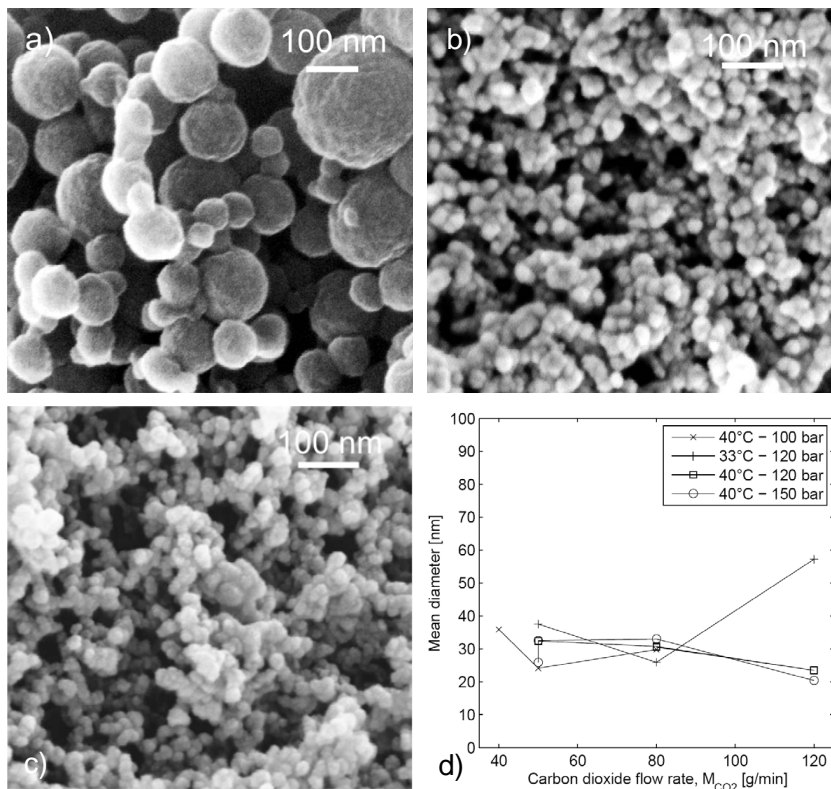


Figure 1.14: Precipitation of Lysozyme using the PCA process, showing products obtained in the a) subcritical, b) supercritical and c) liquid region of the CO_2 -DMSO mixture. d) Effect of the CO_2 flow rate on the mean size of lysozyme particles at different supercritical operating conditions (Fusaro et al., 2009)

jet-break up into droplets, yields particles that are larger than the ones obtained in the supercritical or liquid region. On the other hand, no general trend could be observed when varying the operating point in a rather wide range of supercritical operating conditions or when changing the CO₂ flow rate, as is illustrated in Figure 1.14d.

Modeling of the PCA Process: Also for the PCA process, particle formation has been described using a mathematical model (Fusaro, 2008). Modeling this process is mathematically challenging, since on top of the equations that have been mentioned in the description of the GAS model, the effect of mixing of solution and antisolvent under turbulent flow conditions needs to be described using computational fluid dynamics (CFD). Nevertheless, the model allowed to investigate in computer simulations the effect of important operating parameters in PCA, such as the ratio of CO₂ and solution flow rates, on the size distribution of product particles. It was found, for instance, that an increased CO₂ flow rate should lead to smaller product particles. As may be seen in a comparison of Figures 1.12 and 1.14, this trend predicted by the model is also observed experimentally for crystalline paracetamol, however not for amorphous lysozyme.

1.5.3 Conclusions from previous work

The precipitation of crystalline substances using scCO₂ antisolvent processes can be rationalized in terms of the classical nucleation and growth concept, and models relying on this concept give predictions that are qualitatively correct. On the other hand, for amorphous substances such as lysozyme, a convincing dependence of the product quality on operating parameters strongly affecting supersaturation has not been ob-

served. This hypothesis is suggested by experimental findings obtained from both GAS and PCA processing. Along with recent observations of the phase behavior of lysozyme in the system CO₂-DMSO (Fusaro et al., 2009), these results suggest that amorphous particles are indeed formed by liquid-liquid phase separation involving spinodal decomposition, and not by nucleation and growth. Considering that the formation of drug-polymer co-formulations is targeted in this work, and that many polymeric excipients are amorphous, this aspect is of major importance, defining some of the challenges that shall be addressed in the scope of this thesis.

First, drug-polymer co-formulation often involves two substances that fall into the two different categories described, i.e. crystalline and amorphous materials; leading to the question by which mechanisms composite particles are formed if they are co-precipitated using scCO₂ as antisolvent.

Second, it seems that control of particle size in the precipitation of amorphous polymers is hardly achieved by variation of operating conditions; posing the question whether and how the size of polymeric particles can be controlled otherwise.

1.6 Structure of the thesis

The combination of active pharmaceutical ingredients (APIs) with polymeric excipients into functional drug-polymer co-formulations bears huge potential for innovations in the field of drug formulation technology. Supercritical fluid technology, especially processes using scCO₂ as antisolvents and solvent extracting agents, represents an interesting and innovative class of processes that may be exploited for the direct manufacturing

of high quality composites exhibiting a maximum degree of purity. The aim of this work is to contribute to the development of such technology towards practical implementation on an industrial scale. First, pharmaceutical applications are identified where drug-polymer composites represent an especially promising strategy towards innovative products. Then, an experimental setup implemented at the Separation Processes Laboratory at ETH is used to evaluate the potential of supercritical processes on this field, especially by highlighting the quality of manufactured products using suitable analytical techniques.

Chapter 2 concerns the preparation of co-formulations of the sparingly soluble anticonvulsant phenytoin and the water-soluble polymer poly-(vinyl pyrrolidone)-K30 (PVP). In this case, composites are prepared in order to improve the bioavailability of the drug upon oral administration. The morphology of co-precipitates obtained from solutions exhibiting different drug to polymer ratios is determined, and also the influence of varying the operating conditions is investigated. The stability of product composite particles is checked after one year of storage at ambient conditions.

Chapter 3 focuses on the manufacturing of micro- and nanoparticles of the bio-compatible and bio-degradable polymer poly-lactic-co-glycolic acid (PLGA), a water-insoluble polymer that is widely used for the administration of sensitive biopharmaceuticals and in order to achieve controlled and prolonged drug release. The potential of manufacturing such particles by Supercritical Fluid Extraction of Emulsions (SFEE) is investigated, paying special attention to possible mechanisms that allow to control the size of PLGA particles. Finally, different methods for the encapsulation of lysozyme into composite particles are investigated and compared.

In Chapter 4 the encapsulation of the non-steroidal antiinflammatory

drug ketoprofen (KET) into PLGA is investigated using SFEE. Here, the stability of composite nanoparticles is of interest, and is investigated during one week of storage in aqueous suspension. The observed phase behavior may be rationalized assuming a solubility of KET in PLGA, and a method is presented that allows to determine this solubility experimentally by equilibration of PLGA nanoparticles with crystalline KET.

Based on this concept, the solubility of KET in PLGA is determined in an extended range of temperatures in Chapter 5. Also the effect of KET chirality on the equilibrium is investigated by using two different crystalline forms of KET, namely enantiopure S-KET and a racemic compound, RS-KET, in equilibration experiments. Experimental solubility data of KET in PLGA are also used to parameterize a model describing the polymer solution based on the Sanchez-Lacombe equation of state.

Manufacturing of biocompatible magnetic nanocomposites by SFEE is described in Chapter 6. Such particles are composed of functionalized magnetite nanocrystals dispersed in PLGA nanospheres. The influence of parameters affecting the final particle size distribution and morphology, i.e. the concentration of emulsifier and the magnetite content, is investigated, so as to optimize the process. Also, for magnetite nanoparticles, the effect of different types of surface functionalization on the obtained morphology of product composites is investigated.

Finally, conclusions are drawn in Chapter 7, and an outlook is presented.

Chapter 2

Drug-polymer co-formulation by CO₂ anti-solvent precipitation ¹

2.1 Introduction

2.1.1 Drug-Polymer Co-Formulation

For most organic drug substances, pharmaceutical activity is based on the non-covalent, reversible molecular binding to a specific target, i.e. a biological receptor or an enzyme, involving the interaction of complementary parts of the molecular structure of the active compound and of the receptor. The aptitude of the overall molecular structure for such specific interactions explains why molecules exhibiting pharmaceutical activity usually contain different functional groups and moieties, each characterized by specific properties with respect to charge, polarity and the presence of hydrogen bonding sites. Besides forming the basis of

¹The work in this chapter has been carried out in co-operation with Francesco Fusaro and has been published as Kluge et al. (2009a).

pharmaceutical activity, the overall molecular structure also determines the interactions among drug molecules themselves, and therefore also the formation of crystals with high lattice energies as well as the tendency to polymorphism and pseudo-polymorphism. These aspects are of high relevance because the morphology of a drug product largely determines pharmacokinetics, downstream processability in terms of e.g. flowability or compactability, and long-term stability, which are crucial characteristic properties that define the overall quality of a pharmaceutical product. Compared to pharmaceutical activity, which is assessed at the discovery stage, all these properties are assessed only during the drug development phase.

An important group of orally administered drugs, which are defined as Class II substances, is characterized by very low solubility in aqueous media, and high permeability across gastrointestinal membranes. For this class of active compounds, there is a correlation between in-vivo bio-availability and in-vitro kinetics of dissolution (Amidon et al., 1995). Therefore, many research studies aim at the development of formulation techniques that enhance in-vitro dissolution rates, thus promising enhanced bio-availability.

Among the possible approaches to achieve this, the co-formulation of such drugs with water-soluble polymeric carriers has generally great potential in this area. The presence of such polymers in the drug formulation may improve bio-availability mainly by two mechanisms. First, the dispersion of pharmaceutical crystals in water-soluble excipients improves wetting and tablet disintegration, thus leading to accelerated dissolution. This effect can also be achieved by mere physical mixing of the two compounds and does not involve any change in drug morphology. The second mechanism aims at dissolving the drug in the polymer matrix at a molecular level, so as to stabilize the drug in an amorphous

state, i.e. in a so called solid dispersion or solid solution (Leuner and Dressman, 2000). By this, the formation of a stable crystal lattice is hindered, and the solubility of the drug is increased, thus leading to a great enhancement of bio-availability.

The production of such co-formulations requires the specification of a certain drug to polymer ratio. The amount of polymer must be high enough to guarantee a sufficient shelf life of the pharmaceutical product, whereas the content of the required excipients should be minimized to keep dosages small. The solution of this optimization problem requires an improved understanding of the thermodynamics of the system drug - polymer, which remains a major challenge. In this work, an attractive production process for co-formulations, namely the precipitation using a compressed fluid anti-solvent (PCA), is investigated in this context.

2.1.2 PCA Process

Supercritical fluids, and especially supercritical CO₂, have been widely applied for the production of particulate products, especially for pharmaceuticals and fine chemicals. Existing processes involve supercritical fluids either as solvents (Phillips and Stella, 1993; Subramaniam et al., 1997) or as anti-solvents (Subramaniam et al., 1997). The main advantage in the application of compressed CO₂ as process medium is that a dry product with low residual solvent content is obtained in a single-step process at mild operating temperatures. Furthermore, CO₂ is cheap and its application helps reducing the consumption of organic solvents. Research in this field over the past few years has paid special attention to the processing of class II pharmaceuticals. Here, processes involving supercritical CO₂ promise enhanced dissolution and increased bio-availability either by micronization of the compounds (Perrut et al.,

2005a) or by their co-formulation with polymers and other well-soluble excipients like cyclodextrins (Perrut et al., 2005b).

Within the field of supercritical fluid processes, the formation of polymeric particles has its own research record (Yeo and Kiran, 2005). Also in this case, supercritical fluids have been applied both as solvents (Petersen et al., 1987) and as anti-solvents (Dixon et al., 1993). The phase behavior of the polymer - solvent - anti-solvent system has been discussed previously (Dixon et al., 1993), and particularly with reference to its effect on particle formation in such processes (Palakodaty and York, 1999). Research has soon focused on biodegradable polymers for pharmaceutical controlled release applications (Debenedetti et al., 1993; Ghaderi et al., 2000). More recently, also water-soluble pharmaceutical excipients and the formation of solubility-enhancing co-formulations with sparingly soluble drugs have been studied (Moneghini et al., 2001; Charoenchaitrakool et al., 2002; Perez de Diego et al., 2005; Moneghini et al., 2006).

In line with these studies, it has recently been shown that the co-formulation of the sparingly soluble drug phenytoin with the water-soluble polymer poly-(vinyl pyrrolidone) (PVP K30) results in a significantly improved dissolution rate of the drug (Franco et al., 2001; Muhrer et al., 2006). The present study is a continuation of this research effort, and presents more systematic and comprehensive experimental data for the system phenytoin - PVP K30 obtained in an extended range of operating conditions.

2.2 Materials and Methods

2.2.1 Materials

The compounds 5,5 diphenyl hydantoin (phenytoin), $C_{15}H_{12}N_2O_2$, $M_W = 252.3$ Da, $T_M = 568.3$ K, $\Delta H^f = 34.2$ kJ/mol (Chow et al., 1995) (Sigma-Aldrich, Buchs, Switzerland), poly(vinylpyrrolidone) K30 purum (PVP K30; Sigma-Aldrich, Buchs, Switzerland; product number 81420), ethanol (analytical grade, Scharlau, Sentmenat, Spain), acetone (analytical grade, J.T. Baker, Deventer, Netherlands) and carbon dioxide (99.9%, from PanGas, Schlieren, Switzerland) were all used as received. We presume that PVP K30 corresponds to the BASF product Kollidon 30, which has a number average molecular weight $M_N = 12$ kDa and a weight average molecular weight in the range $M_W = 44 - 54$ kDa hence a polydispersity of about 4 (Bühler, 2003). Prior to anti-solvent precipitation, solutions of PVP and phenytoin were prepared. Based on the experience from previous experiments (Muhler et al., 2006), a solvent mixture consisting of 76 wt.% acetone and 24 wt.% ethanol was used for all experiments.

2.2.2 Experimental Setup and Procedure

A scheme of the experimental setup used for the PCA experiments is shown in Figure 2.1. CO_2 is drawn from a dip tube cylinder and precooled in a pressure module (PM101, NWA GmbH, Lörrach, Germany) before being delivered to the reactor by a piston pump (PP200, Thar Design Inc., Pittsburgh PA, USA). Pump heads are cooled to $5^\circ C$ by a cryostat (minichiller, Huber, Offenburg, Germany). The stream then passes a back pressure regulator (Thar Design Inc., Pittsburgh

PA, USA) set to 10 bar above the desired reactor pressure, in order to reduce stream fluctuations generated by the piston pump. The solution is delivered by an HPLC pump (PU2080 plus, Jasco). Before entering the reactor, both the CO₂ and the solution feed stream are brought to the operating temperature (CC230, Huber).

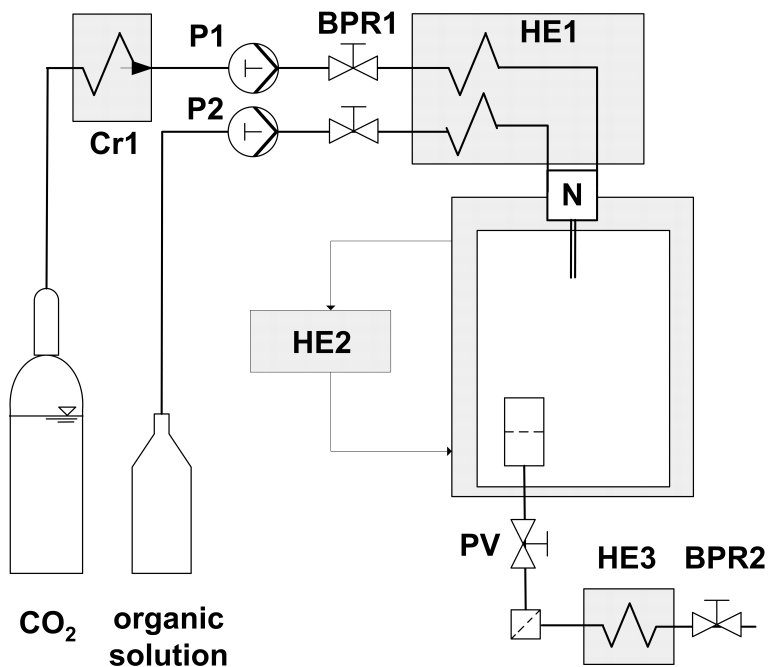


Figure 2.1: Scheme of the PCA setup used for the co-precipitation experiments.

Both streams are mixed at the inlet of the reactor by a two substance nozzle (Schlick, Untersiemau, Germany). The reactor (Premex, Lengnau, Switzerland) has a volume of 900 ml and is kept at the operating temperature by another thermostat (CC240, Huber). The particles formed

are retained within the reactor by a filter bag made of Teflon tissue, and two sinter metal filters are placed at the outlet of the reactor in order to remove all particles from the off-gas stream. The pressure inside the reactor is controlled by a backpressure regulator located downstream, through which the off-gas stream expands to atmospheric pressure and is vented. Due to the Joule-Thomson effect, this expansion leads to strong cooling; therefore the CO₂ stream is heated up in a thermostated waterbath prior to expansion, and the temperature in the backpressure regulator is controlled using heating elements.

A typical PCA experiment is divided into six subsequent stages. First, the reactor is filled with CO₂. Then, feed of all streams is started and back pressure regulators are switched on and adjusted. At this stage, pure organic solvent is fed to the reactor until steady state is reached with respect to operating temperature, pressure and flow rates. During the third stage, the previously prepared organic solution is fed to the reactor for precipitation. In step four, the two reservoirs are swapped, so as to purge all the lines of the setup with pure solvent. During stage five, the feed of solvent is terminated, and the reactor content is flushed with pure CO₂, in order to remove residual solvent from reactor and product. Finally, in the last step the reactor is depressurized and the product is removed from the vessel.

2.2.3 Product characterization

Morphology, size and shape of the product particles were investigated by X-ray powder diffraction (XRPD) and scanning electron microscopy (SEM). The samples for SEM analysis were sputter-coated with 5 nm platinum, and photomicrographs were obtained from a Zeiss Gemini 1530 FEG scanning electron microscope in order to determine size and shape

of the precipitated particles. XRPD patterns of starting materials and products were used to assess morphology changes, and especially to detect traces of crystalline phenytoin as described later on.

Two different spectroscopic methods have been developed in order to quantify both compounds present in the co-formulation, namely the polymer poly(vinyl-pyrrolidone) and the drug phenytoin. Before the analysis, products were dried overnight at 40°C in a vacuum oven in order to remove residual solvent and adsorbed moisture.

For the analysis of PVP, a solution was prepared by dissolving 100 mg of product in 50 ml of ethanol. 1 ml of this solution was mixed with 25 ml of 0.2 M citric acid solution and 10 ml of iodine solution (0.81 g/l of sublimed iodine and 1.44 g/l of potassium iodine dissolved in 1000 ml water). The mixture was topped up to 100 ml with 15% ethanol - water mixture. Ten minutes after mixing, light absorption of the formed PVP-iodine complexes was measured at 413 nm (Bühler, 2003) with a UV-Vis Spectrophotometer (Beckman Coulter, DU 520). For calibration, three independent solutions containing 50 mg of both phenytoin and PCA-processed pure PVP were prepared and analyzed with the described method.

For the analysis of phenytoin, a solution was prepared by dissolving an amount of product equivalent to 10 mg phenytoin in 10 ml of ethanol. 100 μ l of solution and 2 ml of ethanol were mixed in a cuvette, and phenytoin content was determined by UV spectroscopy at 250 nm. The following molar extinction coefficients were obtained and used for conversion of absorption units to molar concentrations: phenytoin at a wavelength of 250 nm, 1105 AU/(mol/l); PVP with an assumed molecular weight of 40kDa at a wavelength of 413 nm, 11.87 AU/(mmol/l).

2.3 Experimental Results

2.3.1 Co-Precipitation of PVP and Phenytoin

The behavior of both the polymer PVP K30 and the drug phenytoin during precipitation with compressed carbon dioxide has already been investigated in a previous study (Muhrer et al., 2006). As can be seen from the images shown in Figure 2.2, pure PVP K30 precipitates in the form of sub-micron and spherical particles, while pure phenytoin forms needle-like crystals that are several orders of magnitude larger.

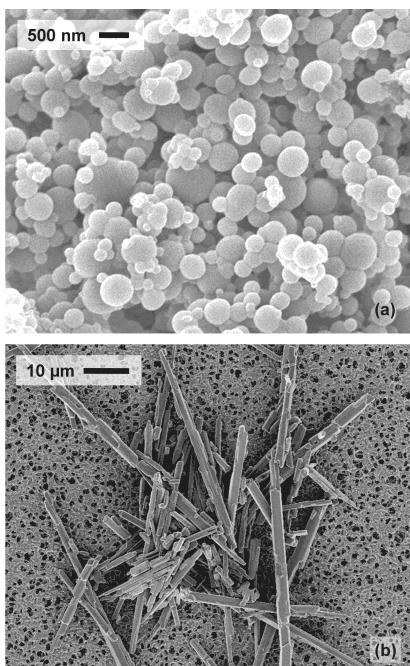


Figure 2.2: Particles of pure PVP (run 1) and PCA-processed pure phenytoin. (Muhrer et al., 2006).

As shown in Figure 2.3, an investigation by X-ray powder diffraction (XRPD) reveals the fully amorphous structure of PVP K30, while crystalline phenytoin yields an XRPD pattern with sharp characteristic peaks at 2θ diffraction angles of 11.27, 12.89, 16.49, 17.19, 18.10, 20.28, 22.31, 22.78 and 25.76° (Franco et al., 2001).

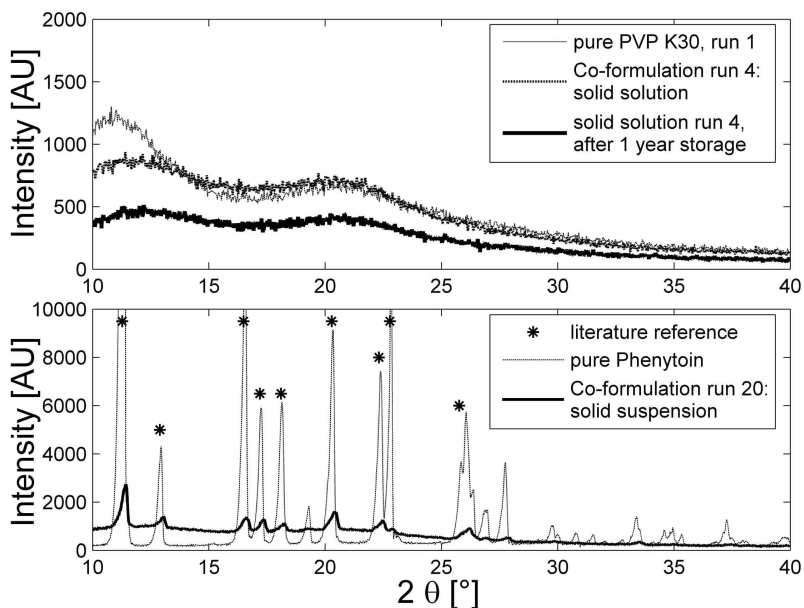


Figure 2.3: X-ray powder diffraction patterns of the amorphous polymer PVP and a drug-polymer co-formulation representing a fully amorphous solution (above); and of pure crystalline phenytoin and a drug-polymer co-formulation containing traces of the crystalline drug (below). Stars represent the 2θ position of phenytoin peaks according to a literature reference (Franco et al., 2001).

A summary of all co-precipitation experiments carried out with PVP and phenytoin is reported in Table 2.1.

2.3 Experimental Results

Table 2.1: Overview of experimental conditions and the results of product analysis.

Run	Operating Conditions		Initial Solution		Product Analysis		
	p [bar]	T [C]	c_{PVP} [wt. %]	$c_{Phenytolm}$ [wt. %]	polymer content ² [wt. %]	drug content ² [wt. %]	morphology ¹
1	80	25	2.00	-	-	-	a
2	80	25	2.00	0.50	70.8	21.0	a
3	80	25	2.00	1.00	60.5	34.6	a
4	80	25	2.00	1.33	57.2	39.4	a
5	80	25	1.00	0.75	55.3	40.8	a + c
6	80	25	2.00	1.50	53.9	41.4	a + c
7	80	25	3.00	2.25	53.5	42.5	a + c
8	80	25	1.00	0.80	53.8	41.0	a + c
9	80	25	2.00	1.60	54.4	43.5	a + c
10	80	25	3.00	2.40	51.9	43.9	a + c
11	80	25	2.00	1.80	50.4	47.3	a + c
12	80	25	2.00	2.00	47.3	49.3	a + c
13	80	25	1.00	2.00	31.2	66.5	a + c
14	80	25	0.50	2.00	19.2	78.8	a + c
15	150	40	2.00	-	-	-	a
16	150	40	2.00	1.00	61.4	32.2	a
17	150	40	2.00	1.20	62.4	35.7	a
18	150	40	2.00	1.40	55.8	38.2	a
19	150	40	2.00	1.60	58.8	39.8	a
20	150	40	2.00	1.80	52.2	44.4	a + c
21	150	40	2.00	2.00	48.3	49.4	a + c

^a*a* represents the amorphous phase and *c* represents crystalline phenytoin

^bIn the cases where the product is a mixture of amorphous and crystalline phase, the measured mixture composition does not represent the composition of one of the single phases

For each experiment, the relevant process variables are operating temperature and pressure and the concentration of solutes in the initial solution. All other operating parameters were kept constant during all experiments. Namely, these were the solvent composition, i.e. 76 / 24 wt.% acetone / ethanol, flow rates of the solution, 0.67 ml/min, and of CO₂, 80 g/min, and the amount of make-up CO₂ used for flushing the particulate product in the vessel to remove residual solvents, i.e. 3 kg.

On the righthand side of the table, the results of product analysis are presented. As described above, polymer and drug content of the products have been measured with independent methods. The fact that the sum of both figures is always less than 100% might indicate either the presence of traces of an unknown impurity in the product or a small systematic error in the measurement. The last column of the table contains a short description of product morphology, indicating whether a fully amorphous one phase product or a two phase mixture containing also crystalline phenytoin had been obtained. When both phenytoin and PVP K30 are co-precipitated from a common solution, products have been observed to contain in fact only these two typical constituents: amorphous sub-micron and spherical particles and, particularly at high drug to polymer ratios, crystalline phenytoin. The presence or absence of phenytoin crystals in the product is evident either from SEM pictures at low resolution (compare e.g. run 12 in Figure 2.4b and run 3 in Figure 2.4e) or from the XRPD pattern of the product (compare that of run 20 in Figure 2.3, bottom, and that of run 4 in Figure 2.3, top). It is worth mentioning that the results of both XRPD and SEM analysis were always consistent with each other and clear in assessing whether crystalline phenytoin was present or not. On the other hand, spherical sub-micron particles of the amorphous phase were present in all co-precipitates of PVP and phenytoin. According to high-resolution

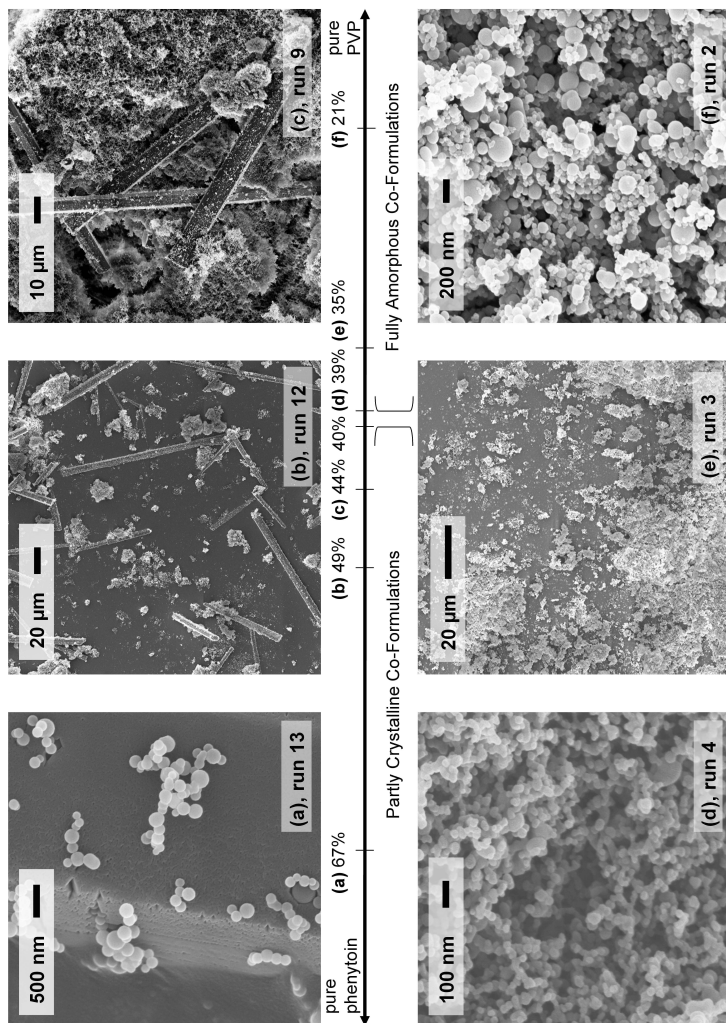


Figure 2.4: Products obtained at 80 bar and 25°C. Runs are indicated on the images. (a) Spherical polymeric particles on a phenytoin crystal. (b) and (c) Needle-like phenytoin crystals interspersed with polymer particles. (d) Fully amorphous polymeric particles, containing 39 wt.% phenytoin. (e) Fully amorphous product, 35 wt.% phenytoin. Note the absence of phenytoin crystals. (f) Spherical, fully amorphous particles, 21 wt.%phenytoin.

SEM pictures shown e.g. for run 13, Figure 2.4a), or for run 2, Figure 2.4f), there is no change in their visual appearance throughout all investigated co-formulation products.

2.3.2 Effect of Drug to Polymer Ratio

For co-precipitates of phenytoin and PVP K30, the effect of drug to polymer ratio has been studied at two different sets of operating conditions; this is illustrated in Figures 2.4 and 2.6. First, in the runs 1 to 14, precipitation experiments were carried out at 80 bar and 25°C while the ratio of drug to polymer in the initial solution was increased from 1:4 to 4:1. Experimental conditions were chosen equivalent to a series of experiments that were performed on a different PCA unit and reported in detail previously (Muhrrer et al., 2006). In good agreement with the results reported earlier, fully amorphous products were obtained for pure PVP K30 and for low drug to polymer ratios, while the amorphous phase appears together with crystalline phenytoin for high drug to polymer ratios. In experiments 3 to 12, this transition in product morphology has been investigated more closely by precipitating solutions with intermediate drug to polymer ratios between 1:2 and 1:1. The transition from fully amorphous products to products containing phenytoin crystals was located at a drug to polymer ratio between 2:3 and 3:4, at a measured drug content of approximately 40%. Precipitates obtained from solutions with a drug to polymer ratio below this threshold value were fully amorphous, while higher initial drug to polymer ratios always led to precipitates containing at least traces of crystalline phenytoin. It can be seen from a comparison of Figures 2.2a (run 1) and 2.4f (run 2) that particles of pure PVP and of amorphous co-precipitates have indeed a very similar appearance. Products containing crystalline phenytoin dispersed

in an increasing amount of polymeric particles are shown in Figures 2.4a to 2.4c. In Figure 2.5, a summary of analytical results is illustrated by plotting the peak intensity of the XRPD spectra at $2\theta = 11.27^\circ$ - a semi-quantitative measure of the fraction of crystals present - against the measured drug content for each experiment. It can be seen that up to 40% drug content, no crystals are detected in the product, while the fraction of crystals is steadily increasing above this threshold.

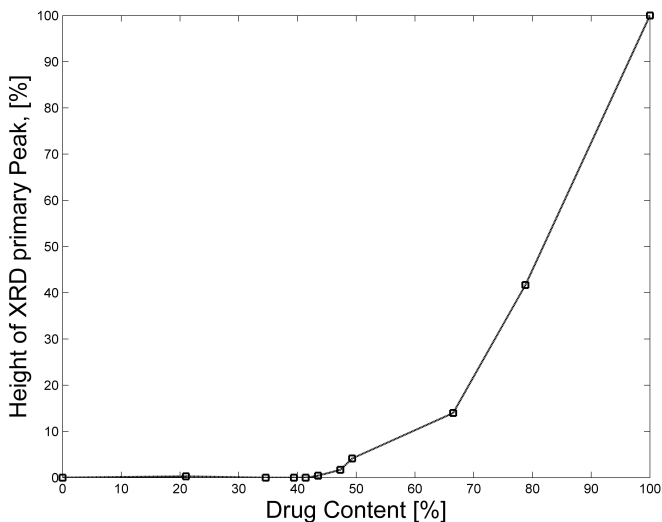


Figure 2.5: Dependence of the crystalline fraction of the drug-polymer co-formulation on the overall drug content. Evaluation is based on the XRPD peak intensity at $2\theta = 11.27^\circ$ (pure drug = 100%). Up to about 40%, the co-formulation is fully amorphous.

While at 80 bar and 25°C it is subcritical, CO_2 is supercritical at 150 bar and 40°C , i.e. where experiments 15 to 20 were carried out. Nevertheless, these two states exhibit similar CO_2 density, i.e. about 775 g/L, and

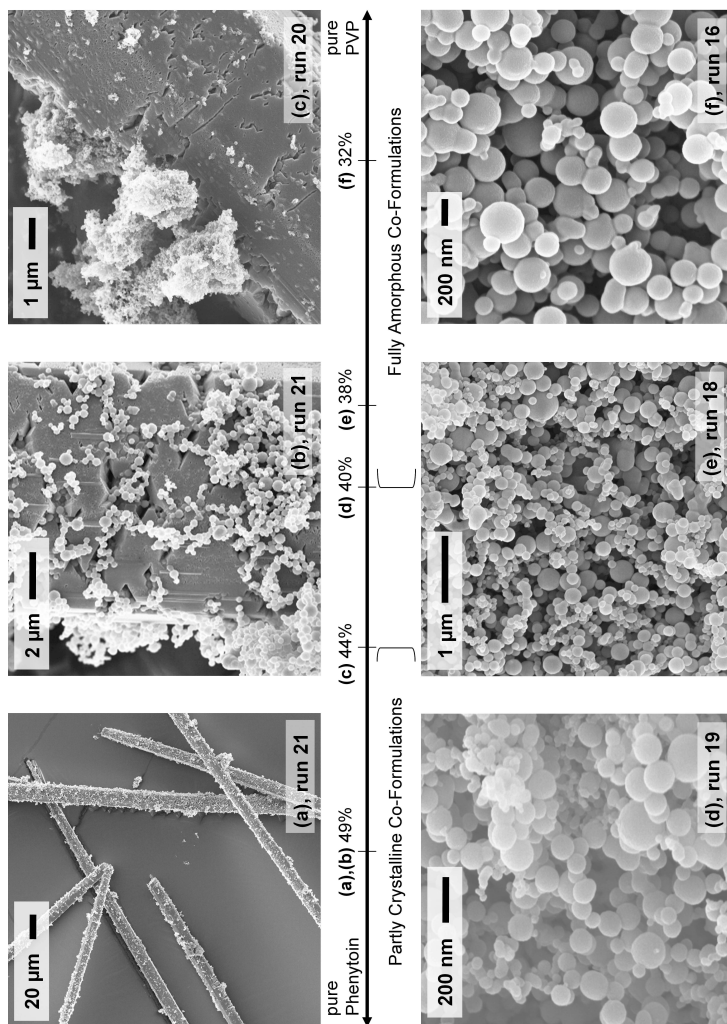


Figure 2.6: Schematic overview on products obtained at 150 bar and 40°C. The corresponding runs are indicated on the images. (a) Phenytoin crystals coated with polymer particles. (b) Close-up picture of a crystal in (a). (c) Polymeric particles together with a phenytoin crystal. (d), (e) and (f) Sub-micron spherical particles of fully amorphous precipitation products. (e) and (f) were taken after one year of storage at ambient conditions.

similar viscosity, i.e. about 6.7×10^{-5} Pa.s. Mixtures of CO₂, ethanol and acetone are fully miscible at these conditions. Therefore, we conjecture that mass transfer properties should also be similar under these rather different temperature and pressure conditions, hence comparable product morphologies could be expected. In experiments 15 to 20, the drug to polymer ratio was varied in the interesting range of intermediate drug to polymer ratios between 1:2 and 1:1, and also pure PVP K30 was precipitated. The transition to products containing crystalline phenytoin was now found at slightly higher drug to polymer ratios in the initial solution, namely between 4:5 and 9:10. However, looking at the phenytoin content found for these products, it can be seen that the previously determined threshold concentration of approximately 40% is valid also at these operating conditions. The corresponding product particles are shown in Figure 2.6. Precipitates from run 20 and 21 (insets a, b and c) contain phenytoin crystals, while products from experiments 15 to 19 are all fully amorphous (insets d, e and f).

2.3.3 Effect of Concentration Changes in the Initial Solution

In experiments 5 to 7 and 8 to 10, solutions with constant drug to polymer ratios were precipitated at three different concentration levels, i.e. 1, 2 and 3 wt.% of polymer. The drug to polymer ratios of 0.75 and 0.8 were chosen in the vicinity of the threshold, in order to assess whether or not there is an influence of the concentration level on its position. For the corresponding products, the measured drug contents ranged from 40.8% in run 5 to 43.9% in run 10, and all samples contained traces of crystalline phenytoin that were in some cases close to the detection limit. Thus, the main conclusion that can be drawn from these experiments is

that changes in the concentration level do not have an obvious influence on the position of the threshold, which remains at approximately 40% drug content.

Looking at the measured drug content for experiments with the same drug to polymer ratio in the initial solution, one finds that it is not constant, but decreases slightly with the concentration level in the initial solution. This may be rationalized. For dilute initial solutions, the product is precipitated and separated from an excess of solvent using an excess of CO₂ anti-solvent. The decrease in drug content may thus be explained by a slightly increased fraction of phenytoin being leached out of the reactor with the efflux.

2.3.4 Long-Term Stability of Co-Formulations

All fully amorphous co-formulation products were analyzed by XRPD after one year of storage at ambient conditions. As can be seen for the example of run 4 in Figure 2.3, no changes in the diffraction pattern could be observed, indicating that a recrystallization of phenytoin from the polymer matrix did not occur. Additional evidence for this comes from SEM analysis. While all other photomicrographs have been obtained within days after the corresponding experiments, the images of samples from run 16 and 18 shown in Figure 2.6f and 2.6d were taken after one year of storage. Photomicrographs of comparable products, such as the one of run 19 shown in Figure 2.6d, show that no visible change in particle morphology has occurred over this time period.

2.4 Discussion and Conclusions

When investigating the long-term stability of amorphous polymers and drug-polymer co-formulations, it is necessary to discuss the meaning of the term "stability" itself. Glassy materials such as amorphous polymers are from a rigorous thermodynamic viewpoint in a durable non-equilibrium state, and it is therefore not possible to relate their stability to the condition of thermodynamic equilibrium. Other criteria have to be applied, and from the viewpoint of pharmaceutical applications, one major concern is whether the product exhibits physical stability throughout a sufficiently long shelf life period. Therefore, long term stability studies are commonly used to address this issue, namely by distinguishing between the following two cases.

If the co-formulation is supersaturated with respect to the drug, the nucleation of drug crystals in the product may be temporarily inhibited by the presence of the polymer (Konno and Taylor, 2006). However, nucleation kinetics is only decelerated and during long-term storage, a crystalline phase will eventually be formed. This may be detected as an alteration in product morphology. On the other hand, if the amorphous and glassy co-formulations are, like the pure polymer, in a steady state where all intensive properties, including the chemical potential of the species belonging to the glassy phase, do not change in time, this state can be viewed as pseudo-equilibrium state.

Our findings indicate that all products are in a long-term stable pseudo-equilibrium state. Further, a threshold in drug content separates fully amorphous from partly crystalline co-formulations, and is approximately independent of operating conditions such as temperature, pressure, or concentration level in the initial solution. This suggests that product morphology is explained by the thermodynamic properties of the system

PVP K30 - phenytoin rather than by the kinetics of precipitation. Under this premise, the observed threshold can be interpreted as the pseudo-equilibrium solubility of the drug in the polymer (Marsac et al., 2006b; Sarti and Doghieri, 1998; Vasanthavada et al., 2004, 2005), such that fully amorphous and stable co-formulations of phenytoin and PVP K30 will always be obtained as long as the drug content of the co-formulation is below 40%, while such co-formulations inevitably contain crystalline phenytoin if their drug content exceeds this solubility limit.

The experimental results presented above can be summarized in two important conclusions. First, co-formulation products may contain two different phases, namely an amorphous phase consisting of sub-micron spherical polymeric particles, and crystalline phase consisting of needle-like phenytoin crystals. As illustrated in Figure 2.5, the fractions of these phases in the product depend on its overall drug to polymer ratio, and for this ratio there is a threshold below which crystals do not appear in the product. Second, PCA-produced co-formulation products exhibit long-term stability, consequently it seems meaningful that this threshold is interpreted as the solubility of the drug in the polymer.

These observations are on one hand relevant for practical design problems. If, for example, a stable and fully amorphous co-formulation with maximal drug loading is the objective, one can directly read from Figure 2.5 that this is possible up to a drug content of 40 wt.%. Then, one of the most frequent problems related to the practical application of drug-polymer co-formulations as pharmaceutical drug delivery systems is insufficient physical stability (Konno and Taylor, 2006; Marsac et al., 2006a,b). Therefore, if PCA co-formulation products exhibit long-term stability, this is a very interesting aspect, and the question is whether it can be rationalized.

The combination of two characteristics of the PCA process may con-

tribute to the formation of long-term stable products. First, the PCA process takes place at supercritical conditions characterized by fast mass transfer. This is well-known and also exploited for other processes like supercritical impregnation (Rodier et al., 2005), or supercritical extraction e.g. of natural products (Reverchon and De Marco, 2006). Under enhanced mass transfer conditions, the phases present at the end of the precipitation are relaxed to pseudo-equilibrium, in the sense clarified above, with no residual supersaturation to be consumed. Second, the PCA process yields product particles at temperatures that are similar to the conditions of long-term storage, i.e. ambient temperatures. This is essentially different for all thermal processes for the production of co-formulations like melt extrusion (Six et al., 2002) or spray drying and solvent evaporation at elevated temperatures (Tanno et al., 2004). Therefore, the amorphous co-formulation particles are already relaxed at room temperature, which means that if no phenytoin crystals have formed at the end of the PCA process, no crystals will form by recrystallization during storage.

2.4.1 Thermodynamics of a four-component system

In the following, we present a theoretical framework where the experimental findings summarized above can be analyzed and interpreted in view of the multi-component phase behavior of the system under investigation in the CO₂ anti-solvent precipitation of a drug and a polymer. This requires a number of simplifying assumptions, in order to focus on the essentials. First, let us consider the binary solvent mixture used in the experiments as made of only one component, which is referred to as "solvent" in the following. Second, PVP K30 shall also be considered as single compound, which clearly implies a major simplification, as poly-

mers consist in fact of a mixture of different polymer chains, typically characterized by a certain chain length distribution. These assumptions allow us to focus on the four-component system drug - polymer - solvent - CO₂ in the forthcoming qualitative thermodynamic analysis. The key to the understanding of the four-component system is a sound representation of the corresponding binary and ternary sub-systems. The four ternary sub-systems are illustrated in the following. Here, it is worth mentioning a few details.

Ternary system phenytoin - solvent - CO₂

The ternary system of type crystalline drug - solvent - anti-solvent has already been introduced in Section 1.4, and is shown here once more for the present system of consideration in Figure 2.7.

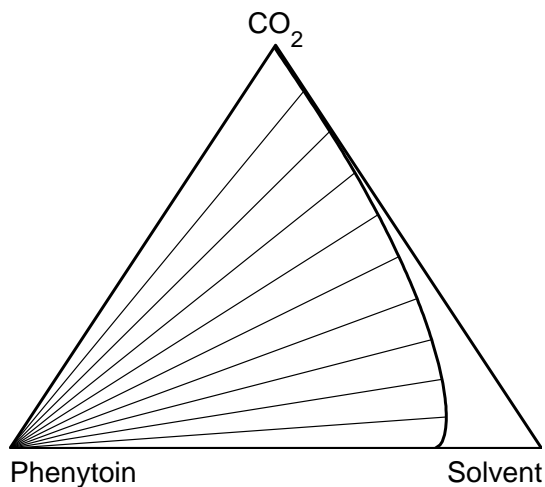


Figure 2.7: Scheme of the ternary system phenytoin - solvent - CO₂

Pure crystalline phenytoin is on the left vertex of the triangle, and a fluid phase with a certain solubility for phenytoin on the right. The fact that CO_2 acts as an anti-solvent is manifested in the concave shape of the solubility curve. Typically in a PCA process, a homogeneous solution of drug and solvent is intimately contacted with pure CO_2 . As the solubility limit is reached, the mixture becomes supersaturated and consequently crystals nucleate and grow. A picture of pure phenytoin precipitated through PCA is shown in Figure 2.2b.

Ternary system PVP - solvent - CO_2

The ternary system of type amorphous polymer - solvent - anti-solvent has already been introduced in Section 1.4, and is shown here once more for the present system of consideration in Figure 2.8.

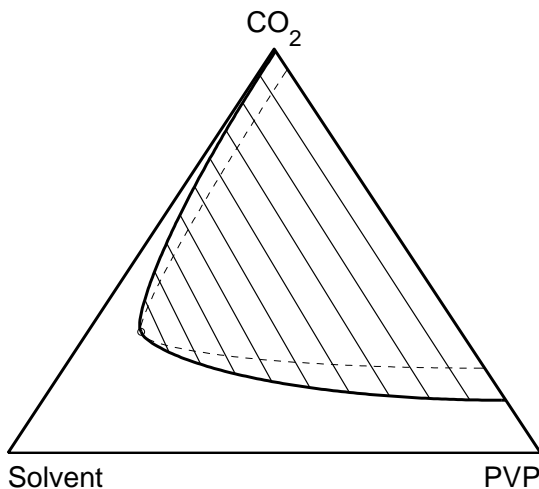


Figure 2.8: Scheme of the ternary system PVP - solvent - CO_2

It is based on assuming complete miscibility of the binary systems polymer - solvent and solvent - CO₂, while the system polymer - anti-solvent is characterized by a large miscibility gap. In Figure 2.8, we have assumed that CO₂ absorbs in the polymer. Polymer solubility in CO₂ - solvent mixtures close to the CO₂ vertex are typically not detected if such systems are studied experimentally (Lai et al., 1998; Perez de Diego et al., 2005), therefore it is assumed that the critical point of the ternary system lies close to the CO₂ - solvent line. This has major consequences for the processing of such polymers by PCA. The process starts with a dilute polymer solution that is then mixed with supercritical CO₂. Therefore, the operating line of the process is bound to enter the two-phase region in the vicinity of the critical point, where the tie lines connecting phases in equilibrium with each other are short. This means that the two newly formed phases have similar composition and density, leading to the important conclusions that first, both phases are initially fluid phases, and second, the surface energy of the newly formed interface is rather small. Surface energy is the basis for the concept of nucleation as a possible mechanism of phase separation; in the absence of surface energy, the phase split more likely occurs by spinodal decomposition rather than by nucleation and growth (Debenedetti, 1996). Therefore, we come to the conclusive hypothesis of this section: in the system under consideration, the precipitation of PVP with a supercritical anti-solvent is achieved by a liquid-liquid phase split and the mechanism of phase separation is likely to be spinodal decomposition rather than nucleation and growth. A picture of PCA- processed PVP is shown in Figure 2.2a. The spherical, droplet-like morphology of the amorphous particles provides further evidence that they might be formed by a fluid-fluid phase split.

Ternary system PVP - Phenytoin - solvent

The triangle for this ternary system is shown in Figure 2.9. Because of the complete miscibility of solvent and polymer, it looks qualitatively similar to the diagram drug - solvent - CO₂. Pure crystalline phenytoin is in the left vertex of the triangle, and a fluid phase with a certain solubility for phenytoin on the right. According to our experimental findings, the solubility of drug in the polymer is high, namely about 45% (w/w). There is no evidence whether solvent and PVP act as co-solvents or as anti-solvents for phenytoin, therefore the solubility line connecting the saturated solutions of phenytoin in the pure compounds is represented as a straight line.

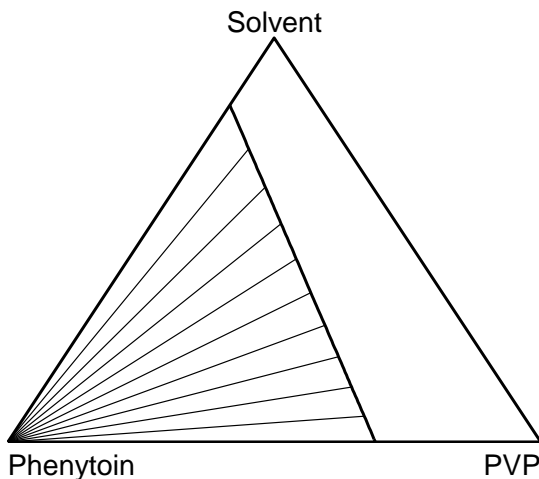


Figure 2.9: Scheme of the ternary system PVP - Phenytoin - solvent

With respect to the PCA processing of co-formulations, this ternary sub-system is important because it contains the possible starting and

end points of the process, namely the initial solutions and the final co-formulation products, respectively. The solution points are located close to the solvent vertex, since only diluted solutions are used. Depending on whether a polymer-rich or a drug-rich initial solution is processed, the initial solution point will be closer to the polymer-solvent or to the drug-solvent edge. The final co-formulation products are found on the bottom line connecting PVP and phenytoin.

Ternary system PVP - Phenytoin - CO₂

This ternary system, shown in Figure 2.10, is characterized by a three-phase region with co-existing crystalline phenytoin, saturated polymer and a CO₂-rich phase.

The overall picture is based on the assumption that CO₂ is a bad solvent

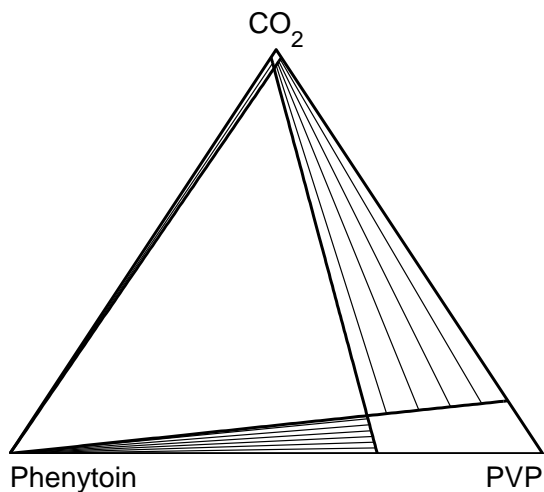


Figure 2.10: Scheme of the ternary system PVP - Phenytoin - CO₂

for both phenytoin and PVP, thus leading to a very small one-phase region close to the CO₂-vertex. On the other hand, PVP is a good solvent for phenytoin, and moreover it takes up a certain fraction of CO₂ by absorption and swelling. This leads to a larger one-phase region close to the PVP vertex. In between the two vertices there is a two-phase region with co-existing polymer-rich and CO₂-rich phase, where phenytoin is only present in solution. For simplicity, all connecting lines are assumed to be straight.

In the PCA processing of co-formulations, this particular ternary subsystem contains the possible end-points of the process, corresponding to the final product of the precipitation after the solvent has been removed from the particles by flushing with pure CO₂. Under the assumption that the reactor contains mostly CO₂, all end-points are located close to the CO₂-vertex. If the product is rich in polymer, the end-point lies close to the polymer-CO₂ edge in the polymer-CO₂ two-phase region. For products with higher drug loadings, the end-point lies in the drug-polymer-CO₂ three-phase region.

Quaternary system PVP - Phenytoin - solvent - CO₂

The quaternary phase diagram shown in Figure 2.11 is a tetrahedron, whose faces are the four ternary diagrams shown in Figures 2.7 to 2.10, the system PVP - phenytoin - CO₂ being the base. Phase transitions originating from the different faces continue inside the tetrahedron and need to be interconnected in a physically consistent way. This again requires some simplifying assumptions, namely that the solubility of phenytoin in the fluid phases can be linearly interpolated from the solubility in the solvent - anti-solvent mixture and the solubility in the polymer fraction, and that the presence of phenytoin does not interfere

with the phase transition originating from the ternary system PVP - solvent - CO₂. Therefore, the interior of the tetrahedron contains two surfaces that intersect each other. The dark blue surface separates the region on its left, where phenytoin is present in crystalline form, from the region on the right side, where phenytoin is present only in dissolved form. The light green surface separates the region above with only one fluid phase from the region below, where there are two fluid phases, namely a PVP-rich phase and a CO₂-rich phase.

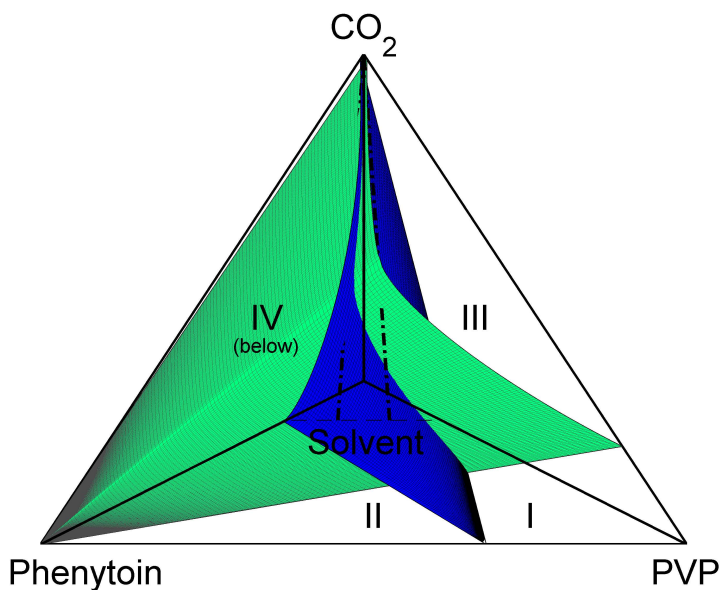


Figure 2.11: Scheme of the quaternary system PVP - Phenytoin - solvent - CO₂. The dashed lines represent two operating lines, one leading to fully amorphous composites (right), the other to products containing also crystalline phenytoin (left).

Consequently, the volume of the tetrahedron is divided into four parts. First, a one-phase fluid region connecting the vertices of PVP, solvent and CO₂, (region I in Figure 2.11). Second, in the direction of the phenytoin vertex, a two-phase fluid-solid region containing crystalline phenytoin in equilibrium with the aforementioned fluid phase (region II). Third, between the vertices of PVP and CO₂, a two-phase fluid-fluid region where a polymer-rich phase is in equilibrium with a CO₂-rich phase (region III). Finally, in the direction of the phenytoin vertex, a three-phase fluid-fluid-solid region where both the CO₂-rich and the PVP-rich fluid phases are in equilibrium with crystalline phenytoin (region IV).

Operating lines in the Quaternary diagram

With the quaternary phase diagram shown in Figure 2.11, drug - polymer co-precipitation processes by PCA can now be rationally explained and visualized by an operating line. The process starts from a dilute solution, close to the solvent vertex, on the PVP - phenytoin - solvent plane. The solution is then mixed with pure CO₂, which means that the operating line goes from its initial start point straight towards the CO₂-vertex. The attainable proximity to the CO₂ vertex largely depends on the flow rate ratio CO₂ to solution.

Two operating lines are drawn in Figure 2.11. On the right-hand side, precipitation from a polymer-rich solution is shown. The operating line enters the fluid-fluid two-phase region. There, a phase-split into a polymer-rich and a CO₂-rich fluid phase leads to the formation of phenytoin-loaded polymer particles. No crystalline phenytoin is formed in this case. Pictures of a product corresponding to this operating line are shown in the insets d, e and f of Figures 2.4 and 2.6. It can be observed that the product looks very similar to the pure PCA- processed

polymer shown in Figure 2.2a.

The line on the left represents the precipitation from a phenytoin-rich solution. The corresponding operating line first enters the fluid-solid two-phase region, thus indicating that crystalline phenytoin is precipitated. Then, it enters the three-phase region, where a polymer-rich and CO₂-rich fluid phase are formed in another liquid-liquid phase split. Upon pressure relaxation, the product consists of crystalline phenytoin interspersed with polymeric precipitate. Products precipitated according to this operating line can be seen in insets a, b, and c of Figures 2.4 and 2.6. In Figures 2.4b and 2.6a, phenytoin crystals are clearly visible at low resolution. Figures 2.4a and 2.6b exhibit spherical and amorphous polymer particles on the background of phenytoin crystals. As compared to Figures 2.4f and 2.6c, the morphology of the polymer-rich phase remains unchanged in the presence of crystalline phenytoin.

Also the effect of concentration changes in the initial solution, as investigated in experiments 11 to 13, can be discussed with the help of the quaternary diagram. For the initial solution point, a change in concentration at constant drug to polymer ratio corresponds to a shift on the line connecting it with the solvent vertex. Experimental results have shown that concentration changes have no influence on the position of the concentration threshold separating fully amorphous and partly crystalline products. This is consistent with the shape of the quaternary phase diagram of Figure 2.11.

2.5 Conclusion

Co-formulations of the sparingly soluble drug phenytoin and the water-soluble polymer PVP have been produced by CO₂ anti-solvent precipi-

tation. At a drug content of about 45 wt.%, a major change in product morphology can be observed. Below this threshold concentration, fully amorphous and homogeneous solid solutions of phenytoin in PVP were obtained, while for higher drug concentrations the polymeric phase was interspersed with crystalline phenytoin particles, which were clearly discernible both by SEM and XRPD analysis. Therefore, if suitable operating conditions are chosen, fully amorphous and homogeneous solutions of phenytoin in PVP can be obtained, exhibiting favorable pharmaceutical properties like optimal drug loading, fast release kinetics and long term stability.

The co-precipitation of drug and polymer by PCA is a process where at least four different components are involved. We have introduced for the system PVP - phenytoin a typical quaternary phase diagram, which can be used to visualize operating lines of a co-precipitation step by PCA. The model is in good agreement with our major experimental findings, namely the transition from fully amorphous products to products containing crystalline phenytoin with increasing drug to polymer ratio. The apparent insensitivity of this transition to changes in operating conditions implies that the transition is indeed imposed by thermodynamic limitations rather than by kinetic effects. Changes in pressure and temperature are expected to slightly modify the location of phase transitions in the quaternary diagram; however, experimental results provide evidence that the overall structure of the diagram remains the same in the investigated ranges of temperature and pressure, i.e. 25 to 40°C and 80 to 150 bar. We believe that this type of behavior is not unique, i.e. it occurs also for other drugs and polymers.

Chapter 3

PLGA micro- and nanocomposites¹ by SFEE: Encapsulation of lysozyme

3.1 Introduction

The biocompatible and biodegradable polymer poly-lactic-co-glycolic acid (PLGA) is a promising and widely used constituent for drug-polymer co-formulations serving specific pharmaceutical purposes such as controlled release or targeted drug delivery (Gander et al., 2001). In this framework, both products and manufacturing processes must meet a number of quality criteria. For pharmaceuticals in general, a high degree of product purity is required while processes must be reproducible and scalable. Many applications require particulate products where the size of the polymeric particles plays an important role and thus represents an important specification. This applies e.g. to pulmonary drug delivery, where a size range of 1 to 3 μm has been shown to behave most efficiently

¹The work in this chapter has been carried out in cooperation with Nathalie Casas and Francesco Fusaro, and has been published as Kluge et al. (2009b).

when targeting the alveolar system (Gupta and Hickey, 1991). In the context of controlled release applications, important parameters such as degradation kinetics of PLGA or drug distribution within the particle have been shown to depend on the size of PLGA particles in a range between 10 to 100 μm (Berkland et al., 2003); thus, the production of uniform particles in the desired size range is a key prerequisite for a precise control of drug release rates (Berkland et al., 2002).

PLGA composite particles combine at least two different materials, i.e. the polymeric excipient PLGA and one or more active pharmaceutical ingredients. This leads therefore to a number of quality criteria, e.g. drug loading (i.e. the drug fraction in the drug-polymer co-formulation), encapsulation efficiency (i.e. the fraction of the drug used in the process that is encapsulated in PLGA), or homogeneity and stability of the produced co-formulations. Finally, there are further aspects of product quality related to pharmaceutical activity that may be assessed in specific testings either *in vitro* or *in vivo*.

The present study demonstrates the feasibility of producing sub-micron particles of PLGA through a novel process, namely supercritical fluid extraction of emulsions (SFEE). It is further studied how the above-mentioned aspects of product quality are met by this process. In particular, it is shown how the size distribution of product particles may be controlled by changes in the initial emulsion. Further, the encapsulation of the water-soluble peptide lysozyme into PLGA is investigated using three different approaches. Lysozyme was dispersed in the PLGA / ethylacetate solution in the form of solid nanoparticles, or alternatively as a solution in two different solvents, namely DMSO and water (the first being miscible and the latter immiscible with the PLGA solution). Drug-polymer dispersions were subsequently processed by SFEE, and the three different products were analyzed and compared, for instance in terms of encapsulation efficiency of lysozyme.

3.2 Background

3.2.1 Formation of PLGA particles

Three different methods are reported in the literature for the formation of particles from an organic PLGA solution (see Table 3.1): spray drying, phase separation (coacervation), and solvent extraction/evaporation from an emulsion (Jain, 2000; Freitas et al., 2005).

In spray drying, the solution is atomized by spraying with a carrier gas, and solid particles are formed upon solvent evaporation from the droplets. In coacervation, mixing the solution with an anti-solvent induces a liquid-liquid phase split yielding droplets of a polymer-rich phase that undergo hardening in a surplus of anti-solvent. Solvent extraction from an emulsion is a two-step process. First, the organic PLGA solution is dispersed in an aqueous phase forming an oil in water (o/w) emulsion. In a second step, the solvent is extracted or evaporated from the emulsion droplets, thus yielding rigid PLGA spheres.

3.2.2 PLGA particles by supercritical fluid processes

Supercritical fluid and dense gas technology is very interesting for pharmaceutical processing (Fages et al., 2004; Perrut et al., 2005a; Byrappa et al., 2008), especially for the formation of particles from sensitive biodegradable compounds (Mishima, 2008) and polymers (Yeo and Kiran, 2005), and also for drug-polymer co-formulations (Shekunov et al., 2006a; Perrut et al., 2005b). As a major advantage, dense gas processes lead to pure and solvent-free products while working at mild operating conditions. They also offer several degrees of freedom with respect to process setup and operating conditions, which may be exploited to tune

Table 3.1: Comparison of methods for the manufacturing of drug-loaded PLGA particles.

	Spray drying	Phase Separation (Coacervation)	Solvent Extraction / Evap- oration from Emulsions
Suitability for temperature-sensitive compounds	- (Freitas et al., 2005)	+	+
Suitability for water-soluble compounds	+(Jain, 2000)	+(Jain, 2000)	-(Jain, 2000)
Control of Particle Size	-(Freitas et al., 2005)	-(Freitas et al., 2005)	+
Low yield, agglomeration of sticky particles	-(Jain, 2000)	-(Jain, 2000)	+
Solvent Residuals	+	-(Jain, 2000; Freitas et al., 2005)	+
Scalability	+(Freitas et al., 2005)	-(Jain, 2000)	+

size and shape of product particles (Fusaro et al., 2004, 2005; Muhrer et al., 2006). Considerable scientific efforts have been made to apply supercritical fluid technology to the manufacturing of micro-particles of PLGA and of poly-L-lactic acid, P_LLA (Debenedetti et al., 1993; Falk et al., 1997; Falk and Randolph, 1998; Ghaderi et al., 1999, 2000; Chattopadhyay et al., 2006; Kang et al., 2008; Della Porta and Reverchon, 2008), and also of drug-PLGA composites (Ghaderi et al., 2000; Chattopadhyay et al., 2006; Kang et al., 2008; Della Porta and Reverchon, 2008; Dave et al., 2006; Lee et al., 2006).

As to the classification made in section 3.2.1, compressed gases have been used in ‘spray drying’ processes for the production of PLGA particles, either as solvent itself in a process called rapid expansion of supercritical solutions, RESS (Debenedetti et al., 1993), or as atomizing and solvent extracting agent in a process called solution-enhanced dispersion by supercritical fluids, SEDS (Ghaderi et al., 2000). Moreover, scCO₂ has widely been used as phase-separating anti-solvent; for instance, the precipitation with compressed antisolvent (PCA) process has been applied by Randolph and coworkers for the precipitation of P_LLA (Falk et al., 1997; Falk and Randolph, 1998) or similarly, the supercritical anti-solvent (SAS) technique was used for the manufacturing of drug-loaded particles of both P_LLA and PLGA (Lee et al., 2006). As demonstrated for other compounds forming amorphous precipitates, e.g. the protein lysozyme (Muhrer and Mazzotti, 2003; Fusaro, 2008), such phase separating processes can also be carried out batch-wise, e.g. in the gas anti-solvent (GAS) process. Anti-solvent processes, such as PCA, SAS or SEDS, that are based on the continuous mixing of solution and dense CO₂ e.g. in a nozzle resemble more the spray-drying process. Miscibility may be seen as the decisive criterion: CO₂ acts as anti-solvent if it is fully miscible with the solution, whereas it acts as solvent-extracting

agent if CO_2 and solution exhibit a miscibility gap so as the latter forms droplets from which the solvent evaporates. Interestingly, supercritical fluid technology allows to access domains of miscible as well as of immiscible conditions for the same solvent - CO_2 system, i.e. by simply changing the operating pressure and temperature. The transition from one domain to the other and its effect on size and morphology of product particles has been studied e.g. for PLLA (Perez de Diego et al., 2005) and for lysozyme (Fusaro et al., 2009).

sc CO_2 has also been used for the production of particles by supercritical fluid extraction of solvent from an emulsion (SFEE). The process was introduced for the manufacturing of drug - PLGA composites (Chattopadhyay et al., 2006), and recent research activities have focused further on producing PLGA microparticles (Della Porta and Reverchon, 2008). Particles produced by SFEE exhibit a characteristic high degree of uniformity.

PLGA is able to uptake CO_2 by sorption, leading to swelling of the hydrophobic polymer matrix and to a significant decrease in glass transition temperature (Pini et al., 2008). This means that at pressure and temperature conditions convenient for a CO_2 process, PLGA is in the liquid or rubbery state, thus forming droplets rather than particles. Problems associated to this behavior, such as agglomeration of PLGA particles resulting in irregular shapes (Kang et al., 2008) or a low yield of PLGA caused by ‘a strong tendency to form a film at the base or on the wall of the reactor’ (Ghaderi et al., 1999) have been reported for the supercritical CO_2 antisolvent processing of PLGA. It may be expected that also the SFEE process leads first to the formation of PLGA droplets. However, since these are formed in an emulsion, they remain dispersed in water throughout the process, and the formation of agglomerates or the sticking of particles to the reactor wall is inhibited.

3.2.3 PLGA composite particles

In pharmaceutical applications, PLGA is primarily used in drug-PLGA composite particles. Figure 3.1 shows different possible approaches to encapsulate an active pharmaceutical ingredient into PLGA.

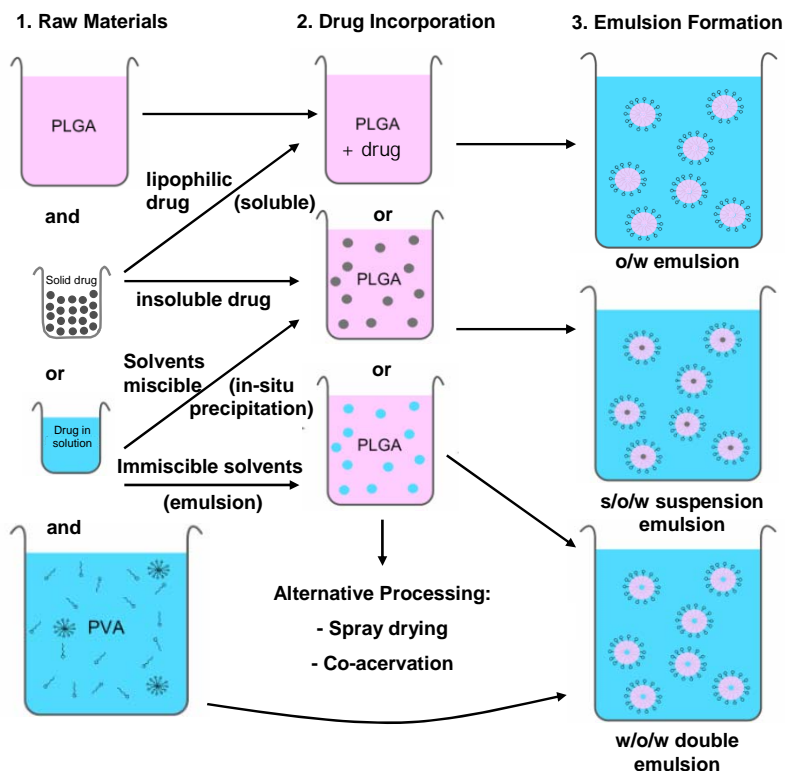


Figure 3.1: Strategies for drug encapsulation into PLGA particles.

The left column of Figure 3.1 indicates the raw materials used for encapsulation. While the drug may be used in different states, i.e. as solid

or as a solution, the polymer is always added in the form of a solution. The middle column of Figure 3.1 shows how drug incorporation into the PLGA solution is achieved. In the simplest case, drug and polymer may be co-dissolved in a common solvent, where they form a fully homogeneous solution (Figure 3.1, top). If otherwise the drug is insoluble in the PLGA solution, it may be dispersed therein as finely pulverized solid, thus forming a suspension (Figure 3.1, center). If the drug can be neither co-dissolved with PLGA nor obtained in a sufficiently micronized form, it may be dissolved in a different solvent before mixing with the PLGA solution. There are now two possibilities: the two solutions may be immiscible, thus forming an emulsion when mixed (Figure 3.1, bottom). Alternatively, if the two solutions are miscible, the drug is likely to precipitate and form a suspension *in situ* (Figure 3.1, center).

The right hand side of Figure 3.1 shows how the aforementioned drug-polymer dispersions are transformed into emulsions, as required for particle formation by SFEE. Depending on whether the drug has been incorporated into a solution, a suspension or a w/o-emulsion, the final mixing step yields an o/w emulsion, a s/o/w suspension emulsion or a w/o/w double emulsion.

The o/w emulsion method has been applied for the PLGA encapsulation of mainly uncharged and lipophilic drugs such as piroxicam (Berkland et al., 2002, 2003; Della Porta and Reverchon, 2008), ketoprofen (Barichello et al., 1999; Gavini et al., 2003; Chattopadhyay et al., 2006) or indomethacin (Barichello et al., 1999; Chattopadhyay et al., 2006), using SFEE as well as conventional methods for solvent extraction. The s/o/w approach has been used to prepare PLGA composites incorporating inorganic nanoparticles such as magnetite (Liu et al., 2007). Moreover, it is especially interesting for the encapsulation of sensitive protein drugs that are more likely to retain their activity in the solid state. How-

ever, in the case of the encapsulation of human growth hormone into PLGA, considerable efforts had to be spent in producing protein microparticles that were sufficiently small for encapsulation (Takada et al., 2003). In the case of insulin, such particles were precipitated in situ by adding an insulin-DMSO solution to an organic PLGA solution prior to the production of composite particles by the in situ s/o/w approach (Bao et al., 2006). Encapsulation efficiencies larger than 90% have been achieved with this method, while considerably lower values ranging from 50% to 80% were obtained using the w/o/w double emulsion method. While the latter approach is of major importance due to the fact that PLGA particles are considered the most attractive drug delivery system especially for strictly water-soluble biomolecules (Mundargi et al., 2008), it is also well-known that leakage of drug from the dispersed to the continuous water phase may lead to poor encapsulation efficiencies (Jain, 2000). This issue has been addressed by Cho and Sah, who have used the double emulsion approach to encapsulate lysozyme into PLGA (Cho and Sah, 2005). They have found that different parameters, e.g. emulsion stirring time and lysozyme to PLGA ratio, cause the encapsulation efficiency to vary in a rather wide range, i.e. from 10% to 75%.

3.3 Materials and Methods

3.3.1 Materials

Carbon dioxide (CO₂; 99.9%, from PanGas, Schlieren, Switzerland), poly(lactic-co-glycolic) acid 5050 DLG 5A (PLGA; Lakeshore Biomaterials, Birmingham AL, United States), poly(vinyl alcohol) 4-88 (PVA), hen egg white lysozyme, dichloromethane (DCM), ethyl acetate, trifluoroacetic acid (TFA), dimethyl sulfoxide (DMSO), and acetonitrile (all

from Sigma-Aldrich, Buchs, Switzerland) were used as received from the suppliers.

3.3.2 Emulsion Preparation

Poly(lactic-co-glycolic) acid (PLGA) was dissolved in ethyl acetate saturated with water, and a 1 %wt. solution of PVA was prepared in water saturated with ethyl acetate. The organic solution (20 g) and the aqueous PVA solution (80 g) were used to form an o/w emulsion upon mixing with a Polytron mixing device (Kinematica AG, Luzern, Switzerland). The stirring rate was adjusted as specified for each experiment, and stirring was applied for 2 minutes.

In order to incorporate water-soluble lysozyme in PLGA particles, the following modified methods were used for the preparation of the organic PLGA solution.

w/o/w Double Emulsion method. An amount of 0.1 g of lysozyme was dissolved in 1 g of water, and 2 g of PLGA were dissolved in 40 g of ethyl acetate. Both solutions formed a w/o emulsion upon mixing at high stirring rates. This primary emulsion was then used as described previously for the PLGA solution to prepare a w/o/w double emulsion. In this case, a low stirring speed of 3,700 rpm was applied for 2 minutes in the final mixing step.

s/o/w Suspension Emulsion. For the preparation of the suspension-emulsion, solid lysozyme nano-particles were prepared by a supercritical CO₂ antisolvent precipitation step as described elsewhere (Fusaro , 2008). An amount of 0.1 g of lysozyme particles were mixed with a solution of 2 g PLGA in 30 g ethyl acetate to form a suspension, which

was then used as described previously for the PLGA solution to prepare a s/o/w suspension emulsion.

In situ s/o/w Suspension Emulsion. A solution of 0.1 g lysozyme in 2 g DMSO was mixed with a solution of 2 g PLGA in 30 g ethyl acetate. Since ethyl acetate is miscible with DMSO but it is an anti-solvent for lysozyme, the latter precipitates and forms solid particles within the PLGA solution. The suspension thus formed was then used as described previously for the PLGA solution to prepare a s/o/w suspension emulsion.

3.3.3 SFEE: Experimental Setup and Procedure

A scheme of the experimental setup used for SFEE experiments is shown in Figure 3.2. The setup is in fact very similar to the one described previously in section 2.2.3 and Figure 2.1. The main difference here is that in SFEE the accumulation of the product suspension at the bottom of the reactor requires that the off-gas stream leaves the reactor through an outlet at the top. Also the operation of the plant is almost identical to the procedure described earlier in section 2.2.3; especially the delivery of the CO₂ stream is fully equivalent. In SFEE, the second stream fed to the reactor is an emulsion that is delivered by an HPLC pump (PU2080 plus, Jasco). Before entering the reactor, both the CO₂ and the emulsion feed stream are brought to the operating temperature (CC230, Huber). Both streams are mixed at the inlet of the reactor in a two substance nozzle (Schlick, Untersiema, Germany). Particles are formed by solvent extraction from the organic emulsion droplets, and remain suspended in the continuous water phase throughout the whole process. The product suspension accumulates at the bottom of the reactor and the outlet there

may be used to withdraw the product suspension continuously throughout the extraction process. This makes it possible to operate SFEE as a continuous process, while PCA is a semi-continuous process, i.e., precipitation is continuous, but operation of the plant needs to be discontinued for product recovery.

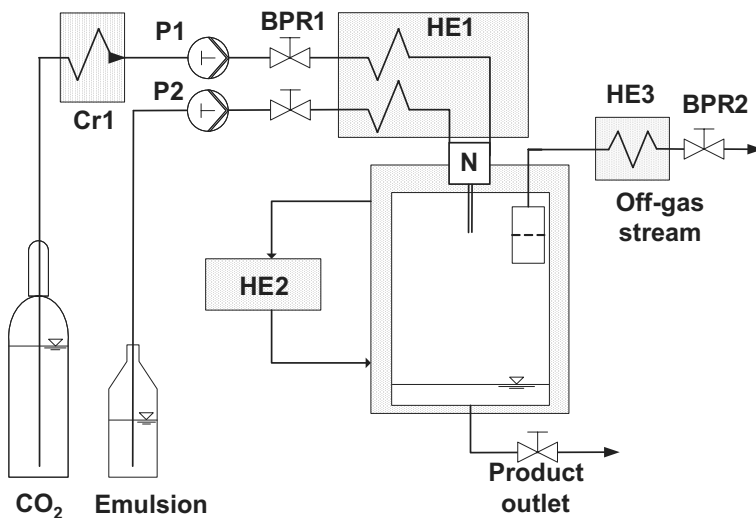


Figure 3.2: Scheme of the SFEE setup used for solvent extraction experiments.

A typical SFEE experiment is divided into five stages. First, the reactor is filled with CO_2 . Then, feed of all streams is started and back pressure regulators are adjusted. At this stage, water instead of emulsion is fed to the reactor until steady state is reached with respect to operating temperature, pressure and flow rates. During the third stage, the emulsion is fed to the reactor for solvent extraction. In step four, the emulsion feed line is again purged with water. Finally, the CO_2 feed stream is stopped and the product suspension is withdrawn from the reactor before the experiment is terminated by the depressurization of the reactor.

3.3.4 Product Characterization

Particle Size Distribution Particle size distributions were measured by static light scattering (Mastersizer 2000, Malvern, UK). Samples of the product suspensions were diluted to a suitable optical density and directly injected into the system.

Morphology by Scanning Electron Microscopy (SEM) For sample preparation, particles were recovered from the suspension and separated from the surfactant PVA. After centrifugation at 20,000 rpm for 15 min (Avanti J-20, Beckman, USA) the supernatant was discarded, and sedimented particles were re-suspended in pure water and subsequently freeze-dried (FlexiDry, FTS Systems, USA). Dried samples were sputter-coated with 5 nm platinum for SEM analysis, and photomicrographs were obtained using a Zeiss Gemini 5 1530 FEG scanning electron microscope in order to determine the morphology of the precipitated particles.

Characterization of Lysozyme Content Approximately 10 mg of freeze-dried particles were dissolved in DCM, and 1 ml of 0.1 vol.% TFA in water was added to extract lysozyme from the solution by vigorous agitation. The lysozyme content of the aqueous supernatant was determined by high-pressure liquid chromatography (Agilent 1100, Agilent Technologies, USA) on a ProntoSIL 120-3-C18 column, applying a gradient method with two mobile phases: 0.1 vol.% TFA in water (buffer A) and 5 vol.% buffer A + 95 vol.% acetonitrile (buffer B). The linear elution gradient was 25 to 80 vol.% B over 17 minutes at a flow rate of 0.5 ml/min (the method is proposed by the supplier of the column). Lysozyme was detected by UV spectroscopy at 210 nm.

3.4 Experimental Results

3.4.1 SFEE processing of PLGA

A summary of all pure PLGA experiments is provided in Table 3.2. For each experiment, the relevant variables are the parameters selected for the preparation of the emulsion, namely the concentration of PLGA in the dispersed organic phase and the stirring rate during emulsification. All the other parameters, especially the operating parameters of the SFEE process, were kept constant during all experiments, namely temperature and pressure conditions inside the extraction vessel (45°C, 80 bar) and the flow rates of the emulsion (2 ml/min) and of CO₂ (80 g/min). Constant emulsion parameters were the concentration of surfactant in the aqueous phase (1% wt.) and the o/w ratio (1:4). On the right hand side of the table, the obtained particle size distributions are described through the values of x_{10} , x_{50} and x_{90} of the volumetric distribution. Also, Figures containing scanning electron micrographs of the corresponding products are indicated. As can be seen in all images, spherical and non-agglomerated PLGA particles with a smooth surface have been obtained in all SFEE experiments.

3.4.2 Effect of PLGA Concentration

For SFEE processing of PLGA, the effect of PLGA concentration in the organic droplets has been studied at two different emulsion stirring rates. First, in runs 1 to 9, emulsions were stirred at a constant rate of 9,400 rpm while the PLGA concentration in the initial solution was increased from 1% to 15%. Equivalently, in runs 10 to 18, emulsions were stirred at the increased rate of 30,000 rpm while varying the PLGA concentration between 1% and 20%.

3.4 Experimental Results

Table 3.2: Experimental parameters and the results of product analysis.

Run	Polymer Concentration [gPLGA/gSolvent]	Emulsion Stirring [rpm]	Particle Size Distribution			Images
			x ₁₀ [nm]	x ₅₀ [nm]	x ₉₀ [nm]	
1	1%	9,400	104	183	267	3.3a
2	2.5%	9,400	112	176	257	
3	5.5%	9,400	109	179	290	
4	7%	9,400	125	278	362	3.3b
5	8.5%	9,400	135	255	512	
6	10%	9,400	229	310	405	
7	11.25%	9,400	477	791	1'211	3.3c
8	12.5%	9,400	485	781	1'202	
9	15%	9,400	501	1'020	1'795	
10	1%	30,000	59	109	177	3.4a
11	2%	30,000	87	125	170	
12	3.5%	30,000	90	133	181	
13	5%	30,000	106	137	177	3.4b
14	7.5%	30,000	112	139	169	
15	10%	30,000	106	138	181	
16	12.5%	30,000	116	166	227	3.4c
17	15%	30,000	227	331	505	3.5a
18	20%	30,000	125	304	891	
19	10%	820	316	895	1'531	
20	10%	3,700	279	674	1'102	3.5b
21	10%	5,400	259	500	1'027	
22	10%	11,800	136	289	381	
23	10%	14,800	113	179	337	3.5c
24	10%	17,200	132	274	401	
25	10%	20,500	121	277	471	

Results are summarized in Figures 3.3 (9,400 rpm) and 3.4 (30,000 rpm), where obtained particle sizes and size distributions are shown together with photomicrographs of the corresponding product particles. It can be seen that for both stirring rates, the average particle size increases as the concentration of PLGA increases. However, the increase is more pronounced at the lower stirring rate.

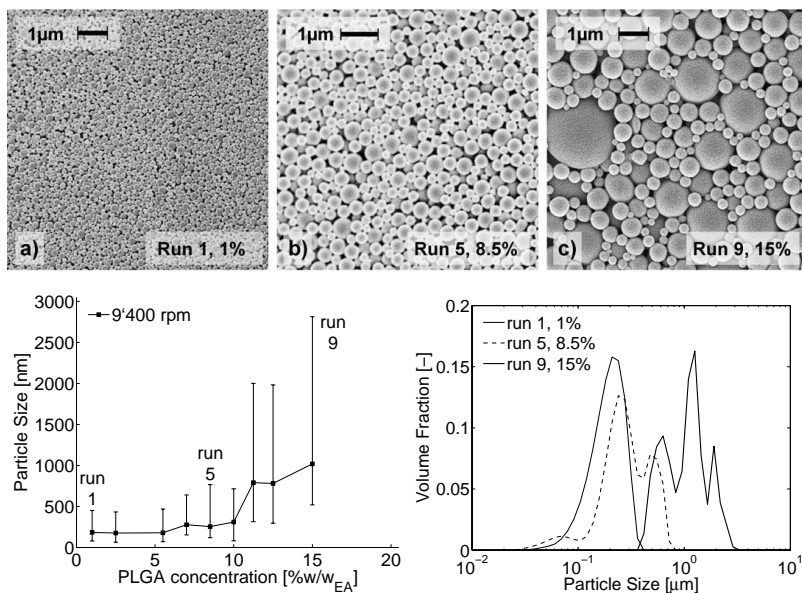


Figure 3.3: PLGA particles produced from emulsions stirred at 9'400 rpm with varying concentration in the dispersed organic phase. Top: photomicrographs of product particles. Bottom left: Average particle size as obtained from light scattering. Symbols represent the x_{50} of distributions, while vertical bars cover the range between x_{10} and x_{90} . Bottom right: Corresponding particle size distributions (selected runs only).

It is further observed that higher PLGA concentrations also lead to an increased breadth of the size distribution. Moreover, such broad distri-

3.4 Experimental Results

butions are rather inhomogeneous and characterized by the presence of distinct classes of particle size, as it may be seen in Figure 3.3c for the case of run 9. A similar behavior is also observed at the higher stirring rate, as it may be seen in Figure 3.4 from the broad and multimodal distribution obtained for run 18. These findings may be rationalized by the fact that increasing PLGA concentrations lead to a higher viscosity of the dispersed organic phase, hence favoring the formation of larger droplets during emulsification.

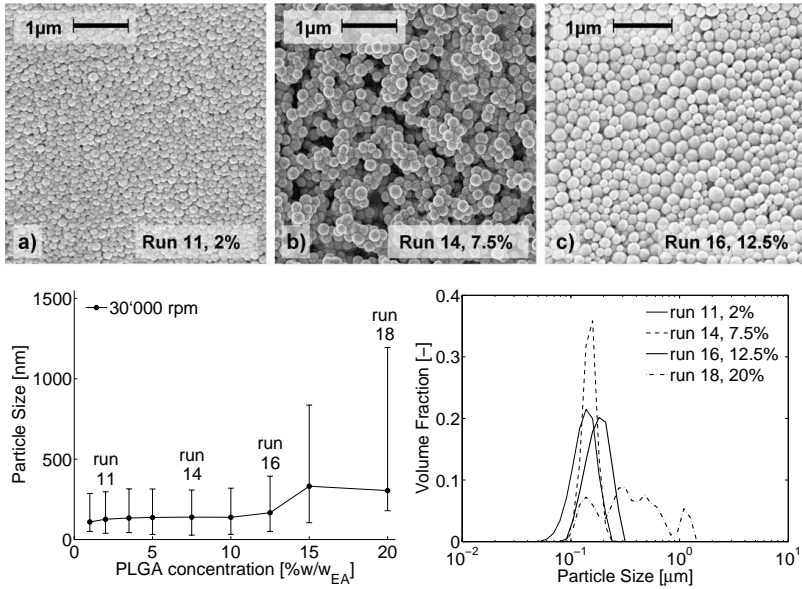


Figure 3.4: PLGA particles produced from emulsions stirred at 30'000 rpm with varying concentration in the dispersed organic phase. Top: photomicrographs of product particles. Bottom left: Average particle size as obtained from light scattering. Symbols represent the x_{50} of distributions, while vertical bars cover the range between x_{10} and x_{90} . Bottom right: Corresponding particle size distributions (selected runs only).

On the other hand, the PLGA concentration might influence the size of emulsion micelles by a synergistic stabilizing effect with the surfactant PVA. This mechanism would favor larger droplets at low levels of PLGA, and could explain the rather invariant particle sizes observed at low PLGA levels where an influence of PLGA on viscosity may be neglected.

3.4.3 Effect of Emulsion Stirring Rate

The effect of stirring rate during emulsion preparation was investigated in experiments 6, 15 and 19 to 25. A constant PLGA concentration of 10 wt.% in the organic phase was used for all these experiments, while the stirring rate was increased from 820 rpm (run 19) to 30,000 rpm (run 15). Results are summarized in Figure 3.5 where particle sizes and size distributions are shown together with photomicrographs of product particles. It can be readily seen that the average particle size decreases with increasing emulsion stirring rate, while particle size distributions become generally narrower. This trend is very pronounced for stirring rates up to 15,000 rpm. For higher stirring rates, the trend seems less persistent; however, the smallest and most uniform particles were indeed produced at the highest stirring rate, namely 30,000 rpm. This may be explained as follows. On the one hand, there is a minimal droplet size distribution that may be stabilized by the surfactant molecules, and it seems reasonable that higher and higher energy inputs eventually lead to this lower bound being gradually approached. On the other hand, high stirring rates, i.e. above 15,000 rpm, caused the entrainment of air into the emulsion during stirring. This makes the attainable energy input by stirring generally smaller and less predictable, and consequently the reproducibility of emulsion formation with our setup might be reduced specifically under these conditions.

3.4 Experimental Results

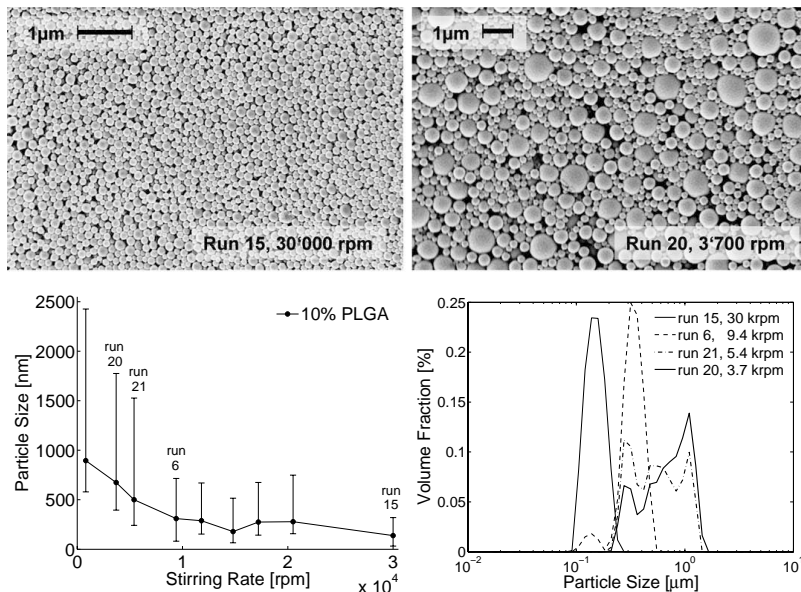


Figure 3.5: PLGA particles produced by SFEE at a constant PLGA concentration of 10% with varying stirring rate during emulsion preparation. Top: photomicrographs of particles produced at high (a) and low (b) stirring rate. Bottom left: Average particle size as obtained from light scattering. Symbols represent the x_{50} of distributions, while vertical bars cover the range between x_{10} and x_{90} . Bottom right: Corresponding particle size distributions (selected runs only).

3.4.4 Encapsulation of Lysozyme

The encapsulation of lysozyme into PLGA was investigated in three experiments. As described in section 3.3.2, each approach used a different strategy for embedding lysozyme in the polymer solution during

emulsion preparation. Emulsions were then SFEE processed, and product particles were recovered and freeze dried. The lysozyme content of freeze-dried particles was then analyzed according to the procedure described in section 3.3.4.

Two key results may be derived from this study: first the loading, i.e. the measured fraction of lysozyme in the co-formulation sample; second, the encapsulation efficiency, which is the ratio of the measured loading and the maximal attainable loading of 4.76 wt.%, i.e. that corresponding to the amounts used in each experiment, namely 100 mg lysozyme and 2 g PLGA. Both figures are reported in Table 3.3 together with photomicrographs of the product particles.

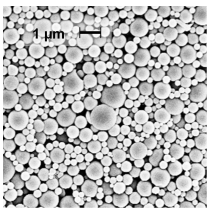
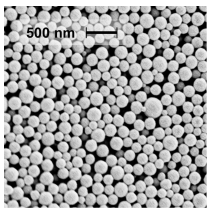
High encapsulation efficiencies of 37.0% and 48.5% were achieved when solid lysozyme precipitates were used for encapsulation in experiments L2 and L3, respectively. In run L1, lysozyme is encapsulated as aqueous solution using the double emulsion approach. It has been described earlier that with this method, reasonable encapsulation efficiencies are only achieved if the droplets of lysozyme solution in the primary w/o emulsion are much smaller than the particle-forming organic droplets in the final double emulsion. Hence, the final w/o/w emulsification step in run L1 was carried out at a much lower stirring speed (3,700 rpm) as compared to the formation of the primary w/o emulsion (30,000 rpm). This leads to larger particles of rather irregular size as compared to the particles obtained in run L3 using a high stirring rate of 30,000 rpm. While the achieved encapsulation efficiency of 10.9% was still relatively low, it is worth mentioning that the double emulsion approach is generally applicable to all water-soluble bio-molecules, and seems especially advantageous regarding the preservation of protein activity during the encapsulation process.

The results shown here on the encapsulation of lysozyme into PLGA

3.4 Experimental Results

should be regarded as a valuable proof of concept, which refers to a typical water-soluble biological macromolecule. Although the ratio of lysozyme to PLGA was chosen irrespective of pharmaceutical specifications, the loading values attained, in the range of 1 to 2 wt.%, are comparable to those in a similar study where the conventional double emulsion method was applied and the influence of stirring on the encapsulation efficiency was explored (Cho and Sah, 2005).

Table 3.3: Co-formulation of PLGA and Lysozyme using different encapsulation methods. Overview of experimental parameters and the results of product analysis.

Run	L1	L2	L3
Method of Encapsulation	w/o/w double emulsion	s/o/w suspension emulsion	s/o/w in situ suspension emulsion
Emulsion Stirring [rpm]	3,700	30,000	30,000
Lysozyme Loading [wt.%]	0.52	1.76	2.31
Encapsulation Efficiency [%]	10.9	37.0	48.5
Micrographs			

3.5 Discussion and Conclusions

PLGA is a system where control of particle size is very important. When investigating SFEE as a possible production process for PLGA particles, it is therefore necessary to understand which mechanisms have an effect on particle size. In a previous study, solvent extraction by SFEE has been compared to the conventional solvent evaporation method. In both processes, products with very similar particle size distributions have been obtained. It has also been shown that the average size of particles is clearly related to the average size of droplets in the original emulsion. These findings have been rationalized by assuming that each organic emulsion droplet forms one PLGA particle upon solvent removal provided that neither droplets nor particles coalesce or aggregate (Della Porta and Reverchon, 2008). Under this assumption, the size of PLGA particles is solely dependent on the amount of PLGA entrapped in the dispersed droplets of the organic solution. For stable emulsion systems, this key property is entirely determined during emulsion formation, and does not change during solvent removal.

In the present study, we have accounted for these findings by highlighting the influence of emulsion parameters directly linked to this key factor, namely the PLGA concentration in the organic phase (Figures 3.3 and 3.4) and the stirring rate, i.e. the energy input during emulsification (Figure 3.5). By variation of these parameters, it has been shown how particles featuring very narrow distributions and with average sizes between 100 nm and a few μm can be produced in a selective and reproducible manner. On the other hand, the influence of SFEE operating parameters such as temperature, pressure or the flowrate ratio of emulsion and CO_2 has not been investigated in the scope of this study. While these parameters are known to influence size and morphology of product

particles in other supercritical scCO₂ antisolvent processes such as PCA (Muhrrer et al., 2006), comparable effects are not expected in the case of SFEE.

It is worth highlighting at this point the great potential of SFEE as process for the production of solvent-free PLGA particles and the many advantages arising from the application of scCO₂ as solvent-extracting agent. For instance, a high product purity and a low content of residual solvents may be achieved at the same time, at moderate operating temperatures and with reasonable CO₂ consumption (Della Porta and Reverchon, 2008). Thus, compared to conventional extraction or evaporation processes, SFEE constitutes an easily scalable and adaptable unit operation.

The pharmaceutical application of PLGA particles, e.g. as delivery devices for drug administration, requires the co-formulation of PLGA with active pharmaceutical ingredients. In this context, we have developed the framework shown in Figure 3.1, thus presenting an overview about different feasible encapsulation approaches depending on the nature of the drug. We conclude that from the perspective of processing, drug encapsulation is generally more challenging for strictly hydrophilic compounds such as peptides and proteins, where PLGA is nevertheless the most widely studied delivery system (Mundargi et al., 2008). More specifically, it may be seen in Table 3.1 that solvent extraction from an emulsion, as carried out in SFEE, is in spite of many other advantages not ideally suited for the encapsulation of hydrophilic compounds. Particles are produced from an emulsion, i.e. in a continuous aqueous surrounding that is prone to extract the drug dispersed in the organic droplets or particles. In this context, the encapsulation efficiency, i. e. the fraction of drug that is actually encapsulated and not lost to the aqueous phase, becomes an important parameter to assess the quality of an encapsula-

tion process. As it may be seen in Table 3.3, we have demonstrated for the case of lysozyme that the choice of the encapsulation method has a considerable influence on the attainable encapsulation efficiency. The latter was only 11% when the double emulsion method was applied, and increased to almost 50% for the in-situ suspension emulsion method that also yielded much smaller composite particles.

The SFEE process relies on an emulsion system that is characterized by the omnipresence of phase interfaces and is moreover exposed to a high pressure process surrounding. However, scCO₂ processing and exposure to organic solvents may affect the stability of proteins, as has been investigated previously for a number of representative proteins such as lysozyme and insulin (Winters et al., 1996). The observed biological activity of re-dissolved precipitation products was generally high, thus demonstrating that scCO₂ precipitation of proteins is feasible in spite of the high pressures involved. Nevertheless, the study highlights the need of clarifying this question, i.e., to what extent the processed proteins are able to retain their activity, especially when comparing and evaluating different process alternatives.

Besides the results presented in this work, the SFEE process can be applied to the co-formulation of PLGA with small hydrophobic drug molecules, as reported elsewhere (Kluge et al., 2009b).

Chapter 4

PLGA micro- and nanocomposites by SFEE: Encapsulating ketoprofen¹

4.1 Introduction

Particles of the biocompatible and biodegradable polymer poly-lactic-co-glycolic acid (PLGA) offer an attractive delivery system platform for a wide range of active pharmaceutical ingredients. The production of such particles may be achieved by processes such as spray drying, coacervation (phase separation) and emulsion processes with subsequent solvent extraction or evaporation (Freitas et al., 2005). A recent and very promising approach involves the application of supercritical CO₂ as solvent extracting agent in a process called supercritical fluid extraction of emulsions (SFEE) (Kluge et al., 2009b; Della Porta and Reverchon, 2008;

¹The work in this chapter has been published as Kluge et al. (2009c).

Chattopadhyay et al., 2006). In the previous chapter 3, we have demonstrated that SFEE enables the production of highly pure PLGA micro- and nanoparticles with controllable size and narrow size distribution while working at mild operating conditions suitable for the treatment of sensitive biomaterials. A detailed description of the process had been provided along with a comprehensive summary of different strategies for the encapsulation of drugs. Moreover, drug encapsulation into PLGA has been investigated experimentally for the case of the water-soluble model peptide lysozyme.

The present investigation extends our study about the feasibility of encapsulation of drug compounds by SFEE to a group of drugs designated as class II substances according to the biopharmaceutical classification system (BCS) (Amidon et al., 1995). Due to a low molecular weight, such drugs are characterized by good permeability, and are thus generally suitable for uptake through the gastrointestinal membranes. However, another characteristic of class II compounds is their poor solubility in the gastrointestinal fluids, a property that may reduce oral bioavailability and thus interfere with the suitability for oral administration. For such substances, the bioavailability in vivo is correlated with the performance in dissolution studies in vitro, and the use of class II compounds in drug-polymer co-formulation studies is wide-spread.

With a molecular weight of 254.28 g/mol and a low aqueous solubility of 0.25 mg/ml for the undissociated molecule, the nonsteroidal and anti-inflammatory drug ketoprofen (KET) is a typical representative of BCS class II (Sheng et al., 2006). The drug is further characterized by a short therapeutic half life (2 - 2.5 h) along with a tendency to induce gastric irritation and an unpleasant taste. These properties highlight some of the most relevant co-formulation applications - e.g. enhancement of bioavailability, controlled drug release, parenteral drug delivery, or sim-

ple taste masking - and explain why KET is widely used in drug-polymer co-formulation studies. The polymer types used most frequently in such studies include PLGA (Blasi et al., 2007; Chattopadhyay et al., 2006; Gavini et al., 2003; Gabor et al., 1999; Castelli et al., 1998), Eudragit (Rassu et al., 2008; Eerikainen et al., 2004a,b) and poly-vinylpyrrolidone (PVP) (Manna et al., 2007; Di Martino et al., 2004). These polymers are all fully amorphous in structure, and for instance PVP is well-known for the ability to stabilize typically crystalline drugs in an amorphous state (Kluge et al., 2009a; Marsac et al., 2008; Konno and Taylor, 2006; Marsac et al., 2006a). Hence, most of the aforementioned studies aim at the production and characterization of amorphous, homogeneous and stable dispersions of KET within the polymer matrix. Since there are common solvents for all of the systems described above, co-formulation processes start in most cases from a homogeneous solution of KET and polymer from which the solvent is subsequently removed e.g. by spray drying (Rassu et al., 2008; Eerikainen et al., 2004a,b; Gavini et al., 2003), extraction (Chattopadhyay et al., 2006; Gabor et al., 1999) or simply evaporation at reduced pressure (Blasi et al., 2007; Di Martino et al., 2004).

It may be assumed that in such processes the mixture of KET and polymer stays fully homogeneous unless the two compounds exhibit a miscibility gap at the chosen conditions that causes demixing. In order to provide evidence whether this is the case or not, most studies investigate product morphology and physicochemical interactions of drug and polymer by using one or several of the following techniques: X-Ray powder diffraction (XRD) may be used to detect the presence or absence of crystalline KET (Chattopadhyay et al., 2006; Di Martino et al., 2004; Eerikainen et al., 2004a). Differential scanning calorimetry (DSC) is frequently used to identify crystalline KET by its melt endotherm at 95

°C (Blasi et al., 2007; Eerikainen et al., 2004a,b; Gavini et al., 2003). Moreover, DSC may be used to identify the glass transition temperature (T_G) of amorphous materials. Foreign molecules embedded in a polymer often cause a plasticization of the material, and indeed many studies report a decreasing T_G for KET-polymer mixtures as compared to the pure polymer (Blasi et al., 2007; Eerikainen et al., 2004a,b; Di Martino et al., 2004). The extent of this decrease is concentration-dependent, and this relationship may be determined experimentally in order to verify whether a KET-polymer system is fully miscible, as it is the case for amorphous KET and PVP (Di Martino et al., 2004), or it exhibits a miscibility gap, as demonstrated for KET and PLGA (Blasi et al., 2007). Infrared Spectroscopy has been used in some of the studies to assess specific molecular interactions between KET and the aforementioned polymers such as hydrogen bonding mechanisms.

The given examples underline how a thoughtful combination of these methods may provide valuable information about the interior state of co-formulations. However, it is also of interest whether the described states are stable, particularly in the light of possible pharmaceutical applications requiring long-term stability. The stability of mixtures is usually assessed by investigating whether or not the above-mentioned properties are invariant over a certain time period. For instance, a DSC-based stability study on spray-dried co-formulations of KET with Eudragit RS and RL (drug to polymer weight ratio of 1:3) showed that the drug had been effectively stabilized in amorphous state over a time period of 30 days (Rassu et al., 2008). However, conclusions drawn in the scope of such studies are often limited to the specific conditions investigated, whereas there is a lack of studies providing information about stability of co-formulations for the drug-polymer system in general.

In this context, the present study introduces a novel and simplified ap-

proach. First, co-formulations of KET and PLGA are manufactured by SFEE, yielding spherical composite nanoparticles dispersed in an aqueous phase. The evolution of the drug content in the suspended particles has been measured throughout one week of storage in order to investigate the stability of the co-formulation. Moreover, it has been studied how an equilibration of the suspensions with crystalline KET affects the composition of particles. The presented findings allow detailed conclusions about the interior state of the co-formulations. Further, the study provides valuable information for pharmaceutical processing, such as operating conditions that maximize the KET load while leading to co-formulations that are long-term stable. Finally, an interpretation of the obtained results in the light of the Flory-Huggins theory of polymer solutions provides - qualitatively - further evidence about the nature of KET-PLGA interactions in the mixture.

4.2 Materials and Methods

4.2.1 Materials

Carbon dioxide (CO₂; 99.9%, from PanGas, Schlieren, Switzerland), poly(lactic-co-glycolic) acid 5050 DLG 5A (PLGA; Lakeshore Biomaterials, Birmingham AL, United States), poly(vinyl alcohol) 4-88 (PVA), racemic Ketoprofen (KET), dimethylsulfoxide (DMSO) and

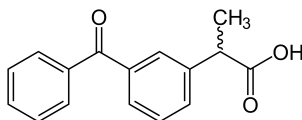


Figure 4.1: Chemical structure of Ketoprofen.

ethyl acetate (all from Sigma-Aldrich, Buchs, Switzerland) were used as received.

4.2.2 Emulsion Preparation and SFEE processing

PLGA (5 wt.%) and a specified amount of KET were both dissolved in ethyl acetate saturated with water. A 1 %wt. solution of PVA was prepared in water saturated with ethyl acetate. The organic and aqueous solution were used at a weight ratio of 1:4 to form an (o/w) emulsion upon ultrasonication with a Branson Sonifier 450 (Skan AG, Basel, Switzerland). Per 100 ml of emulsion, a sonication time of 2 minutes was applied at maximal power output while cooling the emulsion in an ice bath.

Directly after emulsion preparation, the organic solvent was extracted from the dispersed micelles using scCO₂ as extracting agent in the supercritical fluid extraction of emulsions (SFEE) process. The experimental setup used for SFEE experiments is the same the one shown previously in Figure 3.2. A detailed description of the process is available in the previous sections 2.2.3 and 3.3.3.

4.2.3 Product Characterization

Recovery of amorphous particles. The recovery of amorphous co-formulation particles was carried out in two steps. First, KET crystals (if present) were removed from the suspension by 2×10 min centrifugation at a medium rotation speed of 4000 rpm (Eppendorf Centrifuge 5810R, Vaudaux-Eppendorf AG, Basel, Switzerland), thus sedimenting all crystals, but leaving polymeric nanoparticles suspended in the crystal-free

supernatant. The latter was then subjected to 15 minutes of ultracentrifugation at 20,000 rpm (Avanti J-20, Beckman, USA) in order to sediment nanoparticles, while the surplus of PVA surfactant could be discarded with the particle-free supernatant. Sedimented polymeric nanoparticles were re-suspended in pure water and subsequently freeze-dried for further analysis (FlexiDry, FTS Systems, USA).

Light Microscopy (LM) and Scanning Electron Microscopy (SEM). A light microscope (Zeiss Axioplan, Carl Zeiss AG, Feldbach, Switzerland) was used for the observation of particles in aqueous suspension. In order to assess the morphology and size of nanoparticles, SEM photomicrographs were obtained from dried samples sputter-coated with about 5 nm platinum using a Zeiss Gemini 5 1530 FEG scanning electron microscope.

Characterization of Ketoprofen content. A known amount of freeze-dried polymeric nanoparticles containing approximately 10 mg Ketoprofen was dissolved in 10 ml of DMSO. A volume of 100 μ l of the solution was pipetted into a cuvette containing 2 ml DMSO, and the concentration of KET was determined by UV spectroscopy (Beckman Coulter, DU520). For calibration, five independent solutions containing 10 mg KET were analyzed as described. At a wavelength of 300 nm, a molar extinction coefficient of 1228.43 AU/(mol/l) was determined and used for the conversion of absorption units into molar concentrations.

Preparation of Ketoprofen seed crystals. KET crystals for seeding experiments as shown in Figure 4.2b were prepared by using pure KET instead of PLGA for the preparation of an emulsion and subsequent SFEE processing, as described above. KET precipitated in the form of

amorphous nanoparticles, which were allowed to recrystallize following the process illustrated in Figure 4.3. In order to remove all crystal fragments too small for sedimentation, KET crystals were repeatedly spun down at 4000 rpm (Eppendorf Centrifuge 5810R) and resuspended in pure water until the supernatant was clear to the eye and thus considered free of suspended solids. The obtained fraction of large KET crystals was resuspended in water and used in seeding experiments. Approximately 0.5 g of KET crystals were used to seed about 200 ml of product suspension, i.e. an equivalent of about 2.5 g of PLGA were present as nanoparticles.

Stability of PLGA-KET co-formulations. PLGA-KET co-formulation products obtained from SFEE processing as suspensions were observed over a total time of seven days. Where indicated, KET seed crystals were initially added to half of the product suspension, while the other half was used for control measurements. Suspension samples were taken at specified time points, and the amorphous polymeric particles were recovered and characterized with respect to their KET content as described above.

4.3 Experimental Results

A summary of experimental results is given in Table 4.1. The composition of the organic solution used for emulsion preparation according to section 5.2.2 is specified on the left. The right side contains the results of stability studies as described in section 4.2.3, reporting the KET concentration measured within the co-formulation particles over the time span of one week. Finally, SEM images of product particles are referenced in the last column of the table.

Table 4.1: Overview of experimental parameters and the results of product analysis.

Run	Organic solution		Stability Analysis: c_{KET}		Images
	c_{PLGA} [wt. %]	$c_{\text{KET}}/c_{\text{KET}}+c_{\text{PLGA}}$ [%]	[wt. % in amorphous phase]		
1	5.00	-	0.0	-	Fig. 4.2a
1s			4.5	4.4	Fig. 4.4a
2	-	5.00	100	4.3	Fig. 4.2b
3	5.00	0.20	3.9	-	
4	5.00	0.30	5.7	-	
5	5.00	0.40	7.4	-	
6	5.00	0.50	9.1	-	Fig. 4.4b
7	5.00	0.80	13.8	-	
8	5.00	1.20	19.4	-	Fig. 4.4c
9	5.00	5.00	50.0	8.2	
10	5.00	0.80	13.8	7.5	
10s			13.8	5.6	
11	5.00	1.20	19.4	10.2	
11s			19.4	6.3	
				6.3	
				5.2	
				4.9	
				10.3	
				10.3	
				5.6	
				5.4	

4.3.1 SFEE processing of pure PLGA and pure Ketoprofen

SFEE processing of pure PLGA and pure KET was carried out in runs 1 and 2, respectively. Figure 4.2 illustrates the difference in the outcome of these two experiments. In agreement with results reported previously (Kluge et al., 2009b; Della Porta and Reverchon, 2008; Chattopadhyay et al., 2006), Figure 4.2a shows spherical and uniformly distributed PLGA nanoparticles in a size range between 100 - 200 nm that were obtained in run 1. On the other hand, equivalent processing of KET yielded an unstable product that eventually transformed into the large and clearly crystalline platelets of KET shown in Figure 4.2b.

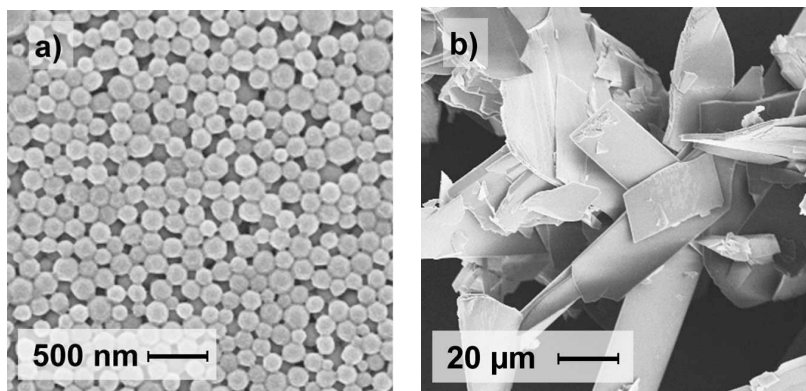


Figure 4.2: Scanning electron photomicrographs of a) PLGA particles and b) recrystallized Ketoprofen, each obtained by SFEE processing of the pure compound.

Details of KET transformation within the solvent-free product suspension can be highlighted and analysed by looking at Figure 4.3. Like pure PLGA, also KET was initially obtained in the form of spherical and non-

sedimenting particles as shown in Figure 4.3a, where we presume that only the larger particles are visible by optical microscopy. In the time course of about 10 min, the formation of crystalline KET could be observed as shown in Figure 4.3b, where an agglomerate of needle-shaped KET crystals (top right) is shown along with some of the aforementioned spherical KET particles. After about 30 min (see Figure 4.3c) an even more advanced state of transformation is observed. Spherical KET precursors have completely vanished by transforming into KET crystals. Interestingly, two different types of crystals, namely agglomerated needles and rectangular platelets possibly representing different polymorphs of KET, are visible on Figures 4.3b and c.

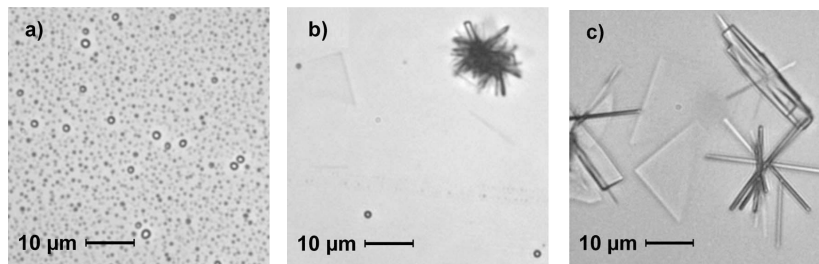


Figure 4.3: Microscope images capturing the solid state transformation of Ketoprofen. a) spherical and presumably amorphous particles obtained by SFEE processing of pure Ketoprofen, b) onset of Ketoprofen recrystallization from the spherical precursor particles and c) completely recrystallized Ketoprofen. Time span between a) and c): approximately 30 min.

It is worth mentioning that the described transformation was also observable by eye. Immediately after processing, the product suspension had a homogeneous and milky appearance. Then, the onset of recrystallization could be observed through the formation of a sediment. Finally, a clear and transparent supernatant together with large and fast-sedimenting KET crystals (Figure 4.2b) indicated the completion

of KET transformation. The spherical KET particles are presumably amorphous, and based on the low glass transition temperature of -3°C that is reported for amorphous KET (Blasi et al., 2007; Di Martino et al., 2004), a liquid or rubbery state should be expected at room temperature. Thus, the formed KET entities are droplets rather than particles. A verification of the amorphous state by XRD proved to be difficult: SEM analysis of freeze-dried samples showed few crystals embedded in a mass devoid of any particulate structure (not shown here). While the former proves that KET recrystallized at least partly while being recovered from the suspension, the latter may be explained assuming full coalescence of KET droplets during recovery.

4.3.2 Co-formulation of PLGA and Ketoprofen via SFEE

The co-formulation of KET and PLGA by SFEE was investigated in runs 3 to 9. As shown in Table 4.1, the nominal KET:PLGA ratio was increased from 4 wt.% (run 3) to a ratio of 1:1 (run 9). Since both PLGA and KET yield particles with an initially similar appearance (compare Figures 4.2a and 4.3a), it is not surprising that also composite particles are primarily characterized by the same spherical morphology. This may be seen in Figures 4.4b and c, i.e. for the case of particles obtained in runs 6 and 8, respectively.

Moreover, all product suspensions had initially a milky and homogeneous appearance to the eye. However, as described for the case of pure KET, the formation of large and sedimenting KET crystals could be observed in co-formulation suspensions with very high KET content. As described in section 4.2.3, it is possible to isolate amorphous co-formulation particles for separate analysis. Hence, the development of KET content

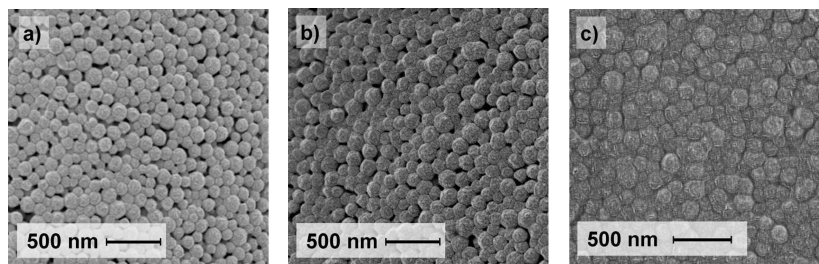


Figure 4.4: SEM photomicrographs of PLGA-Ketoprofen co-formulation particles. a) run 1s on day 1, 4.54% KET, b) run 6 on day 7, 6.11% KET, c) run 8 on day 1, 14.32% KET. Note that particles with high drug content appear softer and are also characterized by a rougher surface.

in the amorphous particles may be monitored during the progress of KET re-crystallization in the product suspension. For experiments 3 to 9, Figure 4.5 and Table 4.1 report the result of such investigation over a span of one week while product suspensions were stored at ambient conditions. KET concentrations in the amorphous particles were determined immediately after the experiment and after seven days. Further, KET concentration was also determined after 1, 2 and 4 days in the case of run 9. Table 4.1 shows that the measured KET content was in all cases lower than the nominal ratio of KET and PLGA in the emulsion. This indicates a certain loss of KET during the process, i.e. by solubility in the supercritical mixture of CO_2 and solvent. Regarding product stability, Figure 4.5 shows that co-formulations with relatively low levels of KET, as obtained for runs 3 to 7, were found to exhibit a constant KET content. Also, recrystallized KET was not observed in the corresponding samples, whereas in runs 8 and 9, KET crystals were indeed formed during storage of product suspensions. As observed in Figure 4.5, the consumption of KET originating from crystal formation

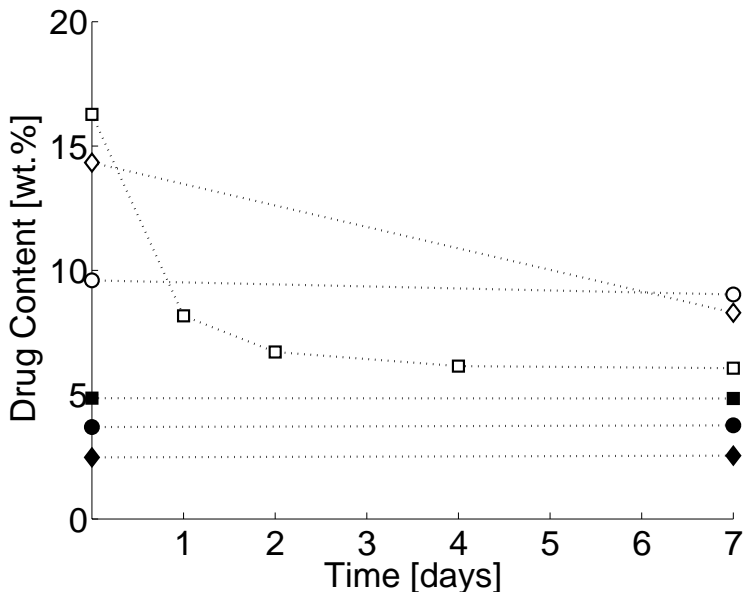


Figure 4.5: Stability of PLGA-Ketoprofen co-formulations. Co-formulations exhibiting constant drug content: \blacklozenge run 3, \bullet run 4, \blacksquare run 5. Co-formulations with decreasing drug content: \circ run 7, \diamond run 8 and \square run 9.

in these two runs was compensated by a decreasing KET content in the corresponding amorphous product fractions.

4.3.3 Stability of co-formulations upon seeding

One more important detail is highlighted in Figure 4.5: Whereas the initially determined KET content for run 9 (16.3 wt.%) is higher than the one in run 8 (14.3 wt.%) and run 7 (9.6 wt.%), this order is reversed after seven days of storage, with run 7 (9.0 wt.%) exhibiting a higher concentration than run 8 (8.3 wt.%) and run 9 (6.1 wt.%). This result

implies that with the described method, the KET content - i.e. the only parameter that has been varied in runs 3 to 9 - is obviously not the only criterium to influence product stability. However, beside KET content there is only one further difference between runs 7 and 9, which is the absence or the presence of KET crystals in the product suspension.

The question whether or not the presence of crystalline KET may have an influence on the outcome of the previously described stability study was addressed with the particles obtained in runs 10 and 11. In both cases, the obtained product suspension was split in two parts, and one fraction was mixed with the previously prepared seed crystals (see Figure 4.2b), while the other was observed as a control. Results of the stability study are shown in Table 4.1 and Figure 4.6, respectively. There, it may be seen that runs 10 and 11 representing the unseeded control experiments each show a constant level of KET. On the contrary the very same products exhibit clearly decreasing KET contents when seeded with crystalline KET in runs 10s and 11s.

We presume that the product suspension is a system where all phases present approach during the observed period of storage a state where they are in equilibrium with each other. Obviously, a depletion of KET from the polymeric co-formulation particles requires KET to accumulate within the suspension in a different phase, namely KET crystals, whose nucleation and growth consumes KET from the environment. Both processes may only take place in a supersaturated environment. Further, it is well-known that nucleation is an activated process where a certain energy barrier needs to be overcome hence it requires a higher supersaturation as compared to the growth of an already existing crystal surface. The experiments presented in Table 4.1 may thus be grouped into three different categories. The first category, best represented by run 9, includes instable products with a very high KET content. There, the high

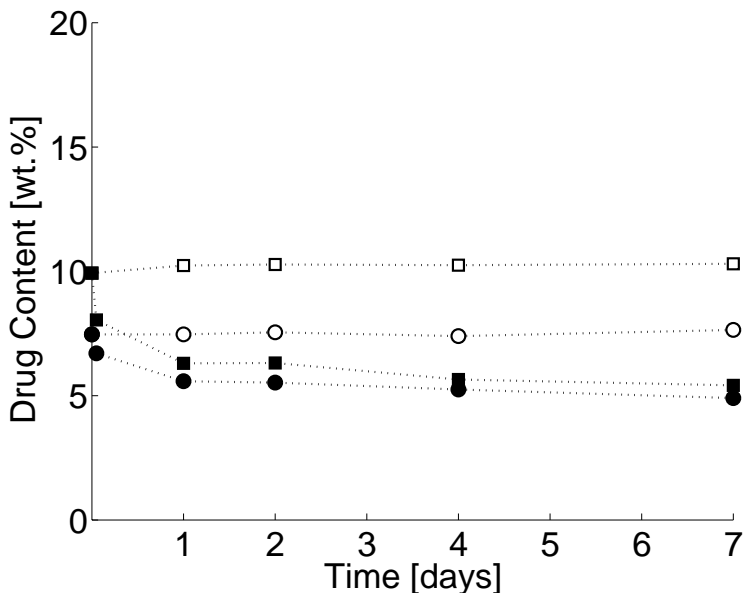


Figure 4.6: Stability of PLGA-Ketoprofen co-formulations. Unseeded product suspensions are metastable: \circ run 10, \square run 11. When seeded with KET crystals, the same products exhibit a decreasing drug content: \bullet run 10s, \blacksquare run 11s. Two data points on day 0 represent concentrations measured before and after mixing with seed crystals.

supersaturation in the suspension causes eventually the nucleation and growth of KET crystals, thus leading to a depletion of KET in the polymeric particles. The second category, best represented by runs 10 and 11, includes metastable products with intermediate KET content. In such suspensions, the level of KET supersaturation is not high enough to induce the nucleation of crystals in the observed time span. However, supersaturation is consumed for crystal growth as soon as seed crystals are provided. Finally, the third category, best represented by runs 3 and

4, contains suspensions with KET levels below the solubility limit, hence stable products.

4.3.4 Co-Formulation by Impregnation

The interpretation of the results presented in the previous section allows two important conclusions. First, seeding of product suspensions with KET crystals leads to an equilibration of polymeric co-formulation particles with the crystalline drug. Second, a time frame of one week is sufficient to observe this equilibration. It is now interesting to investigate whether this equilibration also takes place in the case of seeding previously unsaturated PLGA particles. This would actually require a change in the direction of mass transfer during equilibration, involving the dissolution of seed crystals and impregnation of KET into the polymeric particles.

This question was assessed experimentally using pure PLGA particles from run 1 (see Figure 4.2a). As in previous experiments, KET seed crystals obtained from run 2 were added to the product suspension. During one week of storage for equilibration, samples were withdrawn and the content of KET in the polymeric particles was analyzed. Particles obtained from this impregnation experiment are shown in Figure 4.4a. Also, results are reported in detail in Table 4.1 and are shown in Figure 4.7, together with the results of experiments previously classified as unstable (run 9), metastable (runs 10s and 11s) and stable (runs 3 and 4) which are reported for the sake of comparison. It may be seen that the impregnation of PLGA particles results in the instantaneous uptake of KET up to a level of 4.5 wt.%, which is then maintained during the observed period of storage. It is further observed that this level falls slightly below the level attained by desupersaturation in runs 9, 10s

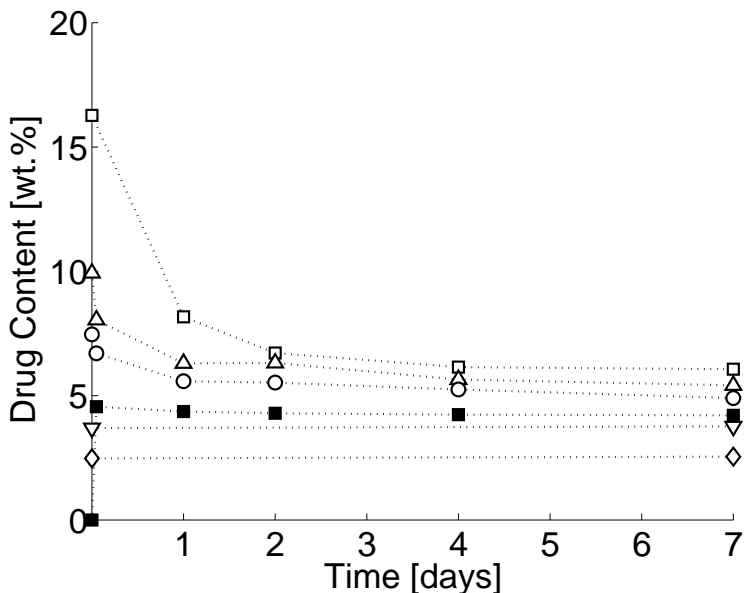


Figure 4.7: Impregnation of pure PLGA particles with crystalline KET: ■ run 1s. Note that the attained concentration level falls exactly between stable co-formulations (◇ run 3 and ▽ run 4) and instable co-formulations (○ run 10s, △ run 11s and □ run 9). Two data points on day 0 represent concentrations measured before and after mixing with seed crystals.

and 11s, and above the stable runs 3 and 4. We conclude that the equilibrium solubility of KET in PLGA under the given conditions lies in the narrow range between the lowest value attained by the depletion of supersaturated particles, i.e. 4.9 wt.% in run 10s, and the highest value attained by the saturation of undersaturated particles, i.e. 4.5 wt.% in run 1s.

4.3 Experimental Results

Table 4.2: Material properties of KET and PLGA used for Flory-Huggins modeling.

Property	Units	KET	PLGA	Source
MW	(g/mol)	254.3	54 800	(Dwan'Isa et al., 2007)
Density	(g/cm ³)	1.253	1.35	(Blasi et al., 2007)
Mol. Volume	(cm ³ /mol)	202.95	40 600	
T_m	(K)	367.7	-	(Lu and Ching, 2004)
T_G	(K)	270.2	319.4	(Di Martino et al., 2004; Blasi et al., 2007) / supplier
ΔH^f	(kJ/mol)	27.38	-	(Lu and Ching, 2004)
$\delta_{polarity}$	(J/cm ³) ^{1/2}	6.8	9.1	(Dwan'Isa et al., 2007; Schenderlein et al., 2004)
$\delta_{dispersion}$	(J/cm ³) ^{1/2}	20.0	17.4	(Dwan'Isa et al., 2007; Schenderlein et al., 2004)
$\delta_{hydrogen}$	(J/cm ³) ^{1/2}	8.0	10.5	(Dwan'Isa et al., 2007; Schenderlein et al., 2004)

4.3.5 KET solubility in PLGA

The solubility of KET in PLGA may be described using material properties of both compounds obtained from the literature and summarized in Table 5.2. Key steps of the approach shall be described briefly, in order to clarify the assumptions on which these predictions are based.

Solubility of a crystalline solute (Prausnitz et al., 1986). The solubility of a crystalline solute at the temperature T may be described using the Schröder-van Laar Equation:

$$\ln(\gamma^s x^s) = -\frac{\Delta H^f}{RT_m} \left(\frac{T_m}{T} - 1 \right) \quad (4.1)$$

Here, x^s is the solubility mole fraction of the solid, T_m is its melting temperature, ΔH^f is its enthalpy of fusion and γ^s is its activity coefficient at saturation, hence the only solvent-dependent parameter in the equation. Thus, the right-hand side of the equation contains only solute parameters and can be calculated using the material properties of the drug compound given in Table 5.2. If γ^s in equation 5.4 is equal to unity, the solution is ideal and solubility does not depend on the solvent. This is a physically unrealistic result, and therefore the activity coefficient is needed to describe the solute-solvent interactions.

The activity coefficient in a polymeric solvent (Flory, 1953).

Since in this work, the "solvent" is PLGA, we rely on the Flory-Huggins solution theory, which is used to describe polymeric solutions. In this framework, we consider a 3D lattice where each site has a volume that corresponds to the molecular volume of the solute molecules. We assume that the lattice is fully occupied by the two species present, i.e. n_1 sites are occupied by n_1 solute molecules, and rn_2 sites are occupied by n_2 molecules of the polymer, each consisting of r subunits each occupying one site ($r = 200$ is calculated from the molar volumes given in Table 5.2). Thus, $n = n_1 + rn_2$ is the total number of sites, and $\Phi_1 = n_1/n$ and $\Phi_2 = 1 - \Phi_1$ are the volume fractions of solute and polymeric solvent, respectively. According to the Flory-Huggins theory of polymer solutions, the activity coefficient of the solute may be calculated using the following expression:

$$\ln(\gamma x) = \ln \Phi_1 + \left(1 - \frac{1}{r}\right)\Phi_2 + \chi(\Phi_2)^2 \quad (4.2)$$

The first two terms constitute the contribution of the excess entropy of mixing, while the last term, including the dimensionless interaction parameter χ , represents the excess enthalpy of mixing for the two species.

This expression may be related to Equation 5.4 for the case of a saturated solution, i.e. where $\gamma x = \gamma^s x^s$:

$$-\frac{\Delta H^f}{RT_m} \left(\frac{T_m}{T} - 1 \right) = \ln \Phi_1 + \left(1 - \frac{1}{r} \right) \Phi_2 + \chi (\Phi_2)^2 \quad (4.3)$$

Equation 5.12 relates the solubility of a solid in an amorphous polymer, which corresponds to the volume fraction Φ_1 , to specific molecular interactions between the two compounds, represented by the dimensionless interaction parameter χ . Thus, χ may be calculated from the experimentally determined solubility of KET in PLGA, i.e. a weight fraction of 4.7 wt.%. Assuming isometric mixing and using the densities given in Table 5.2, a volume fraction Φ_1 of 5.0% is obtained. It is found that the values calculated for χ are very sensitive to changes in temperature. Since equilibration experiments were carried out without temperature control, the ambient temperature is assumed to lie in the range from 293 to 295 K. This translates into χ having a negative value between -0.26 and -0.17 .

It is worth comparing this result to figures estimated from material properties using the Hansen-modified Scatchard-Hildebrand theory. In this approach, χ is calculated from a three-dimensional solubility parameter where each component takes into account a specific type of molecular interactions, namely forces of dispersion ($\delta_{dispersion}$), permanent dipole forces ($\delta_{polarity}$), and hydrogen bonds ($\delta_{hydrogen}$). These components may be determined e.g. by molecular modeling or from solubility experiments, and are available from the literature for both Ketoprofen and PLGA (Table 5.2). Using this approach, a value of $\chi = 1.5$ is obtained

from the solubility difference Δ as to the following equation:

$$\Delta = [(\delta_s - \delta_p)_{dispersion}^2 + (\delta_s - \delta_p)_{hydrogen}^2 + (\delta_s - \delta_p)_{polarity}^2]^{1/2}$$

$$\chi = \Delta^2 \frac{V_m}{RT} \quad (4.4)$$

where V_m is the molecular volume of the solute KET. It is worth highlighting that in agreement with the underlying Scatchard-Hildebrand regular solution theory, Equation 5.14 restricts χ to positive values. However, negative values of χ (i.e. deviations from the regular solution theory) have been observed in many polar systems with specific solute-solvent interactions such as hydrogen bonding, and indicate systems with good solubility (Marsac et al., 2006b; Prausnitz et al., 1986). Therefore, the negative value of χ derived from our experimental findings suggests that specific polar solute-solvent interactions such as hydrogen bonds are indeed present in KET-PLGA solid solutions.

4.4 Discussion and Conclusions

4.4.1 SFEE processing of pure PLGA and Ketoprofen

Concerning the SFEE processing of pure PLGA, the result shown in Figure 4.2a is in full agreement with more detailed previous investigations (Kluge et al., 2009b; Della Porta and Reverchon, 2008; Chattopadhyay et al., 2006). However, the concept of particle formation by SFEE has been applied to only few pure substances other than PLGA, including Eudragit (Chattopadhyay et al., 2006) and the drugs cholesterol acetate, megestrol acetate and griseofulvin (Shekunov et al., 2006b). In the case

of griseofulvin, clearly crystalline microparticles of very uniform size have been obtained. This is remarkable, since phase formation by nucleation - which is characteristic of crystalline materials - does not naturally support the conclusion that one emulsion micelle forms exactly one particle. It is therefore useful to discuss the latter hypothesis, which has been thoroughly verified, however mainly for the case of PLGA, in the light of results obtained for SFEE processing of KET. Here, the size and spherical morphology of presumably amorphous precursor particles shown in Figure 4.3a suggests that they are indeed formed each out of one emulsion droplet. However, this pattern is obviously not preserved during the subsequent recrystallization (Figures 4.3b and c), and the crystals eventually formed are by orders of magnitude larger than particles precipitated out of emulsion micelles (compare Figure 4.4a and b). The observed behavior, i.e. the formation of unstable amorphous precursors and a subsequent recrystallization into larger crystals, is likely to occur also in the SFEE processing of other crystalline compounds. In cases where an observation of the transition shown in Figure 4.3 is not possible because of unfavorable kinetics, the present findings may be helpful to rationalize experimental results.

4.4.2 KET-PLGA co-formulation

Spherical KET-PLGA nano-composites of the morphology shown in Figure 4.4 have significant potential to be used directly as final drug product for in vitro and in vivo studies. This emphasizes the importance of an assessment of their long-term stability, which represents a decisive criterion regarding the possibility to bring such a product on the market. In this context, the determination of the solubility of KET in PLGA represents an important milestone since it enables the design of long-term

stable composites.

It is further worth discussing the present results in the light of a previous study on the same binary system KET-PLGA investigating in detail their interaction (Blasi et al., 2007). This may be helpful in order to highlight some details that might be overlooked otherwise. For instance, it has been described how the presence of KET decreases the glass transition temperature of co-formulations. For pure PLGA, a T_G of 42°C is reported, and co-formulation with KET leads to further decreases in T_G down to 26°C at a KET fraction of 20 wt.%, i.e. values that are actually only slightly above ambient temperature (Blasi et al., 2007). This may be related to a change in particle morphology, which is clearly visible in Figure 4.4. With increasing KET content, particles appear softer and more blurred, especially if compared to the pure PLGA particles in Figure 4.2a.

Further, the described changes in glass transition temperature have been used to assess co-formulation homogeneity (see in section 5.1), and it is concluded that KET is molecularly dispersed into the polymeric matrix at fractions up to 20 wt.% (Blasi et al., 2007). This observation is confirmed by the present findings: The behavior of products in (de)saturation experiments as summarized in Figure 4.7 may only be explained by assuming that all corresponding co-formulation products being equilibrated with crystalline KET represent single phases and are thus homogeneous.

Finally, upon analysis of co-formulations by Fourier-transformed infrared spectroscopy it was concluded that molecular interactions involve the binding of KET carboxylic groups to carbonyl groups along the PLGA polymer chain (Blasi et al., 2007). This result is again consistent with our present findings. Based on a simple lattice model, a dimensionless Flory-Huggins interaction parameter has been determined using the ex-

perimentally observed solubility. Its negative value indicates indeed the presence of polar molecular interactions such as hydrogen bonding.

4.4.3 Concluding remarks

The following conclusions may be drawn regarding the stability and impregnation studies carried out with KET-PLGA co-formulations. First, as shown in Figure 4.7, co-formulations and also particles of pure PLGA finally attain comparable levels of KET when equilibrated with KET crystals in suspension. This has been rationalized by conjecturing that the co-formulation represents a single phase and that there is a certain level where KET dissolved in PLGA is in equilibrium with crystalline KET, i.e. a solubility of KET in PLGA. For pharmaceutical manufacturing, the determination of a solubility is of major importance since it defines the range in which a production of thermodynamically stable products is possible. Secondly, as shown in Figure 4.6, co-formulations may exhibit levels of supersaturation that are too low to induce the autonomous nucleation of KET crystals in the observed period of time, i.e. suspended co-formulations particles may be metastable. Also this information is of relevance for pharmaceutical manufacturing, since the metastable zone width provides a valuable guideline, e.g. in order to prospect the performance of overloaded co-formulations in long-term stability studies.

As an important consequence, it has been shown that KET-PLGA co-formulations may be achieved by common SFEE processing as well as by impregnation of KET into pure PLGA particles. While the former has the advantage that also overloaded metastable co-formulations may be achieved, the latter constitutes a safe and also surprisingly fast process for the formation of stable co-formulations, and it may also help

increasing the reduced KET yield observed in SFEE processing.

4.5 Nomenclature

Roman Symbols

c	Concentration	[wt.%]
ΔH^f	Enthalpy of fusion	[J/mol]
MW	Molecular Weight	[g/mol]
r	Number of lattice sites per molecule	[-]
R	Ideal Gas Constant	[J/(mol K)]
T	Temperature	[K]
T_G	Glass Transition Temperature	[K]
T_m	Melting Temperature	[K]
V_m	Molar volume	[m ³ /mol]

Greek Symbols

γ	Activity coefficient	[-]
$\delta_{polarity}$	Solubility parameter (polarity)	[(J/cm ³) ^{1/2}]
$\delta_{dispersion}$	Solubility parameter (dispersion)	[(J/cm ³) ^{1/2}]
$\delta_{hydrogen}$	Solubility parameter (hydrogen)	[(J/cm ³) ^{1/2}]
Φ	Volume fraction	[-]
χ	Interaction parameter	[-]

Chapter 5

Solubility of Ketoprofen in Colloidal PLGA¹

5.1 Introduction

The microencapsulation of active pharmaceutical ingredients into polymeric drug delivery systems is a promising and widely used method in drug formulation technology, enabling a number of interesting novel pharmaceutical delivery concepts. For instance, in controlled drug release, encapsulation enhances and prolongs the effectiveness of active ingredients, while in drug targeting, polymeric particles are used as carriers for the targeted delivery of the drug to a specific site of action.

In many cases, the co-formulation of drug and polymer aims at producing a solid solution where the drug is dispersed in the amorphous polymer matrix at a molecular level. However, the entrapment of the

¹The work in this chapter has been submitted for publication in the International Journal of Pharmaceutics.

active ingredient into the polymeric material may be thermodynamically unfavorable, especially if high drug loadings are desired, or if the mutual affinity between drug and polymer is low. Such co-formulations bear the risk of reduced long-term stability and shelf life, representing a major hurdle with respect to potential applications (Vasanthavada et al., 2005). Hence, the design and development of such co-formulations could strongly benefit from a priori information about the compatibility of drug and polymer, in order to select promising polymer excipients forming stable co-formulations and allowing for maximal drug load. However, there is still a lack of such data, as well as of robust and reliable experimental methods to generate such information in an accurate and efficient manner.

A crucial step in this direction is the determination of the level of drug present in the polymer phase if the latter is fully equilibrated with the pharmaceutical compound in the crystalline state, i.e., the solubility of the drug in the polymeric matrix, which in this case represents the solvent. In practice, equilibration is hardly achieved in short times since it is based on the slow diffusion of molecules inside the polymer phase. However, the equilibration process may be facilitated by using polymeric nanoparticles, where diffusion distances are short, and consequently, equilibration is fast. We have successfully demonstrated in Chapter 4 that solvent-free PLGA nanoparticles as obtained by SFEE processing may be used to investigate the equilibration of PLGA with crystalline ketoprofen (KET), a chiral molecule belonging to the class of nonsteroidal anti-inflammatory drugs (NSAIDs) (Kluge et al., 2009c).

In order to further underline the potential that arises from SFEE as a viable manufacturing technique and in order to highlight a novel application of and opportunity for this process, this work presents the results of an extended study, investigating the temperature dependence

of the phase equilibrium between KET and PLGA in the range between 0°C and 50°C , as well as the effect of KET chirality. While it may be anticipated that the solubility of KET in PLGA increases with the temperature, the expected effect of chirality on equilibrium needs to be elaborated in more detail. As a chiral molecule, KET exists in nature as two mirror-symmetric enantiomers, S-KET and R-KET. In the solid state KET forms a racemic compound, i.e. a crystal structure with a

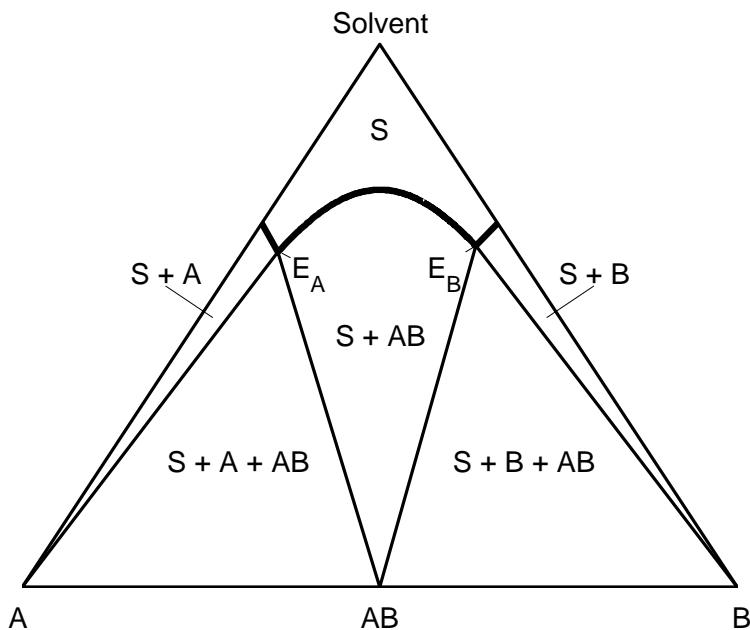


Figure 5.1: Scheme of a ternary phase diagram for the solution of a compound forming chiral system such as KET. (A) is S-KET, (B) R-KET, (AB) represents the crystalline compound RS-KET and (S) the solution. The bold line represents the solubility of the relevant solid form of KET in PLGA. Eutectic points are designated as E_A and E_B , respectively.

one to one ratio of S-KET and R-KET, which is crystallographically different from the enantiopure crystals of S-KET and R-KET (Lu et al., 2009). The characteristic symmetric behavior of such a system in solution is shown qualitatively in Figure 5.1. At temperatures below the melting point, there are three thermodynamically stable solids of KET, namely crystalline S-KET (A), crystalline R-KET (B), and the racemic crystalline compound further referred to as RS-KET (AB). Depending on the ratio of the two enantiomers in the solution, equilibrium is always established with the relevant solid. Only in the transition from one domain to the other, the solution is simultaneously in equilibrium with two solids, i.e. with one of the enantiopure crystals and with the racemic compound. The fixed composition of the solution in these transition points is referred to as the eutectic composition, and is designated with E_A and E_B in Figure 5.1.

Racemic RS-KET as well as enantiopure S-KET are commercially available, and have been used for the preparation of seed crystals. Hence, if PLGA is equilibrated with crystals of S-KET or RS-KET, solutions of enantiopure or racemic composition, respectively, are obtained. If PLGA is equilibrated with both crystalline forms simultaneously, a solution with eutectic composition is attained.

5.2 Experimental

5.2.1 Materials

Carbon dioxide (CO₂; 99.9%, from PanGas, Schlieren, Switzerland), poly(lactic-co-glycolic) acid 5050 DLG 5A (PLGA; Lakeshore Biomaterials, Birmingham AL, United States), poly(vinyl alcohol) 4-88 (PVA),

racemic Ketoprofen (RS-KET), enantiopure S-Ketoprofen (S-KET), dimethylsulfoxide (DMSO), trifluoroacetic acid (TFA), ethyl acetate (all from Sigma-Aldrich, Buchs, Switzerland), ethanol (analytical grade, Scharlau, Sentmenat, Spain), and n-hexane (Merck KGaA, Darmstadt, Germany) were used as received.

5.2.2 Emulsion Preparation and SFEE processing

The organic solutes, i.e. PLGA, RS-KET or S-KET, or specified mixtures thereof, were dissolved at 10 %wt. in ethyl acetate saturated with water. A 1 %wt. solution of PVA was prepared in water saturated with ethyl acetate. The organic and aqueous solutions were used at a weight ratio of 1:4 to form an oil-in-water (o/w) emulsion upon ultrasonication with a Branson Sonifier 450 (Skan AG, Basel, Switzerland). Using 100 ml of emulsion, a sonication time of 2 minutes was applied at maximal power output while cooling the emulsion on ice.

Directly after emulsion preparation, the organic solvent was extracted from the dispersed micelles using scCO₂ as extracting agent in the supercritical fluid extraction of emulsions (SFEE) process. The experimental setup used for SFEE experiments has been shown previously in Figure 3.2. A detailed description of the process is available in the previous sections 2.2.3 and 3.3.3.

5.2.3 Preparation of Ketoprofen crystals

Seed crystals of the racemic compound RS-KET and of enantiopure S-KET were prepared as described previously in section 4.2.3 for the case of RS-KET. The procedure for S-KET was fully analogous. The obtained fraction of large crystals of either RS-KET or S-KET was resuspended in

water and stored in 40 ml aliquots containing approximately 1 gram of crystals each, these were directly used for equilibration experiments. Figure 5.2 allows for a comparison of seed crystal morphology as compared to the corresponding raw material. It can be seen that the recrystallized material consists of larger and well-developed crystals that have a much more regular shape as compared to the raw material.

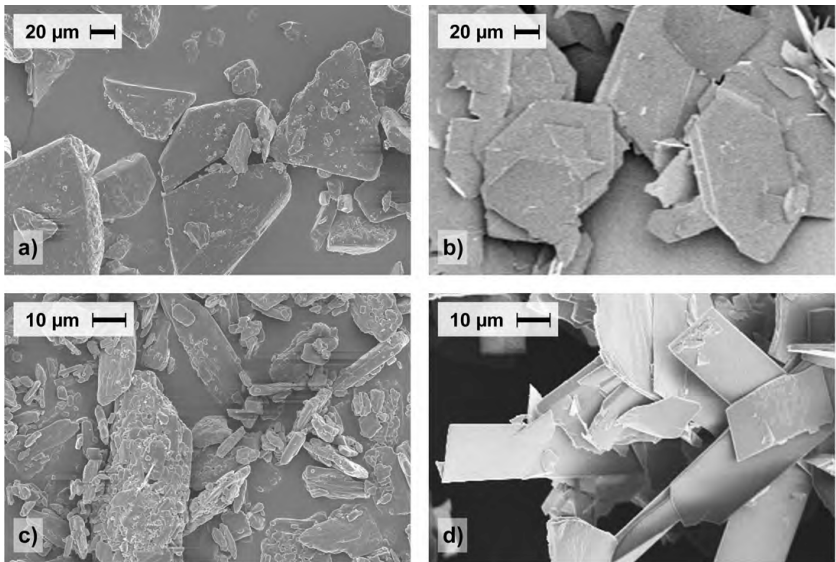


Figure 5.2: Raw materials (left) respectively recrystallized seed crystals (right) of S-KET (top) and RS-KET (bottom). The recrystallized seeds are generally larger and of more regular structure as compared to the raw material.

5.2.4 Equilibration-Impregnation Experiments

Experiments for equilibration by impregnation were carried out in a thermostated shaking water bath (GFL 1086, GFL, Burgwedel, Germany).

Pure PLGA nanoparticles were mixed and equilibrated in suspension with Ketoprofen crystals, namely with RS-KET, S-KET and also with mixtures thereof. Three 200 ml samples of PLGA product suspension, each containing about 2.5 g PLGA as suspended nanoparticles, were mixed with 40 ml aliquots containing KET crystals while being kept on ice, i.e. with RS-KET, S-KET or both RS-KET and S-KET, respectively. For equilibration, the mixed suspensions were put in the shaking water bath and kept at a constant temperature of 0°C for one day before samples were taken to analyze the amount of KET uptaken by PLGA through impregnation. The temperature was then increased to 50°C in steps of 10°C each. Samples were always taken after at least one day of equilibration at constant temperature.

5.2.5 Equilibration by De-supersaturation

Supersaturated KET-PLGA nanoparticles were produced in three separate SFEE experiments, using each 2.5 g PLGA as solute, and 0.5 g RS-KET or 0.5 g S-KET or a mixture of 0.3 g S-KET and 0.2 g RS-KET, respectively; these KET:PLGA ratios were selected according to previous experiences from impregnation experiments. Equilibration-de-supersaturation experiments were carried out in the thermostated shaking water bath. The obtained product suspensions, i.e., three 200 ml samples each containing about 3 g of supersaturated KET-PLGA co-formulation in the form of suspended particles, were mixed with 40 ml aliquots containing KET crystals while being kept at 20°C, i.e., with RS-KET or S-KET or both RS-KET and S-KET, respectively. For equilibration, the mixed suspensions were put in the shaking water bath and kept at 20°C for four days before samples were drawn to analyze the amount of KET remaining in PLGA after equilibration by de-supersaturation. The

temperature was then decreased to 10°C and 0°C. Samples were taken as specified, i.e., after at least four days of equilibration at constant temperature. Also, part of the samples were kept at constant temperature in a separate vessel, in order to monitor further concentration changes in the polymer phase during the following days.

5.2.6 Product Characterization

The isolation of equilibrated PLGA particles from the suspension of the equilibration experiment was carried out as described in section 4.2.3, i.e. using two centrifugation steps at different rotation speed. Throughout the entire process, all samples were carefully kept at the equilibration temperature of the corresponding sample. The crystalline sediment obtained from the centrifugation step was recycled to the equilibration experiment. The polymeric nanoparticles were re-suspended in pure water and subsequently freeze-dried for further analysis. SEM imaging and analysis of KET content by UV Spectroscopy were carried out as described in section 4.2.3. For calibration, five independent solutions containing 10 mg KET were analyzed as described. At a wavelength of 300 nm, a molar extinction coefficient of 1217.01 AU/(mol/l) was determined and used for the conversion of absorption units into molar concentrations. The described method, which could not distinguish between the two enantiomers of KET, was used for the determination of KET content in all samples.

Enantiomeric Composition by HPLC For PLGA samples equilibrated with both RS-KET and S-KET crystals, the enantiomeric composition was determined by High Performance Liquid Chromatography (HPLC). Liquid samples were obtained by extracting both KET enan-

tiomers from a small amount of dried product using ethanol. Enantioseparation of KET in the extract was carried out on a 4.6×250 mm chiral chromatographic column Chiralpak AD (Daicel Chemical Industries Ltd., Japan). The mobile phase was a mixture of 20% ethanol and 80% n-hexane (v/v) containing 0.01% TFA, and a flow rate of 0.7 ml/min was used. Depending on the sample concentration, amounts between 2 and 50 μ l were injected, and injections were repeated three times. Monitoring of the outlet stream by UV spectroscopy at 260 nm showed that baseline separation was successfully achieved in all cases. At the conditions of the analysis R-KET had a retention time of 7.6 min, while S-KET was the more retained species, and was eluted after 9.7 min. The enantiomeric composition in the sample was directly calculated from the two peak areas, assuming linear UV response.

Crystallinity by X-ray Powder Diffraction (XRPD) Analysis

The crystalline sediment obtained during sample preparation in the first centrifugation step was freeze-dried and investigated using XRPD in order to determine the structure of the crystalline residual.

5.3 Results and Discussion

In order to determine the influence of temperature as well as of KET chirality on the equilibrium solubility of KET in PLGA, the equilibration of amorphous PLGA nanoparticles with different crystalline forms of KET was studied in aqueous suspension. Both KET and PLGA are virtually insoluble in water, which indicates that the degree of physicochemical interaction between water and both solids is small. Hence, the presence of water is assumed to have negligible influence on the equilibrium established between KET and PLGA.

Equilibration may be achieved from initial concentrations of the PLGA phase either below or above the solubility limit. The two cases differ only with respect to the direction of KET flux. In the first case, the polymer phase is initially undersaturated, and is equilibrated by impregnation, i.e. by KET dissolving from the crystalline phase, and diffusing through the aqueous phase into the polymer matrix, until the polymer phase is saturated. In the second case, where the polymer phase is initially supersaturated, equilibration is achieved by supersaturation depletion, i.e., by KET diffusing out of the polymer matrix, through the aqueous phase until it is consumed by growth of KET crystals.

A proper combination of impregnation and de-supersaturation experiments as outlined above is a reliable way to investigate whether or not equilibrium has indeed been achieved. For example, it has been demonstrated for the case of RS-KET at ambient conditions that an equivalent level, i.e., the equilibrium solubility of KET in PLGA, is ultimately attained by following either procedure (Kluge et al., 2009c). On the other hand, if equilibrium is not reached, impregnation and de-supersaturation experiments still provide a lower and an upper bound, respectively, for the solubility of KET in PLGA.

In that sense, this work represents an extension of our previous investigation on the equilibrium between PLGA and KET, namely to temperatures in a range between 0°C and 50°C, and to a broader range of feasible KET solid states, namely to enantiopure S-KET, racemic RS-KET and a combination thereof. The work is structured as follows: first, the results of the equilibration experiments carried out by both impregnation and by de-supersaturation are presented, then experimental results are integrated in a mathematical model describing the solubility of a chiral compound in a polymeric solvent, and finally conclusions are drawn by comparing experimental results with model predictions.

5.3.1 Equilibration-Impregnation Experiments

Equilibration of PLGA by impregnation has been studied in three experiments using enantiopure S-KET, racemic RS-KET or a mixture of the two solids, respectively, and varying the temperature between 0°C and 50°C. Experiments started with initially pure PLGA nanoparticles at 0°C, and the temperature was increased in steps of 10°C. Assuming that the equilibrium solubility increases with temperature, this means that at each temperature level, PLGA particles are initially undersaturated, and that equilibration is always attained by impregnation of KET into PLGA. A previous study has shown that impregnation at ambient temperatures leads to rapid equilibration (Kluge et al., 2009c), hence a relatively short impregnation time of one day was used.

Experimental results are summarized in Table 5.1, and illustrated in Figures 5.3 to 5.6. It can be readily observed that in all three experiments, the level of KET impregnated into PLGA increases with increasing temperature, starting from levels around 1 wt.% at 0°C, and reaching a peak value of above 40 wt.% at 50°C. At each temperature level, the concentration of KET impregnated into PLGA is lower for equilibration with RS-KET, significantly higher for equilibration with S-KET, and the highest for simultaneous equilibration with both crystalline species. For samples that had been equilibrated simultaneously with RS-KET and S-KET, also the eutectic composition has been determined at each temperature level. The composition was found to remain rather constant, i.e. with S-KET at around 93% and R-KET at around 7%, except for the samples at 0°C and 50°C, which exhibit a lower content of S-KET.

During storage at 50°C it was observed that the crystalline residual of S-KET disappeared completely, hence equilibrium could no longer be established since solid S-KET had been completely consumed through

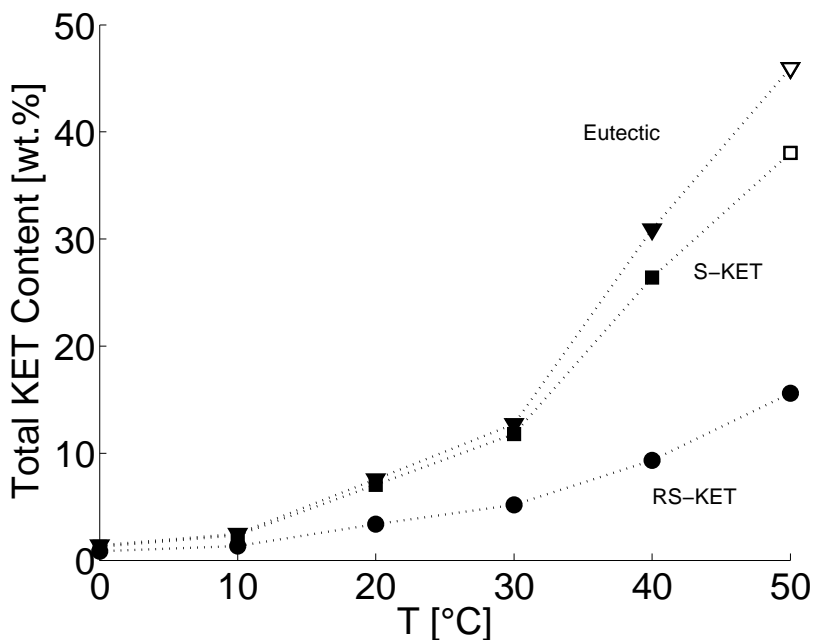


Figure 5.3: Total KET content (sum of both enantiomers) of PLGA equilibrated at different temperatures with crystals of RS-KET (●), S-KET (■) and with both crystal forms together (▲). Open symbols: experiments at 50°C where equilibrium has not been reached due to complete dissolution of crystals.

dissolution and impregnation. The situation was different for RS-KET, where crystals were still present, thus preserving the equilibrium. In the case of simultaneous equilibration with S-KET and RS-KET, XRPD analysis of the crystalline residual showed that S-KET crystals had completely dissolved whereas RS-KET was still present. Hence, PLGA was equilibrated with RS-KET, but not with S-KET, and indeed the corresponding sample is characterized by a lower content of S-KET, i.e.

around 89%, as compared to the other samples exhibiting the eutectic composition of roughly 93%. In Figure 5.3, the two experiments at 50°C where equilibrium was not reached are indicated by open symbols, and they are obviously not considered in the further analysis and discussion of KET-PLGA equilibrium. Nevertheless, the KET loadings measured at 50°C are clearly higher as compared to those determined at 40°C, thus proving that at 40°C the amounts of crystalline KET present were still sufficient to enable equilibration in all impregnation experiments.

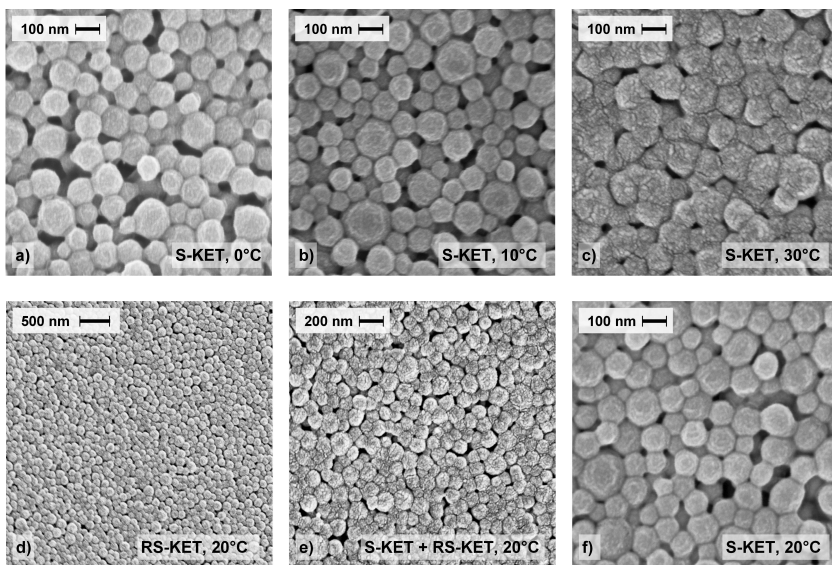


Figure 5.4: a) - c): Co-formulation particles obtained at different temperature stages by impregnation of PLGA with S-KET. d) - f): Co-formulation particles obtained at 20°C by impregnation of PLGA using different crystalline morphologies of KET.

Co-formulation particles obtained at different temperature levels by impregnation of PLGA with S-KET are shown in Figure 5.4a - c, whereas

particles obtained at 20°C by impregnation of PLGA using the different crystalline morphologies of KET available are shown in Figure 5.4d - f. In agreement with previous results (Kluge et al., 2009c), it is noticed that particles exhibiting a high KET content, such as those displayed in Figure 5.4c, appear generally softer and more blurred, and are also characterized by a rougher surface. Otherwise, polymeric particles exhibit in all cases a very similar morphology. Co-formulations equilibrated at 40°C and 50°C were observed to recrystallize promptly upon storage at ambient conditions, obviously because they were highly supersaturated at room temperature. Product properties such as the overall KET content and the enantiomeric composition of the samples were not affected by recrystallization, and could still be determined. Indeed, these recrystallization events underline the significance of determining equilibrium data for the manufacturing of long-term stable drug-polymer composites.

5.3.2 Equilibration by De-supersaturation

Equilibration of PLGA by de-supersaturation has been studied in three experiments using enantiopure S-KET, racemic RS-KET or a mixture of the two solids, respectively, and by investigating the temperature range between 0°C and 20°C. Experiments were initiated by mixing crystals and nanoparticles of previously prepared KET-PLGA composites at 20°C. After at least four days, the level of KET in PLGA was determined and subsequently the equilibration temperature was decreased in steps of 10°C. Thus, each experiment at a new temperature starts with PLGA particles that are initially supersaturated, hence equilibration is always achieved by diffusion of KET out of the supersaturated PLGA particles. A previous one-week study investigating the equili-

Table 5.1: Overview of the results of product analysis. Weight fractions given in roman numbers are assumed to represent equilibrium data, whereas weight fractions in *italic* do not correspond to equilibrium state, as explained in the text.

Temp.	Equilib.	Time	RS-KET	S-KET	RS-KET + S-KET:	Images
°C	[days]	[wt.%]	[wt.%]	[wt.%]	[wt.%]	[% S-KET]
Impregnation:						
Initial	-	<i>0.00</i>	<i>0.00</i>	<i>0.00</i>	<i>0.00</i>	N.A.
0	1	<i>0.83</i>	<i>1.24</i>	<i>1.37</i>	<i>1.37</i>	89.8
10	1	<i>1.29</i>	<i>2.27</i>	<i>2.42</i>	<i>2.42</i>	93.2
20	1	3.30	6.88	7.41	7.41	93.6
30	1	5.07	11.53	12.43	12.43	93.5
40	1	9.13	25.83	30.24	30.24	92.6
50	1	15.25	<i>37.22</i>	<i>44.96</i>	<i>44.96</i>	89.3
De-supersaturation:						
Initial	-	<i>11.12</i>	<i>10.03</i>	<i>11.62</i>	<i>11.62</i>	81.6
20	4	3.63	6.83	7.06	7.06	-
	8	3.44	6.56	6.80	6.80	94.1
10	4	<i>3.20</i>	<i>5.15</i>	<i>5.93</i>	<i>5.93</i>	-
	21	<i>3.21</i>	<i>5.09</i>	<i>5.97</i>	<i>5.97</i>	94.2
0	7	<i>3.10</i>	<i>5.08</i>	<i>5.91</i>	<i>5.91</i>	-
	14	<i>3.12</i>	<i>5.08</i>	<i>5.85</i>	<i>5.85</i>	94.0
	30	<i>3.04</i>	<i>5.04</i>	<i>5.77</i>	<i>5.77</i>	-

bration of PLGA and KET at ambient temperatures has shown that de-supersaturation is significantly slower as compared to impregnation (Kluge et al., 2009c). Based on experiences from that study, an equilibration time of at least 4 days was selected, and part of the samples was kept at constant temperature in a separate vessel, in order to check and exclude further concentration changes.

Experimental results are summarized in Table 5.1, and illustrated in Figure 5.5. The level of KET in the polymeric nanoparticles is initially above 10 wt.% in all three experiments, and therefore supersaturated with respect to the solubilities expected at the initial temperature of 20°C. Thus, equilibration at 20°C leads to a considerable decline in KET content in all three experiments, and the KET levels measured after four days of equilibration are indeed very close to the levels attained by impregnation at the same temperature. This indicates that at 20°C, both impregnation and de-supersaturation lead to complete equilibration, and measured concentrations correspond to the solubility of KET in PLGA that is attained in equilibrium with the relevant KET solid states. Since equilibration depends on temperature-dependent kinetic phenomena such as diffusion and crystal dissolution and growth, respectively, i.e., processes that are generally faster at elevated temperatures, it may be concluded that de-supersaturation and impregnation lead to complete equilibration also at temperatures above 20°C. In further de-supersaturation experiments carried out at lower temperatures, i.e., 10°C and 0°C, only small decreases in the KET content have been observed, as shown in Figure 5.5. In all cases, the measured KET contents remained clearly above the concentration levels obtained in impregnation experiments at the same temperature. As shown in Table 5.1, even changes in the drug content upon longer equilibration times are negligibly small as compared to the gap remaining between the out-

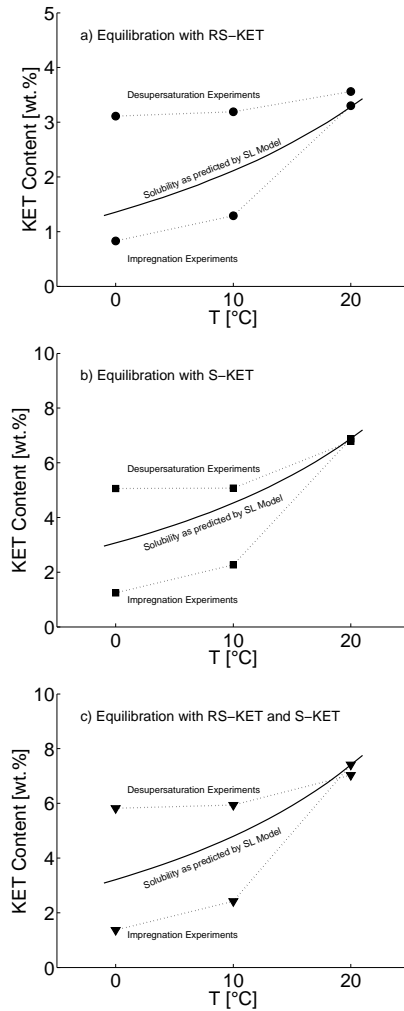


Figure 5.5: Experimental data points obtained by equilibration through impregnation and de-supersaturation using a) crystalline RS-KET, b) crystalline S-KET and c) a mixture thereof at temperatures of 0°C, 10°C and 20°C as compared to the corresponding liquidus lines obtained by extrapolation of the SL-model.

come of de-supersaturation and impregnation experiments. Therefore it is concluded that either impregnation or de-supersaturation - or presumably both - do not lead to complete equilibration at lower temperatures, since the kinetics of equilibration are too slow at 10°C and below. Also, it is worth mentioning that the rather small variance, observed, e.g., in the evaluation of 0°C samples taken at different points in time, suggests that the accuracy of the selected experimental methods is high enough to detect even small concentration changes.

Summarizing, de-supersaturation experiments yielded equilibrium data at 20°C only. From the major disagreement between the outcome of impregnation and de-supersaturation experiments at 10°C and 0°C, it is concluded that these measurements do not represent equilibrium data, but should be seen as lower and upper bounds, respectively, for the corresponding equilibrium states.

5.3.3 Modeling Equilibrium between KET and PLGA

In this section, a model is introduced to describe the equilibria of ketoprofen, as a compound-forming chiral system, and PLGA, as a polymeric solvent. The description of equilibrium between solid KET and amorphous, polymeric PLGA includes three different equilibrium situations, namely equilibrium of the polymer either with the racemic solid, RS-KET, or with the enantiopure solid, S-KET, or with both solids at the same time. In the following section, the species S-KET, R-KET and PLGA are indicated by subscripts 1, 2 and 3, respectively. Subscripts *RS* and *S* refer to the two crystalline forms RS-KET and S-KET, respectively.

Table 5.2: Physico-chemical and material properties of KET and PLGA and pure component parameters used in the Sanchez-Lacombe Equation of State.

Property	Units	RS-KET	S-KET	PLGA	Source
MW number av.	(g/mol)	254.3	254.3	33 400	(Dwan'Isa et al., 2007) / supplier
T^m	(K)	367.7	348.6	-	(Lu and Ching, 2004)
T^G	(K)	270.2	270.2	319.4	(Di Martino et al., 2004; Blasi et al., 2007) / sup- plier
ΔH^f	(kJ/mol)	27.38	22.79	-	(Lu and Ching, 2004)
Parameter	Units	S-KET	R-KET	PLGA	Source
P^*	(MPa)	662.3	662.3	572.7	(Liu and Tomasko, 2007; Coimbra et al., 2006; Gauter and Heidemann, 2000)
T^*	(K)	806.0	806.0	649.6	(Liu and Tomasko, 2007; Coimbra et al., 2006; Gauter and Heidemann, 2000)
ρ^*	(kg/m ³)	1169	1169	1452	(Liu and Tomasko, 2007; Coimbra et al., 2006; Gauter and Heidemann, 2000)

Equilibrium of PLGA with an enantiopure solute such as S-KET at a temperature T may be described using the Schröder-van Laar Equation (Lorenz and Seidel-Morgenstern, 2002; Worlitschek et al., 2004):

$$\ln(a_1^s) = -\frac{\Delta H_S^f}{RT_S^m} \left(\frac{T_S^m}{T} - 1 \right) \quad (5.1)$$

where T_S^m is the melting temperature of S-KET and ΔH_S^f is its enthalpy of fusion; a_1^s is the activity of solute S-KET in a polymer solution that is in equilibrium with crystalline S-KET. On the other hand, equilibrium

between solid racemic RS-KET and a ternary solution of both enantiomers in PLGA is described by the Prigogine-Defay Equation (Lorenz and Seidel-Morgenstern, 2002; Worlitschek et al., 2004):

$$\frac{1}{2} \ln(4a_1^s a_2^s) = -\frac{\Delta H_{RS}^f}{RT_{RS}^m} \left(\frac{T_{RS}^m}{T} - 1 \right) \quad (5.2)$$

where T_{RS}^m is the melting temperature and ΔH_{RS}^f the enthalpy of fusion of the racemic compound RS-KET; a_1^s and a_2^s are the activities of S-KET and R-KET, respectively, in a polymer solution that is in equilibrium with RS-KET. Thus, the right-hand sides of equations 5.1 and 5.2 are formally comparable, and since they contain only solute parameters they can be calculated using the material properties of either S-KET or RS-KET as given in Table 5.2. The activities are functions of temperature and composition, and are described using the Sanchez-Lacombe (SL) equation of state. This equation is based on a lattice fluid theory, and has found a broad use in the modeling of phase equilibria involving polymers (Pini et al., 2008). The SL equation of state is given by (McHugh and Krukonis, 1994):

$$\tilde{\rho}^2 + \tilde{P} + \tilde{T} \left[\ln(1 - \tilde{\rho}) + \tilde{\rho} \left(1 - \frac{1}{r^0} \right) \right] = 0 \quad (5.3)$$

Here, $\tilde{\rho}$, \tilde{P} and \tilde{T} are the reduced density, pressure and temperature, respectively. The variables are reduced using the so-called characteristic quantities:

$$\tilde{\rho} = \frac{\rho}{\rho^*} = \frac{\rho r^0 v^*}{MW}, \quad \tilde{P} = \frac{P}{P^*} = \frac{P v^*}{\epsilon^*}, \quad \tilde{T} = \frac{T}{T^*} = \frac{TR}{\epsilon^*} \quad (5.4)$$

where ρ^* , P^* and T^* are the characteristic density, pressure and temperature. These are in turn functions of the Sanchez-Lacombe lattice

parameters, namely of v^* , the volume of one mole of lattice sites, r^0 , the number of lattice sites per molecule, and ϵ^* , the interaction energy per lattice site. R is the ideal gas constant and M_W is the molecular weight, i.e. the number average molecular weight in the case of polymers. Hence, three of the characteristic quantities are needed to completely characterize a pure fluid. For PLGA 5050, SL characteristic parameters have been reported previously (Liu and Tomasko, 2007), and for KET, they may be estimated from the critical parameters (Coimbra et al., 2006) using a set of equations proposed elsewhere (Gauter and Heidemann, 2000). Numerical values of the pure component characteristic parameters used in this study are reported in Table 5.2.

Mixing rules according to the so-called van der Waals 1 theory have been applied in order to extend these equations to the case of a mixture (McHugh and Krukoni, 1994; Prausnitz et al., 1986). A first mixing rule describes the volume of lattice sites in a ternary mixture:

$$v^* = \sum_{i=1}^3 \sum_{j=1}^3 \Phi_i \Phi_j v_{ij}^*, \quad v_{ij}^* = \frac{v_i^* + v_j^*}{2} (1 - \eta_{ij}) \quad (5.5)$$

where i and j are component indices and the parameters η_{ij} correct for deviations from the arithmetic mean. We assume that there is no such deviation for mixing of the two enantiomers (1 and 2), and that it is the same for mixing of the KET enantiomers (1 or 2) with PLGA (3):

$$\eta_{12} = \eta_{21} = 0, \quad \eta_{13} = \eta_{23} = \eta_{31} = \eta_{32}. \quad (5.6)$$

The variable Φ_i is the volume fraction of the i th component in the mix-

ture and is related to its weight fraction w_i :

$$\Phi_i = \frac{\frac{w_i}{\rho_i^* v_i^*}}{\sum_{j=1}^3 \frac{w_j}{\rho_j^* v_j^*}} \quad (5.7)$$

A second mixing rule defines the characteristic interaction energy per lattice site, ϵ^* , for the case of a mixture:

$$\epsilon^* = \frac{1}{v^*} \sum_{i=1}^3 \sum_{j=1}^3 \Phi_i \Phi_j \epsilon_{ij}^* v_{ij}^*, \quad \epsilon_{ij}^* = \sqrt{\epsilon_i^* \epsilon_j^*} (1 - k_{ij}) \quad (5.8)$$

where k_{ij} is a binary interaction parameter. Here, we assume interactions both between the two enantiomers (1 and 2) and between either of the enantiomers (1 or 2) and achiral PLGA (3):

$$k_{12} = k_{21}, \quad k_{13} = k_{23} = k_{31} = k_{32}. \quad (5.9)$$

Finally, the number of sites occupied by one mole of the mixture, r , is calculated using the third mixing rule:

$$\frac{1}{r} = \sum_{i=1}^3 \frac{\Phi_i}{r_i}, \quad r_i = \frac{r_i^0 v_i^*}{v^*} \quad (5.10)$$

Hence the number of lattice sites occupied by one mole of component i in the mixture, r_i , differs from the one in the pure fluid, r_i^0 .

At equilibrium, temperature, pressure and the chemical potentials of all species are equal in both phases. Using the set of mixing rules presented

above, the chemical potential of component i in the mixture is:

$$\begin{aligned} \mu_i = RT & \left[\ln \Phi_i + \left(1 - \frac{r_i}{r} \right) \right] \quad (5.11) \\ & + r_i \left\{ -\tilde{\rho} \left[\frac{2}{v^*} \left(\sum_{j=1}^3 \Phi_j \epsilon_{ij}^* v_{ij}^* - \epsilon^* \sum_{j=1}^3 \Phi_j v_{ij}^* \right) + \epsilon^* \right] \right\} \\ & + r_i \left\{ \frac{RT}{\tilde{\rho}} \left[(1 - \tilde{\rho}) \ln(1 - \tilde{\rho}) + \frac{\tilde{\rho}}{r_i} \ln \tilde{\rho} \right] + \frac{P}{\tilde{\rho}} \left[2 \sum_{j=1}^3 (\Phi_j v_{ij}^*) - v^* \right] \right\} \end{aligned}$$

For KET, the standard chemical potential of the pure subcooled liquid state is obtained by solving Equation 5.11 for pure species 1:

$$\mu_1^\ominus = \mu_2^\ominus = r_1^0 \left\{ -\tilde{\rho}_1 \epsilon_1^* + \frac{RT}{\tilde{\rho}_1} \left[(1 - \tilde{\rho}_1) \ln(1 - \tilde{\rho}_1) + \frac{\tilde{\rho}_1}{r_1^0} \ln \tilde{\rho}_1 \right] + \frac{P}{\tilde{\rho}_1} v_1^* \right\} \quad (5.12)$$

Using Equations 5.11 and 5.12, the activities of species 1 and 2 in the mixture can be calculated:

$$\ln a_1 = \frac{1}{RT} (\mu_1 - \mu_1^\ominus), \quad \ln a_2 = \frac{1}{RT} (\mu_2 - \mu_2^\ominus) \quad (5.13)$$

5.3.4 Results

At fixed temperature, there are three independent parameters that need to be assigned to characterize equilibrium in the ternary system of the two enantiomers of KET and the polymeric solvent PLGA, namely η_{13} , k_{12} and k_{13} . As it may be expected for a system containing polar species, these mixture parameters are dependent on temperature (McHugh and Krukoni, 1994), and are therefore expressed using linear functions of T :

$$\eta_{13} = c_1 T + c_2, \quad k_{12} = c_3 T + c_4, \quad k_{13} = c_5 T + c_6. \quad (5.14)$$

For the experiments where equilibrium has been reached (see Table 5.1), the activities as given by Equation 5.13 should be equal to the activities in equilibrium, as given by Equations 5.1 and 5.2. For this set of experiments, the coefficients c_1 to c_6 in (5.14) have been obtained by optimization using a Nelder-Mead Simplex algorithm, solving the set of equations 5.1-5.14, further called the SL model, while minimizing an objective function for which the following contribution has been considered at each temperature level:

$$\begin{aligned} \Psi(T) = & \left(\frac{\ln a_1 - \ln (a_1^s)}{\ln (a_1^s)} \right)^2 \Big|_{S-KET} \\ & + \left(\frac{\ln (4a_1 a_2) - \ln (4a_1^s a_2^s)}{\ln (4a_1^s a_2^s)} \right)^2 \Big|_{RS-KET} \\ & + \frac{1}{2} \left[\left(\frac{\ln a_1 - \ln (a_1^s)}{\ln (a_1^s)} \right)^2 + \left(\frac{\ln (4a_1 a_2) - \ln (4a_1^s a_2^s)}{\ln (4a_1^s a_2^s)} \right)^2 \right] \Big|_{Eutectic} \end{aligned} \quad (5.15)$$

The numerical values of the coefficients obtained upon optimization are:

$$\begin{aligned} c_1 &= 1.085 \times 10^{-3} K^{-1}, c_2 = -0.358; \\ c_3 &= 6.86 \times 10^{-4} K^{-1}, c_4 = -0.220; \\ c_5 &= -4.98 \times 10^{-5} K^{-1}, c_6 = 0.0525. \end{aligned} \quad (5.16)$$

Using these coefficients and assuming equilibrium between the polymer solution and the relevant solid phase, i.e., $a_1 = a_1^s$ and $a_2 = a_2^s$, the SL model has been used to calculate the range of compositions corresponding to the liquidus line of the polymer solution in the range of 20°C to 40°C. These are shown in Figure 5.6 together with experimental data points obtained at these temperatures. It can be seen that the model is able to describe the effect of temperature rather well, and also the

influence of chirality on the solubility of KET in PLGA.

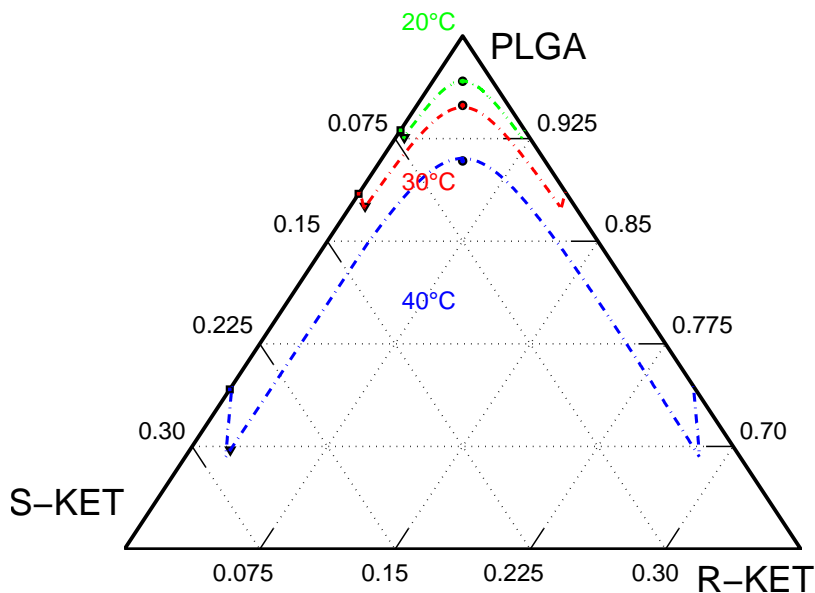


Figure 5.6: Comparison of experimental data points obtained by impregnation at 20°C (green), 30°C (red) and 40°C (blue) to the liquidus lines obtained from the SL model at these temperatures.

An extrapolation of the model to lower temperatures of 0° and 10°C is shown in Figure 5.5, together with the corresponding data points obtained by impregnation and de-supersaturation experiments. It can be seen that at these conditions the model predictions are always above the experimental values obtained by impregnation, and below the levels obtained by de-supersaturation. This is in agreement with our previous findings, namely that the results from impregnation and de-supersaturation experiments at 10°C and 0°C represent lower or

upper bounds for the corresponding equilibrium states rather than equilibrium states, respectively. We conclude that the model can also be used in a predictive manner to estimate equilibrium under conditions where its experimental determination is difficult.

5.3.5 Equilibration and Glass Transition Temperature

A major remaining question is why equilibration is much slower below 10°C as compared to temperatures above 20°C. This may be explained by looking at the interplay of the operating conditions and of the glass transition temperature T^G that is expected for the polymeric particles.

Upon vitrification, i.e., the transformation of the polymer from the rubbery liquid state to the glassy state induced by cooling below the glass transition temperature, foreign molecules trapped in the polymer matrix lose their mobility, thus leading to a decrease in their diffusivity by several orders of magnitude (Foss et al., 2009). Hence the glass transition is expected to have a strong influence on the kinetics of equilibration, and might explain the observed behavior. Now pure PLGA has a T^G around 45°C, i.e. far above the observed transition. However, there are two additional effects having a diminishing influence on T^G . First, PLGA is not pure, but contains KET that is dissolved at a molecular level. The effect of KET on the glass transition of PLGA has been investigated by Blasi et al. (Blasi et al., 2007), and a decrease of roughly 0.83 and 1.49°C per wt.% KET has been determined experimentally using two different types of PLGA, respectively. Secondly, equilibration is carried out in aqueous suspension, and also the presence of water has a diminishing effect on T^G that has been assessed experimentally by Blasi et al. (Blasi et al., 2005). Depending on the duration and temperature of incubation

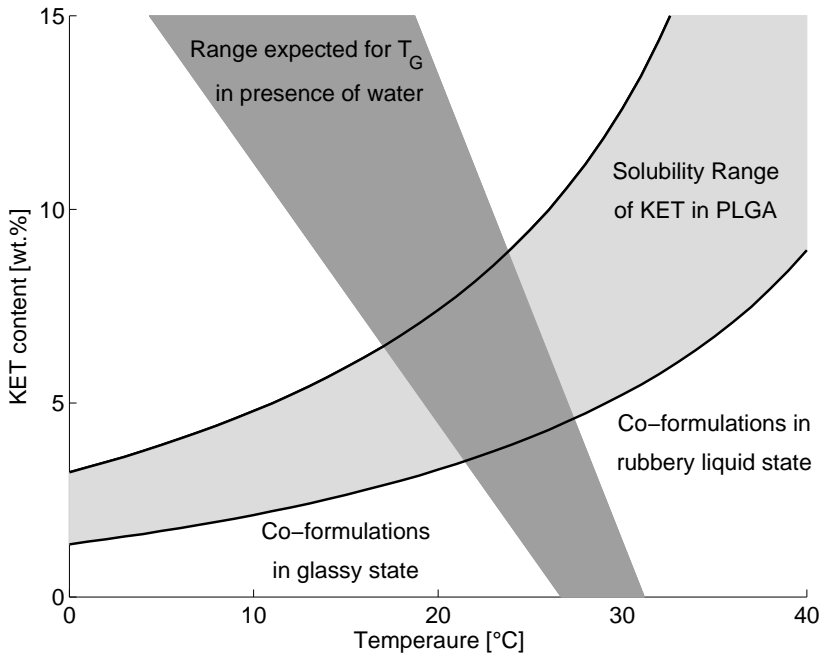


Figure 5.7: Solubility range of KET in PLGA as calculated using the SL-model (light grey zone) together with the expected range of the glass transition temperature of KET-PLGA composites suspended in water as a function of the KET content (dark grey zone). The glass transition separates the region of glass state (left) from the region of rubbery liquid state (right).

in water, wet PLGA samples exhibited glass transition temperatures in the range between 26.7 and 32.7°C, i.e., significantly below the T^G observed for dry PLGA (45°C). Assuming that both effects are additive, the expected T^G of KET-PLGA co-formulations is shown in Figure 5.7 as a function of the KET content, together with the range of possible temperature dependent equilibrium concentrations of KET in PLGA as

determined from the SL model presented in section 5.3.3.

Figure 5.7 illustrates how the equilibrated polymer phase is clearly in the rubbery liquid state for temperatures of 30°C and above, leading to facilitated diffusion of KET molecules into the polymer matrix and to rapid equilibration of the polymer phase with its surroundings. On the other hand, if equilibration is carried out at 10°C or below, the polymer phase is clearly in the glassy state, and consequently the movement of KET molecules within the polymer matrix is largely inhibited so as the polymer phase does not easily equilibrate with its surrounding. Judging from Figure 5.7, the situation is less clear for equilibration at 20°C, leading to compositions that are located in the transition region. However at 20°C, i.e. ambient conditions, it is evident from the results presented in Chapter 4 that complete equilibration is achieved during the selected experimental times by impregnation as well as by de-supersaturation.

5.4 Conclusion

The solubility of the chiral non-steroidal anti-inflammatory drug ketoprofen in PLGA, i.e. one of the pharmaceutically most relevant polymer systems, has been determined experimentally and modeled using standard thermodynamic methods. The presented results are interesting from a fundamental point of view, since equilibrium data involving a chiral crystalline drug and a bio-compatible polymer have been determined in detail and presented for the first time. Further, the present findings allow for a number of practically relevant conclusions with respect to potential applications of PLGA as drug delivery system for KET, such as the level of drug that may be loaded into the polymer to achieve long-term stable co-formulations with acceptable shelf-life. Further, it has

been demonstrated that the capacity of PLGA for S-KET is more than twice as high as compared to the racemic compound, RS-KET. Considering that the pharmaceutical activity of KET resides in S-KET whereas R-KET is inactive (Lu et al., 2009), the application of enantiopure S-KET allows stable drug loadings that are more than four times higher than the loadings achieved with racemic RS-KET. The presented approach to determine drug-polymer equilibrium seems also suitable for the comparison and the evaluation of different polymers with respect to their suitability as drug delivery systems for KET.

Experimental findings show that drug-polymer equilibrium is temperature dependent, and may be described using the Sanchez-Lacombe Equation of State, i.e. a thermodynamic standard model that is typically applied in the description of equilibria involving polymers. It has been demonstrated that equilibration is fast for temperatures above the glass transition temperature of the polymer phase, but becomes very slow if the temperature of the equilibration process is lowered below T^G . Consequently, the experimental investigation of equilibrium for a polymer in glassy state seems to be more difficult as compared to a polymer in liquid-rubbery state. There are two conclusions about how to handle this problem. First, if a model is available, equilibrium for temperatures below T^G may be estimated by extrapolation of the model, as is shown in Figure 5.5. Second, the experimental investigation of equilibrium may be extended and facilitated by lowering the T^G of PLGA, which can be achieved for instance by applying a high-pressure CO₂ atmosphere (Pini et al., 2008). It is also interesting whether or not the presence of an additional T^G -lowering component in the system, such as water in this case, has a strong influence on the investigated equilibrium.

5.5 Nomenclature

Roman Symbols

a_i	Activity of component i in the polymer solution	[-]
$c_1 - c_6$	Constant coefficients	as specified
ΔH^f	Enthalpy of fusion	[J/mol]
k_{ij}	Binary interaction parameter	[-]
P	Pressure	[bar]
r^0	Number of lattice sites per molecule	[-]
R	Ideal gas constant	[J/(mol K)]
T	Temperature	[K]
T^G, T^m	Glass transition resp. melting temperature	[K]
v	Lattice site volume	[m ³ /mol]
w_i	Weight fraction of component i	[-]

Greek Symbols

ϵ	mer-mer interaction energy	[J/mol]
η_{ij}	Binary volumetric interaction parameter	[-]
μ_i	Chemical potential of component i	[J/mol]
ρ	Density	[g/cm ³]
Φ_i	Volume fraction of component i	[-]

Subscripts and Superscripts

S	S-KET	[-]
RS	RS-KET	[-]
i, j	Generic component	[-]
*	Characteristic quantity	[-]
~	Reduced component	[-]

Chapter 6

Design of biocompatible magnetite-PLGA nano-composites using SFEE ¹

6.1 Introduction

Biocompatible polymer nanoparticles composed of biodegradable polymers such as polylactic acid (PLA), poly(lactic-co-glycolic)acid (PLGA) and poly(ϵ -caprolactone) (PCL) are drawing a considerable interest in the scientific community because they can be used in medicine as biodegradable support materials and drug delivery vehicles (Musyanovych et al., 2008; Niwa et al., 1994; Coulembier et al., 2006; Anderson and Shive, 1997). The advantage of these particles is their capability of encapsulating drug molecules inside them, so that they can be released in the body (Niwa et al., 1994; Soppimath et al.,

¹The work in this chapter has been carried out in co-operation with Marco Furlan and Marco Lattuada (Institute for Chemical and Bioengineering) and has been published as Furlan et al. (2010).

2001; Anderson and Shive, 1997; Hans and Lowman, 2002; Panyam and Labhasetwar, 2003) as the polymer matrix progressively degrades. By tuning the composition and molecular weight of the biocompatible polymer matrix, it is possible to control the rate of drug release inside the body (Anderson and Shive, 1997). The effectiveness of such particles can be further enhanced by encapsulating inside them another material, which imparts an additional functionality. One particularly interesting material is magnetite, especially in the form of magnetite nanocrystals, which are already used in diagnostic applications as contrast agent in magnetic resonance imaging (MRI) (Gupta and Gupta, 2005; Neuberger et al., 2004). Not only can magnetic nanocrystals be accumulated in a specific region of a body through the application of an external magnetic field, but they can also be used to locally increase the temperature of the tissue where they are accumulated, so as to attack cancer cells by hyperthermia, for example. By combining the biodegradability of the aforementioned polyester particles with the superparamagnetic properties of magnetite nanocrystals one can prepare a magnetically responsive drug delivery system (Asmatulu et al., 2005; Yang et al., 2006; Neuberger et al., 2004; Jurgons et al., 2006; Koneracka et al., 2007; Liu et al., 2008; Dobson, 2006) which can be simultaneously used for diagnostic applications. The superparamagnetic properties conferred by magnetic nanocrystals encapsulated into biodegradable particles allow them to be accumulated in a specific part of the body by applying an external magnetic field and release there a previously loaded active pharmaceutical ingredient (Dobson, 2006; Jurgons et al., 2006; Gupta and Gupta, 2005; Yang et al., 2006; Asmatulu et al., 2005).

In the last thirty years, tens of recipes for the preparation of magnetite nanocrystals have been published in the literature (Massart, 1981; Kang et al., 1996; Sun and Zeng, 2002; Kim et al., 2003; Woo et al., 2004; Teja

and Koh, 2009; Wan et al., 2007). They can be grouped into two main categories: the coprecipitation method, pioneered by Massart (Massart, 1981; Kang et al., 1996; Kim et al., 2003), and high temperature routes (Sun et al., 2004; Wan et al., 2007). The main differences between the two methods are that high temperatures methods permit a much better control of particle size and size distribution, while the coprecipitation method allows one to produce larger quantities of magnetite at lower cost and in shorter time.

In order to have a better control of the release of the hydrophobic drug and of the magnetic properties of the polymer-magnetite composite nanoparticles, it is very important to prepare them with uniform size, controlled size distribution and high magnetite nanocrystals content (Moghimi et al., 2001). In order to have homogeneous degradation between the nanoparticles all the polymer chains should have ideally the same properties, *i.e.* molecular weight and, in the case of a copolymer, composition. This situation is very difficult to achieve when the polymer is formed after the encapsulation, as it happens for example for polymers prepared via miniemulsion free radical polymerization. Since biodegradable polymers are mainly polyesters, which cannot be easily prepared by emulsion polymerization, one needs to use a preformed polymer. The advantage of preformed polymers, such as commercially available PLGA, is that their properties can be well controlled during their preparation.

For many drug-delivery applications it is essential to prepare nanoparticles with controlled size and morphology. This can be achieved using different methods, such as solvent extraction, solvent diffusion and nanoprecipitation (Musyanovych et al., 2008). Not surprisingly, the first two aforementioned processes are based on the preparation of emulsions. Since single particles are directly formed out of the emulsifier-stabilized droplets, their size may be well controlled during the emulsification step.

Therefore, particles produced from emulsions are typically very uniform in size. Furthermore, they are characterized by a low degree of agglomeration, since the emulsifier stabilizes the droplets throughout the process.

However, solvent removal, especially in the case of solvent extraction method, is a challenging task. There are different methods for extracting the solvent, such as dialysis, evaporation, and supercritical CO₂ solvent extraction. Supercritical fluid extraction offers a high potential in the field of particle formation, since it leads to pure and solvent-free products while operating at mild temperatures. These advantages are especially promising for the manufacturing of polymeric particles (Yeo and Kiran, 2005). Due to their disordered amorphous structure, polymeric particles are prone to retain embedded solvent residuals that are otherwise difficult to remove, especially if manufacturing is constrained to mild temperatures, and could be potentially toxic. Furthermore, supercritical fluid processes offer certain degrees of freedom with respect to setup and operating conditions. Overall, it has been thoroughly demonstrated how different operating conditions may be exploited to tune size and shape of the product particles (Fusaro et al., 2009; Perez de Diego et al., 2005). In this context, processes employing supercritical CO₂ as antisolvent have been used to manufacture micro-particles of PLGA and of poly-L-lactic acid, PLLA (Perez de Diego et al., 2005; Debenedetti et al., 1993; Falk et al., 1997; Falk and Randolph, 1998; Ghaderi et al., 1999, 2000), and also magnetite-PLGA composites (Lam et al., 2008; Chattopadhyay and Gupta, 2002).

The supercritical fluid extraction method, when combined with the preparation of particles via an emulsion process, is called supercritical fluid extraction of emulsions (SFEE). This process has in fact been investigated mainly for producing PLGA particles and drug - PLGA composites (Chattopadhyay et al., 2006; Della Porta and Reverchon,

2008). A more systematic evaluation of this process, both with respect to alternative manufacturing techniques and to possible ways of achieving drug encapsulation, has been presented previously (Kluge et al., 2009b,c).

In this work we have applied the SFEE process to prepare well controlled magnetite-PLGA composite nanoparticles. Magnetite nanocrystals stabilized by ricinoleic acid have been first prepared using Massart's coprecipitations method, and then dispersed with pre-formed PLGA in dichloromethane. After emulsification by sonication of the oil phase in an aqueous solution containing polyvinyl alcohol (PVA) as stabilizer, a stable emulsion of droplets containing magnetite, PLGA and dichloromethane was obtained. The solvent extraction was performed via SFEE leading to a stable and solvent-free suspension of polymer-magnetite nanoparticles. Since controlling the particle size and size distribution is of paramount importance for the design of drug delivery systems, we have focused our study on the influence of some important parameters that affect these crucial product properties. In particular, the effects of sonication time, surfactant amount and magnetite amount have been investigated with respect to their impact on the particle morphology.

6.2 Materials and Methods

6.2.1 Materials

Chemicals were obtained from the following suppliers: castor oil (refined, puris.) from Riedel-de Haën, poly(lactic-co-glycolic) acid (PLGA) (Resomer RG 503) from Boehringer Ingelheim, polyvinyl alcohol 4-88,

iron(II)chloride tetrahydrate ($\geq 98\%$), hydrochloric acid (37% fuming), acetone, toluene and ether from Fluka, iron(III)chloride hexahydrate (99+%, extra pure) and dichloromethane from Acros Organics, absolute ethanol from Scharlau Chemie S.A., potassium hydroxide from Synopharm, 2-ethylhexanoic acid tin(II) salt (95%) and tetrahydrofuran from Sigma Aldrich, crystalline lactic acid from ABCR, lactide from PURAC, magnesium sulfate anhydrous (99.5% min) from Alfa Aesar, methanol (HPLC grade) from Fisher Scientific, ethyl acetate from J.T. Baker and carbon dioxide 99.9% from PanGas. If not specified otherwise, all chemicals were of analytical grade and were used as obtained.

6.2.2 Preparation of magnetite nanocrystals

Synthesis of Ricinoleic Acid

The synthesis of ricinoleic acid from castor oil is a slight modification of a recipe described in the literature earlier (Vaisman et al., 2008). In a typical experiment 10 g KOH and 50 g of castor oil were dissolved in 100 ml of Ethanol and refluxed for 1 hr in order to carry out the reaction at a temperature close to the boiling point of ethanol. After that ethanol was evaporated under reduced pressure. The obtained dry product was washed three times with 100 ml of ether and then dissolved in 300 ml of deionized water. Once the product was dissolved the solution was acidified with HCl until pH 1 was reached. The product was extracted with 300 ml ethyl acetate. Ethyl acetate was evaporated under reduced pressure and ricinoleic acid was obtained as yellowish oil. The obtained ricinoleic acid was used without any further purification step as a ligand for the preparation of magnetite nanocrystals.

Synthesis of Fe_3O_4

The synthesis of Fe_3O_4 follows the coprecipitation method developed by Massart (Massart, 1981). In a typical experiment 1.30 g of FeCl_2 and 3.57 g of FeCl_3 were dissolved in 60 ml of deionized water. In a separate flask 1.90 g of the previously produced ricinoleic acid were dissolved in 1.6 g of acetone; the two solutions were then mixed and heated up to 80°C . Once the temperature of 80°C was reached 9 ml of ammonia were added. The solution turned instantly black, indicating precipitation of magnetite, and was left reacting for an additional 30 min. The product was separated by means of a magnet and washed with Acetone and deionized water. The black product was dried at room temperature for one night.

Synthesis of PLA ligands

The preparation of the PLA follows the recipe from Yu et al. (Yu et al., 2009). The carboxyl terminated PLA with a molar mass of 3 kDa was synthesized via bulk polymerization at 130°C . The reaction was carried out in a glove box to avoid water contamination. Before the reaction the L,L-Lactide (LA) was recrystallized in toluene and dried overnight at 30°C under vacuum. In a typical experiment, 20 g of lactide were melted at temperature below 100°C in a stirred flask, followed by addition of 0.056 g $\text{Sn}(\text{Oct})_2$ and 0.072 g of crystalline lactic acid previously dissolved in toluene (10 wt%). The reaction mixture was then heated to 130°C and allowed to react for 1 hr.

Preparation of PLA capped Fe_3O_4

The preparation of PLA capped Fe_3O_4 follows a typical ligand exchange method (Lattuada and Hatton, 2007), where ligands are PLA chains with a terminal carboxylic end-group prepared as described in the section on the synthesis of PLA ligands. In a typical experiment 1 g of Fe_3O_4 stabilized with ricinoleic acid were mixed with 4 g of PLA in 60 ml of THF and heated at 60°C for 24 hr. The product is then precipitated in a 50:50 v:v methanol water mixture, then redispersed in dichloromethane, treated with MgSO_4 in order to remove water, and finally filtered. The solution was then concentrated for further use.

6.2.3 Preparation of polymer composites

Preparation of Fe_3O_4 @PLGA Miniemulsion

For the preparation of the miniemulsions, two solutions were first prepared. In the first solution, the water phase, PVA was dissolved in deionized water in a weight fraction between 1 and 5%. In the second solution, the oil phase, 2 g of PLGA was dissolved together with 0, 0.4 or 0.8 g of Fe_3O_4 produced as previously described in 24 g of dichloromethane. The oil phase was then mixed with 80 g of the water phase and sonicated under magnetic stirring at 250 rpm using a Branson Sonifier 450D (BRANSON Ultrasonics Corporation, USA). The sonication amplitude was set to 70% and a cycle of 0.5 sec was chosen. To avoid heat accumulation the solution was cooled in an ice bath.

Supercritical Fluid Extraction of Emulsions

A scheme of the experimental setup used for SFEE experiments is shown in Figure 3.2. CO₂ is drawn from a dip tube cylinder and precooled in a pressure module (PM101, NWA GmbH, Lörrach, Germany) before being delivered to the reactor by a piston pump (PP200, Thar Design Inc., Pittsburgh PA, USA). Pump heads are cooled to 5°C by a cryostat (minichiller, Huber, Offenburg, Germany). The stream then passes a back pressure regulator (Thar Design Inc., Pittsburgh PA, USA) set to 10 bar above the desired reactor pressure, in order to reduce stream fluctuations generated by the piston pump. The emulsion is delivered by an HPLC pump (PU2080 plus, Jasco). Before entering the reactor, both the CO₂ and the miniemulsion feed stream, prepared as described before, are brought to the operating temperature (CC230, Huber).

Both streams are mixed at the inlet of the reactor by a two substance nozzle (Schlick, Untersiemau, Germany). The reactor (Premex, Lengnau, Switzerland) has a volume of 900 ml and is kept at the operating temperature by another thermostat (CC240, Huber). The particles are formed by solvent extraction from the organic emulsion droplets, and remain suspended in the continuous water phase throughout the whole process. The product suspension accumulates at the bottom of the reactor and may be withdrawn continuously or at the end of the process through an outlet at the bottom of the reactor. The off-gas stream leaves the reactor through an outlet at the top. The pressure inside the reactor is controlled by a backpressure regulator located downstream, through which the off-gas stream expands to atmospheric pressure to be vented. Due to the Joule-Thomson effect, this expansion leads to strong cooling; therefore the CO₂ stream is heated up in a thermostated waterbath prior to expansion, and the temperature in the backpressure regulator is

controlled using heating elements.

A typical SFEE experiment is divided into five stages. First, the reactor is filled with CO₂. Then, feed of all streams is started and back pressure regulators are adjusted. At this stage, water is fed to the reactor until steady state is reached with respect to operating temperature, pressure and flow rates. During the third stage, the emulsion is fed to the reactor for solvent extraction. In step four, the emulsion feed line is again purged with water. Finally, the CO₂ feed stream is stopped and the product suspension is withdrawn from the reactor before the experiment is terminated by the depressurization of the reactor.

Dialysis

The extraction of the solvent via dialysis was done as follows: one droplet of the previously prepared miniemulsion was diluted in 20 ml of water so that all the solvent can diffuse out of the droplets. The obtained suspension was then used for the light scattering measurements.

6.2.4 Samples characterization

Light scattering measurements have been performed with a Zeta Nano ZN (Malvern Instruments, UK). The mean hydrodynamic diameter was obtained by fitting the autocorrelation function with the cumulant method, which also gives the polydispersity index (PDI), which is defined as (Zemb and Lindner, 2002):

$$PDI = \frac{R_4 R_6}{(R_5)^2} - 1 \quad (6.1)$$

where R_i is the i^{th} moment of the particle size distribution. For average diameter measurements the error bar indicates the width of the distribu-

tion and for the PDI measurements the error bar indicates the standard deviation calculated from three measurements.

For the preparation of samples for transmission electron microscopy TEM, one drop of the product suspension was diluted with 10 ml water. 40 μ l of the obtained solution were deposited on a copper grid (400 mesh), previously covered with a carbon layer of 8 nm thickness, and after 30 seconds the droplet was removed. Images were taken with a FEI Morgagni 268 Transmission Electron Microscope (FEI company, USA).

For the preparation of samples for the scanning electron microscopy SEM, particles were recovered from the suspension and separated from the surfactant PVA. After centrifugation at 20'000 rpm for 15 min (Avanti J-20, Beckman, USA), the supernatant was discarded, and sedimented particles were re-suspended in pure water and subsequently freeze-dried (FlexiDry, FTS Systems, USA). Dried samples were sputter-coated with 5 nm platinum for SEM analysis, and photomicrographs were obtained from a Zeiss Gemini 5 1530 FEG scanning electron microscope in order to determine the morphology of the precipitated particles.

6.3 Results and Discussion

6.3.1 Process Design

In this work, we investigate the preparation of novel biodegradable and magnetically responsive composite nanoparticles. The emulsification method was chosen due to its great versatility, broad range of applications, and the possibility to fine tune parameters such as the particle size and size distribution (PSD). Previous investigations suggest that

the PSD of the produced particles is directly related to the size and size distribution of the emulsion droplets (Chattopadhyay et al., 2006; Della Porta and Reverchon, 2008; Kluge et al., 2009b).

With reference to biomedical applications, FDA approved ingredients have been selected in order to create particles suitable for drug delivery applications. PLGA is one of the most studied biodegradable polymers and its chemical composition, crystallinity, and hydrophobicity can be tuned by varying the ratio between lactic and glycolic acid units. Since our goal is the preparation of composite nanoparticles containing many magnetic nanocrystals, a high uniformity in the size distribution of magnetite nanocrystals was not required. Therefore the Massart's coprecipitation method (Massart, 1981) was chosen to prepare magnetite nanocrystals. Ricinoleic acid was used as biocompatible ligand for the production of hydrophobic nanocrystals in most of the experiments, because it guarantees good dispersibility in apolar and mildly polar organic solvents, such as dichloromethane. Since the type of ligand may affect the distribution of magnetite nanocrystals inside the polymer matrix, we have also performed one experiment with poly lactic acid (PLA) as stabilizer of the nanocrystals.

The removal of the solvent used to disperse and mix the polymer and the magnetic nanocrystals is of paramount importance for the preparation of particles for biomedical applications. It is well recognized that the solvent elimination process has only a limited influence on the final size of the produced microspheres. For instance, it has been shown that slow solvent removal such as in conventional evaporation under vacuum favors slightly larger particles due to an increased tendency of droplets to aggregate over time (Della Porta and Reverchon, 2008). In order to assure complete solvent removal under mild conditions, we have used the sc-CO₂ extraction process, which is largely preferable with respect to the

much slower solvent evaporation. The SFEE process not only limits the extent of aggregation of particles during solvent removal by drastically reducing the time for the solvent extraction, but also allows one to easily set up a continuous process, which is suitable for scale-up. In addition, it extends the range of solvents that can be used during the emulsification process to high boiling point solvents that cannot be easily removed by evaporation.

In order to assess that the extraction method does not affect the particle size distribution, we have measured the size of particles prepared by using the same recipe until the emulsification step, but

two different procedures to extract the solvent, *i.e.* dialysis and sc-CO₂ extraction. The results shown in Figure 6.1 confirm that, within experimental error, the size is indeed independent of the method of solvent removal. Further, since the particle size distribution obtained from light scattering is in all cases consistent with the scenario of a suspension of monodisperse spheres, we conclude that the SFEE process produces largely non-agglomerated particles. The fact that product particles seem to be physically interconnected in some of the SEM images shown in the following is most likely an artifact of the drying procedure required to prepare samples for SEM.

In the remaining sections we will focus on how to control the particle size, the size distribution, and the morphology of the nanoparticles, and in particular on understanding the effect of magnetite nanocrystals on the particle preparation.

6.3.2 Effect of operating parameters on size and morphology

There are many different parameters affecting the final PSD during the preparation of composite nanoparticles via miniemulsification method, such as polymer amount, surfactant type and concentration, amount of solvent, sonication time, amount and properties of magnetite, and others. The effect of some of these parameters, such as surfactant type and concentration, oil-to-water phase ratio, polymer molecular weight, polymer

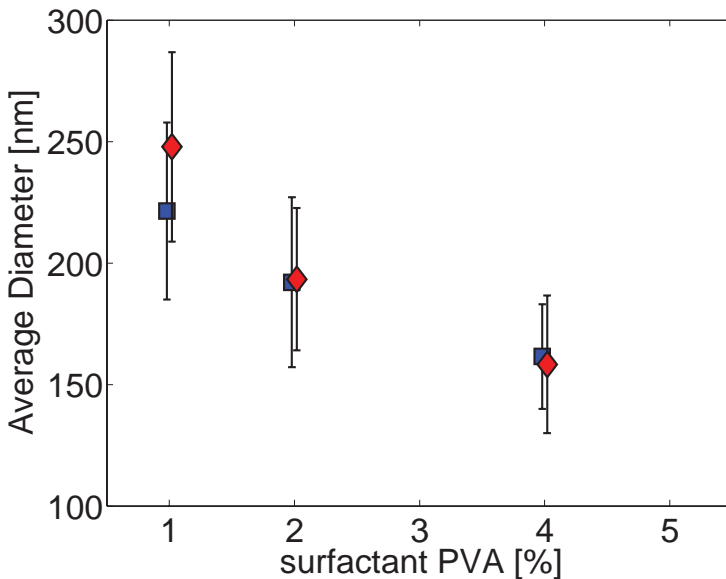


Figure 6.1: Comparison between the average hydrodynamic diameters of particle obtained from the extraction of the solvent using the SFEE method (red ◆) and those obtained from dialysis (blue ■). The error bars indicate the width of the particle size distribution based on the PDI.

concentration and stirring rate have already been studied (Musyanovych et al., 2008; Kluge et al., 2009b). However, most of these studies have not been carried out on composite nanoparticles. Therefore, in order to better characterize and understand the peculiar behavior of our system, we have focused on the influence of four parameters, namely the sonication time, the surfactant amount, the ratio between the amount of magnetite and that of polymer in the oil phase, and the type of ligand stabilizing the magnetite.

Choice of the sonication time

The sonication time is of paramount importance, because if sonication is not applied for sufficiently long time, the resulting particle size distribution will be broad (Antonietti and Landfester, 2002). The ultrasonication is characterized by a complex dynamics of collisions, coalescence, and breakage of droplets, which reaches a dynamic equilibrium only after a sufficient time that increases as the emulsifier concentration decreases (Antonietti and Landfester, 2002). Afterwards, the droplet size distribution stabilizes, being usually characterized by a low polydispersity in the final miniemulsion. In order to assess the influence of magnetite on

Experiment	PVA [%]	after 10 min		after 20 min		after 30 min	
		D [nm]	PDI []	D [nm]	PDI []	D [nm]	PDI []
A	1	228	0.147	222	0.108	221	0.097
B	2	203	0.068	198	0.061	192	0.089
C	4	174	0.051	167	0.058	162	0.046

Table 6.1: List of operating conditions for the experiments performed to study the influence of sonication time on the production of magnetic colloids.

the sonication process, we have focused on three specific systems (see Table 6.1), where three different PVA concentrations (1 wt%, 2 wt% and 4 wt%) were studied, whereas the oil phase contained 15 wt% of magnetite (final solid fraction).

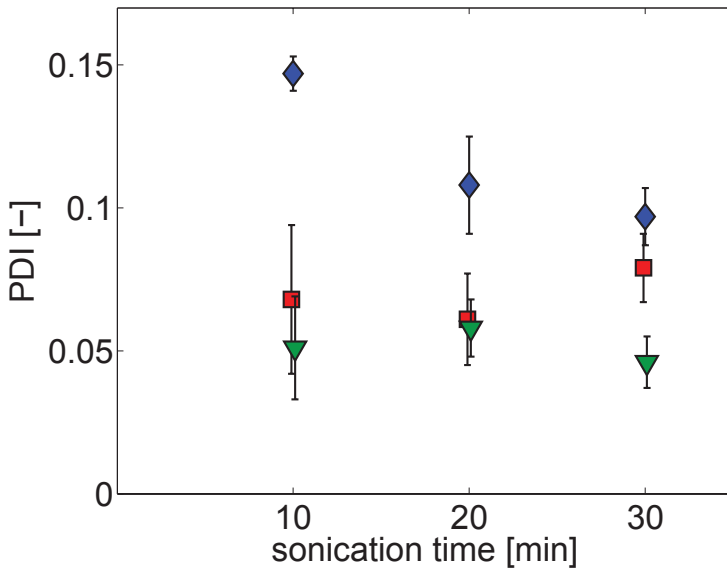


Figure 6.2: Polydispersity Index as a function of the sonication time, for the experiments listed in 6.1 with 1 wt% PVA (blue \blacklozenge), 2 wt% PVA (red \blacksquare) and 4 wt% PVA (green \blacktriangledown). The error bars indicate the standard deviation of the PDI.

For these experiments we have performed size measurements using dynamic light scattering on samples taken at different times during the sonication process. Since we have previously shown that the extraction method does not influence the final particle size and particle size distribution, samples were taken and diluted in an excess of water, thus

allowing the solvent to diffuse out of the droplets. As shown in Table 6.1 and Figure 6.2, the sonication time is only slightly influencing the average particle size, but has a stronger influence on the particle size distribution. The final average size is reached in a few minutes and does not change when longer sonication times are used, while a narrow and stable PSD is reached at much longer times as already reported in the literature (Antonietti and Landfester, 2002). As Figure 6.2 shows, the time needed to reach a stable particle size distribution was maximal for a PVA concentration of 1 wt%. For higher PVA fractions, a stable value for the polydispersity index was already reached after 10 minutes. Therefore, for all our experiments the solution was sonicated for 30 minutes so that a stable value for the polydispersity index could be reached for all the PVA concentrations investigated.

Effect of Surfactant concentration

The amount of emulsifier is probably the parameter that most strongly determines the theoretical final particle size. It is well known that an increasing amount of emulsifier leads to a decrease of particle size, until a minimum value is reached (Schork et al., 2005). While this behavior is general, the type of emulsifier is playing a role, since it is also known that ionic emulsifiers are more effective in stabilizing small particles as compared to steric emulsifiers (Schork et al., 2005; Musyanovych et al., 2008). However, most of the FDA approved emulsifiers are steric, and we have focused on PVA because it is one of the most commonly used emulsifiers in the pharmaceutical industry. In order to demonstrate the effect of the emulsifier on the particle size and size distribution in our system, its concentration was varied in experiments 3-8 (see Table 6.2) at constant magnetite content. Results are shown in Table 6.2 and Figure 6.3.

Exp. #	Emulsion properties					Product properties		
	Aq. phase		Organic phase			D [nm]	PDI []	Morphology
	PVA [%]	PLGA [g]	Fe ₃ O ₄ [%]	DCM [g]				
1	1.5	2	0	24	202	0.006	N.A.	
2	3	2	0	24	176	0.047	N.A.	
3	1	2	15	24	248	0.164	Janus	
4	1.5	2	15	24	215	0.195	Janus	
5	2	2	15	24	193	0.068	Janus	
6	3	2	15	24	162	0.066	Janus	
7	4	2	15	24	158	0.089	Janus	
8	5	2	15	24	144	0.061	Janus	
9	1.5	2	30	24	207	0.177	Janus	
10	3	2	30	24	179	0.100	Janus	
11	3	2	50	24	187	0.121	Janus	
12*	3	2	15	24	184	0.137	Homogeneous	

Table 6.2: List of operating conditions for the experiments performed to study the influence of PVA and magnetite amount on the production of magnetic colloids. Note that the magnetite nanocrystals used in experiment 12* were stabilized by PLA.

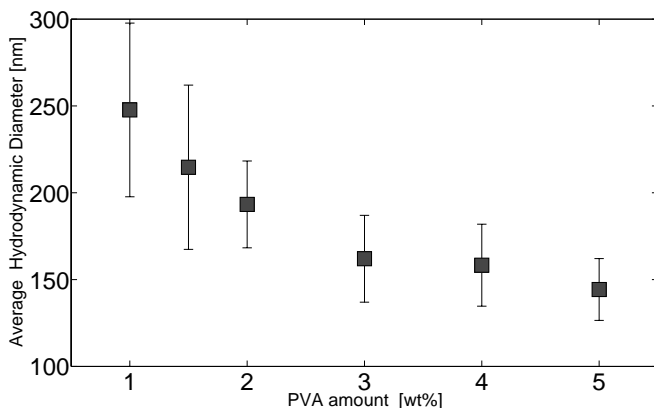


Figure 6.3: Average Particle Hydrodynamic diameter as a function of the PVA amount, for the experiments 3, 4, 5, 6, 7 and 8 reported in Table 6.2. The errorbars indicate the width of the particle size distribution based on the PDI.

As the concentration of PVA is increased, the final particle size decreases first and then reaches a stable value of 150-140 nm for PVA concentrations in water from 3 wt% up to 5 wt%, as expected. However, increasing the amount of emulsifier in water continuously decreases the polydispersity index values of the final product in the entire range of concentrations investigated. This can also be observed in Figure 6.4(a) that shows a SEM picture of particles obtained in an experiment with 1 wt% PVA, and in Figure 6.4(b) that shows a SEM picture of the particle obtained in an experiment with 5 wt% PVA. For low amounts of emulsifiers (Figure 6.4(a)), the particle size distribution is broad, exhibiting many particles with a size substantially smaller or larger than the average. For an experiment with a high amount of emulsifier (Figure 6.4(b)), one can observe that the particle size distribution is much narrower.

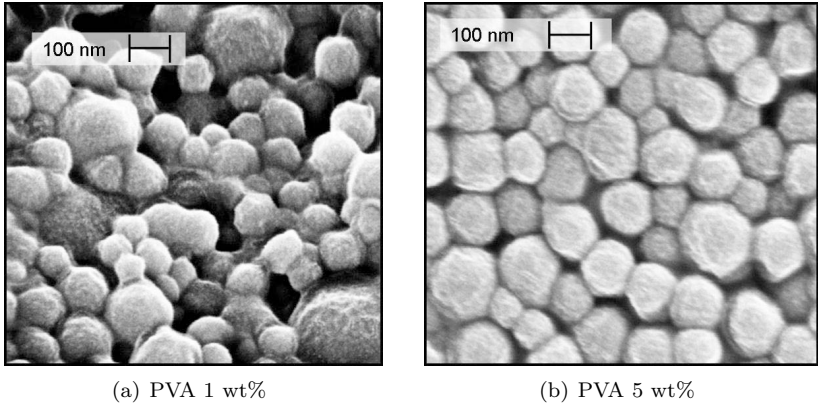


Figure 6.4: SEM pictures of the particles obtained with a PVA amount of 1 wt%, corresponding to experiment 3 in Table 6.2 (left) and with a PVA amount of 5 wt%, corresponding to experiment 8 in 6.2 (right). In both experiments the magnetite content was 15 wt%. The pictures clearly show a decreasing broadness of the particle size distribution with increasing PVA amount.

Effect of Magnetite amount and Particle morphology

The magnetite amount is another factor that can influence the final size and size distribution, but little information is available about its effect on the size and morphology of composite nanoparticles. In order to explain how magnetite can affect the miniemulsification process, it is instructive to look at the morphology of the particles shown in Figure 6.5. One can clearly see that the magnetite nanocrystals are accumulated in clusters at the surface of the particles between the polymer matrix and the emulsifier layer. This phenomenon occurs because magnetite and polymer are probably incompatible, and are both trying to minimize the overall contact surface between each other. Additionally, nanoparticles are accumulating on the surface of the droplets, helping to decrease the interfacial energy between the two phases, a phenomenon

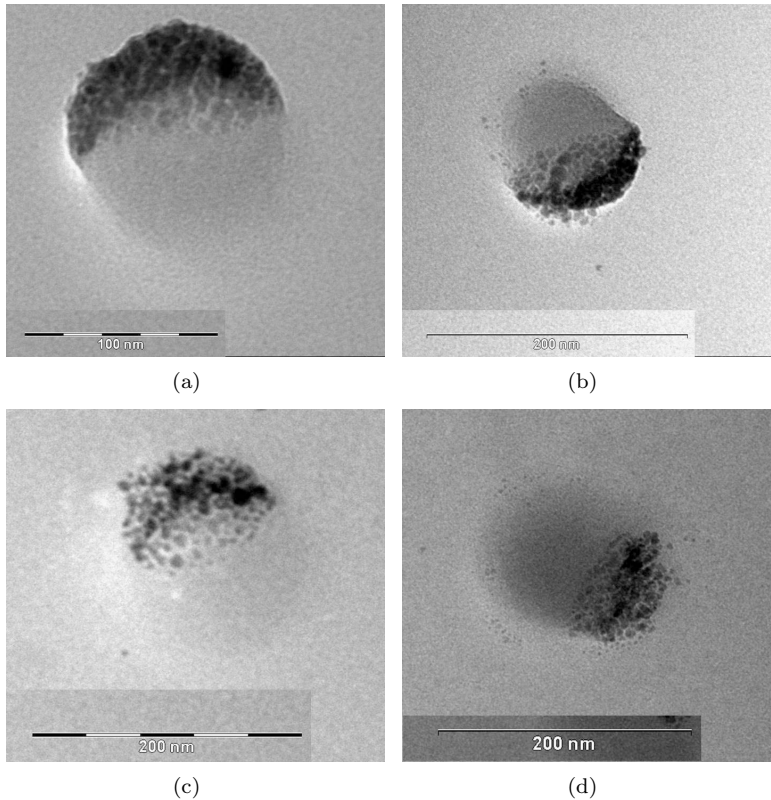


Figure 6.5: TEM picture of typical particles produced in experiments reported in Table 6.2. (a) experiment 3 (1 wt% PVA, 15 wt% Fe_3O_4); (b) experiment 5 (2 wt% PVA, 15 wt% Fe_3O_4); (c) experiment 10 (3 wt% PVA, 30 wt% Fe_3O_4); (d) experiment 7 (4 wt% PVA, 15 wt% Fe_3O_4). For all experiments the ricinoleic acid-capped magnetic nanocrystals are accumulated in one large cluster on one hemisphere of the particles leading to a Janus-type morphology.

called Pickering emulsion (Sacanna et al., 2007). energy gained by keeping nanoparticles at the interface between two phases, even if they are not entirely compatible with either of the two phases, can be enormous

(Binks and Horozov, 2006). Pickering emulsions are used nowadays to prepare composite nanoparticles where the disperse phase, which is often the oil phase, is stabilized solely by nanoparticles. The fact that the nanocrystals are accumulating in clusters at the surface is due to the interfacial tension, which is lower for nanocrystals in close contact with each other than for nanocrystals in contact with the polymer matrix. This effect was also shown by other groups (Montagne et al., 2006; Isojima et al., 2009; Liu et al., 2007), where it was observed that magnetic nanocrystals covered by oleic acid were accumulating on a hemisphere of particles during the seed polymerization of ferrofluid with styrene (Montagne et al., 2006), and in the case of composite particles made of pre-formed polystyrene (Isojima et al., 2009) or PLGA (Liu et al., 2007). The resulting morphology of the composite nanoparticles is of Janus type, as both SEM (see Figure 6.6) and TEM (see Figure 6.5)

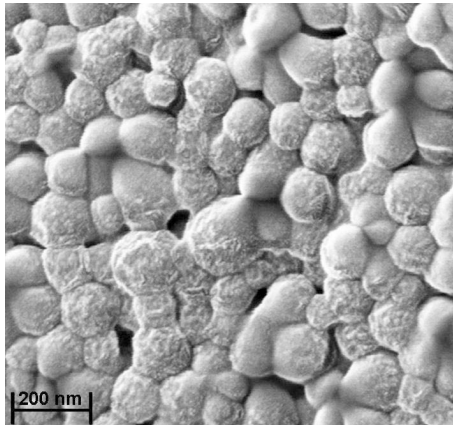


Figure 6.6: SEM picture of a particles produced in experiment 6 as reported in 6.2 (3 wt% PVA, 15 wt% Fe_3O_4). The partially roughness on the surface is due to the presence of magnetite

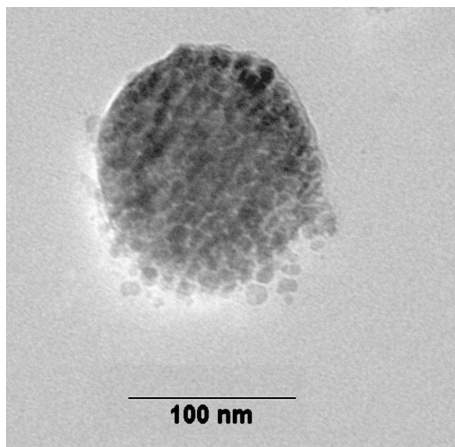


Figure 6.7: TEM picture of a typical particle produced in experiment 11, as reported in 6.2, with 3 wt% PVA and 50 wt% magnetite. The particles are fully covered with magnetic nanocrystals.

pictures indicate. Magnetite nanocrystals tend to accumulate on one side of the particle, thus creating an asymmetric Janus object. This morphology is observed in all the experiments, as Figure 6.5 confirms for Fe_3O_4 amounts of 15 wt% and 30 wt%. When the amount of Fe_3O_4 is increased up to 50 wt% a complete coverage of the particle surface is reached, as shown in Figure 6.7. For the systems with a low amount of emulsifier this phenomenon leads to a high polydispersity of the nanoparticles size distribution. The tendency to form pickering emulsions creates a competition between magnetite nanocrystals and PVA in stabilizing the droplets. This competition explains why the experiments with low amount of surfactant show a broad polydispersity, as shown in Figure 6.8. The small droplets formed during the ultrasonication process can also be partially stabilized by the magnetic nanocrystals, and are therefore more stable than the droplets stabilized only with PVA. This can be

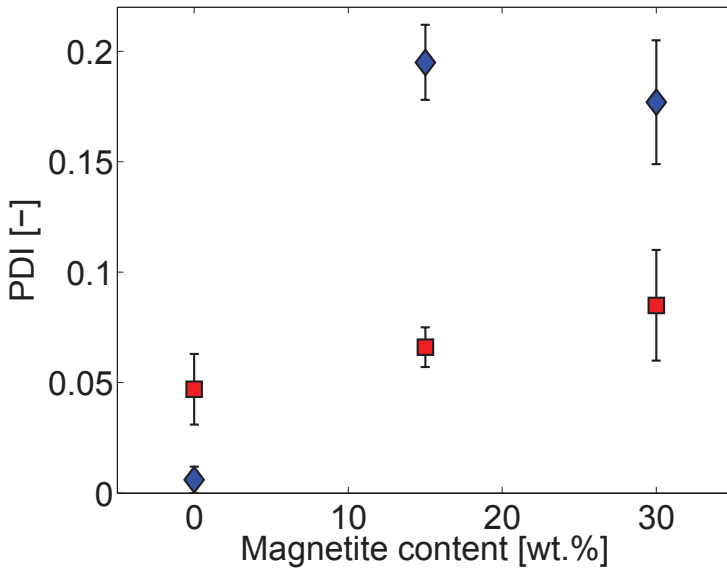


Figure 6.8: Polydispersity Index as a function of Magnetite content. (blue \blacklozenge) experiments carried out with 1.5 wt% PVA (experiments 1, 4 and 9 in 6.2); (red \blacksquare) experiments carried out with 3 wt% PVA (experiments 2, 6 and 10 in 6.2). The error bars indicate the standard deviation of the PDI.

clearly seen in Figure 6.9, where many small particles can be observed that contain a relatively large amount of magnetic nanocrystals covering most of their surface, thus leading to a stabilizing effect.

On the other hand, the large particles in Figure 6.9 have magnetic nanocrystals concentrated in a large cluster on a hemisphere, i.e., only part of the surface is stabilized. For the experiments with high amount of PVA this tendency is weaker, because also particles containing less amount of magnetite nanocrystals can be stabilized very quickly by the large amount of PVA available. However, the behavior is not entirely

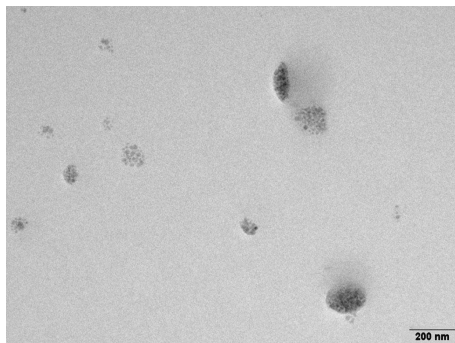


Figure 6.9: TEM picture of particles produced in experiment 3 as reported in Table 6.2, with 1 wt% PVA and 15 wt% magnetite. It can be observed that small particles have a larger amount of surface covered with magnetic nanocrystals than larger particles.

absent, as it can be seen in Figure 6.8, which shows that the polydispersity of PLGA particles prepared without magnetite is significantly smaller than that of particles with magnetite, even at high surfactant concentrations. Surprisingly enough, the average size of the composite nanoparticles is almost unaffected by the presence of magnetite. The data in Figure 6.8, in fact, demonstrate that the average size is independent of magnetite concentration up to weight fractions of magnetite of 30 wt%. In order to obtain an additional proof of this trend, we have carried out an experiment with 50 wt% of magnetite and a PVA content of 3 wt% (see experiment 11 in Table 6.2). The final average size is almost the same of the experiments with 30 wt% of magnetite but as expected the polydispersity of the particles with 50 wt% magnetite is larger than that of all experiments with lower magnetite content (a PDI equal to 0.121 for the experiment with 50 wt% as compared to a value of 0.100 for the experiment with 30 wt%).

6.3.3 Non Janus type morphology

The ligand used for the stabilization of magnetite plays an important role, first of all because it allows for its dispersion in the oil phase. If the dispersion capability is low it is impossible to achieve high magnetite loading inside the final nanoparticles. In all the experiments discussed so far, ricinoleic acid was chosen as ligand. However, regarding the particle morphology observed in Figure 6.5 and Figure 6.9, it is apparent that ricinoleic acid-capped magnetite nanocrystals phase separate from the polymer matrix, leading to large clusters accumulating on one hemisphere of the particles which results in a Janus-type morphology. In order to achieve a more homogeneous distribution of the nanocrystals inside the polymer matrix or at least on the particle surface, we have prepared magnetite nanocrystals capped with PLA through the ligand exchange method (Lattuada and Hatton, 2007). In the case of PLA we cannot apply the direct synthesis method as for the case of ricinoleic acid, because PLA would rapidly degrade in the strong alkaline conditions and at the high temperature required for magnetite precipitation (de Jong et al., 2001), and therefore it cannot be attached to the particle surface during the formation of particles. Even though it is possible to grow PLA from the surface of ricinoleic acid-capped magnetite nanocrystals via ring opening polymerization (ROP) (Lattuada and Hatton, 2007), the production of PLA before capping allows easier control of PLA molecular weight. Even though PLA-capped and ricinoleic acid-capped magnetite nanocrystals seem equally well dispersible in dichloromethane-PLGA mixture, there are strong differences in the morphology of the final polymer particles. By comparing a TEM picture of a typical PLGA particle with PLA-capped nanocrystals, shown in Figure 6.10, with TEM pictures of typical PLGA particles with ricinoleid acid-capped nanocrystals, shown in Figure 6.5, it is clear that

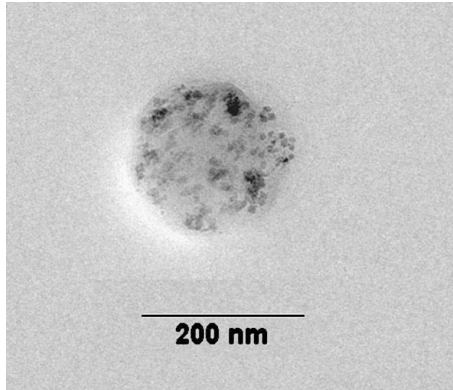


Figure 6.10: TEM picture of a typical particle produced in experiment 12 as reported in Table 6.2, *i.e.* using PLA-capped magnetite. The magnetic nanocrystals are well dispersed inside the particle.

magnetite nanocrystals capped with PLA are better distributed within the PLGA matrix than the magnetite nanocrystals coated with ricinoleic acid, which instead tend to cluster on one hemisphere of the composite particles.

6.4 Conclusions

In this work, we propose a novel strategy for the preparation of PLGA-magnetite composite nanoparticles with controlled size and particles size distribution, suitable for biomedical applications such as targeted drug delivery or teranostic applications. Composite nanoparticles have been prepared by dispersing magnetite and PLGA in a common organic solvent, by miniemulsification through ultrasonication in the presence of a biocompatible emulsifier (PVA), and finally, by removing the solvent through supercritical fluid extraction of the emulsion (SFEE). By chang-

ing the concentration of the emulsifier, the size of the magnetic composite nanoparticles can be tuned between 230 nm (1 wt% PVA) and 140 nm (4 wt% PVA). Surprisingly, the incorporation of magnetite nanocrystals is not affecting the overall particle size, but is instead affecting the particle size distribution by making it broader. This is due to the competition between magnetic nanocrystals and emulsifier during the sonication process. The morphology of the composite nanoparticles tends to be of Janus type, with magnetite accumulated at the surface and usually in one large cluster located on one hemisphere of the particles. More homogenous dispersion of magnetite inside the polymer matrix has been achieved by preparing PLA-capped magnetite nanocrystals.

The advantage of the proposed approach for the preparation of biocompatible magnetic composite nanoparticles is the combination of the emulsification method, which permits a good control of the particles size and morphology, with the use of the supercritical fluid extraction of emulsion technique, a very fast, clean, and efficient process, allowing even high boiling point solvents to be utilized for the emulsification. Since SFEE is a continuous process, the proposed method is particularly promising for the preparation of large quantities of high quality particles for biomedical applications.

Acknowledgements

We thank Professor Massimo Morbidelli for his support. We thank the Electron Microscopy Center of ETH Zurich (EMEZ) and Peter Tittmann for their support on electron microscopy. Financial support by the Swiss National Science Foundation (SNF), grant number 200021-116687, is gratefully acknowledged.

Chapter 7

Conclusions and Outlook

7.1 Conclusions

In this research project, processes based on the application of $scCO_2$ as antisolvent and solvent-extracting agent have been successfully used to design pharmaceutical particles, with a special focus on drug-polymer composites. Such composites may appear rather similar to each other from a material point of view, as they always involve particles composed of a polymer and an additional substance, e.g. an API. However, the specific products described in the individual chapters of this work target entirely different fields of pharmaceutical applications. The co-formulations of phenytoin and PVP described in Chapter 2 are exemplary of composites used in oral drug delivery, in order to increase the bioavailability of sparingly soluble drugs. On the other hand, lysozyme microencapsulated in PLGA, as described in Chapter 3, is representative for a controlled release system intended for parenteral delivery, pro-

longing the therapeutic half-life of sensitive bio-pharmaceuticals. The nano-composites of ketoprofen and PLGA described in Chapters 4 and 5 suggest a broad range of pharmaceutical applications, such as in oral drug delivery (e.g. preventing gastric irritations), in parenteral delivery, or using other delivery pathways, e.g. ophthalmic or transdermal drug delivery (as ingredient in eyedrops or ointments). Finally, the biocompatible and magnetically responsive nano-composites of magnetite and PLGA are intended for drug targeting and theranostic applications. We conclude that the potential of drug-polymer composites manufactured by supercritical fluid technology is not restricted to certain niches, but could potentially provide many different pharmaceutical fields with innovative and added-value products.

Aiming for drug-polymer composites that may be applied in practice and marketed, it is important to address the issue of their long-term stability and, as the basic concept behind, the compatibility of the two materials involved, i.e. a crystalline drug and an amorphous polymer. Here, we have arrived - for two entirely different systems - at the conclusion that there is a solubility of a drug in a polymer, i.e., a level at which the polymer phase is saturated with respect to the solid drug, and is in a pseudo-equilibrium state where its intensive properties, including the chemical potential of the species belonging to the polymer phase, do not change in time. For the system phenytoin-PVP described in Chapter 2, this conclusion remained on the stage of a well-supported hypothesis; major pro-arguments being the reproducible threshold of 40wt.% phenytoin in PVP (below which phenytoin was always fully dissolved in the polymer) in combination with the observed long-term stability. In order to prove this hypothesis, it would have been necessary to consider co-formulations above the threshold and to analyze the polymer phase

separately, in order to confirm whether or not the level of drug in polymer is constant in the presence of crystalline phenytoin - as it should, if it corresponds to the equilibrium solubility. Unfortunately, a separation of crystals and polymeric particles was technically not possible.

In this light, composites of ketoprofen-PLGA produced by SFEE exhibited very interesting properties, as described in Chapter 4. First, some of them were not long-term stable - recrystallization of KET could be observed for composites with levels in excess of 10wt.% KET in PLGA. Second, the environment of an aqueous suspension allowed the separation of polymeric nanocomposites from the much larger crystals by means of centrifugation, and hence their separate analysis. Third, as has been clarified in Chapter 5, the glass transition of these composites in aqueous suspension is around ambient temperatures, which enabled equilibration experiments to be carried out in reasonable time frames. Fourth, a combination of the last two points made impregnation experiments possible, i.e., equilibration could as well be attained using initially undersaturated polymer particles. These points enabled a very clear assessment of the solubility of KET in PLGA, as provided in Chapter 5. An open issue in this context is the possibility to predict drug-in-polymer solubilities. Considering the fact that for each specific drug respectively target application there is a large number of polymeric pharmaceutical excipients that represent potential candidates for the formation of composites, it would be extremely favorable if one could estimate the compatibility of a specific drug and with the different polymer types prior to making a decision which of the polymers should be investigated experimentally. However, it seems that the available shortcut methods, such as the Scatchard-Hildebrand theory described in Chapter 4 which predicts the drug-polymer compatibility on the basis of a three-dimensional set of solubility parameters, have not yet reached

a sufficient degree of accuracy and reliability.

Another issue that is worth being discussed in a synthetic overview is the control of particle size in supercritical fluid processes. It has been shown in Section 1.5 for crystalline compounds such as paracetamol and phenytoin that control of particle size is possible within certain boundaries, firstly by choice of the precipitation technique, i.e., GAS or PCA, and also by modification of operating parameters such as the rate of antisolvent addition in the GAS process or the operating pressure in the PCA process. Moreover, the observed trends have been verified using models describing in detail the precipitation of crystalline substances in GAS (Muhrrer et al., 2002) as well as in PCA (Fusaro , 2008). Provided that material specific information such as the kinetics of crystal nucleation and growth in supercritical fluid mixtures are available, these models allow studying the influence of operating conditions also in simulations.

The situation is entirely different if particles are formed by liquid-liquid phase separation, as shown in Chapter 2 for the precipitation of PVP, or, in more detail, in Section 1.5 for the precipitation of lysozyme. For the latter case it has been shown that the particle size may be influenced by the choice of the precipitation technique (GAS or PCA) and, in PCA, by selecting the operating regime (i.e., supercritical or vapor-liquid regime). On the other hand, it seems that the particle size is almost invariant to changes in operating conditions such the rate of scCO_2 addition, a parameter that had a very strong influence in the precipitation of crystalline species. Moreover, there is no ready-to-use theoretical basis that could give an indication how operating conditions may be expected to influence the size of product particles formed by liquid-liquid phase separation. Although spinodal decomposition may be described using the Cahn-Hilliard Equation, there are two major difficulties that

are still hindering a successful application of this equation in the modeling of precipitation processes. The first hurdle arises from the fact that liquid-liquid separation is usually a process that does not stop until the two liquids are entirely segregated in two separate domains. Hence, for modeling the precipitation of particles by liquid-liquid phase separation, one needs conditions that lead to a termination of the phase separation process by accounting for the fact that one of the two liquids transforms into a glass. However, such conditions are difficult to define and to implement. The second problem is the combination of mixing of solution and antisolvent (as predicted e.g. by the Navier-Stokes equations of fluid flow in the case of PCA) and spontaneous de-mixing by spinodal decomposition (as predicted by the Cahn-Hilliard Equation), which is challenging from a mathematical point of view.

Concerning the possibility to control particle size in amorphous systems, the formation of particles by an emulsion process such as SFEE is clearly more favorable as compared to the formation of particles by liquid-liquid phase separation induced by an antisolvent, such as PCA. This has been described in detail in Chapter 3, where the influence of stirring speed and polymer concentration has been evaluated for the case of PLGA, and in Chapter 6, where the amount of surfactant has been identified as another favorable parameter for controlling the particle size in SFEE.

7.2 Outlook

In the scope of this work we have focused on the manufacturing of polymeric particles, using scCO_2 as antisolvent or solvent extracting agent. However, there have been some preliminary investigations that deviate slightly from this focus, but are nevertheless interesting for future re-

search and also applications, and shall therefore be discussed in this outlook. The first process, scCO₂-assisted high-pressure homogenization, represents a completely solvent free technique for the manufacturing of polymeric micro- and nanoparticles. Here, scCO₂ has the role as a plasticizing agent. In a second part, the potential of SFEE in the processing of crystalline materials shall be addressed.

7.2.1 CO₂-assisted High-Pressure Homogenization

High-Pressure Homogenization (HPH) is a process that was originally used for mixing hydrophilic and lipophilic liquids, in order to form stable and homogeneous emulsions. Another major application is the disintegration of microbial cells obtained from fermentation processes, which is necessary when intracellular products are to be harvested (Harrison, 1991). In both fields, HPH is a well-established technique. On the other hand, the application of HPH for the comminution of solids is rather new, and is often referred to as a special wet milling technique because particles are processed while being suspended in a liquid phase. The process principle of HPH is rather simple: The solid powder is suspended in a liquid, and the suspension is brought to high pressures, typically in the range of 1000 bar, before being relaxed to the original pressure over a homogenizer. Although many commercial homogenization modules have a complex internal geometry, it is worth mentioning that a simple valve causes an equivalent homogenization effect while allowing for better control of the operating pressure. Particles are comminuted while the suspension passes through the homogenizer because the fluid flow experiences an extreme local pressure drop and is therefore highly turbulent. Forces responsible for comminution come mainly from particle-wall collisions, particle-particle collisions, shear forces in the liquid and

cavitation. The suspension may be treated with several passes over the homogenizer until the desired degree of comminution has been achieved. HPH of aqueous suspensions of crystalline pharmaceuticals has been investigated for the micronization of sparingly soluble drugs, forming nano-suspensions to be used in further drug formulation steps (Muller and Peters, 1998). Also the comminution by HPH of particles suspended in liquid CO₂ has been investigated successfully (Muhrrer et al., 2005); unfortunately, this very interesting process has not yet been addressed much in the literature.

It has been discussed in section 1.3.2 that many polymers are able to uptake CO₂ by sorption, leading to swelling of the polymer matrix and to a significant plasticization, i.e., a decrease in the glass transition temperature or melting point. Hence, in the presence of scCO₂ many polymers undergo a transition into the rubbery liquid state; hence, they form melts already at ambient or slightly elevated temperatures. This may be exploited in HPH, since rubbery-liquid polymer particles are much easier to comminute as compared to particles in the glassy state. Moreover, the formation of spherical droplet-like particle morphologies may be expected if the polymer is liquid. Therefore, the preliminary study presented in the following concerns an extension of the original HPH process to the comminution of polymeric particles in an aqueous suspension exposed to an atmosphere of scCO₂.

Experimental: The setup used in this study is shown in Figure 7.1. An aqueous suspension of raw PLGA particles (RG503, Boehringer Ingelheim) was placed in a thermostated and stirred high pressure vessel (Premex, Lengnau, Switzerland), allowing for pressurization of the suspension with CO₂ from the bottle. A stream of the suspension was

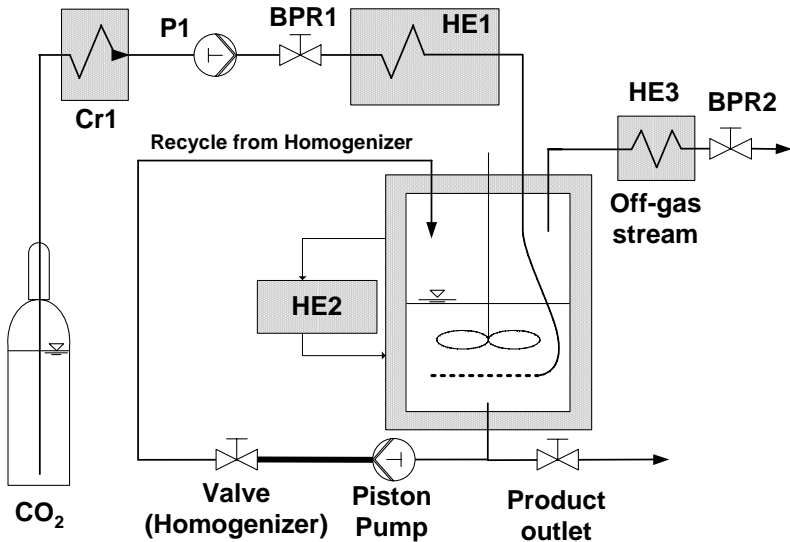


Figure 7.1: Scheme of the setup used for HPH processing.

drawn from the bottom of the vessel and pressurized using an air-driven high-pressure piston pump (Haskel, Burbank CA, USA), achieving operating pressures up to 900 bar using standard pressurized air supply. A micro-metering valve with variable aperture (SITEC-Sieber Engineering, Maur, Switzerland) was used as homogenizer. The homogenized suspension was fed back into the stirred high-pressure vessel, thus allowing the suspension to be treated with several passes over the homogenizer until the desired degree of comminution had been achieved. In order to prevent overheating of the suspension, the vessel temperature was maintained at 25°C . The number of passes over the homogenizer could be estimated from the number of pump strokes, considering that the volume of the pump head is 4.5 ml (i.e., for 225 ml of suspension, 50 pump

strokes correspond to one pass).

Three different homogenization experiments have been carried out, using each time a suspension of 1 g raw PLGA in 225 ml of water containing 1 wt.% PVA as stabilizing surfactant. Run 1 was carried out as reference with a suspension at atmospheric pressure without the plasticizing effect of CO₂. In Run 2, the reactor was initially pressurized with CO₂ up to around 65 bar, until a liquid layer of dense CO₂ could be observed on top of the suspension. Then, homogenization was carried out as in Run 1. In Run 3, the water phase was initially saturated with ethylacetate (EA) at 80 g/l, which may be expected to exert an additional plasticizing effect on the suspended PLGA particles. During all three experiments, samples were drawn through the product outlet while counting the number of passes across the homogenizer, in order to monitor the progress of comminution. Particle size distributions in the aqueous suspension samples were determined subsequently by laser diffraction using a stirred glass cuvette (Helos; Sympatec GmbH, Clausthal-Zellerfeld, Germany). For preparation of SEM images particles were treated as described previously in section 3.3.4.

Results and Discussion: The evolution of PLGA particle size in the three HPH experiments is shown in Figure 7.2, and images of product particles obtained after 150 passes across the homogenizer at approximately 900 bar pressure drop are shown in Figure 7.3. Regarding the final particle size obtained after 150 passes, the largest particles have been observed in the reference Run 1. Moreover, it can be seen in Figure 7.3b that these particles exhibit a rather irregular shape and a very similar morphology as compared to the raw material, Figure 7.3a. In Run 2, CO₂-assisted HPH led to particles that were throughout the whole homogenization process significantly smaller as compared to the reference

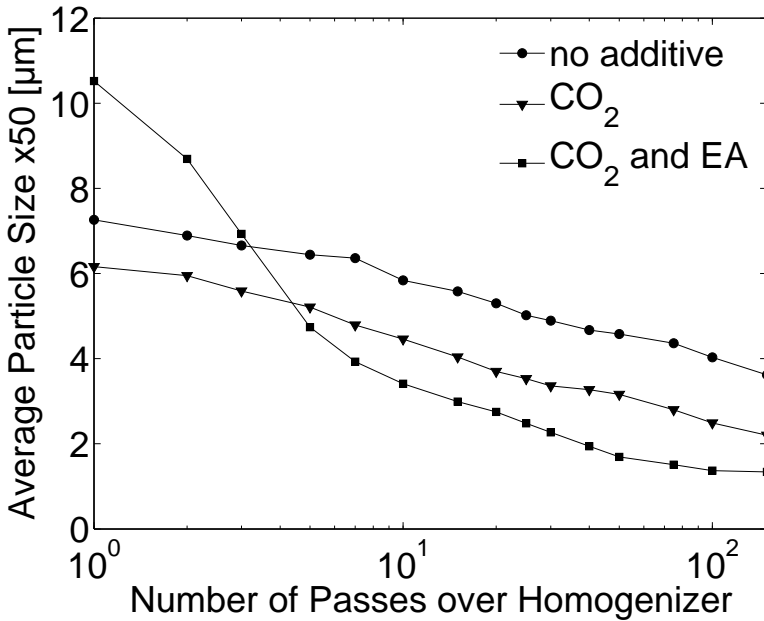


Figure 7.2: Evolution of PLGA particle size in HPH, represented by the average particle size x_{50} of measured distributions. Run 1, reference experiment without plasticizer (●), Run 2, HPH under a liquid CO_2 atmosphere (▼) and Run 3, HPH under a liquid CO_2 atmosphere using EA as additional plasticizer (■)

run, reaching an average particle size of $2.2 \mu\text{m}$ after 150 passes. The plasticizing effect of CO_2 on PLGA is even more evident from Figure 7.3c, showing that particles obtained in Run 2 are spherical and exhibit smooth surfaces. The smallest particles with an average particle size of $1.3 \mu\text{m}$ were obtained using EA as additional plasticizer in Run 3; these particles also exhibit a spherical morphology, as shown in Figure 7.3d. During the preparation of Run 3, it was observed that the presence of

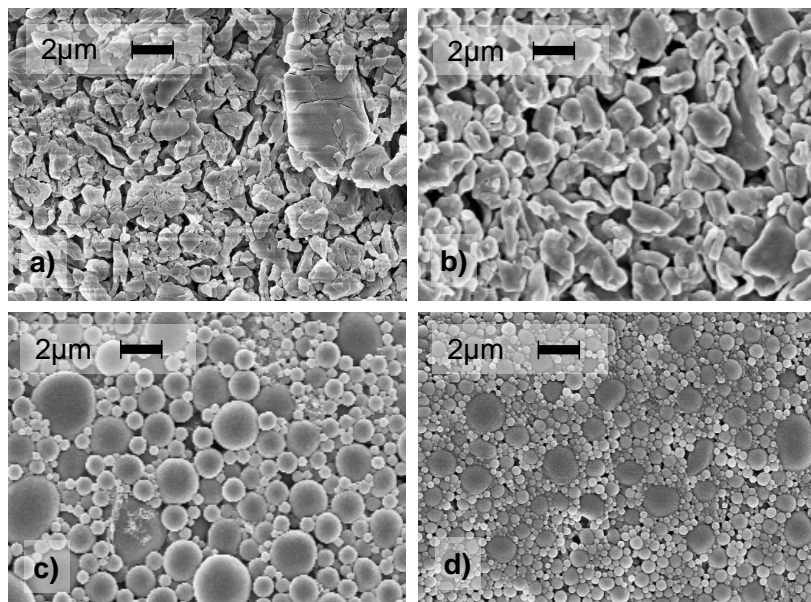


Figure 7.3: SEM images of PLGA particles. a) raw material PLGA RH 503; b) product particles from the HPH reference Run 2 without plasticizer; c) spherical particles obtained from HPH under a liquid CO₂ atmosphere; d) small spherical particles from HPH under a liquid CO₂ atmosphere using EA as additional plasticizer

EA led to formation of aggregates by untimely plasticization of PLGA. Therefore, significantly larger particles were found in Run 3 during the three initial passes.

This preliminary study, and especially Run 2, demonstrates how spherical PLGA microparticles may be obtained in a completely solvent-free process by exploiting the plasticizing effect that scCO₂ exerts on PLGA. Further, as shown in Figure 7.2, particle size may be tightly controlled in this process, firstly by the number of passes across the homogenizer,

but as well by the presence of additional plasticizers such as EA. From previous experiences, it is known that also the operating pressure drop across the homogenizer has a significant effect on particle size. Further investigations should address the issue how drugs may be incorporated into PLGA in this process. Regarding the encouraging results described in Chapters 4 and 5, impregnation seems to be a favorable option for hydrophobic species such as ketoprofen. Since the plasticizing effect of scCO₂ should have a beneficial effect also on the kinetics of impregnation, it seems possible that scCO₂-assisted high-pressure homogenization and impregnation of a drug may be achieved simultaneously.

7.2.2 SFEE processing of crystalline Solids: Recrystallization from Emulsions¹

SFEE can also be applied in the processing of crystalline solids, as has been discussed briefly when describing the formation of ketoprofen seed crystals by recrystallization from an SFEE-processed emulsion in section 4.2.3: When pure KET was used for the preparation of an emulsion and subsequent SFEE processing, KET formed initially amorphous nanoparticles that were obviously metastable, since they recrystallized rather quickly following the process illustrated in Figure 4.3, finally forming crystals that were orders of magnitude larger as compared to their amorphous precursors. An equivalent behavior has been observed in our lab for many other water-insoluble substances (e.g., phenanthrene, nifedipine, ibuprofen, naproxen and flurbiprofen). Figure 7.4 shows different time steps in the emulsion crystallization of phenanthrene as a further example. It is worth highlighting once more the similarity to what is

¹The experimental results reported in this section have been obtained by Lisa Joss in the scope of a Semester Project supervised by Johannes Kluge and Marco Mazzotti.

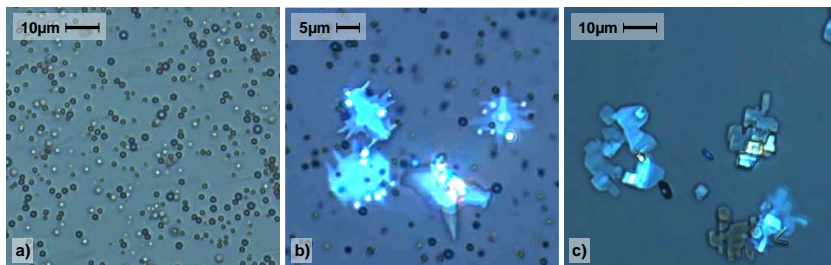


Figure 7.4: Recrystallization of phenanthrene from an emulsion.

shown in Figure 4.3 for the case of ketoprofen. The formation of crystalline nanoparticles by SFEE has also been described in the literature for three different substances, namely griseofulvin, megestrol acetate and cholesterol acetate; however, details of the involved recrystallization have not been mentioned (Shekunov et al., 2006b). In this context, SFEE is clearly a very favorable process, allowing the extraction of high-boiling nonvolatile organic solvents such as toluene, and the efficient large-scale production of undiluted solvent-free aqueous suspensions.

The phase behavior observed during recrystallization from an emulsion, involving the occurrence of a metastable amorphous precursor prior to the formation of crystalline particles, is comparable to what is observed for substances where precipitation involves competition between crystallization and liquid-liquid phase separation, as described in section 1.4. Such competition is often encountered in the precipitation of hydrophobic species with a low melting point, having typically a very high solubility in many organic solvents, as compared to a very low solubility in water. Therefore, such species are often crystallized from mixed solvents exhibiting intermediate solubilities, or by antisolvent precipitation using water as the antisolvent. While both scenarios may lead to oiling out, we focus on the latter for an closer description of the phenomena

occurring, based on the illustration given in Figure 7.5a.

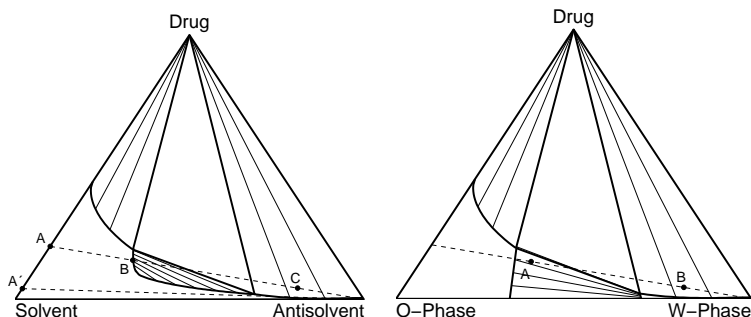


Figure 7.5: a) Oiling out and recrystallization of a drug through antisolvent addition. b) Emulsion crystallization of a drug through antisolvent addition.

If the precipitation process starts with a solution at point A, addition of antisolvent leads first into a liquid-liquid two phase region, and passing beyond point B, liquid-liquid phase separation by spinodal decomposition cannot be avoided - the system oils out, and consists now of two liquid phases, a solute-rich oil phase and a lean aqueous phase. By adding even more antisolvent, the system may reach point C, where in the end the crystalline state is thermodynamically more favorable and crystallization commences. In this case, crystallization starts from a liquid-liquid system, and is in that aspect comparable to what is shown in Figure 7.4 for the case of crystallization from an emulsion. However - and this is the major difference of oiling out as compared to emulsion crystallization - while passing beyond point B, it is likely that liquid-liquid phase separation does not lead to the formation of a stable emulsion, but to complete segregation of the two liquid phases. Since it is usually assumed that the formation of a marketable crystalline product cannot be achieved from this stage, oiling out is generally considered an unwanted phenomenon, and is typically avoided in crystallization

processes. As illustrated in Figure 7.5a, this is possible by starting the crystallization process with a solution at lower concentration in point A'; a compromise requiring on the other hand increased amounts of organic solvents and also larger reactor volumes.

This compromise may now be revised, regarding the possibility to carry out crystallization directly from a stabilized emulsion system where the starting point A is already in the liquid-liquid two-phase region, as illustrated in Figure 7.5b. By adding more antisolvent, or using SFEE as a powerful technique for solvent extraction, the system can be brought to the final state in B. Since the kinetics of crystal formation and possibilities to control particle size in such a system are not yet understood, a preliminary investigation was subject of the study described in the following.

Experimental: Emulsions were prepared by dissolving 10 wt.% of phenanthrene in ethyl acetate, and using a 1 wt.% aqueous PVA solution to form an (o/w) emulsion at a weight ratio of 1:4 by ultrasonication with a Branson Sonifier 450 (Skan AG, Basel, Switzerland). A sonication time of 2 minutes was applied at maximal power output while cooling the emulsion in an ice bath. A simplified method of solvent extraction has been used in this preliminary study, namely dialysis as described in section 6.2.3, allowing the extraction of organic solvents such as ethylacetate that exhibit a certain solubility in water. In order to trigger recrystallization in a controlled and highly reproducible manner, emulsions have been diluted with water at a ratio of 1:9, and recrystallization experiments have been carried out at controlled temperature in a jacketed 1 l glass reactor, using a 4-blade stainless steel impeller with a diameter of 55 mm. Formed crystals were analyzed using a light microscope equipped with two polarizing filters (Zeiss Axioplan,

Carl Zeiss AG, Feldbach, Switzerland) and size distributions were determined by laser diffraction using a stirred glass cuvette (Helos, Sympatec GmbH, Clausthal-Zellerfeld, Germany). Crystallinity of dried particles was confirmed by XRD measurements; for sample preparation, particles were recovered from the suspension by filtration, and subsequently freeze dried (FlexiDry, FTS Systems, USA).

Results and Discussion: The influence of temperature on the recrystallization process was investigated in three experiments where the temperature was increased from 20°C to 60°C while all other parameters, especially the stirring rate of 200 rpm, were kept constant. Images of representative product particles are shown in Figure 7.6. It can be seen that the size of particles increases clearly with temperature; this has been confirmed by determining the PSDs, where the average particle size x_{50} varied from 14 μm at 20°C to 24 μm at 40°C and 86 μm at 60°C. Also the morphology of particles changed visibly with temperature, from heavily agglomerated particles at 20°C to non-agglomerated well-developed crystals with predominantly hexagonal shapes at 60°C; XRD measurements confirmed that the same polymorph has been obtained in all experiments. We conclude that for phenanthrene, carrying out recrystallization experiments at lower temperatures led to higher rates of crystal formation, to smaller particles and also to a more pronounced tendency to form agglomerates. Hence, the temperature is a possible operating parameter to control size and morphology of crystals formed.

The influence of stirring on the recrystallization process was investigated at 20°C, changing the stirring rate from 100 rpm to 300 rpm. Images of representative product particles are shown in Figure 7.7; it can be seen that the size of particles decreases clearly with increasing stirring rate.

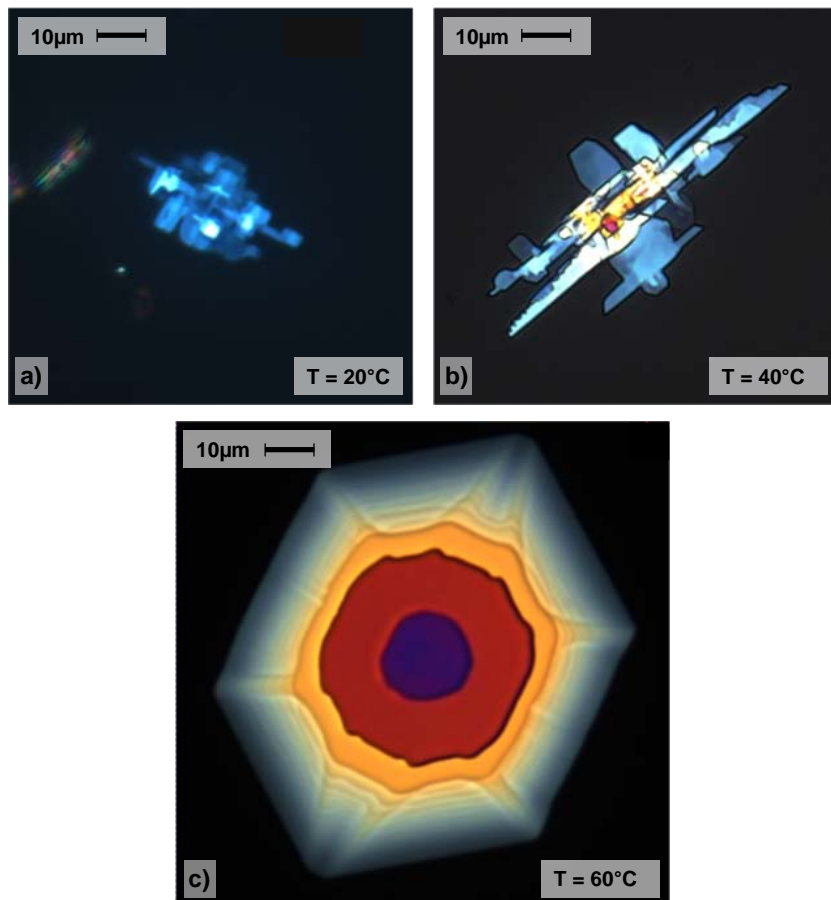


Figure 7.6: Recrystallization of phenantrene from an emulsion. Representative product particles obtained at three different temperatures while stirring at 200 rpm.

This has been confirmed by determining the PSDs, where the average particle size x_{50} decreased from $34\ \mu\text{m}$ (100 rpm) over $14\ \mu\text{m}$ (200 rpm) to $12\ \mu\text{m}$ (300 rpm). While it seems reasonable that at 20°C increased

stirring may lead to reduced agglomeration and hence to smaller particles, it was found that stirring exhibits the same size-reducing effect also at higher temperatures, where agglomeration was absent. Moreover, it has been observed under the microscope that single amorphous precursor droplets crystallized promptly upon contact with already existing crystals. Since the probability of collisions between droplets and crystals increases with increased stirring rate, it seems feasible that stirring influences the rate of crystal nucleation and also the particle size by this mechanism, similarly to secondary nucleation.

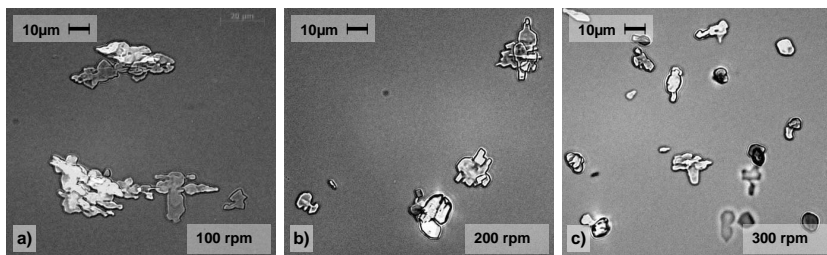


Figure 7.7: Recrystallization of phenanthrene from an emulsion. Representative product particles obtained at 20°C for three different stirring rates.

In order to check how the method of solvent extraction may influence the size of recrystallizing particles, emulsions were also processed by SFEE. In two different experiments, extraction conditions of 45° and 80 bar respectively 60° and 100 bar have been investigated. Phenanthrene was subsequently allowed to recrystallize at the temperature of the experiment. Images of product particles from both experiments are shown in Figure 7.8. It can be seen that obtained particles are generally much smaller as those obtained by dialysis in the previous experiments. It should be highlighted that probably the most important difference between SFEE and dialysis is the density of the suspensions in which crystallization occurs: while the original density of the emulsion is pre-

served in SFEE, dialysis involves dilution by a factor of 10. Therefore, we conclude that it is predominantly the influence of the suspension density that causes the drastic change in particle size. It can be seen in Figure 7.8, and as well from measured PSDs exhibiting an average particle size x_{50} of $3.4\ \mu\text{m}$ at 45°C as compared to $5.7\ \mu\text{m}$ at 60°C , that the previous finding of particle sizes increasing with temperature is confirmed in this case.

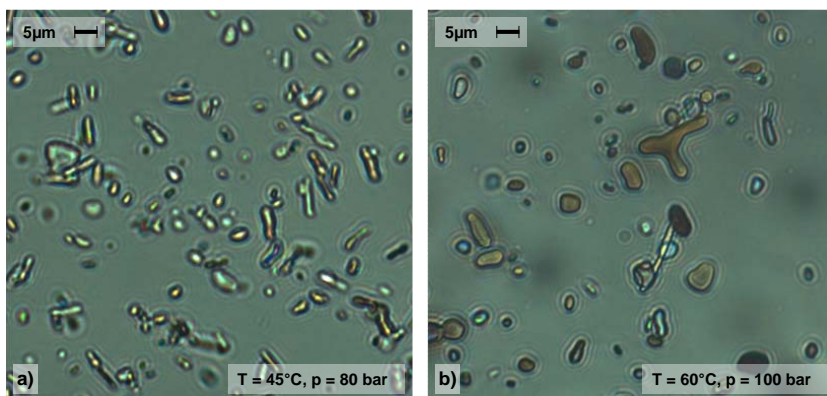


Figure 7.8: Recrystallized phenanthrene from emulsions extracted by SFEE at two different operating conditions.

This preliminary study shows for the case of phenanthrene that recrystallization from emulsions is a process in which the size of product particles could be varied and also controlled in the wide range from $3.4\ \mu\text{m}$ to $84\ \mu\text{m}$, by changing operating parameters such as temperature, stirring rate and suspension density. It has been highlighted that the process might potentially find interesting applications in the crystallization of substances prone to oiling out, as it allows crystallization through the oil phase, instead of avoiding it. Therefore, a more fundamental understanding of the involved mechanisms of crystal formation is required;

especially of the observed nucleation in amorphous precursor droplets upon contact with other crystals. Further, the range of experimental investigations should be expanded also to other materials.

Bibliography

Adami, R., Osseo, L. S., Huopalahti, R., Reverchon, E., 2007. Supercritical antisolvent micronization of PVA by semi-continuous and batch processing. *Journal of Supercritical Fluids* 42 (2), 288–298.

Adami, R., Reverchon, E., Jarvenpaa, E., Huopalahti, R., 2008. Supercritical antisolvent micronization of nalmefene HCl on laboratory and pilot scale. *Powder Technology* 182 (1), 105–112.

Amidon, G. L., Lennernas, H., Shah, V. P., Crison, J. R., 1995. A theoretical basis for a biopharmaceutic drug classification - the correlation of in-vitro drug product dissolution and in-vivo bioavailability. *Pharmaceutical Research* 12 (3), 413–420.

Anderson, J. M., Shive, M. S., 1997. Biodegradation and biocompatibility of PLA and PLGA microspheres. *Advanced Drug Delivery Reviews* 28 (1), 5–24.

Antonietti, M., Landfester, K., 2002. Polyreactions in miniemulsions. *Progress in Polymer Science* 27 (4), 689–757.

Asmatulu, R., Zalich, M. A., Claus, R. O., Riffle, J. S., 2005. Synthesis, characterization and targeting of biodegradable magnetic nanocom-

- posite particles by external magnetic fields. *Journal of Magnetism and Magnetic Materials* 292, 108–119.
- Bao, W. C., Zhou, J. X., Luo, J. F., Wu, D. X., 2006. PLGA microspheres with high drug loading and high encapsulation efficiency prepared by a novel solvent evaporation technique. *Journal of Microencapsulation* 23 (5), 471–479.
- Barichello, J. M., Morishita, M., Takayama, K., Nagai, T., 1999. Encapsulation of hydrophilic and lipophilic drugs in PLGA nanoparticles by the nanoprecipitation method. *Drug Development and Industrial Pharmacy* 25 (4), 471–476.
- Barrett, A. M., Dehghani, F., Foster, N. R., 2008. Increasing the dissolution rate of itraconazole processed by gas antisolvent techniques using polyethylene glycol as a carrier. *Pharmaceutical Research* 25 (6), 1274–1289.
- Berkland, C., Kim, K., Pack, D. W., 2003. PLG microsphere size controls drug release rate through several competing factors. *Pharmaceutical Research* 20 (7), 1055–1062.
- Berkland, C., King, M., Cox, A., Kim, K., Pack, D. W., 2002. Precise control of PLG microsphere size provides enhanced control of drug release rate. *Journal of Controlled Release* 82 (1), 137–147.
- Binks, B., Horozov, T., 2006. *Colloidal particles at liquid interfaces*. Cambridge University Press, Cambridge.
- Blasi, P., D'Souza, S. S., Selmin, F., DeLuca, P. P., 2005. Plasticizing effect of water on poly(lactide-co-glycolide). *Journal of Controlled Release* 108 (1), 1–9.

- Blasi, P., Schoubben, A., Giovagnoli, S., Perioli, L., Ricci, M., Rossi, C., 2007. Ketoprofen poly(lactide-co-glycolide) physical interaction. *AAPS PharmSciTech* 8 (2).
- Bodmeier, R., Wang, H., Dixon, D. J., Mawson, S., Johnston, K. P., 1995. Polymeric microspheres prepared by spraying into compressed carbon-dioxide. *Pharmaceutical Research* 12 (8), 1211–1217.
- Bühler, V., 2003. Kollidon - Polyvinylpyrrolidone for the Pharmaceutical Industry, 7th Edition. BASF Aktiengesellschaft, Pharma Ingredients, 67056 Ludwigshafen, Germany.
- Byrappa, K., Ohara, S., Adschiri, T., 2008. Nanoparticles synthesis using supercritical fluid technology - towards biomedical applications. *Advanced Drug Delivery Reviews* 60 (3), 299–327.
- Castelli, F., Conti, B., Maccarrone, D. E., Conte, U., Puglisi, G., 1998. Comparative study of 'in vitro' release of anti-inflammatory drugs from polylactide-co-glycolide microspheres. *International Journal of Pharmaceutics* 176 (1), 85–98.
- Chang, S. C., Lee, M. J., Lin, H. M., 2008. Role of phase behavior in micronization of lysozyme via a supercritical anti-solvent process. *Chemical Engineering Journal* 139 (2), 416–425.
- Charoenchaitrakool, M., Dehghani, F., Foster, N. R., 2002. Utilization of supercritical carbon dioxide for complex formation of ibuprofen and methyl-beta-cyclodextrin. *International Journal of Pharmaceutics* 239 (1-2), 103–112.
- Charoenchaitrakool, M., Dehghani, F., Foster, N. R., Chan, H. K., 2000. Micronization by rapid expansion of supercritical solutions to enhance the dissolution rates of poorly water-soluble pharmaceuticals. *Industrial & Engineering Chemistry Research* 39 (12), 4794–4802.

- Chattopadhyay, P., Gupta, R. B., 2002. Supercritical CO₂ based production of magnetically responsive micro- and nanoparticles for drug targeting. *Industrial & Engineering Chemistry Research* 41 (24), 6049–6058.
- Chattopadhyay, P., Huff, R., Shekunov, B. Y., 2006. Drug encapsulation using supercritical fluid extraction of emulsions. *Journal of Pharmaceutical Sciences* 95 (3), 667–679.
- Chen, A. Z., Pu, X. M., Kang, Y. Q., Liao, L., Yao, Y. D., Yin, G. F., 2007. Study of poly(L-lactide) microparticles based on supercritical co₂. *Journal of Materials Science-Materials in Medicine* 18 (12), 2339–2345.
- Cho, M., Sah, H., 2005. Formulation and process parameters affecting protein encapsulation into PLGA microspheres during ethyl acetate-based microencapsulation process. *Journal of Microencapsulation* 22 (1), 1–12.
- Chow, A. H. L., Gordon, J. D., Szeitz, A., Young, J. W. M., 1995. Modification of phenytoin crystals .3. influence of 3-butanoyloxymethyl-5,5-diphenylhydantoin on solution-phase crystallization and related crystal properties. *International Journal of Pharmaceutics* 126 (1-2), 11–19.
- Cohen, F. J., 2005. Macro trends in pharmaceutical innovation. *Nature Reviews Drug Discovery* 4 (1), 78–84.
- Coimbra, P., Duarte, C. M. M., de Sousa, H. C., 2006. Cubic equation-of-state correlation of the solubility of some anti-inflammatory drugs in supercritical carbon dioxide. *Fluid Phase Equilibria* 239 (2), 188–199.
- Coulember, O., Degee, P., Hedrick, J. L., Dubois, P., 2006. From controlled ring-opening polymerization to biodegradable aliphatic

- polyester: Especially poly(beta-malic acid) derivatives. *Progress in Polymer Science* 31 (8), 723–747.
- Dave, R., Yulu, W., Yiping, W., Jun, Y., Pfeffer, R., Michniak, B., 2006. The application of a supercritical antisolvent process for sustained drug delivery. *Powder Technology* 164 (2), 94–102.
- de Jong, S. J., Arias, E. R., Rijkers, D. T. S., van Nostrum, C. F., Kettenes-van den Bosch, J. J., Hennink, W. E., 2001. New insights into the hydrolytic degradation of poly(lactic acid): participation of the alcohol terminus. *Polymer* 42 (7), 2795–2802.
- Debenedetti, P. G., 1996. *Metastable Liquids: Concepts and Principles*. Physical Chemistry: Science and Engineering. Princeton University Press, Princeton N.J.
- Debenedetti, P. G., Tom, J. W., Kwauk, X., Yeo, S. D., 1993. Rapid expansion of supercritical solutions (RESS) - fundamentals and applications. *Fluid Phase Equilibria* 82, 311–321.
- Della Porta, G., Reverchon, E., 2008. Nanostructured microspheres produced by supercritical fluid extraction of emulsions. *Biotechnology and Bioengineering* 100 (5), 1020–1033.
- Di Martino, P., Joiris, E., Gobetto, R., Masic, A., Palmieri, G. F., Martelli, S., 2004. Ketoprofen-poly(vinylpyrrolidone) physical interaction. *Journal of Crystal Growth* 265 (1-2), 302–308.
- Dixon, D. J., Johnston, K. P., 1991. Molecular thermodynamics of solubilities in gas antisolvent crystallization. *AIChE Journal* 37 (10), 1441–1449.

- Dixon, D. J., Johnston, K. P., Bodmeier, R. A., 1993. Polymeric materials formed by precipitation with a compressed fluid antisolvent. *AIChE Journal* 39 (1), 127–139.
- Dobson, J., 2006. Magnetic nanoparticles for drug delivery. *Drug Development Research* 67 (1), 55–60.
- Duarte, A. R. C., Gordillo, M. D., Cardoso, M. M., Simplicio, A. L., Duarte, C. M. M., 2006. Preparation of ethyl cellulose/methyl cellulose blends by supercritical antisolvent precipitation. *International Journal of Pharmaceutics* 311 (1-2), 50–54.
- Dwan'Isa, J. P. L., Rouxhet, L., Preat, V., Brewster, M. E., Arien, A., 2007. Prediction of drug solubility in amphiphilic di-block copolymer micelles: the role of polymer-drug compatibility. *Pharmazie* 62 (7), 499–504.
- Eerikainen, H., Kauppinen, E. I., Kansikas, J., 2004a. Polymeric drug nanoparticles prepared by an aerosol flow reactor method. *Pharmaceutical Research* 21 (1), 136–143.
- Eerikainen, H., Peltonen, L., Raula, J., Hirvonen, J., Kauppinen, E. I., 2004b. Nanoparticles containing ketoprofen and acrylic polymers prepared by an aerosol flow reactor method. *AAPS Pharmscitech* 5 (4).
- Elvassore, N., Baggio, M., Pallado, P., Bertucco, A., 2001a. Production of different morphologies of biocompatible polymeric materials by supercritical CO₂ antisolvent techniques. *Biotechnology and Bioengineering* 73 (6), 449–457.
- Elvassore, N., Bertucco, A., Caliceti, P., 2001b. Production of insulin-loaded poly(ethylene glycol)/poly(L-lactide) (PEG/PLA) nanoparticles by gas antisolvent techniques. *Journal of Pharmaceutical Sciences* 90 (10), 1628–1636.

- Fages, J., Lochard, H., Letourneau, J. J., Sauceau, M., Rodier, E., 2004. Particle generation for pharmaceutical applications using supercritical fluid technology. *Powder Technology* 141 (3), 219–226.
- Falk, R., Randolph, T. W., Meyer, J. D., Kelly, R. M., Manning, M. C., 1997. Controlled release of ionic compounds from poly (L-lactide) microspheres produced by precipitation with a compressed antisolvent. *Journal of Controlled Release* 44 (1), 77–85.
- Falk, R. F., Randolph, T. W., 1998. Process variable implications for residual solvent removal and polymer morphology in the formation of gentamycin-loaded poly(L-lactide) microparticles. *Pharmaceutical Research* 15 (8), 1233–1237.
- Filipovic-Grcic, J., Perissutti, B., Moneghini, M., Voinovich, D., Martinac, A., Jalsenjak, I., 2003. Spray-dried carbamazepine-loaded chitosan and HPMC microspheres: preparation and characterisation. *Journal of Pharmacy and Pharmacology* 55 (7), 921–31.
- Flory, P., 1953. *Principles of polymer chemistry*, 3rd Edition. Cornell University Press, Ithaca, N.Y., United States of America.
- Foss, W. R., Anderl, J. N., Clausi, A. L., Burke, P. A., 2009. Diffusivities of dichloromethane in poly(lactide-co-glycolide). *Journal of Applied Polymer Science* 112 (3), 1622–1629.
- Foster, N., Mammucari, R., Dehghani, F., Barrett, A., Bezanehtak, K., Coen, E., Combes, G., Meure, L., Ng, A., Regtop, H. L., Tandy, A., 2003. Processing pharmaceutical compounds using dense gas technology. *Industrial & Engineering Chemistry Research* 42 (25), 6476–6493.
- Franceschi, E., De Cesaro, A. M., Ferreira, S. R. S., Oliveira, J. V., 2009. Precipitation of beta-carotene microparticles from SEDS tech-

- nique using supercritical CO₂. *Journal of Food Engineering* 95 (4), 656–663.
- Franco, M., Trapani, G., Latrofa, A., Tullio, C., Provenzano, M. R., Serra, M., Muggironi, M., Biggio, G., Liso, G., 2001. Dissolution properties and anticonvulsant activity of phenytoin-polyethylene glycol 6000 and -polyvinylpyrrolidone K-30 solid dispersions. *International Journal of Pharmaceutics* 225 (1-2), 63–73.
- Freitas, S., Merkle, H. P., Gander, B., 2005. Microencapsulation by solvent extraction/evaporation: reviewing the state of the art of microsphere preparation process technology. *Journal of Controlled Release* 102 (2), 313–332.
- Furlan, M., Kluge, J., Mazzotti, M., Lattuada, M., 2010. Preparation of biocompatible magnetite-PLGA composite nanoparticles using supercritical fluid extraction of emulsions. *Journal of Supercritical Fluids*, doi:10.1016/j.supflu.2010.05.010.
- Fusaro, F., Hanchen, M., Mazzotti, M., Muhrer, G., Subramaniam, B., 2005. Dense gas antisolvent precipitation: A comparative investigation of the GAS and PCA techniques. *Industrial & Engineering Chemistry Research* 44 (5), 1502–1509.
- Fusaro, F., Kluge, J., Mazzotti, M., Muhrer, G., 2009. Compressed CO₂ antisolvent precipitation of lysozyme. *Journal of Supercritical Fluids* 49 (1), 79–92.
- Fusaro, F., 2008. Production of pharmaceutical microparticles using compressed CO₂ as antisolvent. Dissertation, ETH Zurich, Switzerland.

- Fusaro, F., Mazzotti, M., Muhrer, G., 2004. Gas antisolvent recrystallization of paracetamol from acetone using compressed carbon dioxide as antisolvent. *Crystal Growth & Design* 4 (5), 881–889.
- Gabor, F., Ertl, B., Wirth, M., Mallinger, R., 1999. Ketoprofen-poly(D,L-lactic-co-glycolic acid) microspheres: influence of manufacturing parameters and type of polymer on the release characteristics. *Journal of Microencapsulation* 16 (1), 1–12.
- Gallagher, P. M., Coffey, M. P., Krukonis, V. J., Klasutis, N., 1989. Gas antisolvent recrystallization - new process to recrystallize compounds insoluble in supercritical fluids. *ACS Symposium Series* 406, 334–354.
- Gander, B., Meinel, L., Walter, E., Merkle, H. P., 2001. Polymers as a platform for drug delivery: Reviewing our current portfolio on poly(lactide-co-glycolide) (PLGA) microspheres. *Chimia* 55 (3), 212–217.
- Garay, I., Pocheville, A., Madariaga, L., 2010. Polymeric microparticles prepared by supercritical antisolvent precipitation. *Powder Technology* 197 (3), 211–217.
- Gauter, K., Heidemann, R. A., 2000. A proposal for parametrizing the Sanchez-Lacombe equation of state. *Industrial & Engineering Chemistry Research* 39 (4), 1115–1117.
- Gavini, E., Sanna, V., Juliano, C., Giunchedi, P., 2003. Compressed biodegradable matrices of spray-dried PLGA microspheres for the modified release of ketoprofen. *Journal of Microencapsulation* 20 (2), 193–201.
- Ghaderi, R., Artursson, P., Carlfors, J., 1999. Preparation of biodegradable microparticles using solution-enhanced dispersion by supercritical fluids (SEDS). *Pharmaceutical Research* 16 (5), 676–81.

- Ghaderi, R., Artursson, P., Carlfors, J., 2000. A new method for preparing biodegradable microparticles and entrapment of hydrocortisone in DL-PLG microparticles using supercritical fluids. *European Journal of Pharmaceutical Sciences* 10 (1), 1–9.
- Gupta, A. K., Gupta, M., 2005. Synthesis and surface engineering of iron oxide nanoparticles for biomedical applications. *Biomaterials* 26 (18), 3995–4021.
- Gupta, P. K., Hickey, A. J., 1991. Contemporary approaches in aerosolized drug delivery to the lung. *Journal of Controlled Release* 17 (2), 127–147.
- Hans, M. L., Lowman, A. M., 2002. Biodegradable nanoparticles for drug delivery and targeting. *Current Opinion in Solid State & Materials Science* 6 (4), 319–327.
- Harrison, S. T. L., 1991. Bacterial-cell disruption - a key unit operation in the recovery of intracellular products. *Biotechnology Advances* 9 (2), 217–240.
- Isojima, T., Suh, S. K., Sande, J. B. V., Hatton, T. A., 2009. Controlled assembly of nanoparticle structures: Spherical and toroidal superlattices and nanoparticle-coated polymeric beads. *Langmuir* 25 (14), 8292–8298.
- Jain, R. A., 2000. The manufacturing techniques of various drug loaded biodegradable poly(lactide-co-glycolide) (PLGA) devices. *Biomaterials* 21 (23), 2475–2490.
- Jurgons, R., Seliger, C., Hilpert, A., Trahms, L., Odenbach, S., Alexiou, C., 2006. Drug loaded magnetic nanoparticles for cancer therapy. *Journal of Physics-Condensed Matter* 18 (38), S2893–S2902.

- Kalogiannis, C. G., Pavlidou, E., Panayiotou, C. G., 2005. Production of amoxicillin microparticles by supercritical antisolvent precipitation. *Industrial & Engineering Chemistry Research* 44 (24), 9339–9346.
- Kang, Y. Q., Yin, G. F., Ping, O. Y., Huang, Z. B., Yao, Y. D., Liao, X. M., Chen, A. Z., Pu, X. M., 2008. Preparation of PLLA/PLGA microparticles using solution enhanced dispersion by supercritical fluids (SEDS). *Journal of Colloid and Interface Science* 322 (1), 87–94.
- Kang, Y. S., Risbud, S., Rabolt, J. F., Stroeve, P., 1996. Synthesis and characterization of nanometer-size Fe₃O₄ and gamma-Fe₂O₃ particles. *Chemistry of Materials* 8 (9), 2209–2211.
- Kikic, I., Lora, M., Bertucco, A., 1997. A thermodynamic analysis of three-phase equilibria in binary and ternary systems for applications in rapid expansion of a supercritical solution (RESS), particles from gas-saturated solutions (PGSS), and supercritical antisolvent (SAS). *Industrial & Engineering Chemistry Research* 36 (12), 5507–5515.
- Kikic, I., Vecchione, F., 2003. Supercritical impregnation of polymers. *Current Opinion in Solid State & Materials Science* 7 (4-5), 399–405.
- Kim, D. K., Mikhaylova, M., Zhang, Y., Muhammed, M., 2003. Protective coating of superparamagnetic iron oxide nanoparticles. *Chemistry of Materials* 15 (8), 1617–1627.
- Kluge, J., Fusaro, F., Muhrer, G., Thakur, R., Mazzotti, M., 2009c. Rational design of drug-polymer co-formulations by CO₂ anti-solvent precipitation. *Journal of Supercritical Fluids* 48 (2), 176–182.
- Kluge, J., Fusaro, F., Casas, N., Mazzotti, M., Muhrer, G., 2009a. Production of PLGA micro- and nanocomposites by supercritical fluid extraction of emulsions: I. encapsulation of lysozyme. *Journal of Supercritical Fluids* 50 (3), 327–335.

- Kluge, J., Fusaro, F., Mazzotti, M., Muhrer, G., 2009b. Production of PLGA micro- and nanocomposites by supercritical fluid extraction of emulsions: II. encapsulation of ketoprofen. *Journal of Supercritical Fluids* 50 (3), 336–343.
- Koneracka, M., Muckova, M., Zavisova, V., Tomasovicova, N., Kocansky, P., Timko, M., Jurikova, A., Csach, K., V., K., Lancz, G., 2007. Encapsulation of anticancer drug and magnetic particles in biodegradable polymer nanospheres. In: 11th International Conference on Magnetic Fluids. Iop Publishing Ltd., Kosice, SLOVAKIA.
- Konno, H., Taylor, L. S., 2006. Influence of different polymers on the crystallization tendency of molecularly dispersed amorphous felodipine. *Journal of Pharmaceutical Sciences* 95 (12), 2692–2705.
- Lai, J. Y., Lin, S. F., Lin, F. C., Wang, D. M., 1998. Construction of ternary phase diagrams in nonsolvent/solvent/PMMA systems. *Journal of Polymer Science Part B-Polymer Physics* 36 (4), 607–615.
- Lam, U. T., Mammucari, R., Suzuki, K., Foster, N. R., 2008. Processing of iron oxide nanoparticles by supercritical fluids. *Industrial & Engineering Chemistry Research* 47 (3), 599–614.
- Lattuada, M., Hatton, T. A., 2007. Functionalization of monodisperse magnetic nanoparticles. *Langmuir* 23 (4), 2158–2168.
- Lee, S., Kim, M. S., Kim, J. S., Park, H. J., Woo, J. S., Lee, B. C., Hwang, S. J., 2006. Controlled delivery of a hydrophilic drug from a biodegradable microsphere system by supercritical anti-solvent precipitation technique. *Journal of Microencapsulation* 23 (7), 741–749.
- Lee, S., Nam, K., Kim, M. S., Jun, S. W., Park, J. S., Woo, J. S., Hwang, S. J., 2005. Preparation and characterization of solid dispersions of itraconazole by using aerosol solvent extraction system for

- improvement in drug solubility and bioavailability. *Archives of Pharmaceutical Research* 28 (7), 866–874.
- Lengsfeld, C. S., Delplanque, J. P., Barocas, V. H., Randolph, T. W., 2000. Mechanism governing microparticle morphology during precipitation by a compressed antisolvent: Atomization vs nucleation and growth. *Journal of Physical Chemistry B* 104 (12), 2725–2735.
- Leuner, C., Dressman, J., 2000. Improving drug solubility for oral delivery using solid dispersions. *European Journal of Pharmaceutics and Biopharmaceutics* 50 (1), 47–60.
- Lian, Z. Y., Epstein, S. A., Blenk, C. W., Shine, A. D., 2006. Carbon dioxide-induced melting point depression of biodegradable semicrystalline polymers. *Journal of Supercritical Fluids* 39 (1), 107–117.
- Lin, C., Ng, K. M., Wibowo, C., 2007. Producing nanoparticles using precipitation with compressed antisolvent. *Industrial & Engineering Chemistry Research* 46 (11), 3580–3589.
- Lin, I. H., Liang, P. F., Tan, C. S., 2010. Preparation of polystyrene/poly(methyl methacrylate) blends by compressed fluid antisolvent technique. *Journal of Supercritical Fluids* 51 (3), 384–398.
- Liu, D. H., Li, H. B., Noon, M. S., Tomasko, D. L., 2005. CO₂-induced PMMA swelling and multiple thermodynamic property analysis using Sanchez-Lacombe eos. *Macromolecules* 38 (10), 4416–4424.
- Liu, D. H., Tomasko, D. L., 2007. Carbon dioxide sorption and dilation of poly(lactide-co-glycolide). *Journal of Supercritical Fluids* 39 (3), 416–425.
- Liu, T. Y., Hu, S. H., Liu, K. H., Shaiu, R. S., Liu, D. M., Chen, S. Y., 2008. Instantaneous drug delivery of magnetic/thermally sensi-

- tive nanospheres by a high-frequency magnetic field. *Langmuir* 24 (23), 13306–13311.
- Liu, X. Q., Kaminski, M. D., Chen, H. T., Torno, M., Taylor, L., Rosengart, A. J., 2007. Synthesis and characterization of highly-magnetic biodegradable poly(D,L-lactide-co-glycolide) nanospheres. *Journal of Controlled Release* 119 (1), 52–58.
- Lorenz, H., Seidel-Morgenstern, A., 2002. Binary and ternary phase diagrams of two enantiomers in solvent systems. *Thermochimica Acta* 382 (1-2), 129–142.
- Lu, Y. H., Ching, C. B., 2004. Physicochemical properties, binary and ternary phase diagrams of ketoprofen. *Chirality* 16 (8), 541–548.
- Lu, Y. H., Wang, X. J., Ching, C. B., 2009. Application of preferential crystallization for different types of racemic compounds. *Industrial & Engineering Chemistry Research* 48 (15), 7266–7275.
- Manna, L., Banchemo, M., Sola, D., Ferri, A., Ronchetti, S., Sicardi, S., 2007. Impregnation of PVP microparticles with ketoprofen in the presence of supercritical CO₂. *Journal of Supercritical Fluids* 42 (3), 378–384.
- Marsac, P. J., Konno, H., Rumondor, A. C. F., Taylor, L. S., 2008. Recrystallization of nifedipine and felodipine from amorphous molecular level solid dispersions containing poly(vinylpyrrolidone) and sorbed water. *Pharmaceutical Research* 25 (3), 647–656.
- Marsac, P. J., Konno, H., Taylor, L. S., 2006a. A comparison of the physical stability of amorphous felodipine and nifedipine systems. *Pharmaceutical Research* 23 (10), 2306–2316.

- Marsac, P. J., Shamblin, S. L., Taylor, L. S., 2006b. Theoretical and practical approaches for prediction of drug-polymer miscibility and solubility. *Pharmaceutical Research* 23 (10), 2417–2426.
- Martin, A., Mattea, F., Gutierrez, L., Miguel, F., Cocero, M. J., 2007. Co-precipitation of carotenoids and bio-polymers with the supercritical anti-solvent process. *Journal of Supercritical Fluids* 41 (1), 138–147.
- Massart, R., 1981. Preparation of aqueous magnetic liquids in alkaline and acidic media. *IEEE Transactions on Magnetics* 17 (2), 1247–1248.
- Mayo, A. S., Ambati, B. K., Kompella, U. B., 2010. Gene delivery nanoparticles fabricated by supercritical fluid extraction of emulsions. *International Journal of Pharmaceutics* 387 (1-2), 278–285.
- McHugh, M. A., Krukonis, V. J., 1994. *Supercritical Fluid Extraction - Principles and Practice*, 2nd Edition. Butterworth-Heinemann, Newton. MA.
- Miguel, F., Martin, A., Gamse, T., Cocero, M. J., 2006. Supercritical anti solvent precipitation of lycopene - effect of the operating parameters. *Journal of Supercritical Fluids* 36 (3), 225–235.
- Miguel, F., Martin, A., Mattea, F., Cocero, M. J., 2008. Precipitation of lutein and co-precipitation of lutein and poly-lactic acid with the supercritical anti-solvent process. *Chemical Engineering and Processing* 47 (9-10), 1594–1602.
- Miller, D. A., McConville, J. T., Yang, W., Williams, R. O., McGinity, J. W., 2007. Hot-melt extrusion for enhanced delivery of drug particles. *Journal of Pharmaceutical Sciences* 96 (2), 361–376.

- Mishima, K., 2008. Biodegradable particle formation for drug and gene delivery using supercritical fluid and dense gas. *Advanced Drug Delivery Reviews* 60 (3), 411–432.
- Moghimi, S. M., Hunter, A. C., Murray, J. C., 2001. Long-circulating and target-specific nanoparticles: Theory to practice. *Pharmacological Reviews* 53 (2), 283–318.
- Moneghini, M., Kikic, I., Voinovich, D., Perissutti, B., Alessi, P., Cortesi, A., Princivale, F., Solinas, D., 2003. Study of the solid state of carbamazepine after processing with gas anti-solvent technique. *European Journal of Pharmaceutics and Biopharmaceutics* 56 (2), 281–289.
- Moneghini, M., Kikic, I., Voinovich, D., Perissutti, B., Filipovic-Grcic, J., 2001. Processing of carbamazepine-PEG 4000 solid dispersions with supercritical carbon dioxide: preparation, characterisation, and in vitro dissolution. *International Journal of Pharmaceutics* 222 (1), 129–38.
- Moneghini, M., Perissutti, B., Kikic, I., Grassi, M., Cortesi, A., Princivale, F., 2006. Preparation of theophylline-hydroxypropylmethylcellulose matrices using supercritical antisolvent precipitation: A preliminary study. *Drug Development and Industrial Pharmacy* 32 (1), 39–52.
- Montagne, F., Mondain-Monval, O., Pichot, C., Elaissari, A., 2006. Highly magnetic latexes from submicrometer oil in water ferrofluid emulsions. *Journal of Polymer Science Part a-Polymer Chemistry* 44 (8), 2642–2656.
- Muhrer, G., Lin, C., Mazzotti, M., 2002. Modeling the gas antisolvent recrystallization process. *Industrial & Engineering Chemistry Research* 41 (15), 3566–3579.

- Muhrer, G., Mazzotti, M., 2003. Precipitation of lysozyme nanoparticles from dimethyl sulfoxide using carbon dioxide as antisolvent. *Biotechnology Progress* 19 (2), 549–556.
- Muhrer, G., Mazzotti, M., Muller, M., 2003. Gas antisolvent recrystallization of an organic compound. tailoring product PSD and scaling-up. *Journal of Supercritical Fluids* 27 (2), 195–203.
- Muhrer, G., Meier, U., Fusaro, F., Albano, S., Mazzotti, M., 2006. Use of compressed gas precipitation to enhance the dissolution behavior of a poorly water-soluble drug: Generation of drug microparticles and drug-polymer solid dispersions. *International Journal of Pharmaceutics* 308 (1-2), 69–83.
- Muhrer, G., Schneeberger, R., Wirth, W., Baumberger, A., 2005. Micronization of a pharmaceutically active agent, useful in e.g. inhalation formulations, comprises suspending the agent in a propellant or compressed gas, processing the suspension and obtaining dry powder upon depressurization.
- Muller, R. H., Peters, K., 1998. Nanosuspensions for the formulation of poorly soluble drugs - I. preparation by a size-reduction technique. *International Journal of Pharmaceutics* 160 (2), 229–237.
- Mundargi, R. C., Babu, V. R., Rangaswamy, V., Patel, P., Aminabhavi, T. M., 2008. Nano/micro technologies for delivering macromolecular therapeutics using poly(D,L-lactide-co-glycolide) and its derivatives. *Journal of Controlled Release* 125 (3), 193–209.
- Munos, B., 2009. Lessons from 60 years of pharmaceutical innovation. *Nature Reviews Drug Discovery* 8 (12), 959–968.

- Musyanovych, A., Schmitz-Wienke, J., Mailander, V., Walther, P., Landfester, K., 2008. Preparation of biodegradable polymer nanoparticles by miniemulsion technique and their cell interactions. *Macromolecular Bioscience* 8 (2), 127–139.
- Neuberger, T., Schopf, B., Hofmann, H., Hofmann, M., von Rechenberg, B., 2004. Supermagnetic nanoparticles for biomedical applications: Possibilities and limitations of a new drug delivery system. In: 5th International Conference on Scientific and Clinical Applications of Magnetic Carriers. Elsevier Science Bv, Lyon, FRANCE, pp. 483–496.
- Niu, F. H., Roby, K. F., Rajewski, R. A., Decedue, C., Subramaniam, B., 2006. Paclitaxel nanoparticles: Production using compressed CO₂ as antisolvent: Characterization and animal model studies. *Polymeric Drug Delivery II: Polymeric Matrices and Drug Particle Engineering* 924, 262–277.
- Niwa, T., Takeuchi, H., Hino, T., Kunou, N., Kawashima, Y., 1994. In-vitro drug-release behavior of D,L-lactide/glycolide copolymer (PLGA) nanospheres with nafarelin acetate prepared by a novel spontaneous emulsification solvent diffusion method. *Journal of Pharmaceutical Sciences* 83 (5), 727–732.
- Palakodaty, S., York, P., 1999. Phase behavioral effects on particle formation processes using supercritical fluids. *Pharmaceutical Research* 16 (7), 976–985.
- Panyam, J., Labhasetwar, V., 2003. Biodegradable nanoparticles for drug and gene delivery to cells and tissue. *Advanced Drug Delivery Reviews* 55 (3), 329–347.
- Pasquali, I., Bettini, R., 2008. Are pharmaceuticals really going supercritical? *International Journal of Pharmaceutics* 364 (2), 176–187.

- Pasquali, I., Bettini, R., Giordano, F., 2008. Supercritical fluid technologies: An innovative approach for manipulating the solid-state of pharmaceuticals. *Advanced Drug Delivery Reviews* 60 (3), 399–410.
- Perez, Y., Wubbolts, F. E., Witkamp, G. J., Jansens, P. J., de Loos, T. W., 2004. Improved pca process for the production of nano- and microparticles of polymers. *AIChE Journal* 50 (10), 2408–2417.
- Perez de Diego, Y., Pellikaan, H. C., Wubbolts, F. E., Witkamp, G. J., Jansens, P. J., 2005. Operating regimes and mechanism of particle formation during the precipitation of polymers using the pca process. *Journal of Supercritical Fluids* 35 (2), 147–156.
- Perrut, M., Jung, J., Leboeuf, F., 2005a. Enhancement of dissolution rate of poorly-soluble active ingredients by supercritical fluid processes. part I: Micronization of neat particles. *International Journal of Pharmaceutics* 288 (1), 3–10.
- Perrut, M., Jung, J., Leboeuf, F., 2005b. Enhancement of dissolution rate of poorly soluble active ingredients by supercritical fluid processes. part II: Preparation of composite particles. *International Journal of Pharmaceutics* 288 (1), 11–6.
- Petersen, R. C., Matson, D. W., Smith, R. D., 1987. The formation of polymer fibers from the rapid expansion of supercritical fluid solutions. *Polymer Engineering and Science* 27 (22), 1693–1697.
- Phillips, E. M., Stella, V. J., 1993. Rapid expansion from supercritical solutions - application to pharmaceutical processes. *International Journal of Pharmaceutics* 94 (1-3), 1–10.
- Pini, R., Storti, G., Mazzotti, M., Tai, H. Y., Shakesheff, K. M., Howdle, S. M., 2008. Sorption and swelling of poly(DL-lactic acid)

- and poly(lactic-co-glycolic acid) in supercritical CO₂: An experimental and modeling study. *Journal of Polymer Science Part B-Polymer Physics* 46 (5), 483–496.
- Pourmortazavi, S. M., Hajimirsadeghi, S. S., 2005. Application of supercritical carbon dioxide in energetic materials processes: A review. *Industrial & Engineering Chemistry Research* 44 (17), 6523–6533.
- Prausnitz, J. M., Lichtenthaler, R. N., Gomes de Azevedo, E., 1986. *Molecular Thermodynamics of Fluid Phase Equilibria*, 2nd Edition. Prentice-Hall Inc., Englewood Cliffs, N.J. 07632, U.S.A.
- Rajendran, A., Bonavoglia, B., Forrer, N., Storti, G., Mazzotti, M., Morbidelli, M., 2005. Simultaneous measurement of swelling and sorption in a supercritical CO₂-poly(methyl methacrylate) system. *Industrial & Engineering Chemistry Research* 44 (8), 2549–2560.
- Randolph, T. W., Randolph, A. D., Mebes, M., Yeung, S., 1993. Sub-micrometer-sized biodegradable particles of poly(L-lactic acid) via the gas antisolvent spray precipitation process. *Biotechnology Progress* 9 (4), 429–435.
- Rassu, G., Gavini, E., Spada, G., Giunchedi, P., Marceddu, S., 2008. Ketoprofen spray-dried microspheres based on eudragit RS and RL: Study of the manufacturing parameters. *Drug Development and Industrial Pharmacy* 34 (11), 1178–1187.
- Reverchon, E., Antonacci, A., 2006. Chitosan microparticles production by supercritical fluid processing. *Industrial & Engineering Chemistry Research* 45 (16), 5722–5728.
- Reverchon, E., De Marco, I., 2006. Supercritical fluid extraction and fractionation of natural matter. *Journal of Supercritical Fluids* 38 (2), 146–166.

- Reverchon, E., De Marco, I., Caputo, G., Della Porta, G., 2003. Pilot scale micronization of amoxicillin by supercritical antisolvent precipitation. *Journal of Supercritical Fluids* 26 (1), 1–7.
- Reverchon, E., De Marco, I., Della Porta, G., 2002. Rifampicin microparticles production by supercritical antisolvent precipitation. *International Journal of Pharmaceutics* 243 (1-2), 83–91.
- Reverchon, E., De Marco, L., 2004. Supercritical antisolvent micronization of cefonicid: thermodynamic interpretation of results. *Journal of Supercritical Fluids* 31 (2), 207–215.
- Reverchon, E., Lamberti, G., Antonacci, A., 2008. Supercritical fluid assisted production of HPMC composite microparticles. *Journal of Supercritical Fluids* 46 (2), 185–196.
- Rodier, E., Lochard, H., Sauceau, M., Letourneau, J. J., Freiss, B., Fages, J., 2005. A three step supercritical process to improve the dissolution rate of effucimibe. *European Journal of Pharmaceutical Sciences* 26 (2), 184–193.
- Roy, C., Vega-Gonzalez, A., Subra-Paternault, P., 2007. Theophylline formulation by supercritical antisolvents. *International Journal of Pharmaceutics* 343 (1-2), 79–89.
- Sacanna, S., Kegel, W. K., Philipse, A. P., 2007. Thermodynamically stable pickering emulsions. *Physical Review Letters* 98 (15).
- Sarti, G. C., Doghieri, F., 1998. Predictions of the solubility of gases in glassy polymers based on the NELF model. *Chemical Engineering Science* 53 (19), 3435–3447.

- Schenderlein, S., Luck, M., Muller, B. W., 2004. Partial solubility parameters of poly(D,L-lactide-co-glycolide). *International Journal of Pharmaceutics* 286 (1-2), 19–26.
- Schork, F., Luo, Y., Smulders, W., Russum, J., Butt, A., Fontenot, K., 2005. Miniemulsion polymerization. In: *Polymer Particles. Advances in Polymer Science*. Springer, Berlin, pp. 129–255.
- Sethia, S., Squillante, E., 2002. Physicochemical characterization of solid dispersions of carbamazepine formulated by supercritical carbon dioxide and conventional solvent evaporation method. *Journal of Pharmaceutical Sciences* 91 (9), 1948–57.
- Sethia, S., Squillante, E., 2004. Solid dispersion of carbamazepine in PVP K30 by conventional solvent evaporation and supercritical methods. *International Journal of Pharmaceutics* 272 (1-2), 1–10.
- Shariati, A., Peters, C. J., 2003. Recent developments in particle design using supercritical fluids. *Current Opinion in Solid State & Materials Science* 7 (4-5), 371–383.
- Shekunov, B. Y., Chattopadhyay, P., Seitzinger, J., 2006a. Engineering of composite particles for drug delivery using supercritical fluid technology. In: *Polymeric Drug Delivery II: Polymeric Matrices and Drug Particle Engineering*. Vol. 924 of ACS Symposium Series. pp. 234–249.
- Shekunov, B. Y., Chattopadhyay, P., Seitzinger, J., Huff, R., 2006b. Nanoparticles of poorly water-soluble drugs prepared by supercritical fluid extraction of emulsions. *Pharmaceutical Research* 23 (1), 196–204.
- Sheng, J. J., Kasim, N. A., Chandrasekharan, R., Amidon, G. L., 2006. Solubilization and dissolution of insoluble weak acid, ketoprofen: Ef-

- fects of pH combined with surfactant. *European Journal of Pharmaceutical Sciences* 29 (3-4), 306–314.
- Sievers, R. E., Huang, E. T. S., Villa, J. A., Kawamoto, J. K., Evans, M. M., Brauer, P. R., 2001. Low-temperature manufacturing of fine pharmaceutical powders with supercritical fluid aerosolization in a bubble dryer. *Pure and Applied Chemistry* 73 (8), 1299–1303.
- Six, K., Berghmans, H., Leuner, C., Dressman, J., Van Werde, K., Mullens, J., Benoist, L., Thimon, M., Meublat, L., Verreck, G., Peeters, J., Brewster, M., Van den Mooter, G., 2003. Characterization of solid dispersions of itraconazole and hydroxypropylmethylcellulose prepared by melt extrusion, part II. *Pharmaceutical Research* 20 (7), 1047–1054.
- Six, K., Leuner, C., Dressman, J., Verreck, G., Peeters, J., Blaton, N., Augustijns, P., Kinget, R., Van den Mooter, G., 2002. Thermal properties of hot-stage extrudates of itraconazole and eudragit E100 - phase separation and polymorphism. *Journal of Thermal Analysis and Calorimetry* 68 (2), 591–601.
- Snavely, W. K., Subramaniam, B., Rajewski, R. A., Defelippis, M. R., 2002. Micronization of insulin from halogenated alcohol solution using supercritical carbon dioxide as an antisolvent. *Journal of Pharmaceutical Sciences* 91 (9), 2026–39.
- Soppimath, K. S., Aminabhavi, T. M., Kulkarni, A. R., Rudzinski, W. E., 2001. Biodegradable polymeric nanoparticles as drug delivery devices. *Journal of Controlled Release* 70 (1-2), 1–20.
- Subra, P., Laudani, C. G., Vega-Gonzalez, A., Reverchon, E., 2005. Precipitation and phase behavior of theophylline in solvent-supercritical CO₂ mixtures. *Journal of Supercritical Fluids* 35 (2), 95–105.

- Subramaniam, B., Rajewski, R. A., Snavely, K., 1997. Pharmaceutical processing with supercritical carbon dioxide. *Journal of Pharmaceutical Sciences* 86 (8), 885–890.
- Sun, S. H., Zeng, H., 2002. Size-controlled synthesis of magnetite nanoparticles. *Journal of the American Chemical Society* 124 (28), 8204–8205.
- Sun, S. H., Zeng, H., Robinson, D. B., Raoux, S., Rice, P. M., Wang, S. X., Li, G. X., 2004. Monodisperse $m\text{Fe}_2\text{O}_4$ ($m = \text{Fe}, \text{Co}, \text{Mn}$) nanoparticles. *Journal of the American Chemical Society* 126 (1), 273–279.
- Takada, S., Yamagata, Y., Misaki, M., Taira, K., Kurokawa, T., 2003. Sustained release of human growth hormone from microcapsules prepared by a solvent evaporation technique. *Journal of Controlled Release* 88 (2), 229–242.
- Tanno, F., Nishiyama, Y., Kokubo, H., Obara, S., 2004. Evaluation of hypromellose acetate succinate (HPMCAS) as a carrier in solid dispersions. *Drug Development and Industrial Pharmacy* 30 (1), 9–17.
- Taylor, L. T., 2009. Supercritical fluid chromatography for the 21st century. *Journal of Supercritical Fluids* 47 (3), 566–573.
- Teja, A. S., Koh, P. Y., 2009. Synthesis, properties, and applications of magnetic iron oxide nanoparticles. *Progress in Crystal Growth and Characterization of Materials* 55 (1-2), 22–45.
- Turk, M., 2009. Manufacture of submicron drug particles with enhanced dissolution behaviour by rapid expansion processes. *Journal of Supercritical Fluids* 47 (3), 537–545.

- Vaisman, B., Shikanov, A., Domb, A. J., 2008. The isolation of ricinoleic acid from castor oil by salt-solubility-based fractionation for the biopharmaceutical applications. *Journal of the American Oil Chemists Society* 85 (2), 169–184.
- Varde, N. K., Pack, D. W., 2004. Microspheres for controlled release drug delivery. *Expert Opinion on Biological Therapy* 4 (1), 35–51.
- Vasanthavada, M., Tong, W. Q., Joshi, Y., Kislalioglu, M. S., 2004. Phase behavior of amorphous molecular dispersions I: Determination of the degree and mechanism of solid solubility. *Pharmaceutical Research* 21 (9), 1598–1606.
- Vasanthavada, M., Tong, W. Q., Joshi, Y., Kislalioglu, M. S., 2005. Phase behavior of amorphous molecular dispersions - II: Role of hydrogen bonding in solid solubility and phase separation kinetics. *Pharmaceutical Research* 22 (3), 440–448.
- Verreck, G., Decorte, A., Heymans, K., Adriaensen, J., Liu, D. H., Tomasko, D. L., Arien, A., Peeters, J., Rombaut, P., Van den Mooter, G., Brewster, M. E., 2007. The effect of supercritical CO₂ as a reversible plasticizer and foaming agent on the hot stage extrusion of itraconazole with EC 20 CPS. *Journal of Supercritical Fluids* 40 (1), 153–162.
- Verreck, G., Decorte, A., Heymans, K., Adriaensen, J., Liu, D., Tomasko, D., Arien, A., Peeters, J., Van den Mooter, G., Brewster, M. E., 2006a. Hot stage extrusion of p-amino salicylic acid with ec using co₂ as a temporary plasticizer. *International Journal of Pharmaceutics* 327 (1-2), 45–50.
- Verreck, G., Decorte, A., Li, H. B., Tomasko, D., Arien, A., Peeters, J., Rombaut, P., Van den Mooter, G., Brewster, M. E., 2006b. The effect

- of pressurized carbon dioxide as a plasticizer and foaming agent on the hot melt extrusion process and extrudate properties of pharmaceutical polymers. *Journal of Supercritical Fluids* 38 (3), 383–391.
- Wan, J., Cai, W., Meng, X., Liu, E., 2007. Monodisperse water-soluble magnetite nanoparticles prepared by polyol process for high-performance magnetic resonance imaging. *Chemical Communications* (47), 5004–5006.
- Weidner, E., Steiner, R., Knez, Z., 1996. Powder generation from polyethyleneglycols with compressible fluids. In: vonRohr, P. R. T. C. (Ed.), *High Pressure Chemical Engineering. Vol. 12 of Process Technology Proceedings*. Elsevier Science Publ B V, Amsterdam, pp. 223–228.
- Werling, J. O., Debenedetti, P. G., 1999. Numerical modeling of mass transfer in the supercritical antisolvent process. *Journal of Supercritical Fluids* 16 (2), 167–181.
- Winters, M. A., Knutson, B. L., Debenedetti, P. G., Sparks, H. G., Przybycien, T. M., Stevenson, C. L., Prestrelski, S. J., 1996. Precipitation of proteins in supercritical carbon dioxide. *Journal of Pharmaceutical Sciences* 85 (6), 586–594.
- Won, D. H., Kim, M. S., Lee, S., Park, J. S., Hwang, S. J., 2005. Improved physicochemical characteristics of felodipine solid dispersion particles by supercritical anti-solvent precipitation process. *International Journal of Pharmaceutics* 301 (1-2), 199–208.
- Woo, K., Hong, J., Choi, S., Lee, H. W., Ahn, J. P., Kim, C. S., Lee, S. W., 2004. Easy synthesis and magnetic properties of iron oxide nanoparticles. *Chemistry of Materials* 16 (14), 2814–2818.

- Worlitschek, J., Bosco, M., Huber, M., Gramlich, V., Mazzotti, M., 2004. Solid-liquid equilibrium of troger's base enantiomers in ethanol: Experiments and modelling. *Helvetica Chimica Acta* 87 (2), 279–291.
- Wu, K., Li, J., Wang, W. N., Winstead, D. A., 2009. Formation and characterization of solid dispersions of piroxicam and polyvinylpyrrolidone using spray drying and precipitation with compressed antisolvent. *Journal of Pharmaceutical Sciences* 98 (7), 2422–2431.
- Yang, J., Park, S. B., Yoon, H. G., Huh, Y. M., Haam, S., 2006. Preparation of poly epsilon-caprolactone nanoparticles containing magnetite for magnetic drug carrier. *International Journal of Pharmaceutics* 324 (2), 185–190.
- Yeo, S. D., Kiran, E., 2005. Formation of polymer particles with supercritical fluids: A review. *Journal of Supercritical Fluids* 34 (3), 287–308.
- Yu, Y. C., Storti, G., Morbidelli, M., 2009. Ring-opening polymerization of L,L-lactide: Kinetic and modeling study. *Macromolecules* 42 (21), 8187–8197.
- Zemb, T., Lindner, P., 2002. Neutrons, X-rays and light: scattering methods applied to soft condensed matter. Elsevier Science & Technology, Amsterdam.

List of Figures

1.1	Multidisciplinary background of this thesis project.	2
1.2	Product morphologies obtained by scCO ₂ antisolvent precipitation of pure drug substances. a) Paracetamol, compact crystals (Fusaro et al., 2004); b) Theophylline, crystalline platelets (Roy et al., 2007); c) Phenytoin, crystalline needles (Muhrrer et al., 2006); d) undisclosed compound, amorphous submicron spherical particles (Muhrrer et al., 2003).	13
1.3	Product morphologies obtained by scCO ₂ antisolvent precipitation of polymers. a) L-PLA, a water-insoluble semicrystalline polymer (Chen et al., 2007); b) Ethylcellulose, a water-insoluble amorphous polymer (Duarte et al., 2006); c) PVA, a water-soluble semi-crystalline polymer (Adami et al., 2007); d) Dextran, a water-soluble amorphous polymer (Perez et al., 2004).	17

1.4	Drug-Polymer composite particles obtained by scCO ₂ antisolvent precipitation. a) Theophylline + L-PLA: Rhombic theophylline crystals can be clearly distinguished from micron-sized polymeric particles (Roy et al., 2007); b) Cholesterol + PLGA: Elongate crystals of cholesterol coated by polymeric droplets (Dave et al., 2006); c) Insulin + PLA + PEG: Submicron composite particles (Elvassore et al., 2001b); d) Felodipine + HPMC: The drug is stabilized in amorphous composite particles, crystals are not present (Won et al., 2005). . . .	20
1.5	a) Precipitation of a crystalline solid using CO ₂ as an antisolvent. b) Precipitation of a polymer using CO ₂ as an antisolvent.	24
1.6	Competition between crystallization and liquid-liquid phase separation. a) Kinetic competition, b) Thermodynamic competition	25
1.7	Sequence of Steps in Gas AntiSolvent recrystallization (GAS).	27
1.8	Paracetamol crystals precipitated by the GAS process, using specific rates of CO ₂ addition of 0.1 min ⁻¹ (a), 0.6 min ⁻¹ (b), and 2 min ⁻¹ (c). Average particle size vs. specific rate of CO ₂ addition for a larger set of experiments (d); (∇) experiments carried out using a different GAS setup (Fusaro et al., 2004).	29

1.9	Phenytoin crystals precipitated by the GAS process, using specific rates of CO ₂ addition of a) 0.07 min ⁻¹ , b) 0.1 min ⁻¹ , c) 0.2 min ⁻¹ , d) 0.5 min ⁻¹ , e) 1 min ⁻¹ , f) 2 min ⁻¹ . The average crystal size decreases with increasing rate of CO ₂ addition (Fusaro , 2008).	30
1.10	Lysozyme precipitation by the GAS process. a) Product precipitated from a 2 g/l solution in DMSO at 25°C, using a CO ₂ addition rate of 50 g/min. b) Effect of CO ₂ addition rate on the average particle size of lysozyme precipitated at 25°C (Muhrer and Mazzotti, 2003)	31
1.11	Precipitation with Compressed Antisolvent (PCA) process.	33
1.12	Precipitation of Paracetamol using the PCA process. Products obtained at 313 K and 150 bar from a 10 g/l solution at a flow rate of 1 ml/min. CO ₂ flow rates are a) 20 g/min, b) 50 g/min and c) 150 g/min. d) Volumetric particle size distributions obtained for these runs (Fusaro , 2008).	35
1.13	Precipitation of Phenytoin using the PCA process. Products obtained at 323 K from a 4 wt.% solution at a flow rate of 1 ml/min, using a CO ₂ flow rate of 80 g/min. Operating pressures are a) 150 bar, b) 120 bar and c) 95 bar (Muhrer et al., 2006).	36
1.14	Precipitation of Lysozyme using the PCA process, showing products obtained in the a) subcritical, b) supercritical and c) liquid region of the CO ₂ -DMSO mixture. d) Effect of the CO ₂ flow rate on the mean size of lysozyme particles at different supercritical operating conditions (Fusaro et al., 2009)	37

2.1	Scheme of the PCA setup used for the co-precipitation experiments.	48
2.2	Particles of pure PVP (run 1) and PCA-processed pure phenytoin. (Muhrrer et al., 2006).	51
2.3	X-ray powder diffraction patterns of the amorphous polymer PVP and a drug-polymer co-formulation representing a fully amorphous solution (above); and of pure crystalline phenytoin and a drug-polymer co-formulation containing traces of the crystalline drug (below). Stars represent the 2θ position of phenytoin peaks according to a literature reference (Franco et al., 2001).	52
2.4	Products obtained at 80 bar and 25°C. Runs are indicated on the images. (a) Spherical polymeric particles on a phenytoin crystal. (b) and (c) Needle-like phenytoin crystals interspersed with polymer particles. (d) Fully amorphous polymeric particles, containing 39 wt.% phenytoin. (e) Fully amorphous product, 35 wt.% phenytoin. Note the absence of phenytoin crystals. (f) Spherical, fully amorphous particles, 21 wt.%phenytoin.	55
2.5	Dependence of the crystalline fraction of the drug-polymer co-formulation on the overall drug content. Evaluation is based on the XRPD peak intensity at $2\theta = 11.27^\circ$ (pure drug = 100%). Up to about 40%, the co-formulation is fully amorphous.	57

2.6	Schematic overview on products obtained at 150 bar and 40°C. The corresponding runs are indicated on the images. (a) Phenytoin crystals coated with polymer particles. (b) Close-up picture of a crystal in (a). (c) Polymeric particles together with a phenytoin crystal. (d), (e) and (f) Sub-micron spherical particles of fully amorphous precipitation products. (e) and (f) were taken after one year of storage at ambient conditions.	58
2.7	Scheme of the ternary system phenytoin - solvent - CO ₂	64
2.8	Scheme of the ternary system PVP - solvent - CO ₂	65
2.9	Scheme of the ternary system PVP - Phenytoin - solvent	67
2.10	Scheme of the ternary system PVP - Phenytoin - CO ₂	68
2.11	Scheme of the quaternary system PVP - Phenytoin - solvent - CO ₂ . The dashed lines represent two operating lines, one leading to fully amorphous composites (right), the other to products containing also crystalline phenytoin (left).	70
3.1	Strategies for drug encapsulation into PLGA particles.	81
3.2	Scheme of the SFEE setup used for solvent extraction experiments.	86

3.3	PLGA particles produced from emulsions stirred at 9'400 rpm with varying concentration in the dispersed organic phase. Top: photomicrographs of product particles. Bottom left: Average particle size as obtained from light scattering. Symbols represent the x_{50} of distributions, while vertical bars cover the range between x_{10} and x_{90} . Bottom right: Corresponding particle size distributions (selected runs only).	90
3.4	PLGA particles produced from emulsions stirred at 30'000 rpm with varying concentration in the dispersed organic phase. Top: photomicrographs of product particles. Bottom left: Average particle size as obtained from light scattering. Symbols represent the x_{50} of distributions, while vertical bars cover the range between x_{10} and x_{90} . Bottom right: Corresponding particle size distributions (selected runs only).	91
3.5	PLGA particles produced by SFEE at a constant PLGA concentration of 10% with varying stirring rate during emulsion preparation. Top: photomicrographs of particles produced at high (a) and low (b) stirring rate. Bottom left: Average particle size as obtained from light scattering. Symbols represent the x_{50} of distributions, while vertical bars cover the range between x_{10} and x_{90} . Bottom right: Corresponding particle size distributions (selected runs only).	93
4.1	Chemical structure of Ketoprofen.	103

- 4.2 Scanning electron photomicrographs of a) PLGA particles and b) recrystallized Ketoprofen, each obtained by SFEE processing of the pure compound. 108
- 4.3 Microscope images capturing the solid state transformation of Ketoprofen. a) spherical and presumably amorphous particles obtained by SFEE processing of pure Ketoprofen, b) onset of Ketoprofen recrystallization from the spherical precursor particles and c) completely recrystallized Ketoprofen. Time span between a) and c): approximately 30 min. 109
- 4.4 SEM photomicrographs of PLGA-Ketoprofen co-formulation particles. a) run 1s on day 1, 4.54% KET, b) run 6 on day 7, 6.11% KET, c) run 8 on day 1, 14.32% KET. Note that particles with high drug content appear softer and are also characterized by a rougher surface. 111
- 4.5 Stability of PLGA-Ketoprofen co-formulations. Co-formulations exhibiting constant drug content: \blacklozenge run 3, \bullet run 4, \blacksquare run 5. Co-formulations with decreasing drug content: \circ run 7, \diamond run 8 and \square run 9. 112
- 4.6 Stability of PLGA-Ketoprofen co-formulations. Unseeded product suspensions are metastable: \circ run 10, \square run 11. When seeded with KET crystals, the same products exhibit a decreasing drug content: \bullet run 10s, \blacksquare run 11s. Two data points on day 0 represent concentrations measured before and after mixing with seed crystals. . . . 114

-
- 4.7 Impregnation of pure PLGA particles with crystalline KET: \blacksquare run 1s. Note that the attained concentration level falls exactly between stable co-formulations (\diamond run 3 and ∇ run 4) and instable co-formulations (\circ run 10s, \triangle run 11s and \square run 9). Two data points on day 0 represent concentrations measured before and after mixing with seed crystals. 116
- 5.1 Scheme of a ternary phase diagram for the solution of a compound forming chiral system such as KET. (A) is S-KET, (B) R-KET, (AB) represents the crystalline compound RS-KET and (S) the solution. The bold line represents the solubility of the relevant solid form of KET in PLGA. Eutectic points are designated as E_A and E_B , respectively. 127
- 5.2 Raw materials (left) respectively recrystallized seed crystals (right) of S-KET (top) and RS-KET (bottom). The recrystallized seeds are generally larger and of more regular structure as compared to the raw material. 130
- 5.3 Total KET content (sum of both enantiomers) of PLGA equilibrated at different temperatures with crystals of RS-KET (\bullet), S-KET (\blacksquare) and with both crystal forms together (\blacktriangle). Open symbols: experiments at 50°C where equilibrium has not been reached due to complete dissolution of crystals. 136

5.4 a) - c): Co-formulation particles obtained at different temperature stages by impregnation of PLGA with S-KET. d) - f): Co-formulation particles obtained at 20°C by impregnation of PLGA using different crystalline morphologies of KET. 137

5.5 Experimental data points obtained by equilibration through impregnation and de-supersaturation using a) crystalline RS-KET, b) crystalline S-KET and c) a mixture thereof at temperatures of 0°C, 10°C and 20°C as compared to the corresponding liquidus lines obtained by extrapolation of the SL-model. 141

5.6 Comparison of experimental data points obtained by impregnation at 20°C (green), 30°C (red) and 40°C (blue) to the liquidus lines obtained from the SL model at these temperatures. 149

5.7 Solubility range of KET in PLGA as calculated using the SL-model (light grey zone) together with the expected range of the glass transition temperature of KET-PLGA composites suspended in water as a function of the KET content (dark grey zone). The glass transition separates the region of glass state (left) from the region of rubbery liquid state (right). 151

6.1 Comparison between the average hydrodynamic diameters of particle obtained from the extraction of the solvent using the SFEE method (red ♦) and those obtained from dialysis (blue ■). The error bars indicate the width of the particle size distribution based on the PDI. 168

-
- 6.2 Polydispersity Index as a function of the sonication time, for the experiments listed in 6.1 with 1 wt% PVA (blue \blacklozenge), 2 wt% PVA (red \blacksquare) and 4 wt% PVA (green \blacktriangledown). The error bars indicate the standard deviation of the PDI. . . . 170
- 6.3 Average Particle Hydrodynamic diameter as a function of the PVA amount, for the experiments 3, 4, 5, 6, 7 and 8 reported in Table 6.2. The errorbars indicate the width of the particle size distribution based on the PDI. 173
- 6.4 SEM pictures of the particles obtained with a PVA amount of 1 wt%, corresponding to experiment 3 in Table 6.2 (left) and with a PVA amount of 5 wt%, corresponding to experiment 8 in 6.2 (right). In both experiments the magnetite content was 15 wt%. The pictures clearly show a decreasing broadness of the particle size distribution with increasing PVA amount. 174
- 6.5 TEM picture of typical particles produced in experiments reported in Table 6.2. (a) experiment 3 (1 wt% PVA, 15 wt% Fe_3O_4); (b) experiment 5 (2 wt% PVA, 15 wt% Fe_3O_4); (c) experiment 10 (3 wt% PVA, 30 wt% Fe_3O_4); (d) experiment 7 (4 wt% PVA, 15 wt% Fe_3O_4). For all experiments the ricinoleic acid-capped magnetic nanocrystals are accumulated in one large cluster on one hemisphere of the particles leading to a Janus-type morphology. 175
- 6.6 SEM picture of a particles produced in experiment 6 as reported in 6.2 (3 wt% PVA, 15 wt% Fe_3O_4 . The partially roughness on the surface is due to the presence of magnetite 176

6.7 TEM picture of a typical particle produced in experiment 11, as reported in 6.2, with 3 wt% PVA and 50 wt% magnetite. The particles are fully covered with magnetic nanocrystals. 177

6.8 Polydispersity Index as a function of Magnetite content. (blue \blacklozenge) experiments carried out with 1.5 wt% PVA (experiments 1, 4 and 9 in 6.2); (red \blacksquare) experiments carried out with 3 wt% PVA (experiments 2, 6 and 10 in 6.2). The error bars indicate the standard deviation of the PDI. 178

6.9 TEM picture of particles produced in experiment 3 as reported in Table 6.2, with 1 wt% PVA and 15 wt% magnetite. It can be observed that small particles have a larger amount of surface covered with magnetic nanocrystals than larger particles. 179

6.10 TEM picture of a typical particle produced in experiment 12 as reported in Table 6.2, *i.e.* using PLA-capped magnetite. The magnetic nanocrystals are well dispersed inside the particle. 181

7.1 Scheme of the setup used for HPH processing. 190

7.2 Evolution of PLGA particle size in HPH, represented by the average particle size x_{50} of measured distributions. Run 1, reference experiment without plasticizer(\bullet), Run 2, HPH under a liquid CO₂ atmosphere (\blacktriangledown) and Run 3, HPH under a liquid CO₂ atmosphere using EA as additional plasticizer (\blacksquare). 192

7.3	SEM images of PLGA particles. a) raw material PLGA RH 503; b) product particles from the HPH reference Run 2 without plasticizer; c) spherical particles obtained from HPH under a liquid CO ₂ atmosphere; d) small spherical particles from HPH under a liquid CO ₂ atmosphere using EA as additional plasticizer	193
7.4	Recrystallization of phenanthrene from an emulsion.	195
7.5	a) Oiling out and recrystallization of a drug through antisolvent addition. b) Emulsion crystallization of a drug through antisolvent addition.	196
7.6	Recrystallization of phenanthrene from an emulsion. Representative product particles obtained at three different temperatures while stirring at 200 rpm.	199
7.7	Recrystallization of phenanthrene from an emulsion. Representative product particles obtained at 20°C for three different stirring rates.	200
7.8	Recrystallized phenanthrene from emulsions extracted by SFEE at two different operating conditions.	201

List of Tables

1.1	Selection of studies concerning the manufacturing of drug, polymer and drug-polymer composite products using scCO ₂ as antisolvent.	12
1.2	Selection of studies concerning the manufacturing of drug, polymer and drug-polymer composite products using scCO ₂ as antisolvent.	16
1.3	Selection of studies concerning the manufacturing of drug, polymer and drug-polymer composite products using scCO ₂ as antisolvent.	19
2.1	Overview of experimental conditions and the results of product analysis.	53
3.1	Comparison of methods for the manufacturing of drug-loaded PLGA particles.	78
3.2	Experimental parameters and the results of product analysis.	89

3.3	Co-formulation of PLGA and Lysozyme using different encapsulation methods. Overview of experimental parameters and the results of product analysis.	95
4.1	Overview of experimental parameters and the results of product analysis.	107
4.2	Material properties of KET and PLGA used for Flory-Huggins modeling.	117
5.1	Overview of the results of product analysis. Weight fractions given in roman numbers are assumed to represent equilibrium data, whereas weight fractions in <i>italic</i> do not correspond to equilibrium state, as explained in the text.	139
5.2	Physico-chemical and material properties of KET and PLGA and pure component parameters used in the Sanchez-Lacombe Equation of State.	143
6.1	List of operating conditions for the experiments performed to study the influence of sonication time on the production of magnetic colloids.	169
6.2	List of operating conditions for the experiments performed to study the influence of PVA and magnetite amount on the production of magnetic colloids. Note that the magnetite nanocrystals used in experiment 12* were stabilized by PLA.	172

Curriculum Vitae

Johannes Kluge

Born in Bad Säckingen, Germany

January 03rd, 1980

Education

- ETH Zurich**, Switzerland
- 09/2005 - today Research assistant at the Institute of Process Engineering,
Ph.D. studies in the Separation Processes Laboratory
under supervision of Prof. Marco Mazzotti.
- 10/1999 - 04/2005 Studies in Mechanical and Process Engineering,
Diploma thesis (Bioprocess Laboratory, Prof. Sven Panke)
awarded with the Prix SGVC 2005 (1st prize).
- Delft University of Technology**, Netherlands
- 09/2002 - 06/2003 Exchange year and research project (Prof. Jack Pronk).
- Scheffelymnasium Bad Säckingen**, Germany
- 09/1990 - 05/1999 Abitur (university-entrance diploma).

Professional Experience

- ETH Zurich**, Switzerland
- 09/2009-02/2010 Department for Mechanical and Process Engineering: Lecturer
Master Class 'Rate-Controlled Separations in Fine Chemistry'.
- 05/2005-06/2005 Research Assistant at the Department of Process Engineering,
Bioprocess Laboratory (Prof. Sven Panke).
- Novartis Pharma AG**, Basel, Switzerland
- 03/2004-06/2004 Internship (Section for Chemical and Analytical Development).

List of Publications

- Kluge, J., Muhrer, G., Mazzotti, M., Solubility of Ketoprofen in Colloidal PLGA. *International Journal of Pharmaceutics*, **2010**, 399: 163–172.
- Furlan, M., Kluge, J., Mazzotti, M., Lattuada, M., Preparation of biocompatible magnetite-PLGA composite nanoparticles using supercritical fluid extraction of emulsions. *Journal of Supercritical Fluids*, **2010**, 54(3): 348–356.
- Kluge, J., Fusaro, F., Muhrer, G., Mazzotti, M., Production of PLGA micro- and nanocomposites by supercritical fluid extraction of emulsions: II. Encapsulation of Ketoprofen. *Journal of Supercritical Fluids*, **2009**, 50 (3): 336–343.
- Kluge, J., Fusaro, F., Casas, N., Muhrer, G., Mazzotti, M., Production of PLGA micro- and nanocomposites by supercritical fluid extraction of emulsions: I. Encapsulation of Lysozyme. *Journal of Supercritical Fluids*, **2009**, 50 (3): 327–335.
- Fusaro, F., Kluge, J., Muhrer, G., Mazzotti, M., Compressed CO₂ anti-solvent precipitation of lysozyme. *Journal of Supercritical Fluids*, **2009**, 49 (1): 79–92.
- Kluge, J., Fusaro, F., Muhrer, G., Thakur, R., Mazzotti, M., Rational design of drugpolymer co-formulations by CO₂ anti-solvent precipitation. *Journal of Supercritical Fluids*, **2009**, 48 (2): 176–182.
- Ottiger, S., Kluge, J., Rajendran, A., Mazzotti, M., Enantioseparation of 1-phenyl-1-propanol on cellulose-derived chiral stationary phase by supercritical fluid chromatography: II. Non-linear isotherm. *Journal of Chromatography A*, **2007**, 1162 (1): 74–82.